Engineering the Sequestration of Carbon Dioxide Using Microalgae

A Thesis Submitted to the

College of Graduate Studies and Research in
Partial Fulfillment of the Requirements for the Degree of
Doctor Of Philosophy (Ph.D.)

In the
Department of Chemical Engineering
University of Saskatchewan

By
Erin Powell

Permission to Use

In presenting this thesis in partial fulfillment of the requirements for a doctorate of philosophy from the University of Saskatchewan, I agree that the Libraries of this University may make it freely available for inspection. I further agree that permission to copy this thesis in any manner in whole or in part, for scholarly purposes may be granted by Dr. Gordon Hill who supervised my thesis work, or in his absence, by the Dean of the College of Engineering. It is understood that any copying, publication, or use of this thesis or parts thereof for financial gain shall not be allowed without my written permission. It is also understood that due recognition shall be given to me and to the University of Saskatchewan in a scholarly use which may be made of the material in my thesis. Requests for permission to copy or to make other use of material in this thesis in whole or part should be addressed to:

Head of the Department of Chemical Engineering

University of Saskatchewan

Saskatoon, Saskatchewan

Canada S7N 5A9

Abstract

With greenhouse gas emissions (of which CO_2 is the major component) being a major environmental concern, mitigation of those emissions is becoming increasingly imperative. The ability to use a fast growing, photosynthetic organism like microalgae that can survive primarily on nutrients such as sunlight and air (with increased CO_2 levels) makes it a desirable agent for CO_2 sequestration. The primary goal of this project is the engineering of the sequestration of CO_2 using the cultivation of the microalgae species *Chlorella vulgaris*. Secondary goals of the project are the exploration and development of valuable by-products of the cultivation and the determination of whether utilizing microalgae to capture CO_2 could be integrated economically into an industrial facility.

The batch growth kinetics of the photosynthetic algal species *C. vulgaris* were investigated using a well-mixed stirred bioreactor. The growth rate was found to increase as the dissolved CO_2 increased to 150 mg/L (10% CO_2 by volume in the gas), but fell dramatically at higher concentrations. Increasing the radiant flux also increased growth rate. With a radiant flux of 32.3 mW falling directly on the 500 mL culture media, the growth rate reached up to 3.6 mg of cells/L-h. Both pH variation (5.5 - 7.0) and mass transfer rate of CO_2 (K_La between 6 h^{-1} and 17 h^{-1}) had little effect on growth rate.

The operation of continuously stirred tank bioreactors (CSTBs) at minimum cost is a major concern for operators. In this work, a CSTB design strategy is presented where impeller stirring speed and aeration rate are optimized to meet the oxygen demand of growing cells, simultaneously minimizing the capital and operating cost. The effect of microbial species, ions in the culture medium, impeller style, as well as changing CSTB size and biomass input density on the optimum operating conditions, is examined. A study of the effects of various parameters on the CSTB design is shown.

Using the kinetic data collected in the batch growth study, a novel external loop airlift photobioreactor (ELAPB) was designed and tested. A model was developed for *C. vulgaris* growth in the ELAPB that incorporated growth behaviour, light attenuation, mass transfer, and fluid dynamics. The model predicts biomass accumulation, light penetration, and transient CO_2 concentrations, and compares predictions to experimental data for radiant fluxes of 0.075 – 1.15

W/m^2 and 0 – 20% CO_2 enrichment of feed air, with a 10% average error. The effect of radiant flux and CO_2 concentration is presented with discussion of radial and vertical profiles along the column. For a fed-batch culture at a biomass density of 170 mg/L, the penetration of the radiant flux was found to decrease by 50% within the first 1 cm, and 75% at 2 cm. Theoretical optimum growth conditions are determined to be 0.30 W/m^2 and 6% CO_2 enrichment of inlet feed air.

The algal culture was observed to be a workable electron acceptor in a cathodic half cell. A net potential difference of 70 mV was achieved between the growing *C. vulgaris* culture acting as a cathode and a 0.02 M potassium ferrocyanide anodic half cell. Surge current and power levels of 1.0 μA/mg of cell dry weight and 2.7 mW/m^2 of cathode surface area were measured between these two half cells. The recently developed photosynthetic cathode was also coupled to a fermentative anode to produce a completely microbial fuel cell. Loading effects and the effect of changing culture conditions on fuel cell operation are reported. The maximum power output measured was 0.95 mW/ m^2 at 90 V and 5000 Ω. A significant increase in this output is achieved with the addition of supplemental glucose to the anodic half cell and the enrichment of the feed air bubbled into the cathodic half cell with 10% CO_2.

Two economic feasibility studies were performed on the integration of ELAPBs into an industrial facility. These integration studies operated the ELAPBs continuously as biocathodes in coupled microbial fuel cells (MFCs) that capture CO_2 from an existing 130 million L/yr bioethanol plant, while generating electrical power and yielding oil for biodiesel to provide operational revenue to offset costs. The anodes for the coupled MFCs are the existing yeast batch fermentors, and the CO_2 to be sequestered comes from the existing bioethanol production. Two different design schemes were evaluated, in both cases the maximum profit was achieved with the maximum number of tall columns operated in parallel. The first design evaluated a batch bioethanol facility with off-site oil processing, and the economic feasibility is demonstrated by the positive Net Present Worth achieved over the 20 year life of the plant, at a 10% rate of return on investment. The second design, for a continuous bioethanol operation, processes both oil and algae biomass on-site, but the economics of this second process are only positive (Internal Rate of Return 9.93%.) if the government provides financial assistance in the form of generous carbon credits (a speculative $100 per tonne of CO_2 not yet attained) and a 25% capital equipment grant.

Acknowledgements

I would like to thank my supervisor Dr. Gordon Hill of the Department of Chemical Engineering for his invaluable guidance. I was fortunate to have a mentor of his caliber throughout my research. I would also like to thank our frequent collaborator on research and publication, Dr. Richard Evitts.

The hard work of Majak Mapiour, John Bolster, and Andrea Vigueras in the laboratory is much appreciated. The collaboration with Divya Sasi was invaluable. I would also like to thank Henry Berg and the Engineering Machine Shops for their help in the construction of the experimental apparatus. LauraLee Powell provided endless hours of assistance with many of the original drawings in the thesis. Heather Lukey and the staff in the office of the College of Graduate Studies and Research were also instrumental in ensuring my scholarship and classes were in order with the complications of my medical leave.

The University of Saskatchewan, the Natural Sciences and Engineering Research Council, and Agriculture Canada are thanked for their financial support.

I would also like to recognize all of the help, friendship and moral support of my friends, colleagues, and office mates in the Department of Chemical Engineering: Aaron, Jean, Kelly, Elizabet, Kyla, Erica, Jason, Mike, Marianne, Reza, Hossain, Janice, Gareth, Ryan, Shayan, Greg, Glynn, and others.

Finally, my heartfelt thanks to my husband Jason, for all of his love and support. And thanks also to my family LauraLee and Myra, and to Jean and George.

TABLE OF CONTENTS

LIST OF TABLES

LIST OF FIGURES

Chapter 1

1. Introduction and Background

1.1. Project Motivation

The primary goal of the Ph.D. research is the engineering of the sequestration of CO_2 using the cultivation of the microalgae species *Chlorella vulgaris*. With greenhouse gas emissions (of which CO_2 is the major component) being a major environmental concern, mitigation of those CO_2 emissions is becoming increasingly imperative. The ability to use a fast growing, photosynthetic biological organism like microalgae that can survive primarily on nutrients such as sunlight and air (with increased CO_2 levels), makes it a desirable agent for CO_2 sequestration and removal. The use of *C. vulgaris* is a natural biological solution that is not environmentally harmful that may produce useful by-products. Present CO_2 scrubbing processes primarily utilize organic chemicals such as amine solvents (such as monoethanolamine) and still require post-removal disposal or sequestration (Amann et al., 2009; Ellison, 2006; Zheng et al., 2004).

The secondary goal of the Ph.D. project is the exploration and development of valuable by-products (either direct or indirect) of the *C. vulgaris* cultivation. This is important in that production of marketable by-products from a microalgae photobioreactor used in CO_2 bioremediation makes the use of this technology more feasible from an economical standpoint. This in turn makes eventual integration on a large scale into an industrial facility more practical.

The final aim of the Ph.D. study tries to answer the practical question of whether utilizing microalgae to capture CO_2 could be integrated into an industrial facility while remaining economically feasible. The concept is to install photosynthetic bioreactors into existing bioethanol plants.

1.2. Carbon Dioxide Emissions and Their Environmental Impact

1.2.1. Canada's Carbon Dioxide Emission Levels and Their Impact

In recent years, Canadians have emitted approximately 747 megatonnes of greenhouse gases annually into the atmosphere, making us the 7th largest emitter in the world per capita (Environment Canada, 2008). The vast majority is CO_2, accounting for 79%, while methane and nitrous oxide contribute the next largest shares at 13% and 7% respectively. Greenhouse gases occur naturally, and are in fact imperative to making the Earth livable by trapping a portion of the sun's heat near the Earth's surface, with the natural atmospheric CO_2 concentration in the atmosphere being 0.03% by volume, although recent measurements indicate it has risen to 0.038% over the course of the last century (Etheridge et al., 1998). Unfortunately, an increase in the greenhouse gas concentration in the Earth's atmosphere increases the greenhouse effect with detrimental environmental consequences, and is now thought to be causing global warming (Environment Canada, 2003). In fact, the need to mediate greenhouse gas emissions and their impact on global temperature has now been accepted by such global bodies as the United Nations Framework Convention on Climate Change (White et al., 2003). Excess atmospheric greenhouse gases and the resulting climate changes affect the Earth as a whole, but will impact Canada specifically in several ways. Air pollution and smog will become increasing problems, and severe and destructive weather events may occur more frequently. Rising temperatures could result in reduced freshwater resources, increasing sea levels, higher incidence of forest fires, and damage to fish populations. The full extent of the damage to the Canadian Arctic with a temperature increase is not fully known but expected to be significant (Environment Canada, 2007).

1.2.2. Sequestration Methods

In December 1997, Canada and 160 other members of the United Nations developed a voluntary agreement to reduce greenhouse gas emissions called the Kyoto Protocol. Canada signed it in April 1998 and it was ratified in 2004. It became legally binding in February 2005. According to the terms of the Protocol, Canada had to reduce its greenhouse gas emissions by

25-30% by 2010. Some of Canada's primary CO_2 emitting industries are fossil fuel industries, coal and oil fired power plants, and transportation (Environment Canada, 2006). The Kyoto Protocol has since been modified by Canada to aim for a 6% reduction over the years 2008-2012 (Environment Canada, 2008). A recent government audit has indicated that this goal may not be attainable with present emissions levels and technology. Canada has already invested more than 3 billion dollars in climate change action programs and initiatives to help reduce emissions across all sectors of the economy. This includes investigation of various methods of bioremediation, both of already emitted atmospheric greenhouse gases, and in-line processes to reduce further emissions from industry and sequester them safely (Environment Canada, 2006). Canadian and American studies have been performed on the sequestration of CO_2 in deep saline aquifers and oil fields (Shafeen et al., 2004; White et al., 2003), as well as in the deep ocean (Herzog et al., 1991) and in unmineable coal beds (White et al., 2003). Research into the use of algae to convert CO_2 to oxygen as a greenhouse gas bioremediation tool, for example of power plant flue gas emissions, is already being performed. Presently, Norway, Japan, Italy, and the United States are all investing in environmental protection research to find economically feasible processes for CO_2 fixation using microalgae applications (Pulz and Gross, 2004). Recent published large scale examples include: an algal CO_2 fixation system that has been economically incorporated into a natural gas power station in Japan (Otsuki, 2001), and a 6000 L algal photobioreactor using industrial effluent gas that has been proven feasible in Germany (Pulz and Gross, 2004). An American study has also been performed on the use of *Botryococcus braunii* for the sequestration of CO_2 separated from flue gas emissions (Feng, 2008). Recent government incentives in Canada such as the Carbon Credit program, which can penalize or reward companies for their level of CO_2 emissions (Haugen-Kozyra, 2007), have made the implementation of CO_2 sequestration technology more cost imperative.

1.3. Microalgae and *Chlorella vulgaris*

The biodiversity of microalgae is enormous and at present represents an almost untapped resource (Pulz and Gross, 2004). It has been estimated that between 200,000 and several million species exist, compared with about 250,000 species of higher plants (Richmond,

2004). Applications range from simple biomass production from food and feed to valuable products for ecological applications. The market is still developing and the uses for microalgae continue to extend into new areas. When the enormous biodiversity of microalgae is considered, and with recent developments in genetic engineering, this group of organisms represents a promising source for new products and applications. With the development of sophisticated culture and screening techniques, microalgal biotechnology can already meet the high demands of both food and pharmaceutical industries (Andersen, 2005). The microalgal biomass market had a size of about 5000 tonnes/year of dry matter in 2004, and generated a turnover of $\$1.25 \times 10^9$/year in 2004 (not including processed products) (Pulz and Gross, 2004).

1.3.1. Species Characteristics

The eukaryotic algae may be defined as those organisms that perform oxygen-evolving photosynthesis and possess chloroplasts (Stanier et al., 1970). They are a highly diverse group, and not all fall into the category of microorganisms. The current primary classification of algae is based on cellular, not organismal, properties (Richmond, 2004). The largest and most varied group is the Chlorophyta (green algae), which spans the full range of organismal diversity. These are characterized by a cellulose cell wall, starch reserves, the presence of chlorophyll a and b and several carotenoids, and most species have flagellate stages with two identical flagella per cell. These can be unicellular, coccoid, filamentous, or plant-like multicellular forms (Stanier et al., 1970).

The Chlorophyceae represent the largest group of Chlorophyta, with about 2,500 species (Richmond, 2004). The best known algae, such as *Chlorella*, *Chlamydomonas*, *Dunaliella* and *Haematococcus*, belong to this group. Many species are cultivated for their value as biomass, while others produce valuable by-products during growth. The extraction of the carotenoid β-carotene from *Dunaliella salina* has already reached large-scale production (Borowitza, 1999). Another promising carotenoid is astaxanthin, a high-value pigmentation source in aquaculture, especially for trout and salmon. Efforts have been made to produce astaxanthin cost-efficiently from *Haematococcus pluvialis* (Garcia-Malea, et al., 2005). Another interesting species, *Botryococcus braunii*, has been investigated as a renewable source of fuel owing to its high hydrocarbon content that can be used for biodiesel production (Richmond,

2004). Most recently, microalgae have been investigated for their value in CO_2 sequestration as a photosynthetic microorganism that requires minimal terrestrial surface area for cultivation (Laws, 1991; Chisti, 2007).

Chlorella vulgaris is a freshwater unicellular species of the Chlorophyta with a high growth rate relative to other microalgae species (Patino et al., 2007; Ogbonna et al., 1997) and ease of cultivation (Andersen, 2005). Cultivated as biomass, it is used in health foods, as a food supplement, and in feed surrogates (Pulz and Gross, 2004). As well as consuming CO_2 and producing oxygen like most photosynthetic microorganisms, *C. vulgaris* has a high chlorophyll content. Like many algae species, *C. vulgaris* also contains oil that can be used to produce biodiesel, at an average content of 28–32% (Chisti, 2007).

1.3.2. Growth Behaviour

The ability of algae to perform photosynthesis confers on them very simple nutrient requirements. Most algae can grow in a completely inorganic medium when in the light. However, some algae also have specific vitamin requirements. The ability to perform photosynthesis also does not necessarily preclude the utilization of organic compounds as the principal source of carbon and energy, and many algae have a mixed metabolism (Ogbonna and Tanaka, 2000).

Chlorella species are capable of growing heterotrophically as well as photoautotrophically. In fact, many large outdoor cultivation systems still use mixotrophic cultivation to compensate for the periods of low light and darkness inherent in an outdoor sun-dependent system (Ogbonna et al., 1997; Endo and Shirota, 1972). Heterotrophic cultivation requires input of an alternate carbon source, typically glucose or acetic acid, in a careful step-wise control or the formation of chloroplasts is suppressed. *Chlorella* species exhibit markedly lower growth rates under heterotrophic growth (Droop, 1974; Richmond, 2004), and given the need for an organic carbon source that may be costly, it could be considered desirable to grow *C. vulgaris* entirely photoautotrophically using a photobioreactor with an artificial light source when sunlight is not available (Andersen, 2005).

When the culture environment is favourable and all nutrients required for cell growth are present in non-growth limiting quantities, unicellular algae like *Chlorella* species reproduce

asexually (Richmond, 2004). The size and biomass of individual cells increase with time, resulting in biomass growth. Eventually the DNA content is doubled in quantity and cell division ensues, with complete division of the cell into two progeny of equal genome and size. This is defined as population growth.

The growth pattern of microalgae generally follows predictable phases in batch culture (Richmond, 2004) as shown in Figure 1.1. The initial lag phase occurs where the specific growth rate is low. This lag can be due to initial adjustment to the culture conditions, or later it may be due to shade-adapted cells being exposed to a higher irradiance. At the late lag phase, cells have adjusted to the new environment and begin to grow and multiply and enter the exponential (or logarithmic) growth phase. Cells grow and divide as an exponential function of time as long as inorganic substrates and light are saturated. During the exponential growth phase, the growth rate of cells is proportional to the biomass of cells (Shuler and Kargi, 2002). The cell concentration of a photosynthetic culture will continue to increase exponentially until it enters the light limited growth phase, described as linear growth (Richmond, 2004; Pirt et al, 1980). Ideally, the theoretical maximum growth rate of an algae culture should be equal to the maximum rate of photosynthesis. This rate, according to Richmond (2004), is approximately 0.2 h^{-1}.

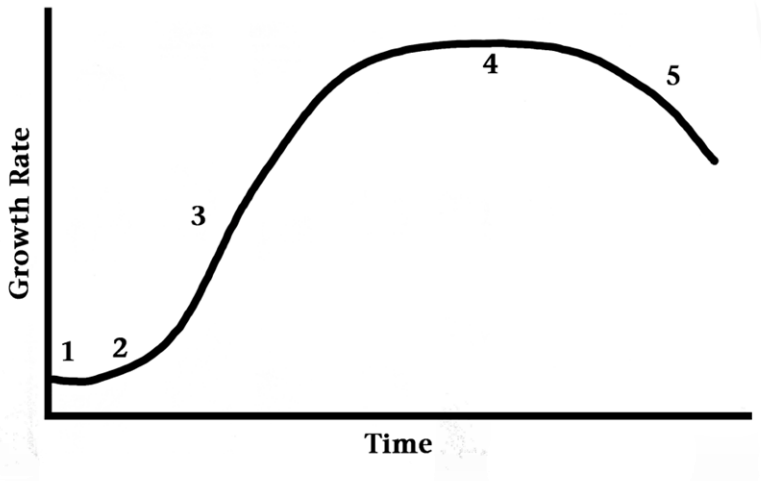

Figure 1.1 Schematic growth curve of microalgae in a batch culture. The growth phases are denoted 1 = lag , 2 = exponential, 3 = linear, 4 = stationary, 5 = decline or death.

1.3.3. Photosynthesis

Photosynthesis as a biological energy conversion system is a remarkable process from the viewpoint of energy accumulation. It is the most abundant energy-storing and life-supporting

process on earth. Algae contribute 40 to 50% of the oxygen in the Earth's atmosphere (Andersen, 2005) and the carbon dioxide fixation rate of most microalgae species is ten times that of the temperate forest (Otsuki, 2001). Photosynthesis is the light mediated conversion of carbon dioxide to organic cell materials. Carbon dioxide is consumed by microalgae and converted to carbohydrate and oxygen using solar energy. Water and carbon dioxide are the substrates utilized according to the following overall reaction (Stryer, 1988):

$$CO_2 + H_2O \overset{LIGHT}{\rightarrow} (CH_2O) + O_2. \quad (1.1)$$

Although the above reaction is very simple, photosynthesis is in fact a complex multi-step process that involves many proteins and specialized molecules. In simple terms, photosynthesis is a two stage process. In the first stage, light energy is absorbed in the 'light reactions' and water is split to release oxygen, reducing power is stored, and the high-energy compound ATP is generated. The second stage is 'the dark reactions' where CO_2 is fixed and biomass is synthesized using the reducing power and ATP generated in the light reactions. The light reactions occur on thylakoid membranes in the chloroplasts, and the dark reactions take place in the stroma.

All photosynthetic microorganisms contain pigments for harvesting light energy. Chlorophylls (green pigments), both Chlorophyll a and b, and carotenoids (yellow and orange pigments) are found in *Chlorella* species (Sansawa and Endo, 2004). All chlorophyll pigments have two major absorption bands: blue or blue-green (450-475 nm) and red (630-675 nm) (Matthijs et al., 1996). Chlorophyll a is present in all oxygenic photoautotrophs as part of the core and reaction centre pigment-protein complexes. In *Chlorella*, in light-harvesting antennae, Chlorophyll a is accompanied by Chlorophyll b. The accessory (antennae) pigments extend the range of light absorption.

The main role of the light reactions is to provide the biochemical reductant ($NADPH_2$) and the chemical energy (ATP) for the assimilation of inorganic carbon. The light energy is trapped in two photoreactions carried out by two pigment-protein complexes, PS I and PS II. The photosystems operate in series connected by a chain of electron carriers. The electron transport reactions proceed energetically downhill, from a lower to a higher redox potential (Stryer, 1988). Upon illumination, two electrons are extracted from water (O_2 is evolved) and transferred through a chain of electron carriers to produce one molecule of $NADPH_2$. Simultaneously, protons are transported from an external space (stroma) into the intra-thylakoid

space (lumen) forming a pH gradient as shown in Figure 1.2. The gradient drives ATP synthesis, which is catalyzed by the protein complex called ATPase (or ATP synthase). This reaction is called photophosphorylation and is summarized by the following equation (Stryer, 1988):

$$2NADP + 2H_2O + 2ADP + 2P_i \xrightarrow[chlorophyll]{light\,energy} 2NADPH_2 + 2ATP + O_2. \quad (1.2)$$

The fixation of CO_2 occurs in the dark reactions using the $NADPH_2$ and ATP produced in the light reactions of photosynthesis. These are so termed because they can occur either in light or dark conditions. The reaction can be expressed by the following equation (Stryer, 1988):

$$CO_2 + 4H^+ + 4e^- \xrightarrow[enzymes]{2NADPH_2, 3ATP} (CH_2O) + H_2O. \quad (1.3)$$

In order to fix one molecule of CO_2, two molecules of $NADPH_2$ and three molecules of ATP are required (representing an energy of 5.2 x 10^4 J or 13 kcal). Regarding the quantum efficiency of CO_2 fixation, a minimum of ten quanta of absorbed light are required for each molecule of CO_2 fixed or O_2 evolved. The conversion of CO_2 to carbohydrate occurs in four distinct phases forming the Calvin-Benson cycle:

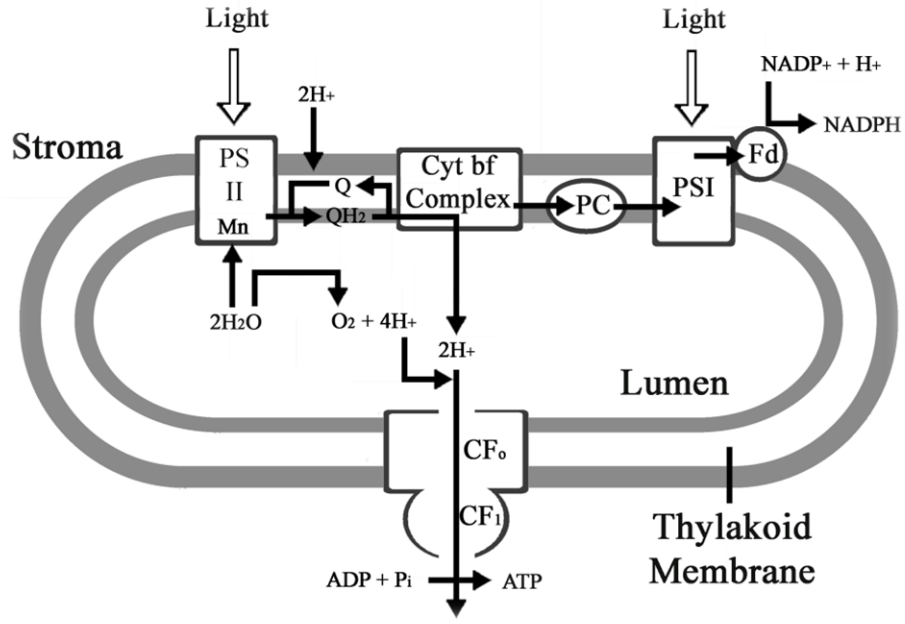

Figure 1.2. Vectorial arrangement of photosystem (PS) I and II within the thylakoid membrane.

i. Carboxylation phase. CO_2 is added to the 5-carbon sugar, ribulose bisphophate (Ribulose-bis-P), to form two molecules of phosphoglycerate (Glycerate-P). This reaction is catalyzed by the enzyme ribulose bisphosphate carboxylase/oxygenase (Rubisco).

ii. Reduction phase. In order to convert Glycerate-P to 3-carbon products (Triose-P), energy must be added in the form of ATP and $NADPH_2$ in two steps.

iii. Regeneration phase. Ribulose phosphate (Ribulose-P) is regenerated for further CO_2 fixation in a complex series of reactions combining 3-,4-,5-,6-,and 7-carbon sugar phosphates.

iv. Production phase. Primary end-products of photosynthesis are considered to be carbohydrates, but fatty acids, amino acids and organic acids are also synthesized in photosynthetic CO_2 fixation. Various end-products can be formed under different conditions of light intensity, CO_2 and O_2 concentrations, and nutrition.

Given the photosynthetic nature of *C. vulgaris*, as expected, previous research has demonstrated that light intensity has been a limiting factor for growth rate. The level of CO_2 present has also been shown to impact the growth rate. Burger et al. (1988) reported that microalgae grown under CO_2 enriched air (> 5% by volume) required different quantum light supplies compared to unenriched air, suggesting there is an interacting effect between CO_2 concentration and light requirements. The limiting effect of light on the growth of *C. vulgaris* is well documented (Morita et al., 2000; Hanagata et al., 1992; Frohlich et al., 1983; Pirt et al., 1980). Algae cultures can collapse under either light deficient or light excessive conditions (Wu and Merchuk, 2002). Sufficient light must be received for the algae species to exceed its light compensation point for its net growth; otherwise the net growth of the culture is poor due to respiratory loss (Andersen, 2005). Increasing the light intensity beyond the compensation point results in an increase in the growth rate, until the culture becomes light saturated, and then even higher light intensities can lead to photoinhibition (Andersen, 2005). Critical light intensity for *C. vulgaris* has been measured at 3.05 mmol m^{-2} s^{-1} (for 30 mmol m^{-2} s^{-1} light supplied, where one mole is 6.02 x 10^{23} photons) by Huisman (1999), but this is dependent on the culture environment including the light intensity to which the cells are exposed. High levels of CO_2 are known to inhibit several metabolic reactions associated with the Krebs cycle. Ammann and Lynch (1967) found that air enriched at the 3% level with CO_2 inhibited the growth of some *Chlorella* species, but Hirata et al. (1999) found *Chlorella* species that were able to tolerate 40% CO_2 by volume in air.

It has been shown that under high photon flux density (PFD), the introduction of a light/dark cycle enhances growth (Wu and Merchuk, 2002; Morita et al., 2000). This may provide a resting stage for cells, and allow algae to utilize very high photon flux density without entering permanent photoinhibition (Merchuk et al., 1998). Lee and Pirt (1981) also found a light/dark cycle to be important to achieving high biomass growth rates in *C. vulgaris,* but they

studied short cycles of intermittent illumination, with a total cycle of 40 s of which an optimum 9.2 s is in darkness, yet still observed enhanced growth. They hypothesized that a very short cycle of intermittent illumination likely differs qualitatively from a long daily diurnal cycle as it is not long enough for substantial variations in the amounts of enzymes and other structural components in the cells.

Photosynthetic microorganisms also undergo photorespiration, where O_2 is metabolized in the place of CO_2. Photorespiration is therefore a competing process to carboxylation, where the organic carbon is converted into CO_2 without any metabolic gain. In this process, Rubisco functions as an oxygenase, catalyzing the reaction of O_2 with Ribulose-bis-P to form phosphoglycolate. After dephosphorylation, glycolate is converted in several steps to serine, ammonia, and CO_2 all without the production of ATP. Photorespiration depends on the relative amounts of O_2 and CO_2, where a high O_2/ CO_2 ratio stimulates this process, and a low ratio favours carboxylation. Rubisco has a low affinity for CO_2, likely because it evolved in an atmosphere with very high carbon dioxide levels compared to the present atmosphere (Moroney and Samanchi, 1999). In some species the rate of photorespiration may be as high as 50% of the net photosynthesis (Richmond, 2004). Microalgae are one of the photosynthetic microorganisms that have adapted to low CO_2 levels by concentrating CO_2 internally (Moroney and Somanchi, 1999). This increases CO_2 fixation and decreases the deleterious oxygenation reaction. This makes microalgae an excellent candidate for cultivation for CO_2 sequestration. For optimal yields in microalgae cultures, it is necessary to minimize the effects of photorespiration. This might be achieved by either stripping of O_2 or by CO_2 enrichment.

1.4. Bioreactor Design for Microorganism Cultivation

Stirred tank, or well-mixed, bioreactors are the most commonly used of the aerated bioreactors in the fermentation industry (Winkler, 1990). A stirred tank bioreactor consists of a vessel containing the liquid growth medium, with the oxygen supplied by sparging compressed air, and a mechanical agitator or stirrer to maintain homogeneous conditions (Winkler, 1990). The often used term well-mixed bioreactor for this design stems from the presumption that mixing is presumed to be sufficiently intense and uniform such that conditions are uniform

throughout the reactor (Bailey and Ollis, 1986). In reality however, the impeller flooding criterion limits the gas throughput of the stirred vessels. When high air gas flow rates are used, the area surrounding the impeller is flooded with gas, rendering the mixing action of the impeller ineffective. The high rate of agitation required causes a high shear zone around the impeller that can cause shear damage to shear sensitive cells (Popovic and Robinson, 1989). The high mechanical energy required to drive the impeller also produces heat, which may have to be removed (Chisti, 1989). For viscous, non-Newtonian fluids, the aeration zone is restricted to the immediate impeller region and channeling of the gas may occur. The use of improved impeller designs and baffles improves mixing and the homogeneity of the conditions (Oldshue, 1983).

For a stirred tank batch reactor, the mass balance equation (assuming Monod growth kinetics) is as follows (Bailey and Ollis, 1986):

$$\frac{dX}{dt} = \frac{\mu_{\max} XS}{S + K_S} \tag{1.4}$$

where X is the biomass concentration (g/L), S is the substrate concentration (g/L), t is time (h), μ_{max} is the maximum specific growth rate (h^{-1}), and K_S is the saturation constant (S at $\mu = \mu_{max}/2$). The substrate balance is given in the form:

$$\frac{dS}{dt} = -\frac{1}{Y}\frac{\mu_{\max} XS}{S + K_S} \tag{1.5}$$

where Y is the biomass yield coefficient on the limiting substrate (g cells/g substrate). If the initial conditions $X(0) = X_0$ and $S(0) = S_0$ apply, then the substrate balance becomes the ordinary differential equation:

$$\frac{dS}{dt} = -\frac{\mu_{\max}}{Y}\frac{\left[X_0 + Y(S_0 - S)\right]S}{S + K_S}. \tag{1.6}$$

Plug flow bioreactors can serve as an alternative to the stirred tank culture. In a plug flow reactor, which is tubular as shown in Figure 1.3, there is no mixing in the axial direction, and the cells flow along the tube with the medium, which initially contains all the substrates and factors required for growth. The plug flow bioreactor is so termed because the contents move with uniform flow along the tube together as an approximation of a plug (Bakker et al., 1997). When fluid moves through a large pipe or channel with a sufficiently large Reynolds number (typically> 2100 in a pipe), it approximates plug flow, meaning that there is no variation in axial velocity over the cross section (Bailey and Ollis, 1986). The fact that both the substrate and

biocatalyst flow together in the whole of the plug flow bioreactor means that the reaction rate is maintained at its maximum (Bakker et al., 1997). Plug flow can be viewed as batch culture with the dimension of time replaced with the dimension of linear space (Voloshin et al., 2005). The rate of reaction is higher, on average, in a plug flow bioreactor than for a conventional stirred tank vessel of the same volume, as a substrate concentration gradient exists along the reactor and substrate is used more efficiently (Bakker et al., 1997). Some bioprocesses can be impractical and costly in plug flow bioreactors however, as aeration is difficult and induces mixing and thus distorts plug flow behavior (Voloshin et al., 2005).

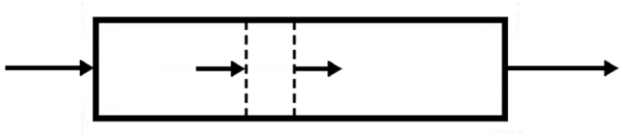

Figure 1.3.Schematic of Plug Flow Bioreactor.

Bioreactors can be operated in batch, fed-batch, or continuous mode. Batch growth of cell populations consists of inoculating the medium with cells only once, and once the culture is initiated nothing is added or removed from it as growth proceeds. The concentrations of nutrients, cells, and products vary with time. In a fed-batch operation, additions are made to the culture during the course of the reaction process. These feed streams can include nutrients, reaction enzymes, and product precursors. When reactors are operated in continuous mode, culture components are added and removed continuously in feed and effluent streams. Growth and product formation can be maintained for prolonged periods in this manner. Once a continuously stirred tank bioreactor (CSTB) reaches steady state, the cell, substrate, and product concentrations remain constant (Shuler and Kargi, 2002).

The addition of a recycle stream to a bioreactor containing concentrated cells can be used to increase biomass and product yield per unit reactor volume per unit time (Shuler and Kargi, 2002). The microorganisms in the recycle stream are usually more concentrated than in the reactor effluent (Warren et al., 1994), and with recycle a dilution rate larger than the organism's specific growth rate is used (Bailey and Ollis, 1986). Therefore with microorganisms growing at the same rate, by employing cell recycle it is possible to process more feed material per unit time and reactor volume than in the nonrecycle situation. This approach is particularly useful for cultures which have a very slow specific growth rate (Richmond, 2004).

Microbial bioreactors can be classed as either suspended or fixed cell growth cultures. In suspended growth systems, the microorganisms are immersed in their nutrient medium, and they are carried along with the fluid movement in the reactor. This is a great advantage in that organisms are in close contact with their environment (Winkler, 1990). Suspended growth systems are principally used in stirred tank and gas sparged fermenters. In fixed, or immobilized, growth systems, the microorganisms are immobilized onto a supporting surface as a biological film or layer, with the outside of the biofilm in direct contact with the nutrient medium. Cell mobility is restricted within a defined space (Shuler and Kargi, 2002). The support surface is usually a biologically inert material that acts as an anchor for the biofilm. The support surface may be packing material through which the nutrient medium is passed, or it may be a porous membrane through which the nutrients reach the cells.

1.4.1. Airlift Design

Pneumatically driven bioreactors offer new solutions to many of the problems historically encountered in the fermentation industry. The bubble column, tower, and airlift bioreactor are bioreactors in which the liquid is partially mixed by the rising bubbles of the gas dispersed by a sparger located at the bottom of the column. The sparged gas passing through the liquid allows for mass transfer between the liquid and gaseous phases. These gas bubbles provide oxygen to the cells in aerobic fermentations. Pneumatic bioreactors have several advantages over stirred tank bioreactors (Nikakhtari and Hill, 2006). In particular they have no moving parts and lower shear rates, making them more suitable for shear-sensitive cells. The interaction between fluid flow and growing cells is complex and not fully understood.

Airlift fermentors are physically divided into two geometrically and hydrodynamically distinct regions. Usually one of these is sparged by gas and the other is not. The different gas holdups in the two zones results in two different bulk densities which induce liquid circulation in the bioreactor. The region of the reactor containing the gassed liquid flowing upwards is called the riser. The section of the reactor containing the liquid flowing downward is termed the downcomer. A loop bioreactor refers to a column bioreactor with a liquid circulation loop. A variety of different loop configurations have been studied (Chisti, 1989). These include the concentric draught tube internal loop, split cylinder internal loop, and external loop bioreactor designs. The classification is based on the positioning of the riser and the downcomer and how

flow occurs between the two regions.

The external loop airlift bioreactor (ELAB) is one type of airlift loop bioreactor in which the two separate columns are connected by horizontal tubes near the top and bottom as shown in Figure 1.4. This external loop allows for liquid circulation between the riser and the downcomer. Compared to the bubble column or basic airlift bioreactor, an ELAB improves the culture condition by circulating the liquid phase, which provides sufficient mixing for the slow process of microbial growth. The turbulence in the liquid is also reduced by damping out the eddies found in bubble columns (Nikakhtari and Hill, 2006). The enhanced mixing in loop airlift columns forms a homogenous environment for microbial growth. In continuous operation, a loop airlift bioreactor also acts more closely to a well-mixed vessel as compared to an ordinary bubble column (Ritchie, 1994). To improve mass transfer between the gas and liquid phases in an ELAB, important hydrodynamic parameters to consider are the two-phase flow pattern, liquid physical properties, gas holdup, liquid circulation velocity, bubble sizes, bubble distribution, dispersion, and turbulence intensity (Cheremisinoff, 1996). Hydrodynamics control the mixing characteristics and are therefore a principal determinant of the light regime that a photosynthetic cell culture would experience (Babcock et al., 2002) with this type of bioreactor design. The continuous flow through all parts of the reactor and mixing effects help prevent algal adhesion (thus reducing the blocking of light) that can inhibit growth in conventional tank reactors.

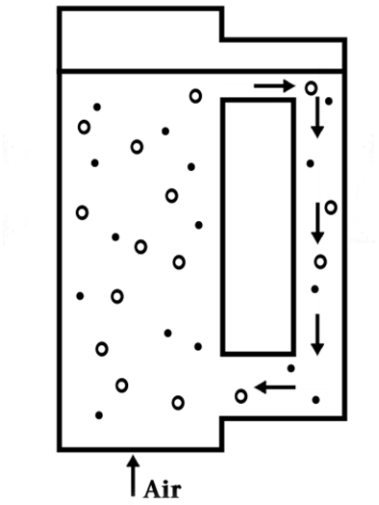

Figure 1.4. Schematic of an ELAB. Gas is sparged into the riser, and liquid flows down in the downcomer. White circles are air bubbles and black dots are cells.

The type and location of gas spargers are design factors which can affect performance. The head space, where the gas-liquid separation takes place, also affects the performance of the reactor. Some other important factors in airlift design include: reactor type, reactor size, ratio of riser to downcomer cross-sectional areas, and internal baffling. This extensive variation in airlift bioreactor design makes the development of design strategies difficult. Packing has been employed in ELABs to permit immobilized biomass holdup attachment to the packing and

enhance gas holdup to improve mass transfer. Enhancement of the oxygen mass transfer rate has been observed using a small amount of either stainless steel mesh or woven nylon packing of very high porosity in the riser section of an ELAB (Nikakhtari and Hill, 2005a; 2005b).

Aeration of bioreactors of any type is a key design factor. Ensuring that sufficient oxygen reaches the cells for microbial growth is important, and therefore many studies have been performed (Nikakhtari and Hill, 2005c; Schell et al., 2001) on the mass transfer of oxygen from the gas phase to the liquid phase, where it can be utilized by the cells. The ELAB provides a well-mixed environment for aerated growth without the need for an impeller (Nikakhtari and Hill, 2005b; Chisti, 1989). More recently, circulating loop airlift bioreactors have been applied as a treatment technology for contaminated air effluents (Nikakhtari and Hill, 2006; Ritchie and Hill, 1995). Bioremediation of volatile organic chemicals (VOCs) provides both oxygen and substrate (VOCs) from the gas phase, and has been shown to be limited by the mass transfer into the liquid phase (Nikakhtari and Hill, 2005d). Such studies and modeling of ELABs where the sparged gas provides substrate for microbial growth provides useful information for the design of a bioreactor for culturing of a photosynthetic microorganism.

The growth of a photosynthetic organism like microalgae requires CO_2 as the substrate that will be delivered by the gas phase. The mass transfer of this substrate into the liquid phase may also be a limiting factor in microalgae culture. The mass transfer of CO_2 is frequently treated as similar to that of oxygen (Hill, 2006; Baquerisse et al., 1999), and the diffusion coefficient correction factor is employed to obtain the mass transfer coefficient, K_La, of CO_2 from that of oxygen. The direct mass transfer of CO_2 has been studied (Hill, 2006; Camacho Rubio et al., 1999) and microalgae have been successfully cultivated in airlift bioreactors (Krichnavaruk et al., 2005; Wu and Merchuk, 2004).

1.5. Light and its Effect on Bioreactor Design and Photosynthetic Cultivation

Light is the energy source that microalgae use for growth. Therefore an understanding of the nature and properties of light, in addition to understanding how it penetrates into the bioreactor, is important to effectively culture microalgae.

1.5.1. Characteristics

Light is electromagnetic radiation, and based on the wavelength; electromagnetic radiation can be divided into several components. Only those wavelengths of radiation between 10^{-3} m and 10^{-8} m are denoted as light. The visible part of the spectrum ranges from the violet at approximately 380 nm to the far red at 750 nm. The wavelengths of visible light also correspond to photosynthetically active radiation (PAR), meaning radiation utilizable for photosynthesis (Fleck-Schneider et al., 2007).

The colour of most objects depends upon the interaction between visible light and the electrons of atoms that make up that object. It is the result of a dynamic process on the molecular level: the absorption of light and the resulting change of a molecule's quantized energy. In simplest terms, for most objects, the colour of the object that an observer will see is the colour of the wavelengths of the light it reflects (Physical Science Study Committee, 1960). Therefore, green microalgae such as *C. vulgaris* appears green because the high levels of chlorophyll pigments reflect mainly green light wavelengths and absorb red and blue in the visible spectrum.

According the quantum theory, light energy is delivered in the form of separated packages called photons. The energy, *E*, of a light quantum, or photon, is given by the following expression (Physical Sciences Study Committee, 1960):

$$E = hf = \frac{hc}{\lambda} \tag{1.7}$$

where *h* is Planck's constant (6.626×10^{-34} J s), f is the frequency (Hz or s^{-1}), λ is the wavelength (m) and *c* is the speed of light (m/s). Since the energy is inversely related to the wavelength, a photon of blue light (about 400 nm) is more energetic that that of red light (around 700 nm). Photosynthetic pigments absorb the energy of photons, and transfer it to the reaction centres where it is utilized for photochemistry. The photon should posses a critical energy sufficient to excite a single electron from one pigment molecule and initiate charge separation (Richmond, 2004). According to Einstein's law, one mole of a compound must absorb the energy of N photons ($N = 6.023 \times 10^{23}$, the Avogadro number) to start a reaction.

In microalgal culture, photons of light are the major energy source for growth of cells. The properties of the light source, such as wavelength and intensity, are critical (Matthijs et al., 1996; Wang et al., 2007), and can greatly influence the growth rate. There are many sources of

light, and not all are suitable for photosynthetic growth. Plants and algae respond best to certain wavelengths of light, and the optimum wavelength can be species specific. The action spectra of green microalgae, including *C. vulgaris*, show preferred absorption ranges: blue (420 - 450 nm) and red (660 – 700 nm) (Lee and Palsson, 1996; Matthijs et al., 1996).

Sunlight is the natural light source for nearly all photosynthetic growth on Earth. Sunlight is the radiation emitted by the chromosphere of the sun at around 6000 K. The thermal radiation emitted is in every region of the spectrum, meaning it has a "continuous spectrum", and it peaks in the visible region of the electromagnetic spectrum, at around 550 nm. Average direct solar irradiance reaching the earth's surface is 1000 W m^{-2} (Miyake et al., 1999) of which approximately 40% (Richmond, 2004) is photosynthetically active radiation (PAR, between 400-750 nm) (Gordon and Polle, 2007). Artificial light sources are available using a variety of commercially available bulbs. These include incandescent light bulbs, fluorescent lights, high-intensity discharge lamps, and light emitting diodes.

The light-emitting diode (LED), is a semiconductor diode that emits narrow-spectrum light when electrically biased. This effect is a form of electroluminescence. Compared to conventional fluorescent and incandescent lamps, LEDs are considered to be optimal light sources for cultivating algae due to their low power consumption, small size, reliability, and long lifetime (Lee and Palsson, 1996; Michel and Eisentraeger, 2004; Wang et al., 2007). LEDs also have a highly efficient conversion of electricity to light so heat generation is minimized (Lee and Palsson, 1996).

Wang et al. (2007) studied the use of LEDs with different light wavelengths for the cultivation of *Spirulina platensis*, a blue-green freshwater microalgae. It was found that LEDs provided an effective and economical light source for microalgae cultivation. Red LED light (620-645 nm) provided the highest growth rate, and blue LED (460-475 nm) light the lowest. White LED light (380-760 nm) provided the second highest microalgae growth rate, and although not as high as the red LED, significantly higher than the yellow, green and blue LEDs, which were minimal in all cases.

Michel and Eisentraeger (2004) found similar growth of green microalgae species using both white LEDs and tubular discharge lamps. Lee and Palsson (1996) obtained comparable cell masses and growth rates for *C. vulgaris* with LEDs and fluorescent light, but found that only the red wavelengths were imperative for photosynthetic growth, although limiting the light to red

wavelengths resulted in cell volume and structure changes. It has been established that photosynthetic microorganisms require both the red and blue spectrum wavelengths of light for optimal growth (Richmond, 2004; Matthijs et al., 1996). Matthijs et al. (1996) also found that red wavelength LEDs are effective for culturing *Chlorella* species, and that the blue spectrum light is not needed. Possible explanations for this are that perhaps the red LED produces sufficient blue photons, or that this blue light is not needed for energy purposes but for enzyme activation and regulation of gene transcription.

1.5.2. Distribution and Penetration

As discussed previously, growth of *C. vulgaris* is light limited. It follows from this that one of the most important factors influencing growth in a photobioreactor is the availability of light to the cells (Merchuk et al., 1998; Evers, 1991). It is therefore necessary to determine the light radiation distribution inside an algae culture vessel. Within a fully lit photobioreactor there can be both regions of high photon flux density and dark regions in which the net biomass production is negative. One way of preventing such negative growth is to increase the volumetric surface area (reduce the depth of the culture) (Wu and Merchuk, 2002), a frequently costly option, or to alter the bioreactor design to reduce shading in the light region. Such a reduction can take a high toll on the economics of the process depending on the photobioreactor design.

An assessment of local light energy is a prerequisite for modeling and analyzing the light energy transfer in a culture vessel. Either incident light intensity or irradiating surface area per unit culture volume has been widely used as an indication of light transfer efficiency (Ogawa et al., 1971; Prokop and Erickson, 1995; Qi and Rorrer, 1995). In the case of "thin" column bioreactors, a simple mean value is frequently taken for the light intensity in many models (Frohlich et al., 1983; Molina Grima et al., 1996), this value being calculated according to the geometry of the reactor. These values are only valid however at low cell concentrations and a narrow light path (Suh and Lee, 2003), and give no information on local light distribution inside the culture. Therefore, mathematical models have been developed to obtain the light distribution profile and average light intensity (Cornet et al., 1992a; Lee et al, 1987; Molina Grima et al., 1997; Rabe and Benoit, 1962). However, since the average light intensity can be identical for completely different conditions (Suh and Lee, 2003), the light distribution profile is required to

describe the irradiance conditions more precisely.

When light passes through a transparent medium, not all of it is transmitted. Depending on the properties of the substance, some of the light may be absorbed, and some scattered from the initial light path. Light from an external source must pass through the vessel wall and a slurry of culture medium and other living cells (Miyake et al., 1999) to reach an individual algae cell as shown in Figure 1.5. The vessel wall used in the novel photobioreactor study carried out in this research is a transparent substance. It is made of 12.7 mm (0.5 inch) acrylic chosen for its transparency. It transmits light, but not perfectly, and some of that light is still absorbed and some is reflected away from the vessel. The average light transmission of visible light through acrylic is 92% (Shackelford, 2001).

When all light effects are considered, not just attenuation by the reactor wall and culture itself, losses, dispersion, and reflection need to be considered in determining the light distribution in a vessel, as shown in Figure 1.5. These can be neglected as minimal relative to attenuation by the culture. Reflection off the vessel wall back to the light source, and losses outside the vessel, are assumed to be included in the vessel wall transmission losses. Dispersion is the spreading out of light in other directions from its original path of travel once it strikes an object. It also spreads out into the spectrum of the wavelengths of which it consists. However, light can still be treated as monodirectional (Wu and Merchuk 2004; Parson, 2007), and once it enters the vessel is considered to either be absorbed by the culture or dissipated as heat. The present models for light distribution in photobioreactors neglect light attenuation, refraction, and losses due to the vessel wall material (Evers, 1991; Wu and Merchuk, 2004; Cornet et al., 1992a). The penetration of light radiation into a cell culture is also highly wavelength-dependant, with the lower wavelengths of light being able to penetrate deeper according to Sorensen (2005) and Miyake et al. (1999). This phenomenon is typically neglected for modeling purposes.

If the slurry of culture medium and living cells is assumed to be absorbing and scattering, nonemitting, and nonfluorescing, and it is assumed that the scattering and absorption are proportional to the biomass concentration (Cornet et al., 1992a), light radiation diminishes rapidly with depth of penetration (through medium and cell culture). Miyake et al. (1999) observed this with the photosynthetic purple bacterium *R. spheroides RV* culture, where for a tank culture, light intensity dropped to 10% at 1 cm depth, and to 1% at 2 cm depth. Li et al. (2008) reported that the maximum microalgae cell density for light penetration is typically 1-5

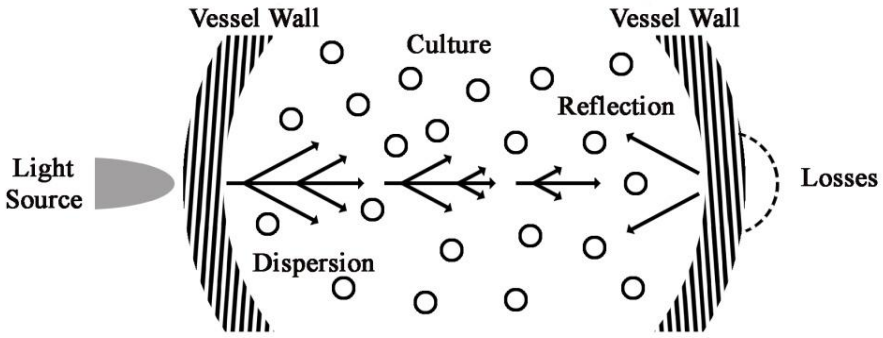

Figure 1.5. Schematic of Light Distribution in the Experimental Photobioreactor.

g/L for most species. The Beer-Lambert law has typically been used to express the exponential attenuation of the radiant energy flux which results from absorption by the culture (Wu and Merchuk, 2004; Evers 1991; Ten Hoopen et al., 1989; Fredrickson et al., 1961). This model is used extensively in photometry and is based on two assumptions: (1) the light field remains parallel throughout the vessel and (2) the scattering by the solid particles (cells) can be neglected. Attenuation by the actual growth medium is generally neglected, only attenuation by the biomass in the culture is taken into account. The Lambert-Beer law for light attenuation by biomass, where I is the light intensity, is (Parson, 2007)

$$I(p,C_x) = I_o \exp(-pK_aC_x) \tag{1.8}$$

where I_o is light intensity (illumance) at the surface (W/m^2), p is the length of the light path (m), C_x is the biomass density, (g/L), and K_a is the absorption coefficient (m^2/g). The absorption coefficient, sometimes called the extinction coefficient, must be determined experimentally and is particular to a microalgae species (Yun and Park, 2003). Yun and Park (2001) obtained a value of 435.3 m^2/kg for K_a of *C. vulgaris* suspensions under full spectrum visible light. Note that Equation 1.8 applies only for one-dimensional propagation, and can be applied for individual wavelengths (Parson, 2007). The Beer-Lambert equation is a simplified description of illuminance attenuation in a bioreactor, as a stricter analysis should take into account the geometry of the system and light scattering. Nevertheless, this uncomplicated approach is used frequently as it is considered to provide a sufficient description of light attenuation and it is simple to incorporate into complicated models of growth kinetics, reactor light distribution, and fluid dynamics.

The Beer-Lambert Law of light attenuation has been applied to airlift loop bioreactors

with light and dark zones. For an externally lit internal loop airlift photobioreactor, Wu and Merchuk (2004) based their determination of photon flux density (PFD) in each region of the photobioreactor on the Beer-Lambert law. For the light-sufficient downcomer, the radial mixing is negligible, apparently due to non-developed laminar flow (Wu and Merchuk, 2003). An algal cell that enters this region at a radial position z' will experience the PFD, I_d ($\mu E\ m^{-2}\ s^{-1}$), from the Beer-Lambert law for light attenuation:

$$I_d = I_O e^{Pz'}, \tag{1.9}$$

during the entirety of its residence time in the downcomer. It is noted that Wu and Merchuk (2004) neglected the scattering effect of the culture by using the Beer-Lambert law for light attenuation yet obtained satisfactory agreement with experimental results. This simplification also allowed for combining of algal kinetics and fluid dynamics with light distribution while keeping the solution of the equations in the model manageable.

Other published models have accounted for the scattering effect on light within a photobioreactor. Cornet et al. (1992a) proposed a model for light attenuation that may be more appropriate for high biomass concentrations (greater than 1 g/L) that considers scattering and absorption phenomena separately. It is an adapted version of Schuster's (1905) hypothesis which assumes: (1) the light field remains isotropic throughout the whole culture and (2) light absorption and scattering are independently accounted for by two coefficients, E_a and E_s, respectively. The scattered intensity is assumed to be emitted by the suspended particles in the main direction of the radiation either positively or negatively. The adapted Schuster and Beer-Lambert models give very different results for dense microbial cultures, indicating the importance of taking into account the scattering effect of dense cultures (Cornet et al, 1992a). It should be noted that this model is also only monodimensional. Also, for cultures with low biomass densities, or for cultures that have minimal scattering properties, this model and the Beer-Lambert provide the same results.

Light distribution in the bioreactor also depends on the shape of the vessel. Evers (1991) described the modeling of a cylindrical vessel, evenly illuminated from all sides. This model assumes that the outside of the column is homogenously illuminated so that each point at the wall can be considered as a light source with illuminance I_o. The cylinder length does not influence the modeling of overall biomass change rate in the vessel if the top and bottom effects are neglected. The direction of the light is not important, due to the assumption of uniform

lighting from all sides. In the case of a cylindrical riser such as an airlift photobioreactor, homogeneous lighting from all sides is a reasonable assumption. According to Evers (1991), in a cylindrical reactor, the path of light to a point inside the reactor is determined from the distance from the vessel outer surface and the angle from the bioreactor centerline. Light was only considered on the horizontal plane, radially through the reactor. The light intensity at a given point in the vessel can therefore be determined as a function of distance, angle, and light attenuation. Wu and Merchuk (2002) have demonstrated however that the improved accuracy of including the effect of reactor geometry (such as with the Evers (1991) model) in their model was not significant, but did greatly increase the complexity of the calculations relative to using the more simple Beer-Lambert Law of light attenuation.

Several other models for the path of light as it penetrates a photobioreactor have been developed. A majority of models simply calculate a value for mean light intensity throughout the reactor based on the geometry (Li et al., 2003; Molina Grima et al., 1994; Iehana, 1990; Camancho-Rubio et al., 1985; Frohlich et al., 1983). Molina Grima et al. (1999) modeled the incident radiation on the surface of a photobioreactor as the total of direct sunlight, reflected radiation from the surroundings and disperse radiation due to particulates in the atmosphere. The disperse and reflected light paths involved similar equations. The solar light beams were modeled to hit the photobioreactor from all angles, rather than each artificial light beam focusing perpendicularly incident to the bioreactor surface. Acien Fernandez et al. (1997) only considered direct and disperse rays of sunlight in their model of light paths in photobioreactors.

1.6. Fundamentals of Modeling Growth in Airlift Photobioreactor

1.6.1. Photosynthetic Microbial Growth

The specific growth rate of microorganisms has been shown to be affected by the substrate concentration. This relationship is most often expressed by the unstructured Monod model of saturation kinetics. The Monod equation (Shuler and Kargi, 2002) is:

$$\mu = \frac{\mu_{max} S}{K_S + S} \tag{1.10}$$

where μ is the specific growth rate (h^{-1}), μ_{max} is the maximum specific growth rate (h^{-1}), S is the rate-limiting substrate concentration, and K_S is the saturation constant (S at $\mu = \mu_{max}/2$). A typical growth curve for a microorganism exhibiting Monod growth kinetics is shown in Figure 1.6.

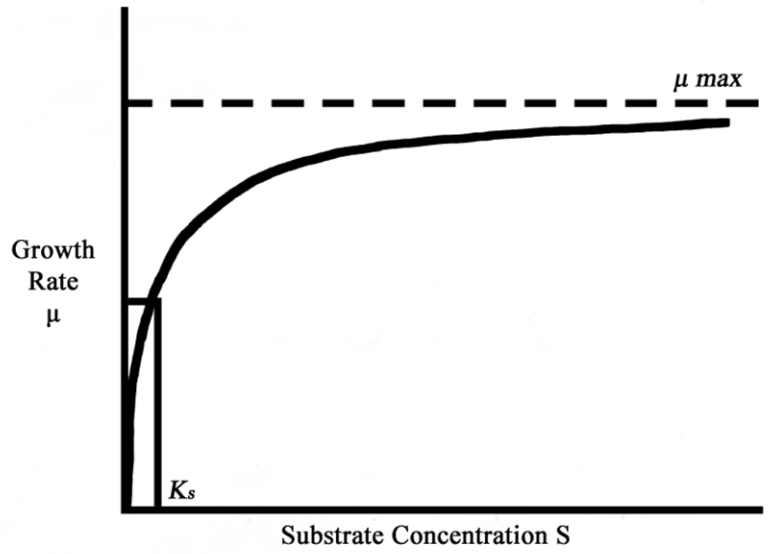

Figure 1.6. Specific growth rate curve for a microbial species exhibiting substrate limited Monod growth kinetics.

According to the Monod equation, increasing the substrate concentration does not affect the specific growth rate after reaching the maximum value. However, it has been observed that in most cases, the specific growth rate actually starts to decrease when the substrate concentration increases beyond a certain value. In the case of photosynthetic microorganisms, this phenomenon has previously been discussed as photoinhibition when light is the substrate. In the case of *C. vulgaris* however, both light and CO_2 are growth substrates, which may both be inhibitory. Data obtained by Brune and Novak (1981) from carbon limited batch and chemostat cultures suggest that the specific growth rate of a variety of algae species including *C. vulgaris* are best represented by the Monod model. However, the Haldane equation (Aiba, 1982) improves the Monod model by including the possible inhibitory effect of excessive light or CO_2:

$$\mu = \frac{\mu_{max} S}{K_S + S + \frac{S^2}{K_I}} \tag{1.11}$$

where the inhibition constant K_I has been included, and when the substrate S becomes the radiant light intensity I, then K_I represents a photoinhibition constant. If S is the CO_2 concentration in the media, then K_I serves as the CO_2 inhibition concentration. The phenomenon of CO_2 inhibition was found to describe the actual microalgae production curve far better than the Monod equation by Rehak et al. (2008).

There is indication that the substrate kinetics of the Monod model are too simplistic an approach for light limitation. This is supplied by examining the P-I curve of microalgae. The classical description of photosynthetic activity is based on measurements of oxygen evolution in proportion to light intensity, termed the light-response or P-I curve (Richmond, 2004). A schematic representation this curve is given in Figure 1.7. The initial slope of $a = P_{max}/I_k$, where I_k represents the saturation irradiance and P_{max} is the maximum rate of photosynthesis. In the dark, there is a net consumption of oxygen as a consequence of respiration (the negative part of Figure 1.7). Therefore, gross photosynthesis is considered as the sum of net photosynthesis (O_2 evolution) and respiration (O_2 uptake). At low irradiance (light-limited region), the rate of photosynthesis depends linearly on light intensity. With increasing light intensity, photosynthesis becomes less and less efficient. Finally, it reaches a plateau – the light-saturated value – where enzymatic reactions utilizing fixed energy become rate limiting. Under prolonged supra-optimal irradiance, photosynthetic rates usually decline from the light-saturated value. This is the photoinhibition previously discussed in Section 1.3.3.

The most commonly used models to calculate the growth of a microalgae culture are the P-I models (Kurano and Miyachi, 2005; Frohlich et al., 1983; Rubio et al. 2002; Molina Grima et al., 1994; Cornet et al., 1992b; Camacho-Rubio and Martinez-Sancho, 1985; Iehana, 1990; Ten Hoopen et al., 1989) which relate productivity, or biomass growth rate, to light intensity. The models differ in the parameters that are included in the model. A mean value is generally taken for light intensity. Monod or Aiba growth kinetics are among the most usual equations appearing in such models. The simple substrate inhibition model was successfully used to simulate the relationship between the specific growth rate and CO_2 response by Kurano and Miyachi (2005). In this case, CO_2 was the sole source of carbon for the growth of the highly CO_2-tolerant green algae species *Chlorococcum littorale* in batch cultures and it was found to inhibit its growth above 20% (by volume). Since we have two limiting substrates, that may be either interacting or independent, the simple Monod equation would need to be modified to

incorporate both factors. This has been done by Baquerisse et al. (1999) for *Porphyridium purpureum* and their work can serve as a guide for the algebraic factors that must be included in the Monod growth model to account for the simultaneous effects of light and CO_2 concentration.

Cornet et al. (1992a; 1992b) also used the Monod model to describe the mean growth rate, but have divided the microalgae biomass into several compartments for the purposes of modeling. The goal was to link the biomass growth of cyanobacteria under light limitation to mineral limitations as they affect the different cellular constituents, including those which directly affect photosynthesis such as chlorophyll. This led to a very intricate set of equations that seems unnecessarily complex and not particularly applicable to *C. vulgaris*, as it is not limited by minerals such as sulphur and nitrogen that were included in this model. The great value of the work of Cornet et al. (1992a; 1992b) is the model of radiative transfer in the photobioreactor, which includes both absorption and scattering by the microalgae culture.

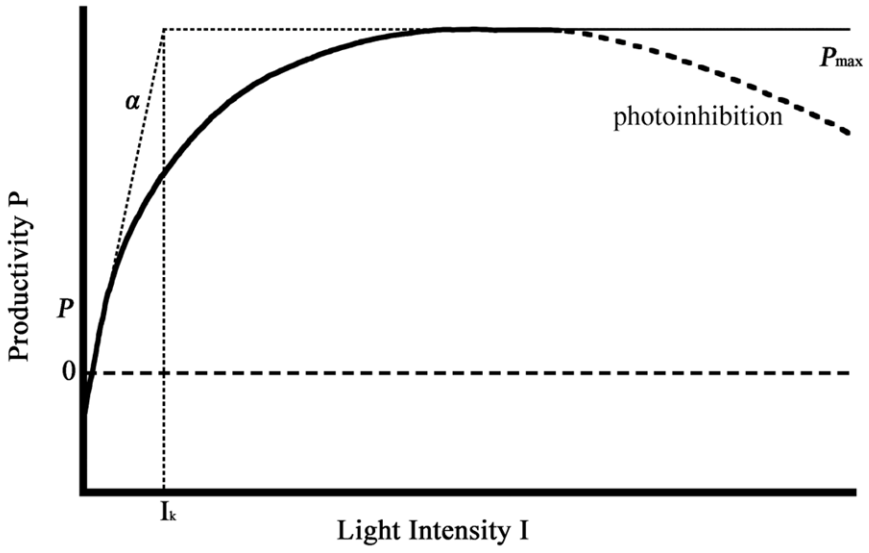

Figure 1.7. Schematic diagram of a microalgal light response curve.

Molina Grima et al. (1999) have developed their own version of the biomass specific growth rate equation that accounts not only for photoinhibition, but also for the dependence of specific growth rate μ (h^{-1}) on the average irradiance, I_{av} ($\mu E\ m^{-2}\ s^{-1}$) varying with the incident irradiance level I_o ($\mu E\ m^{-2}\ s^{-1}$). The biomass growth rate equation is given as:

$$\mu = \frac{\mu_{\max} I_{av}^{\left(b_I + \frac{c_I}{I_O}\right)}}{\left[I_k \left(1 + \left(\frac{I_o}{K_i} \right)^{a_I} \right) \right]^{b_I + \left(\frac{c_I}{I_O}\right)} + I_{av}^{\left(b_I + \frac{c_I}{I_O}\right)}} \tag{1.12}$$

where μ_{max} is the maximum specific growth rate (h^{-1}), I_k is the microalgal affinity for light ($\mu E\ m^{-2}\ s^{-1}$), K_i is the photoinhibition constant ($\mu E\ m^{-2}\ s^{-1}$), and a_I, b_I, and c_I are experimentally determined parameters. This growth model was developed for use with outdoor cultures where cyclic changes in illumination occur over the course of the day and the year. It is designed to account for physiological changes in how microalgae respond to light when the incident light changes. It includes several new experimentally determined kinetic parameters.

Lee and Pirt (1981) present a model that accounts for specific growth rate in both light-sufficient and dark zones in a bioreactor. It also includes an endogenous metabolism maintenance term, which differs for growth in light and in darkness. This model was developed for use with cultures grown under intermittent illumination. Their set of biomass and energy equations is useful in describing growth in a photobioreactor, with a light-sufficient riser and dark zones. The final simplified equations for light-limited growth are:

$$\mu_o = \mu(\alpha_L + \beta_D) - m_r Y_G \{1 - (\alpha_L + \beta_D)\} \tag{1.13}$$

and $$\phi I_o A / XV = \mu_o / Y_G + m' \tag{1.14}$$

where, $$m' = m_r \{1 - (\alpha_L + \beta_D)\} \tag{1.15}$$

and μ_o is the observed specific growth rate (h^{-1}), μ is the specific growth rate (h^{-1}) in the growth zone (light or dark), α_L is the light zone (a fraction of the volume illuminated), β_D is the dark growth zone (a fraction of the total volume where cells continue to grow in the dark), m_r is the maintenance coefficient of resting cells ($J(g\ dw)^{-1}h^{-1}$), Y_G is the true growth yield from light ($g\ dw\ J^{-1}$), ϕ is the fraction of photosynthetically available radiation, Io is incident light intensity ($W\ m^{-2}$), A is total surface area of culture (m^2), X biomass concentration ($g\ dw\ L^{-1}$), V is total culture volume (m^3), and m' is apparent maintenance coefficient of culture ($J(g\ dw)^{-1}h^{-1}$). This model was developed for a simple tubular loop reactor and the heterogeneity of light distribution within the reactor is not considered. The maintenance coefficient of a *Chlorella* culture was reported to be 20 J/g-biomass h^{-1} (Pirt et al., 1980).

Evers (1991) proposed a model for light limited growth in continuous cultures in a chemostat or turbidostat that assumes that light energy uptake rate depends hyperbolically on light intensity and that the maintenance costs are proportional to biomass. This model takes the light distribution in the vessel into account and is analogous to a nutrient-limited chemostat model. In effect, light is modeled as an algae food source. Light is considered taken up only if it

is converted into a form of energy which can be used by the cell. Absorbed light energy can be lost by absorption by components other than photosynthetic pigments, and after absorption by photosynthetic pigments, there will be energy loss by the photosynthetic route since it lacks 100% efficiency. The spectral composition of light is not incorporated into the model. It is assumed that part of the energy is used for maintenance, and the remaining part of the energy is used for growth. Biomass is assumed to be homogeneously distributed. The Evers (1991) formula for the biomass change rate is

$$W' = \mu W - DW = y'\left([a]\frac{I}{I+K} - [m] \right) W - DW \tag{1.16}$$

where W' is biomass change rate (g/L-h), m is specific growth rate (h^{-1}), W is biomass density (g/L), D is dilution rate (h^{-1}), y' is the conversion factor from energy to biomass (g/J), [a] is maximal weight-specific energy uptake rate (J/g-h), I is light intensity (W/m^2), K is saturation constant (W/m^2), and [m] is the maintenance coefficient (J/g-h). Mutual shading of cells cannot be neglected if the biomass density is high enough to influence the light distribution in the vessel significantly, particularly in a chemostat. Light intensity I is then a function of biomass W and depends on the place in the vessel, and as a result, the growth rate also depends on the place in the vessel. The light distribution in the vessel must therefore be known for this model.

Wu and Merchuk (2004) simulated microalgae growth in an externally illuminated internal loop airlift photobioreactor that includes kinetics parameters for a system that includes light/dark cycles. This model constitutes an integration of the kinetics of photosynthesis and photoinhibition with the fluid dynamics of a reactor column, including the effects of shear stress on the kinetics of growth. The maintenance term is modified to take into account the effects of liquid flow in the bioreactor on growth rate. Since light availability varies from point to point in the reaction vessel, the model takes into account the movement of the cells from one region of the bioreactor to another. It also makes possible the prediction of the collapse of cultures under conditions of light deficiency or light excess and the influence of mixing on these critical parameters. This is a dynamic model based on the concept of the photosynthetic factory (PSF) of the light-trapping system (Eilers and Peeters, 1988) and the three possible states (resting, activated, and inhibited) that may occur upon stimulation by a photon of light. It is however limited to cultures that exhibit the characteristics of photoinhibition and requires a large amount of experimental data for solution due to the large number of empirical constants. The kinetic

equations for Wu and Merchuk's (2004) model are:

$$\frac{dx_1}{dt} = -\alpha I x_1 + \gamma x_2 + \delta(1 - x_1 - x_2) \tag{1.17}$$

$$\frac{dx_2}{dt} = \alpha I x_1 - \gamma x_2 - \beta I x_2 \tag{1.18}$$

$$\mu = k\gamma x_2 - Me \tag{1.19}$$

where x_1 designates the resting (open state), x_2 the activated (closed) state, and x_3 the inhibited state. α, β, γ, and δ are experimentally determined rate constants, k is the photosynthesis yield, m is the specific growth rate (h^{-1}), and *Me* is the maintenance term (s^{-1}). The light intensity I is different at every point in the reactor, and since the position of a cell changes with time, *I(t)* is used which is controlled by the fluid dynamics in the reactor. From the above equations, the primary biomass production rate can be calculated as:

$$\frac{dX}{dt} = (\mu - Me)X = (k\gamma x_2 - Me)X \,. \tag{1.20}$$

While this model has been used in other work (Vunjak-Novakovic et al., 2005) with good result and should be applicable to any photosynthetic microbial growth, its application has been found (Wu and Merchuk, 2004) to be best suited to those cultures and experiments where photoinhibition is observed.

1.6.1.1. Carbon Dioxide

CO_2 serves as the carbon source for algal photosynthesis, but it must be transferred from the gas phase into the aqueous phase prior to cell uptake. It exists in the aqueous phase as four different species: CO_2; H_2CO_3; HCO_3^-; and CO_3^{2-} (Hill, 2006). The equilibrium concentration of these species is controlled by the pH. Acidic pH is commonly used to keep essentially all the CO_2 from conversion to HCO_3^- and thus readily available for photosynthesis. It is also possible, as suggested by Brune and Novak (1981), that *C. vulgaris* is capable of efficiently using carbon in equilibrium forms other than carbon dioxide for growth. Other investigators have shown that certain species of *C. vulgaris* can uptake HCO_3^- as well as CO_2 molecules (Aizawa and Miyachi, 1986; Moroney and Somanchi, 1999).

Very little literature exists on the quantification of CO_2 mass transfer coefficients in algal cultivation systems. Mass transfer is dependent on the photobioreactor system used, aeration rate and mixing intensity. What little data is available is for mainly open pond and

outdoor photobioreactors, or is highly system specific. (Babcock et al., 2002). Published work frequently assumes the mass transfer of CO_2 is similar to that of oxygen, and therefore uses the well-known mass transfer rate of oxygen and the diffusion coefficient correction factor (Hill, 2006). A direct study of the rate of carbon dioxide transfer from air bubbles into the aqueous phase has recently been reported by Hill (2006). Hill has developed an empirical equation for predicting the volumetric mass transfer coefficient K_La for CO_2 as a function of temperature, gas flow rate, and mixing speed in a well-mixed baffled reactor. Values ranging from 22 to 120 h^{-1} were obtained.

The substrate term in any biomass growth equations refers to the CO_2 in the liquid phase, but it is the concentration in the gas phase which is likely known from experimental work. Therefore, from the known concentration of CO_2 in the gas phase in g/L, and assuming equilibrium, Henry's Law predicts (Perry and Green, 1997),

$$C_g = H_e S \tag{1.21}$$

where C_g = CO_2 concentration in the gas phase, mol/L; and H_e = Henry's Law constant, mol/L/g/L. Mass transfer considerations for CO_2 in a photobioreactor are dispersion and advection in the gas phase, transfer by diffusion and bulk flow from the rising gas bubbles, and mass transfer from the dissolved liquid phase across the boundary layer to the suspended cell, followed by the rate of uptake across the cell membrane for growth. It is assumed that since the transfer rate of CO_2 from the gas phase to the liquid phase is much faster than the rate at which the cells can uptake the dissolved CO_2, that phase transfer from gas to liquid can be considered instantaneous from a relativistic standpoint. The boundary layer around each cell can also be assumed to be minimal due to the continuous flow around the microalgae particles, and so can be neglected.

1.6.2. Modeling External Loop Airlift Bioreactors

Mathematical modeling of growth in photobioreactors requires the coupling between the metabolism of microorganisms and the physical phenomena of light transfer inside the culture medium. Growth of a photosynthetic microorganism in a photobioreactor is governed by the availability of radiant light energy, which can be very heterogeneous within the culture volume. This spatial heterogeneity results in localized reaction rates (Evers, 1991; Wu and Merchuk, 2002). Although the actual mechanism for transforming light energy into biomass is

photosynthesis, in order to simplify the solution, light can be treated as an algae food source in an unstructured growth equation for the purposes of modeling.

The hydrodynamic equations required for characterization of the system have been developed by other researchers using ELABs for volatile organic chemical (VOC) bioremediation (Nikakhtari and Hill, 2005a; Nikakhtari and Hill, 2005b; Meng et al., 2002). The correlations published are the standard hydrodynamic equations needed to model an ELAB such as gas holdup, superficial gas velocity, liquid velocity in the riser section, gas holdup driving force for liquid circulation, and the Bodenstein number. In the case of a photobioreactor for a photosynthetic microorganism, CO_2 would need to replace VOCs as the modeled key gaseous component required for growth.

The precise magnitude of the effect of mass transfer and hydrodynamics on algal productivity is highly system-specific and not well understood (Babcock et al., 2002). It has been found that there does exist an optimum degree of mixing to maximize productivity, providing sufficient cycling of cells between the light and dark zones, with excessive mixing being counterproductive due to shear (Babcock et al., 2002), particularly in stirred tank reactors. Wu and Merchuk (2004) observed shear stress on the algae cells in an airlift photobioreactor only under high gas velocity, and its effects on the kinetics of algal growth were negligible for this type of bioreactor design.

In a study of mass transfer, two partial differential equations were used to predict the oxygen concentrations with time and position in the gas and liquid phases by Nikakhtari and Hill (2005b). The change in oxygen concentration with time and space is given as:

$$\frac{dc}{dt} = D\frac{\partial^2 c}{\partial z^2} - U_{LR}\frac{\partial c}{\partial z} + K_L a\left(c^* - c\right) \tag{1.22}$$

$$\frac{dy}{dt} = -U_{GR}\frac{\partial y}{\partial z} - K_{La}\frac{1-\theta_{GR}}{\theta_{GR}}\left(c^* - c\right) \tag{1.23}$$

Where c=dissolved oxygen concentration in the liquid phase (g/L), c*=equilibrium oxygen concentration (g/L), D=axial dispersion coefficient (m^2/s), U_{LR}=liquid velocity in the riser section (m/s), U_{GR}=gas velocity in the riser section (m/s), θ_{GR} = gas hold up, and K_La=overall volumetric mass transfer coefficient (s^{-1}). The symbol y=oxygen concentration in the gas phase (g/L), t=time (s), and z=axial distance up the riser section (m). The diffusion coefficient of oxygen in water is 20% higher than that of CO_2 (Perry and Green, 1997), and as such

coefficients such as the mass transfer coefficient for carbon dioxide would be expected to be lower than that for oxygen.

Nikakhtari and Hill (2005c) also presented a model governing the steady state concentration distributions of a VOC in a packed bed ELAB during the continuous steady state phenol biodegradation process. The substrate in the liquid phase, the biomass in the liquid phase, and the substrate in the air phase are represented by three non-linear ordinary differential equations. The model is completed by the specific growth rate equation defined by substrate inhibition kinetics as described in Section 1.6.1. The substrate in the liquid phase with position is given by the equation below for anysubstrate:

$$D\frac{d^2S}{dz^2} - U_{LR}\frac{dS}{dz} + K_L a(S^* - S) - \frac{\mu X_T}{Y_{XS}} = 0 \tag{1.24}$$

$$D\frac{d^2X}{dz^2} - U_{LR}\frac{dX}{dz} + \mu X_T = 0 \tag{1.25}$$

$$-U_{GR}\frac{dy}{dz} - K_{La}\frac{1-\theta_{GR}}{\theta_{GR}}(S^* - S) = 0 \tag{1.26}$$

where S=substrate concentration (mg/L), S*=substrate concentration at interface, D=axial dispersion coefficient (m^2/s), U_{LR}=liquid velocity in the riser section (m/s), U_{GR}= gas velocity in the riser (m/s), K_La=overall volumetric mass transfer coefficient (h^{-1}) and m=specific growth rate (h^{-1}). The symbol X_T=total biomass concentration (mg/L), Y_{XS}=substrate yield factor (mg cell/ mg substrate), y=oxygen concentration in the gas phase (g/L), and z=axial distance up the riser section (m). Again, the model of Nikakhtari and Hill (2005c) can serve as a basis for modeling an airlift loop photobioreactor with a gaseous CO_2 food source.

The model of Wu and Merchuk (2004) for photosynthetic algal growth in an airlift bioreactor that accounts for reactor geometry, fluid flow, and illumination on the biomass uses the PSF three states model of photosynthetic growth discussed in Section 1.6.1. The light history of the photosynthetic cells is controlled by the fluid dynamics in the column. It is necessary for this model to know the fraction of time that each photosynthetic element spends at each photon flux density. The physical and liquid properties of the system are also incorporated into the determination of the cycle time. The photobioreactor of Wu and Merchuk (2004) regarded the riser as the dark zone, and hence the cell kinetics in this region do not depend of the photon flux density (PFD). It has been shown (Merchuk and Yunger, 1990) that perfect mixing can be

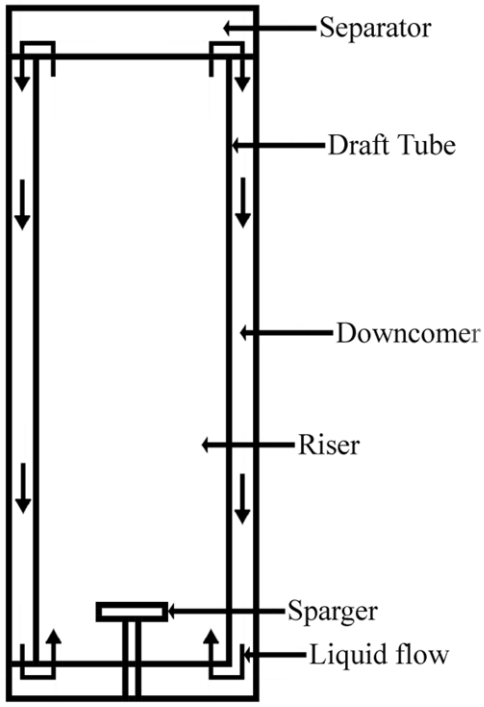

Figure 1.8. Schematic diagram of an internal loop airlift photobioreactor.

assumed in the gas separator, and since the residence time in this region is small, therefore the light history can be approximated as one of constant illumination. The riser however, is the major region where the cells are illuminated, and the fluid dynamics of this region were found to be practically plug flow in the range of interest. The light history of a cell in the airlift photobioreactor of Wu and Merchuk (2004), similar to the one shown in Figure 1.8, can be represented by the scheme shown in Figure 1.9.

The model of Wu and Merchuk (2004) is based on the assumption that under low gas flow rates, there is gas only in the riser and separator, and the gas holdup in the downcomer can be neglected. The light history in each region is then determined from the light distribution for each region of the airlift loop bioreactor. The light intensity attenuation as a function of culture depth is calculated in order to determine the radiant flux for each region, but the effects of geometry are neglected by using the Beer-Lambert model of light attenuation.

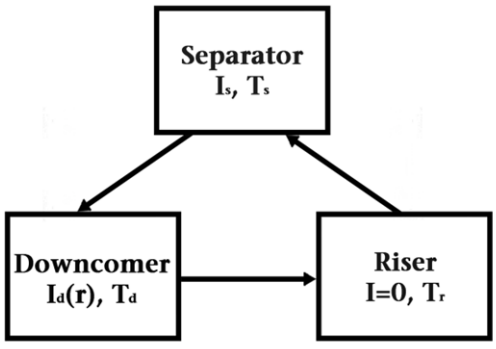

Figure 1.9. Cyclic light history of cells in an ALR of design as shown in Figure 1.8.

1.7. Research Objectives

The objectives of the Ph.D. research are:

i. Study the growth kinetics of *C. vulgaris*. This type of information is sparse in the published literature. This includes growth parameters and CO_2 consumption.

ii. Develop a method for determination of optimum design and operating conditions for well-mixed continuously stirred tank bioreactors used in the growth study.

iii. Discuss and evaluate possible by-products of *C. vulgaris* cultivation. Evaluate experimentally any novel ideas where possible.

iv. Design a novel photobioreactor for *C. vulgaris* cultivation that will improve upon the results achieved using the traditional well-mixed tank design.

v. Evaluate the novel photobioreactor experimentally and model the *C. vulgaris* growth in the photobioreactor, accounting for light intensity and attenuation, CO_2 concentration, cell position, and fluid dynamics.

vi. Evaluate the feasibility of integrating the novel photobioreactor, with its accompanying *C. vulgaris* cultivation for CO_2 sequestration, into a large scale industrial bioethanol facility.

1.8. Organization of the Thesis

The Ph.D. thesis is organized according to the University of Saskatchewan guidelines for manuscript-based theses. This means that in place of presenting raw data and analyzing it for the first time in a uniform manner throughout the thesis, it is presented as a series of journal manuscripts. The bulk of the thesis consists of a series of literary publications of the research that were compiled over the course of the project. These manuscripts were written and submitted for publication as each stage of the Ph.D. project was completed. The manuscripts presented in Chapters 2, 3, 4, 6, and 7 have all been published (or are accepted for publication and in press) in peer-reviewed journals. The manuscript in Chapter 5 was written in the final phase of the Ph.D. project and has only very recently been completed and submitted for review. In each

manuscript-based chapter, three issues are discussed in addition to the manuscript itself. These are the contribution of the Ph.D. candidate, the contribution of the paper to the overall study, and relevant material not in the manuscript (if required). Chapters 1, 8, and 9 are original text in this thesis included to introduce the subject matter and discuss the outcome of the project. Chapter 10 encompasses the references used in all Chapters, with any useful supplementary material given in the Appendices.

1.9. Manuscript Content of the Thesis

The specific topic of each chapter and the way in which it addresses the overall objectives of the thesis are detailed below. The use of a manuscript-based thesis results in some overlap of material between chapters.

In order to assist in the determination of the optimum design of continuously stirred tank bioreactors, Chapter 2 describes an optimization scheme which determines the best bioreactor design and operating conditions for the bioreactor for microbial growth. The study of the growth kinetics of *C. vulgaris* was initially performed using a well-mixed bioreactor, in order to aid in the cultivation of this microalgae species for CO_2 consumption. The details of this study are described in Chapter 3. This manuscript also includes a discussion of the biomass yield on CO_2, and an examination of using the *C. vulgaris* culture as a novel photosynthetic biocathode in a microbial fuel cell. As part of the ongoing search for ways to make microalgae cultivation and CO_2 bioremediation economically feasible with valuable cultivation byproducts, it was further shown that this microalgae biocathode could be coupled to a fermentative anode to form a completely microbiological fuel cell as discussed in the manuscript presented in Chapter 4. With the growth kinetic study completed using a stirred tank bioreactor, Chapter 5 describes the design of an external loop airlift photobioreactor. This novel bioreactor has both light and dark zones for improved growth; and the fluid mixing embedded in the airlift design increases light penetration to each cell by reducing shading and cell adhesion without excessive shear. The details and results of a growth model that includes light and CO_2 effects, reactor cell position, and fluid dynamics are also included in Chapter 5. The economic feasibility of integrating the novel external loop airlift photobioreactor into industrial bioethanol plants is analyzed in

Chapters 6 and 7. This was performed for two cases: batch and continuous bioethanol plant operations. The microbial fuel cell with *C. vulgaris* biocathode concept was used to facilitate integration. Also, both off-site and on-site microalgae oil extraction (for biodiesel) was modeled.

1.10. Nomenclature

A total surface area of culture, m^2

a_I experimentally determined parameter, Eq. 1.12

[a] maximal weight-specific energy uptake rate, J/g-h

b_I experimentally determined parameter, Eq. 1.12

C_g CO_2 concentration in the gas phase, mol/L

C_x biomass density, g/L

c speed of light, m/s

c dissolved oxygen concentration in the liquid phase, g/L

c_I experimentally determined parameter, Eq. 1.12

c* equilibrium oxygen concentration, g/L

D axial dispersion coefficient, m^2/s

D dilution rate, h^{-1}

E energy, J

f frequency, Hz or s^{-1}

H_e Henry's Law constant, mol/L/g/L.

h Planck's constant (6.626×10^{-34}), J s

I actual illuminance, also called PFD or radiant flux, W/m^2 or $\mu E\ m^{-2}\ s^{-1}$

I_{av} average irradiance, $\mu E\ m^{-2}\ s^{-1}$

I_d irradiance in the downcomer, $\mu E\ m^{-2}\ s^{-1}$

I_k microalgal affinity for light, $\mu E\ m^{-2}\ s^{-1}$

I_o incident illuminance level, also called PFD or radiant flux, W/m^2 or $\mu E\ m^{-2}\ s^{-1}$

I_s irradiance in the separator, $\mu E\ m^{-2}\ s^{-1}$

K_a absorption coefficient, m^2/kg

K_I inhibition constant, $(\text{units of substrate})^2$

K_i photoinhibition constant, $\mu E\ m^{-2}\ s^{-1}$

K_{La} overall volumetric mass transfer coefficient, s^{-1}

K_S saturation constant, units of substrate

Me endogenous metabolism coefficient, s^{-1}

m_r maintenance coefficient of resting cells, $J(g\ dw)^{-1}h^{-1}$

m' apparent maintenance coefficient of culture, $J(g\ dw)^{-1}h^{-1}$

[m] maintenance coefficient, J/g-h

N Avogadro's number, 6.023×10^{23}

P extinction coefficient, m^{-1}

P_{max} maximum rate of photosynthesis

p length of light path, m

S substrate concentration in the liquid phase, mg/L

S* substrate concentration at interface, g/L

s distance from vessel surface in (cylindrical vessel), m

T_d downcomer retention time, s

T_r riser retention time, s

T_s separator retention time, s

t time, s

V total culture volume, m^3

W biomass density, g/L

W' biomass change rate, g/L-h

U_{GR} gas velocity in the riser, m/s

U_{LR} liquid velocity in the riser section, m/s

X biomass concentration, g dw L^{-1} or mg/L

X_T total biomass concentration, mg/L

x_1 fraction of biomass in the resting (open state)

x_2 fraction of biomass in the activated (closed) state

x_3 fraction of biomass in the inhibited state

Y biomass yield coefficient, g cells/ g substrate

Y_G true growth yield from light, g dw J^{-1}

Y_{XS} substrate yield factor, mg cell/ mg substrate

y oxygen concentration in the gas phase, g/L

y' conversion factor from energy to biomass, g/J

z axial distance up the riser section, m

z' radial position, m

Greek Letters

α experimentally determined parameter, Eq. 1.17

α_L light zone (fraction of the volume illuminated)

β experimentally determined parameter, Eq. 1.18

β_D dark growth zone (fraction of volume not illuminated)

γ experimentally determined parameter, Eq. 1.17, 1.18

δ experimentally determined parameter, Eq. 1.17

ϕ fraction of photosynthetically available radiation

k photosynthesis yield, dimensionless

λ wavelength, m

μ specific growth rate, h^{-1}

μ_o observed specific growth rate, h^{-1}

μ_{max} maximum specific growth rate, h^{-1}

θ_{GR} gas hold up

Chapter 2

2. Continuous Bioreactor Optimization for Cost Minimization: Effect of Microbial Species and Operating Conditions

A similar version of this chapter has been published in the International Journal of Chemical Reactor Engineering:

Powell, E.E. and G. A. Hill "Optimization of Continuously Stirred Tank Bioreactor Design for Cost Minimization: Effect of Microbial Species and Operating Conditions", International Journal of Chemical Reactor Engineering, 6, A20, (2008).

Contribution of Ph.D. Candidate

The development of the bioreactor optimization scheme was performed by Erin Powell, along with the analysis of the design results predicted by the model. Gordon Hill provided guidance in the program design, and in the selection of parameters to be optimized and analyzed as part of the optimized design. The submitted manuscript was written by Erin Powell, while Gordon Hill provided editorial input.

Contribution of this Paper to Overall Study

The primary object of the Ph.D. research is the cultivation of microalgae for the consumption of CO_2. *Chlorella vulgaris* yields in well-mixed bioreactors has been reported in the literature (Patino et al., 2007; Ogbonna et al., 1997). Although the growth rate of *C. vulgaris*

is considered high relative to other algae species (Patino et al., 2007; Ogbonna et al., 1997), it is still very slow relative to other microbial species such as yeast and many bacteria (Andersen, 2005). The lack of published kinetic growth data for *C. vulgaris* however, requires that kinetic growth data be collected and analyzed as part of the Ph.D. research. This requires the design and operation of well-mixed or continuously stirred tank bioreactors (CSTB). In expectation that future applications will require large scale CSTB studies, and in order to obtain optimum algae levels in a bioreactor, it is important to determine how to best operate a CSTB with multiple factors to consider.

Therefore, how best to design a CSTB for microalgae growth was modeled. The efficient design of a CSTB is important to the successful production and high yield of any microorganism. In order to obtain the desired growth, it is necessary to deliver the necessary aeration, in this case the gas being air and CO_2, to the microalgae cells in the liquid culture medium. In order to aid in future CSTB design with optimum aeration, which can be performed by changing both gas airflow rate and impeller stirring speed in a variety of combinations, an optimization design strategy was developed in this phase of the research. Since most cultures are aerobic, including our study of algae, the determining factor was meeting the oxygen demand of the cells.

2.1. Abstract

The operation of continuously stirred tank bioreactors (CSTBs) at minimum cost is a major concern of operators. In this work, a CSTB design strategy is presented where impeller stirring speed and aeration rate are optimized to meet the oxygen demand of growing cells, simultaneously minimizing the capital and operating cost. The operating cost is limited to the cost of utilities. The optimization scheme assumes a given fermentor tank size, and that the properties of the culture medium and the oxygen respiratory requirements of the microorganisms being cultivated are known. It is possible to choose between two different turbine impellers during the design process. The equations, constraints, and the CSTB design strategy employed by the program are described. The effect of microbial species, ions in the culture medium, impeller style, as well as changing CSTB size and biomass input density on the optimum

operating conditions, is examined. The mass transfer coefficient, gas holdup, mixing speed, and aeration rate are all reported at optimized cost conditions. A study of the effects of various parameters on the CSTB design is shown.

2.2. Introduction

Continuous flow stirred tank bioreactors are advantageous for culturing microorganisms as they offer constant environmental conditions since biological systems can be very sensitive to transient process variations. Once the optimum conditions are determined, they can be maintained on a long term basis in a carefully controlled bioreactor. The main goal of this continuously stirred tank bioreactor (CSTB) design strategy is to minimize cost of both initial equipment and operation over a 5 year period.

A multitude of other optimization programs exist for the selection and modeling of a variety of parameters (Mantzouridou et al., 2002; Yoon, Lee, and Park, 2002; Hill and Robinson, 1989), but these modern programs and strategies, while providing valuable design data, rarely focus on minimizing cost. Hill and Robinson (1989) presents a strategy for designing optimum growth CSTBs in series, three of decreasing size being ideal for growth and minimum residence time. Those optimizations that do focus on cost (Malcata, 1989; Oldshue, 1983) follow a different strategy than that presented here. Malcata (1989) is concerned with the sizes of reactors in series to minimize capital cost. Oldshue (1983) dealt with some of the same fermentor design parameters as this work, but only optimized these parameters individually, not as one interactive design scheme. Some of Oldshue's individual correlations are used in this strategy. Cost is the major real world consideration for the practical operation of any microbial bioreactor, as long as the operational needs of the cultivation are being met. The oxygen supply into the medium constitutes one of the decisive factors of aerobic microbial growth and plays an important role in the economy of an aerated CSTB system.

Since the oxygen mass transfer coefficient (k_La) and the gas holdup (e_G) are calculated as part of the design optimization program, in addition to the mixing speed, aeration rate, and cost; the optimized values for these parameters are also reported for various microorganisms, culture liquids, and impeller styles.

2.3. Design Theory

A schematic of the continuously stirred tank bioreactor set-up that is being designed in this work is shown in Figure 2.1. The components that make up the capital equipment cost include the fermentor, compressor, and mixer. The operating cost consists of the power required to aerate and stir the cell culture over a 5 year period. The starting point of the optimization design is a chosen fermentor size, with a specific microbial culture of known biomass concentration. These parameters are pre-determined in any fermentation process to meet

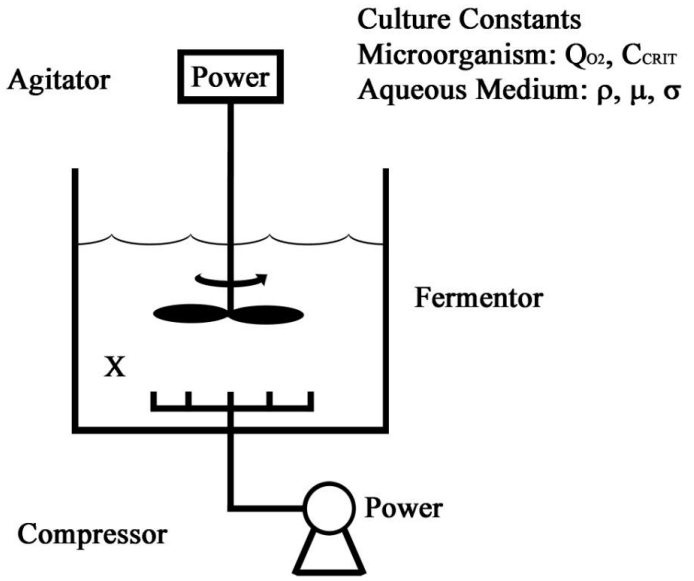

Figure 2.1. CSTB design components that contribute to capital and operating costs. The culture medium and microbial species constants are required for solution of design scheme.

productivity requirements. The program allows the user to input the biomass concentration, but will not allow a value greater than 50 g/l, which is meant to represent the maximum encountered in a practical system. The physical parameters of the liquid culture medium are also required by the program, with standard values for pure water or oceanic salt water being provided for selection if desired. The constants required include surface tension, s, density, r, and dynamic viscosity, m. The respiratory coefficient of the cultured microorganism must be input by the user as well as both the critical oxygen concentration for cell growth and culture temperature.

A flowchart of the entire design optimization strategy used is given in Figure 2.2. The details of each step, with accompanying equations, constraints, and references follow. The main focus of the strategy is to meet the oxygen demand of the cells by varying mixing speed and aeration rate, with the ultimate goal being to minimize the cost of the CSTB. The total cost includes both the capital cost of the equipment and the operating cost. The operating cost over 5 years (with 1000 days total operation), which consists only of utilities in this study, will be evaluated in the results.

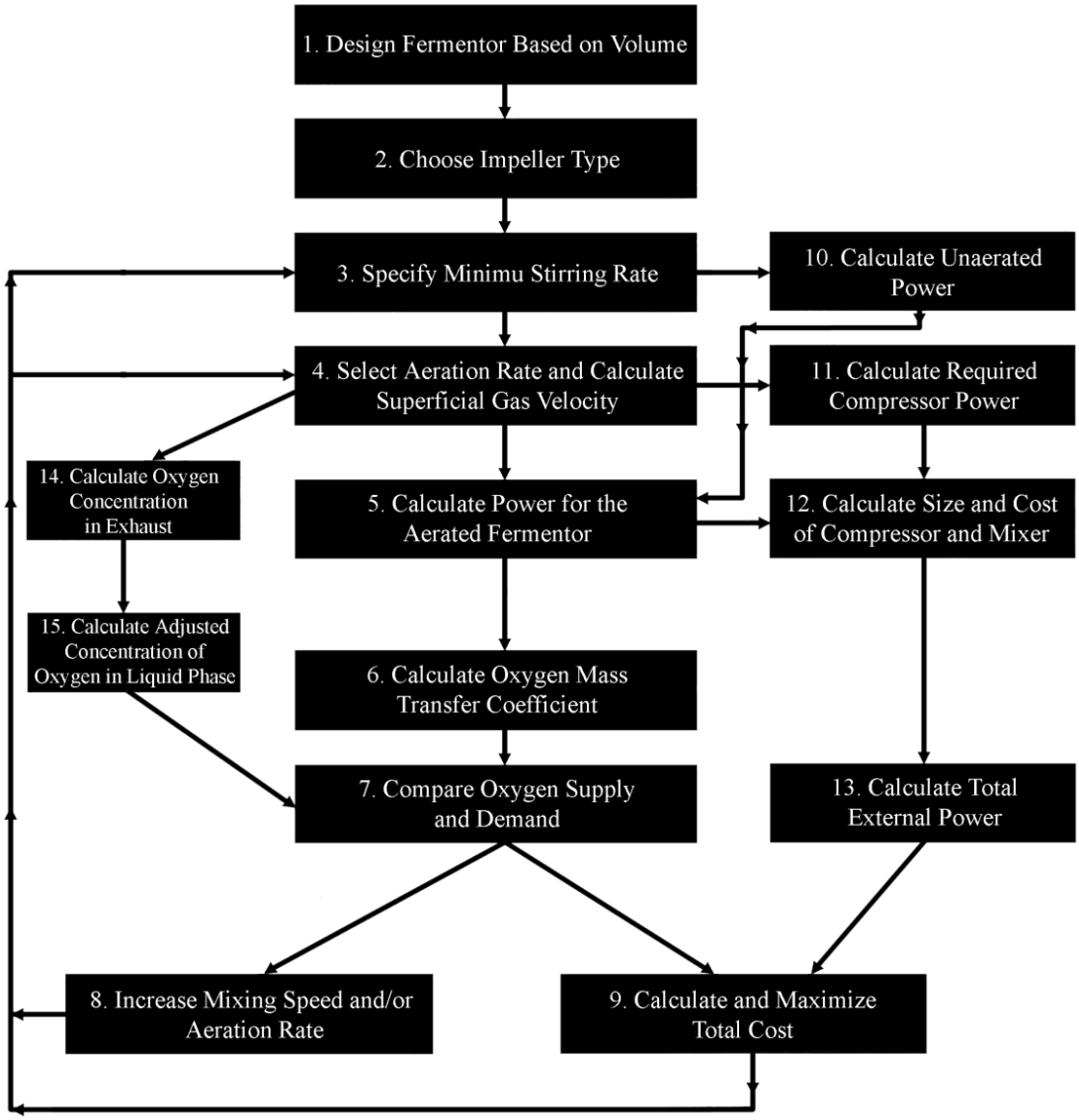

Figure 2.2. Flowchart of optimization strategy for CSTB design.

Flowchart 1. The bioreactor dimensions are determined based on the required reactor volume. The reactor tank is assumed to be cylindrical with a liquid height of 2/3 the tank height and a tank diameter equal to the liquid height. The maximum tank volume is considered to be 150 m^3 (maximum commercially available), with any volume greater than 150 m^3 being divided into a number, n_F, of equally-sized tanks to be operated in parallel. For the tank(s),

$$d = (\frac{4}{\pi} V_W)^{1/3} \tag{2.1}$$

$$\frac{2}{3} H_{TANK} = H_{LIQ} = d \tag{2.2}$$

$$V_{TANK} = \pi(\frac{d}{2})^2 H_{TANK} \tag{2.3}$$

This results in a maximum working volume of 100 m^3 per bioreactor.

Flowchart 2. The impeller type is selected by the user, from one of two options. Impeller diameter is determined relative to tank diameter (Perry and Green, 1997), and is assumed to be independent of all design and culture conditions for the purposes of this work, except impeller style. There is a single impeller in a bioreactor. Impeller type 1 is shown in Figure 2.3. This is a standard six blade radial flow design used most often in bioreactors. It creates a turbulent flow pattern that improves mixing and mass transfer. Impeller type 2 is shown in Figure 2.4. The second turbine impeller has pitched blades, and creates an axial flow pattern that sweeps the contents of the bioreactor efficiently and is considered to be cost-effective in power usage.

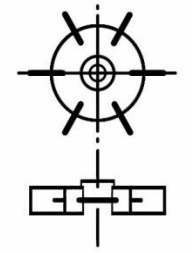

Figure 2.3 Impeller style 1.

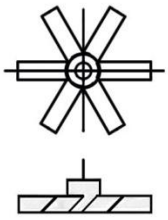

Figure 2.4 Impeller style 2.

For impeller style 1:

$$D_I = 0.40d \tag{2.4}.$$

And for impeller style 2:

$$D_I = 0.60d \tag{2.5}.$$

Flowchart 3. The stirring rate is optimized, with a minimum value (for stirring the liquid media alone) determined from (Oldshue, 1983):

$$N_{MIN} = \left(1.22 + 1.25\frac{d}{D_I}\right)\left(\frac{\sigma g}{\rho_L}\right)^{0.25}\frac{1}{D_I} \ . \tag{2.6}$$

All fluids are assumed to be Newtonian for the purposes of this work. An aqueous culture medium containing a high concentration of cells may behave more like a non-Newtonian fluid, but will still be considered as Newtonian for all cases. This is the starting point for the mathematical optimization of stirring speed, N, for cost minimization in the design scheme.

Flowchart 10. Calculation of the power required for the unaerated reactor is based on a turbine power correlation for the chosen impeller (Perry and Green, 1997).

For impeller style 1 (valid for transitional and turbulent conditions $66 \leq N_{RE} \leq 50{,}000$; for $N_{RE} > 50{,}000$, $N_P = 5$):

$$N_P = 2.5737 N_{RE}^{\ 0.0614} \tag{2.7}$$

For impeller style 2 (valid for conditions $1 \leq N_{RE} \leq 100{,}000$; for $N_{RE} > 100{,}000$, $N_P = 1.31$):

$$N_P = 13.131 N_{RE}^{\ -0.2775} \tag{2.8}$$

where,

$$N_P = \frac{Po}{\rho_L N^3 D_I^5} \tag{2.9}$$

$$N_{RE} = \frac{\rho N D_I^2}{\mu} \tag{2.10}$$

And the power is obtained from:

$$Po = N_P \rho_L N^3 D_I^5 \tag{2.11}$$

Flowchart 4. The aeration rate is optimized to meet the oxygen demand of the cultured cells, but an initial value must be chosen, and the aeration rate is used to determine superficial gas velocity. A low initial guess of 0.1 vvm (volume air / volume liquid / min) (Elizier, 1987) is assumed so $Q = (0.1/60)V_W$ m^3/s. This is the starting point for the mathematical optimization of aeration rate, Q, for cost minimization during the CSTB design procedure. The superficial gas velocity is then given by:

$$\upsilon_S = \frac{Q}{\frac{\pi d^2}{4}} \tag{2.12}$$

Flowchart 11. The required compressor power needed for aeration is determined by the equation (with air source assumed to be at 304 kPa (3 atm) in order to create flow through all spargers and for all fermentor sizes):

$$\overset{o}{W}_C = \frac{2 * R * 298 \gamma \overset{o}{m}_{AIR}}{MW_{AIR}(\gamma - 1)} \left(3^{\frac{\gamma-1}{\gamma}} - 1 \right). \tag{2.13}$$

For air at 25 ^{o}C, ρ_{AIR} = 1.22 kg/ m^3 and MW_{AIR} = 28.96 g/mol (Perry and Green, 1997).

Flowchart 5. In order to determine the power needed for stirring the aerated fermentor, the unaerated power Po (Bailey and Ollis, 1986) is used,

$$P_G = \frac{0.80}{(1 - \in_G) N_A^{0.38} N_{WE}^{0.25}} Po \tag{2.14}$$

where the aeration number is

$$N_A = \frac{Q}{N D_I^3} \tag{2.15}$$

and the Weber number is

$$N_{WE} = \frac{N^2 D_I^3 \rho_L}{\sigma}. \tag{2.16}$$

Equation 14 is valid for $0 \leq N_A \leq 1200$.

The gas holdup for a well mixed bioreactor like this CSTB (Hassan and Robinson, 1977) is determined from the standard equation for pure water as the culture liquid.

$$\in_G = 0.113 \left(\frac{Q N^2}{\sigma} \right)^{0.57} \tag{2.17}$$

For culturing in salt water, the presence of electrolytes changes the gas holdup equation to:

$$\in_G = 0.209 \left(\frac{Q N^2}{\sigma} \right)^{0.44} \tag{2.18}$$

Both gas holdup equations are valid for $\in_G \leq 0.4$.

Flowchart 12. Calculation of the size and cost of the compressor and the mixer required to operate the CSTB is based on an equipment cost correlation. The costs of the compressor and the mixer are capital costs, but are still to be minimized with the operating costs; as they are affected by the determination of the aeration rate and stirring speed. Only one type of compressor and one type of mixer is assumed to be available for the purposes of this CSTB design and optimization. The capital cost correlations are based on the industrial cost data of

Ulrich and Vasudevan (2004). The CE Plant Cost Index (2004) used is 400 for developing both Equation 19 and 20.

The following is for a standard centrifugal carbon steel compressor (excluding drivers) suitable for use with our CTSB. The compressor cost is:

$$C_{BMC} = 2.5\left(932.6\left(\overset{o}{W}_C\right)^{0.9373}\right). \tag{2.19}$$

The correlation is valid for \$35,000 < C_{BMC} < \$ 3,800,000, and 47 kW < W_C < 7000 kW. If W_C < 47 kW, then W_C = 47 kW is used, and if W_C > 7000 kW then multiple compressor units n_C are used requiring equal W_C. The correction factor for carbon steel is 2.5 and is incorporated into equation (2.19) as only one compressor design is available.

The mixer cost correlation is given below for a stainless steel mechanical seal agitator. It is suitable for use with nearly all culture fluids and tolerates pressures up to 8100 kPa. It includes motor, speed reducer, and impeller cost.

$$C_{BMM} = 2.5\left(847.65\left(\frac{P_G}{1000}\right) + 8423.6\right) \tag{2.20}$$

The correlation is valid for \$8,100 < C_{BMM} < \$ 183,000, and 1.3 kW < (P_G/1000) < 206 kW. If (P_G /1000) < 1.3 kW, then (P_G /1000) = 1.3 kW is used; and if (P_G /1000) > 206 kW then multiple compressor units n_M are used requiring equal (P_G /1000). The correction factor for carbon steel is 2.5 and is incorporated into equation (2.20) as only one mixer design is considered to be available.

Flowchart 13. The total external power required by the CSTB is simply the power used by the compressor(s) and mixer(s).

$$P_{EXT} = n_C \overset{o}{W}_C + n_M\left(\frac{P_G}{1000}\right) \tag{2.21}$$

Flowchart 6. The calculation of the oxygen mass transfer coefficient (k_La) is an important hydrodynamic characteristic specific to each CSTB design. The following equations are valid for baffled CSTBs provided $k_La \leq 0.9\ s^{-1}$ (Van't Riet, 1979). The value of k_La is considered to be unaffected by temperature (given the narrow range generally observed for microbial cultures). For pure or low ionic strength water,

$$k_L a = 0.026\left(\frac{P_G}{V_L}\right)^{0.4} \upsilon_S{}^{0.5} \tag{2.22}$$

and for strong ionic solutions, such as sea water,

$$k_L a = 0.002\left(\frac{P_G}{V_L}\right)^{0.7} \upsilon_S{}^{0.2} \tag{2.23}$$

Flowchart 14. Key to the optimization of the CSTB design is the oxygen that must be delivered to the cells. In order to determine the oxygen demand of the culture, the respiratory coefficient Q_{O2} (mgO_2/mgDW-h) of the selected microorganism must be known. The biomass concentration X (mg DW/l) must also either be known or calculated from the following equation for steady-state unlimited growth (Shuler and Kargi, 2002). This is a simplification that neglects cell decay or use of substrate for cell maintenance. For active cultures, this simplification is considered acceptable for the purposes of this work.

$$X = Y_{XS} S \tag{2.24}$$

where

$$S = S_0 - S_1. \tag{2.25}$$

It can be assumed that the oxygen in the fermentor outlet gas is what is remaining from the inlet air supply after meeting the needs of the cells. This outlet oxygen concentration is considered to be the same as the oxygen in the air bubbles and the demand is calculated as (Shuler and Kargi, 2002):

$$N_{O2} = X * Q_{O2} \tag{2.26}$$

Assuming constant flow rate in inlet and outlet flows, the oxygen demand is also:

$$N_{O2} = (C_{O2in} - C_{O2out})Q. \tag{2.27}$$

and the concentration of oxygen in the outlet gas is therefore (with C_{O2in} known to be 267 mg/l or 20.9%):

$$C_{O2AIR}{}^* = C_{O2out} = C_{O2in} - \frac{N_{O2}}{Q}. \tag{2.28}$$

Flowchart 15. The adjusted oxygen concentration in the liquid phase, C*, is now calculated from the Henry's Law Constant for oxygen and ratio of mole fractions in the exhaust and inlet air streams. The Henry's Law Constant depends on temperature, and is determined from the following correlation ($0^oC \le t \le 40^oC$) from Bailey and Ollis (1986):

$$H = 13.866e^{-0.0187t}. \tag{2.29}$$

And:

$$C^* = H\frac{molefractionO_2 exhaust}{molefractionO_2 inlet} \tag{2.30}$$

Flowchart 7. Oxygen supply and demand are compared. Supply must meet demand for the design to be considered valid. This is the primary condition for selecting a suitable aeration rate and stirring speed while minimizing cost. Minimum oxygen supply is

$$N_S = k_L a(C^* - C_{CRIT}) \tag{2.31}$$

where the critical oxygen concentration for growth of the cultured microbes (Shuler and Kargi, 2002) can be input by the user. The default value is 1.0 mg/l.

N_S and N_{O2} are compared in the program. If the oxygen supply is insufficient, then the program proceeds to Step 8, where either stirring speed and/or aeration rate are increased. If the oxygen supply meets the demand, then the program proceeds to Step 9 and the economy of the design.

Flowchart 8. Mixing speed and/or aeration rate are increased by the program to meet the oxygen demand of the cells while still minimizing the overall cost of the fermentor design. If aeration rate only is increased, all steps from 4 must be recalculated. If stirring speed, or stirring speed and aeration rate are increased, then all steps from 3 onward must be recalculated to determine if the oxygen demand is now met. The combination of aeration rate and stirring speed that minimizes cost, while still meeting all design constraints, is determined by forward differentiation using the Newton-Raphson method. This is embedded in the Excel Solver used to determine the optimum designs presented and compared in this work.

Flowchart 9. The final consideration in the program is the total cost of the CSTB as designed. This is an optimization condition in the program and includes both capital and operating costs. Operating costs are for utilities only and are determined for 5 years of operation or 1000 days. The fermentor capital cost is

$$C_F = 40{,}000 * \left(\frac{V_{TANK}}{0.5}\right)^{0.6} * n_F \ . \tag{2.32}$$

The relationship between fermentation vessel volume and cost was obtained from Ratledge and Kristiansen (2006). The base cost and capacity incorporated into the equation are from Perry and Green (1997). For tank volumes of 0.5 m^3 or less the cost is $ 40,000.

The compressor and mixer capital costs are

$$C_C = C_{BMC} * 5 * n_C * n_F, \text{ and} \quad (2.33)$$

$$C_M = C_{BMM} * 5 * n_M * n_F, \text{ respectively.} \quad (2.34)$$

The 5-year operating cost assumes a 10¢ / kW-h cost for power, 200 days of operation in each year, and is calculated by:

$$P_{COST} = n_F * \left(P_{EXT} * 10^{-3}\right)(1000x24)(0.10) \quad (2.35).$$

2.4. Results and Discussion

The optimization strategy as described in the previous section was used to design the optimum fermentors for several types of microorganisms. These include one yeast species (*Saccharomyces cerevisiae*), two bacterial species (*Azotobacter chroococcum* and *Enterobacter aerogenes*), and a representative freshwater algae (as phytoplankton). The required respiratory coefficients are 0.36, 6.0, 0.06 (Altman and Dittmer, 1972), and 0.00625 (DePinto et al., 1996) mg O_2 / mg DW-h, respectively. These microorganisms were selected for their wide ranging differences in oxygen requirements required for growth. In the case of *A. chroococcum*, the optimum design is significantly affected by the high respiratory coefficient of the cells (6.0 mg O2 / mg DW-h). Conversely, algae have a very low respiratory coefficient due to photosynthetic activity and require mainly carbonates and little oxygen for growth. For comparison purposes, this study focuses on a CSTB size of 10 m^3, containing 5 g DW / l biomass in each case, except for *A. chroococcum*. It is important to note that it was not possible to maximize the *A. chroococcum* at 5 g DW /l biomass and meet all design constraints, and so a maximum biomass constraint was also determined as part of the optimization. This was due to the very high respiratory coefficient of *A. chroococcum.* For impeller 1, a maximum biomass of 276 mg DW/l can be input, and when impeller 2 is employed 373 mg DW/l is possible. These maximum biomass concentration values for each impeller style were used for the *A. chroococcum* CSTB designs that were generated. C_{CRIT} was considered to be 1.0 mg/l for all culture types and temperature 25 ^oC. All presented results are for an optimized system with the goal of minimizing cost, meeting all stated constraints, particularly that of the oxygen demand, by adjusting mixing speed and aeration rate.

The values of the oxygen mass transfer coefficients (k_La) for each modeled microorganism being cultured are given in Figure 2.5. This range of values corresponds to those observed in the literature (Galaction et al. 2004; Hoet al., 1987; Van't Riet, 1979; Hassan and Robinson, 1977). It is immediately apparent that only the choice of microbe and the cell density affect the required value of the oxygen mass transfer coefficient. This is logical as the key factor that differentiates the microorganisms is their respiratory coefficients. A greater respiratory coefficient results in a greater required k_La value. A larger respiratory coefficient means a larger oxygen demand. This means that either or both mixing speed and aeration rate must be increased to meet the demand. Since the oxygen mass transfer coefficient is directly dependent on aeration rate, and indirectly affected by mixing speed, it also increases with respiratory coefficient. The style of impeller chosen for stirring the CSTB affects k_La only for *A. chroococcum,* where different cell concentrations were employed for each impeller type as discussed earlier.

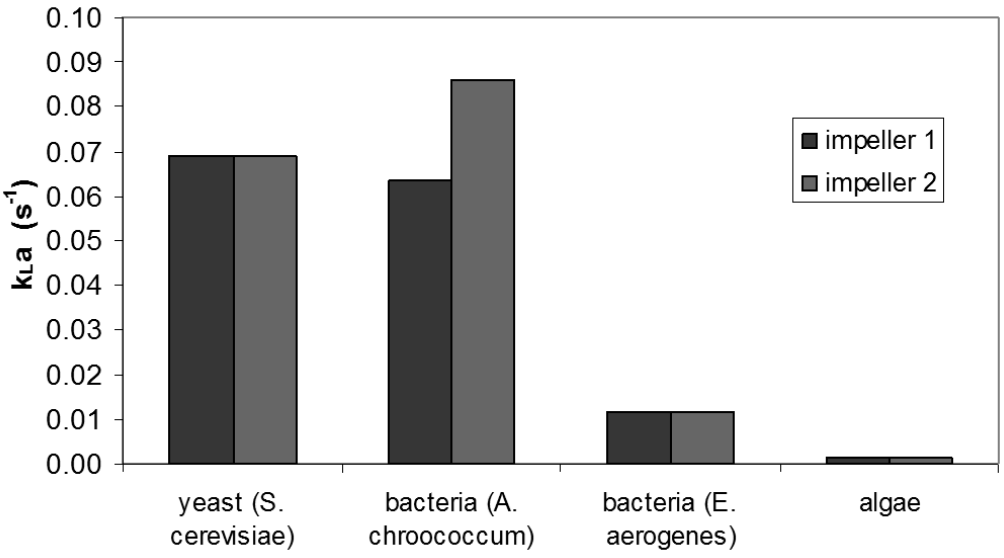

Figure 2.5. Determination of the effect of microorganism and impeller style on oxygen mass transfer coefficient at cost-minimizing culture conditions of aeration and mixing (10 m^3 reactor volume, 5g(DW)l^{-1} cell density (excepting *A. chrococcum*: 0.28g(DW)l^{-1} for impeller 1, 0.37g(DW)l^{-1} for impeller 2), fresh water medium).

The gas holdup for each of the four microorganism types was calculated at the optimized design conditions. The results are shown in Figure 2.6. Since gas holdup increases if mixing speed and/or aeration rate are increased, it is expected that gas holdup will be greater for microbes with greater respiratory coefficients. These have larger oxygen demands and therefore require greater mixing to provide oxygen to the cells. A maximum of 0.4 is observed as this is the maximum value for which the holdup correlation is valid (Hassan and Robinson, 1977), and therefore is a design constraint in the program. A small difference in gas holdup was also observed between impeller styles, with 1 being greater than 2, in cases where the system was not constrained by the maximum gas holdup. A difference in gas holdup was also observed with difference in impeller type by Hassan and Robinson (1977).

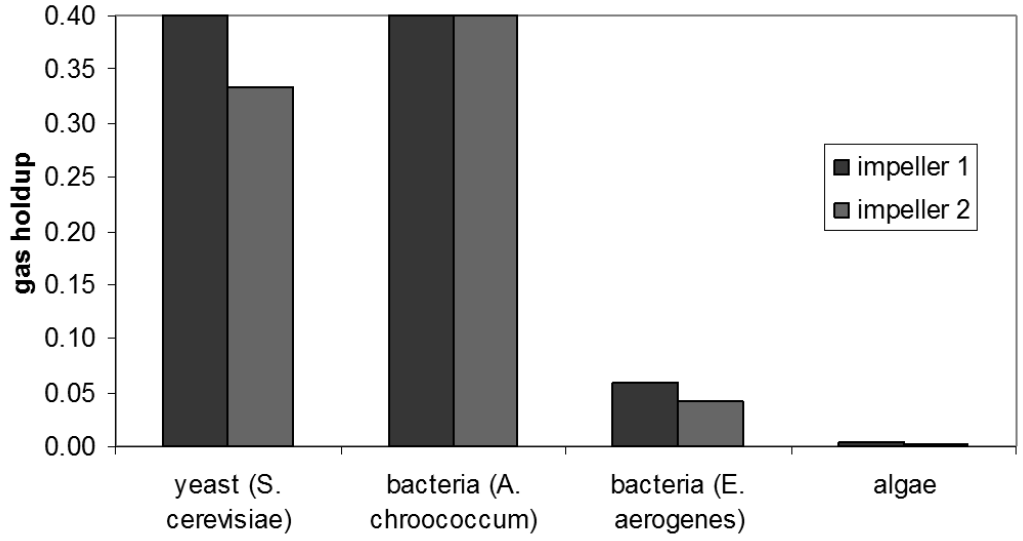

Figure 2.6. Determination of the effect of microorganism and impeller style on gas holdup at cost-minimizing culture conditions of aeration and mixing (10 m^3 reactor volume, 5g(DW)l^{-1} cell density (excepting *A. chrococcum*: 0.28g(DW)l^{-1} for impeller 1, 0.37g(DW)l^{-1} for impeller 2), fresh water medium).

The mixing speed for the various microbes and impeller styles is shown in Figure 2.7. As expected, an organism with a larger respiratory coefficient, and hence oxygen demand, will require more mixing to help transfer oxygen to the cells. Impeller style 1 consistently required greater mixing speed, with the difference between the two types of impellers increasing for those microorganisms that require more oxygen for growth. It is important to note again that the

biomass present in the case of *A. chroococcum* is significantly less than for the other three microorganisms.

The aeration rate for the cost optimized CSTB design is presented in Figure 2.8. For both impeller styles, an increasing trend with increasing respiratory coefficient is observed, even with the significantly lower biomass of *A. chroococcum.* This is predictable given the increased need for oxygen by the cells. The need for greater aeration with impeller style 2 becomes apparent for microorganisms with greater oxygen requirements. From Figures 7 and 8, although the expected need to increase mixing and aeration to meet increased cell oxygen requirements is observed, there is no obvious trend between how the two are optimized for the same culture. The relationship between mixing speed and aeration rate in minimizing CSTB design cost is complex and involves a variety of design parameters.

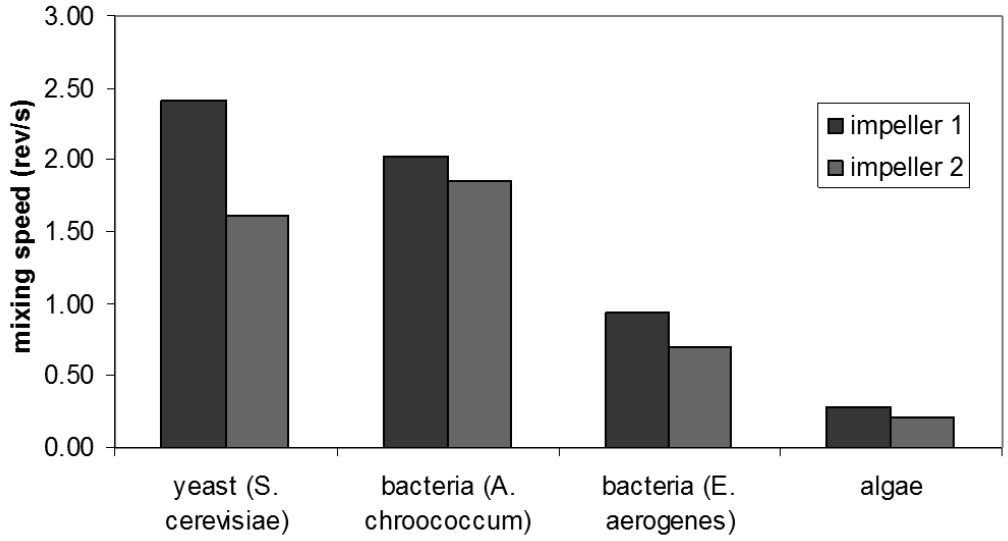

Figure 2.7. Determination of the effect of microorganism and impeller style on optimum mixing speed at cost-minimizing culture conditions of aeration and mixing (10 m^3 reactor volume, 5g(DW)l^{-1} cell density (excepting *A. chrococcum*: 0.28g(DW)l^{-1} for impeller 1, 0.37g(DW)l^{-1} for impeller 2), fresh water medium).

Minimized operating cost as a function of cultured microorganism and CSTB impeller style is given in Figure 2.9. As expected, the bacterial *A. chroococcum* is the most expensive to cultivate, especially when the low biomass density (compared to the other microbes) in the bioreactor is considered. It has the largest oxygen demand and therefore requires the most

mixing and aeration to ensure that sufficient oxygen reaches the cells; which of course increases operating cost. It would also increase the capacity of the compressor and the mixer required, and hence the capital cost. Cost increases with the oxygen demand of the cells for all species. A larger cost was observed using impeller style 2 for *S. cerevisiae* and *A. chroococcum*, the two microorganisms with the greater respiratory coefficients. Although impeller 2 is considered to be a more cost-effective choice to operate, it also must be operated at higher mixing speeds than impeller 1 to achieve the same turbulence and mass transfer.

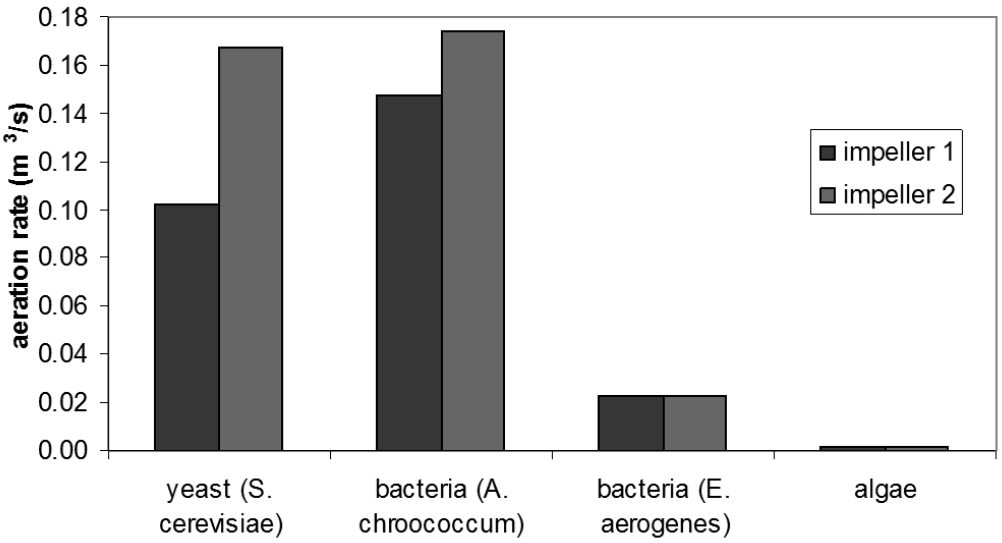

Figure 2.8. Determination of the effect of microorganism and impeller style on optimum aeration rate at cost-minimizing culture conditions of aeration and mixing (10 m^3 reactor volume, 5g(DW)l^{-1} cell density (excepting *A. chrococcum*: 0.28g(DW)l^{-1} for impeller 1, 0.37g(DW)l^{-1} for impeller 2), fresh water medium).

A comparison of optimum design parameters for both fresh water and salt water culture mediums was performed. The fresh water medium was considered to be pure water and the salt water was considered to have 35 g/l of NaCl as present in typical ocean seawater. These represent the extreme limits of the range for typical microbial growth mediums. All bioreactor systems for culture medium comparison were optimized for the *S. cerevisiae* yeast fermentation with the same inputs as used for the microorganism comparisons presented above.

No change of oxygen mass transfer coefficient was observed whether pure water or seawater was used to culture the cells, and regardless of the turbine impeller chosen. The value

of k_La is 0.069 s^{-1} for both pure and salt water, regardless of impeller style. Although the presence of salt in seawater has been shown to increase the value of k_La relative to that of pure water (Van't Riet, 1979) due to the presence of ions, this was not observed in this work. The reason for this is the manner in which the CSTB design scheme is set up. Given identical culture conditions and bioreactor design, the k_La values for the two mediums would differ as expected given their different properties, particularly diffusivity. The CSTB design scheme for cost minimization solves for the needed amount of oxygen that must be transferred into the medium for cell growth, and hence the value of k_La, and designs the CSTB from this determination. This oxygen mass transfer coefficient is determined by the oxygen need of the cells being cultured, and since all the fermentation optimizations for the medium comparison study were performed for the same microbial species and bioreactor size; the k_La values are the same for each case, regardless of the type of culture medium. The effect of the different properties of the two mediums is observed instead when the required operating conditions are determined using the cost minimization design procedure.

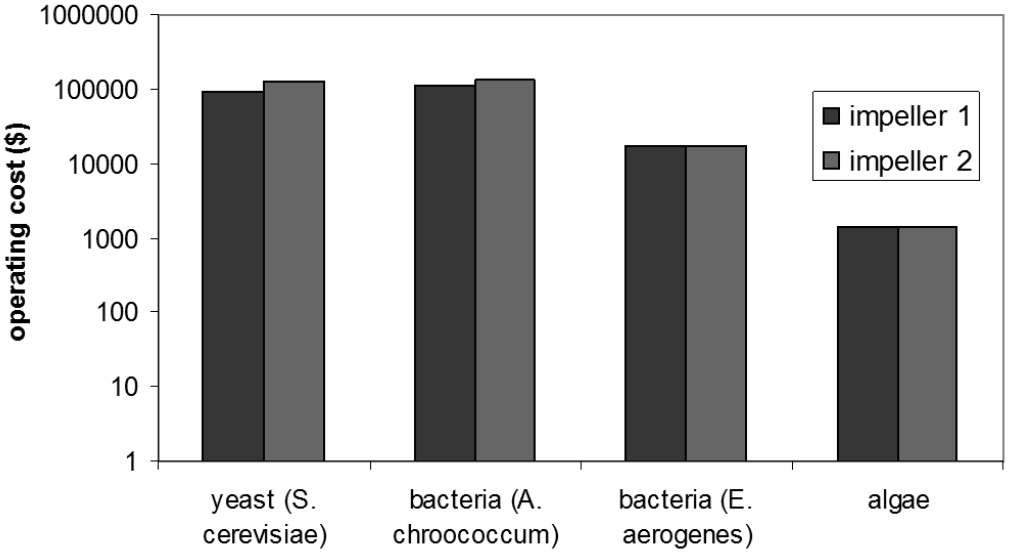

Figure 2.9. Determination of the effect of microorganism and impeller style on minimum operating cost at cost-minimizing culture conditions of aeration and mixing (10 m^3 reactor volume, 5g(DW)l^{-1} cell density (excepting *A. chrococcum*: 0.28g(DW)l^{-1} for impeller 1, 0.37g(DW)l^{-1} for impeller 2), fresh water medium).

The effect of culture medium on gas holdup was insignificant when the design is optimized for cost. For all cases, both pure and salt water, and both impeller styles, the gas holdup is consistently 0.4. This is the maximum value to which the holdup correlation (Hassan and Robinson, 1977) is constrained by the design strategy, and so limits the combination of mixing speed and aeration speed that is determined during cost minimization. From published work, an unconstrained system would perhaps show an increase in gas holdup for saline culture mediums. The addition of ions has been shown to reduce average bubble size, and the frequency of bubble coalescence (Van't Riet, 1979). The holdup therefore has a tendency to become larger compared to pure water (Ho et al., 1987; Hassan and Robinson, 1977).

The mixing speed as determined by the cost optimization program for both pure water and seawater is shown in Figure 2.10. A reduced mixing speed was required for the saline medium when impeller style 1 was employed. No significant difference was observed with the ionic characteristics of the culture medium for impeller 2. The aeration rate is given in Figure 2.11 for the same optimized conditions. No consistent trend with the ionic properties of the culture medium was observed. The results in Figures 2.10 and 2.11 highlight the complex and interacting relationship between mixing speed and aeration rate in meeting both the oxygen demand of the cells and of minimizing the cost of the CSTB system design.

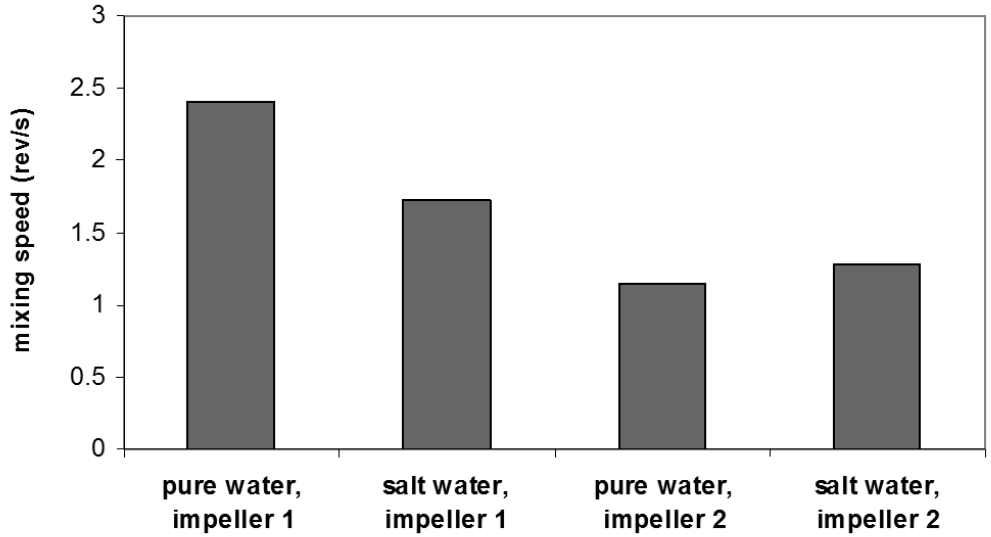

Figure 2.10. Determination of the effect of culture medium and impeller style on mixing speed at cost-minimizing culture conditions (*S. cerevisiae*, 10 m^3 reactor volume, 5g(DW)l^{-1} cell density).

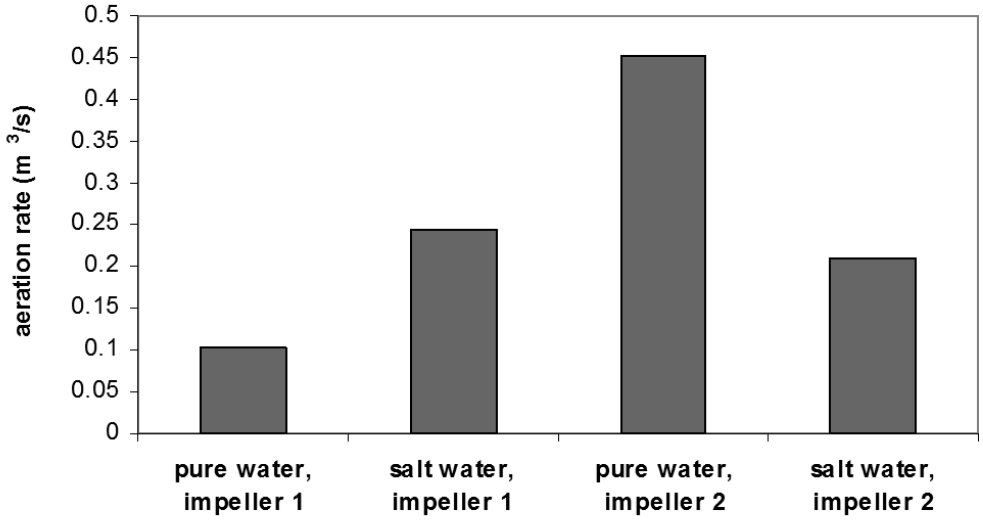

Figure 2.11. Determination of the effect of culture medium and impeller style on aeration rate at cost-minimizing culture conditions (*S. cerevisiae*, 10 m^3 reactor volume, 5g(DW)l^{-1} cell density).

The effect of using seawater instead of pure water as culture medium in a cost-optimized CSTB is presented in Figure 2.12. The presence of ions in the medium had an observable impact on operating cost for both impeller types, but not in a consistent manner. The operating cost is the result of the combination of mixing speed and aeration rate that both provides enough oxygen to the cells and minimizes cost. Many different combinations of mixing speed and aeration rate could meet the oxygen demands of the microorganisms being cultured, but the relationship of these parameters to cost is complex.

Overall, the impact of the culture medium on operating cost and fermentation parameters was generally small. This indicates that the design strategy is much less sensitive to the properties of the medium, as seen from Figures 2.10 through 2.12, than it is to the characteristics of the vessel itself and the microbe being cultured.

All results up to this point were calculated for a vessel of working volume 10 m^3. The effect of vessel size is now presented. (For volumes greater than 100 m^3, vessels of equal size in parallel are used.) The optimization for cost minimization was performed for the *S. cerevisiae* yeast fermentation and all presented results meet the stated constraints, particularly that of the oxygen demand by adjusting mixing speed and aeration rate.

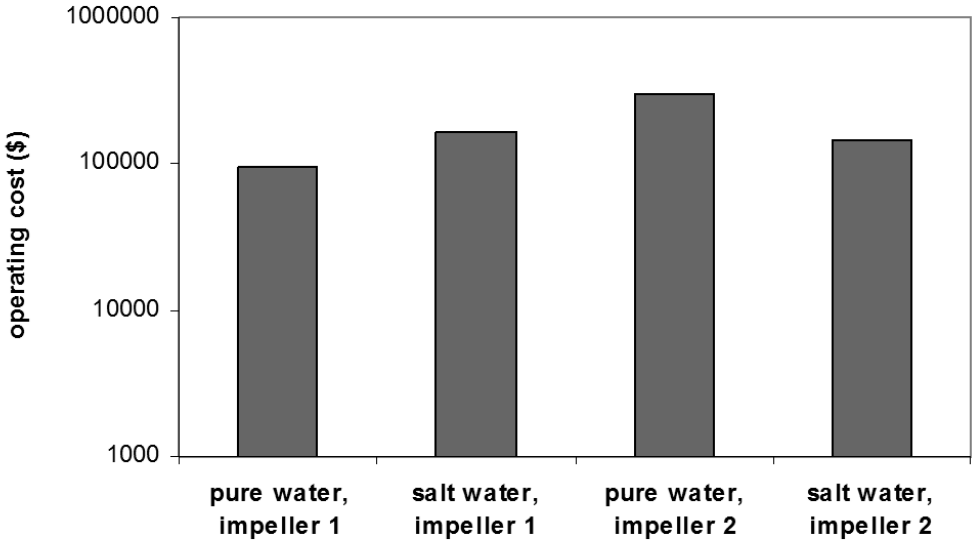

Figure 2.12. Determination of the effect of culture medium and impeller style on the minimum operating cost (over 5 years) at cost-minimizing culture conditions of aeration and mixing (*S. cerevisiae*, 10 m^3 reactor volume, 5g(DW)l^{-1} cell density).

The required mixing speed demonstrated a decreasing trend in Figure 2.13 with increasing fermentor working volume. A similar trendline is observed for both impeller styles, with greater mixing speed required with impeller style 1. The most significant changes in mixing speed are observed with small working volumes. No change in mixing speed is observed once a working volume of 100 m^3 (or tank volume of 150 m^3) is reached, as larger reactors are simply multiple reactors of equal size in parallel. Hassan and Robinson (1977) found that for pure water, tank size had no appreciable effect on hydrodynamic parameters such as gas holdup, but in this work the values have been determined at cost minimizing conditions. Gas holdup depends on both mixing speed and aeration rate. Figure 2.13 provides valuable data for designing a CSTB for minimal operating cost that still meets the growth needs of the cultured cells. The design program can be used to determine this data for any type of growth culture.

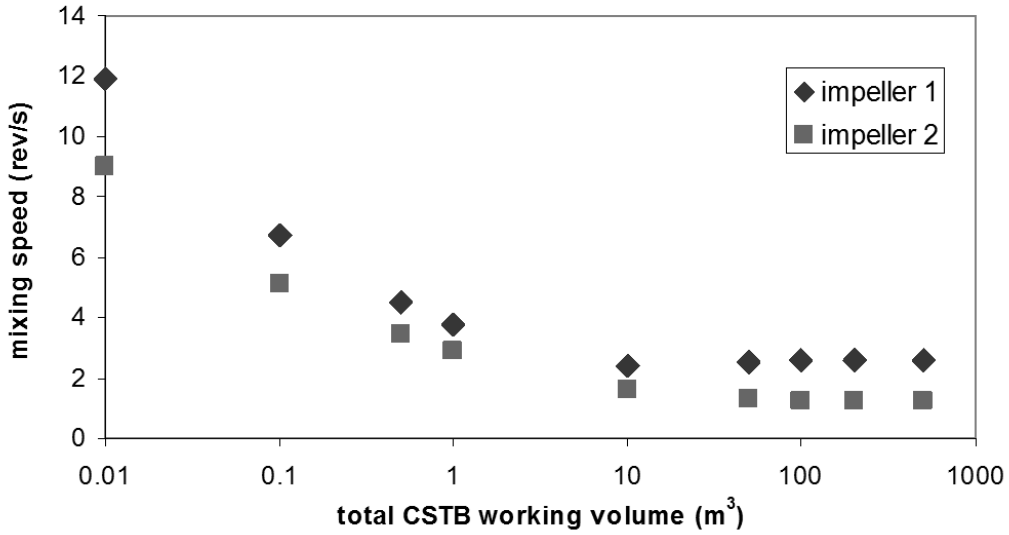

Figure 2.13. Determination of the effect of CSTB volume and impeller style on the required mixing speed for cost-minimization (*S. cerevisiae*, 5g(DW)l^{-1} cell density, fresh water medium).

The operating cost over 5 years, consisting of utilities only, with change in CSTB working volume is given in Figure 2.14. (Again, for working volumes greater than 100 m^3, or tank volumes greater than 150 m^3, vessels of equal size in parallel are used.) The expected increase in cost with increased reactor volume is observed, with the cost of operating being greater for CSTBs employing impeller style 1. Cost minimization information for determining the benefit of larger yield fermentations is given in Figure 2.15. The unit cost for each gram of biomass that can be cultured with increasing CSTB working volume is provided, with cost as both capital and operating, and as operating alone. It is evident that the unit cost initially decreases rapidly as the bioreactor volume increases, indicating that small working volumes are not cost effective. Regardless of the impeller style employed, the unit cost decreases steadily as working volume increases, until the unit cost becomes constant. At this point, the benefit of using a larger working volume and multiple reactors becomes the large desired output while still maintaining the lower unit cost. The value of the cost minimization information provided in Figure 2.15 assumes that the desired product of the cell culture is either the biomass itself or a cell by-product that is directly related to the amount of biomass.

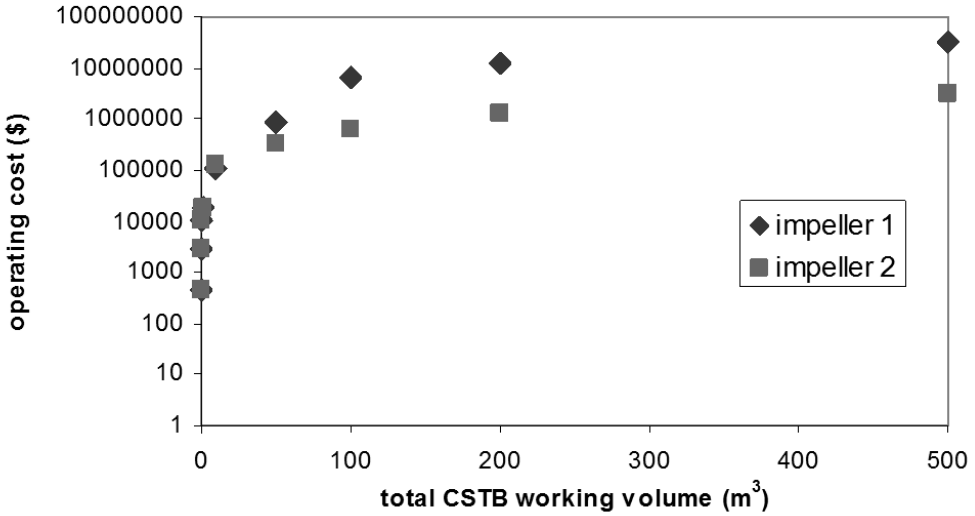

Figure 2.14. Determination of the effect of CSTB volume and impeller style on the minimum operating cost (over 5 years) at cost-minimizing aeration and mixing (*S. cerevisiae*, 5g(DW)l^{-1} cell density, fresh water medium).

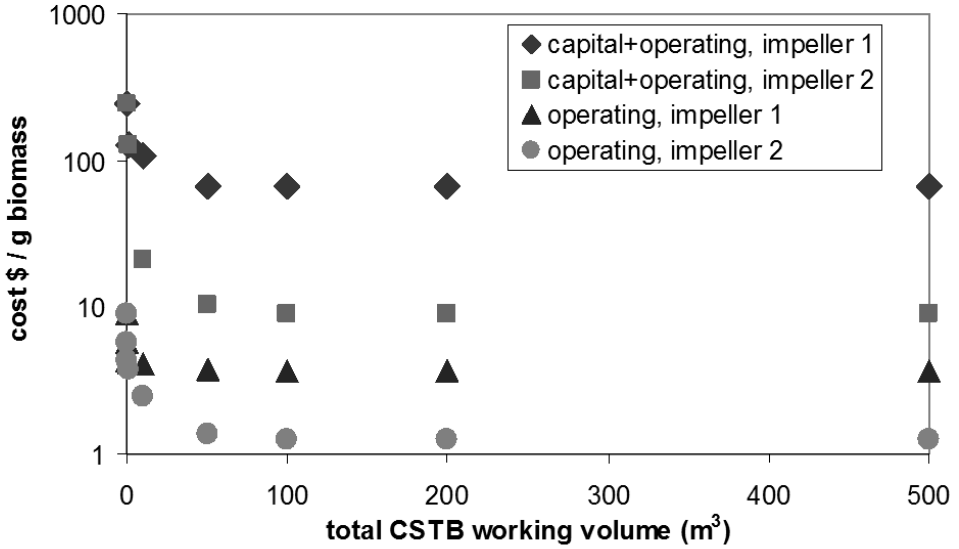

Figure 2.15. Determination of the effect of bioreactor volume and impeller style on minimum production costs for producing biomass (*S. cerevisiae*, 5 g DW / l cell density, fresh water medium).

All CSTB optimizations presented above have been determined using a steady state biomass input of 5 g/l. The effect of biomass cell density is now presented, again using *S. cerevisiae* as an example, and returning to the CSTB volume of 10 m^3. All other inputs are as in the previous optimizations.

The gas holdup as a function of the biomass input is presented in Figure 2.16. Gas holdup increases with cell density, which is expected in order to provide more oxygen for the increased numbers of cells. More oxygen is being input into the CSTB at greater mixing speeds and varying aeration rates. The maximum value of 0.4 for gas holdup is constrained in the program by the upper limit of the gas holdup correlation (Hassan and Robinson, 1977).

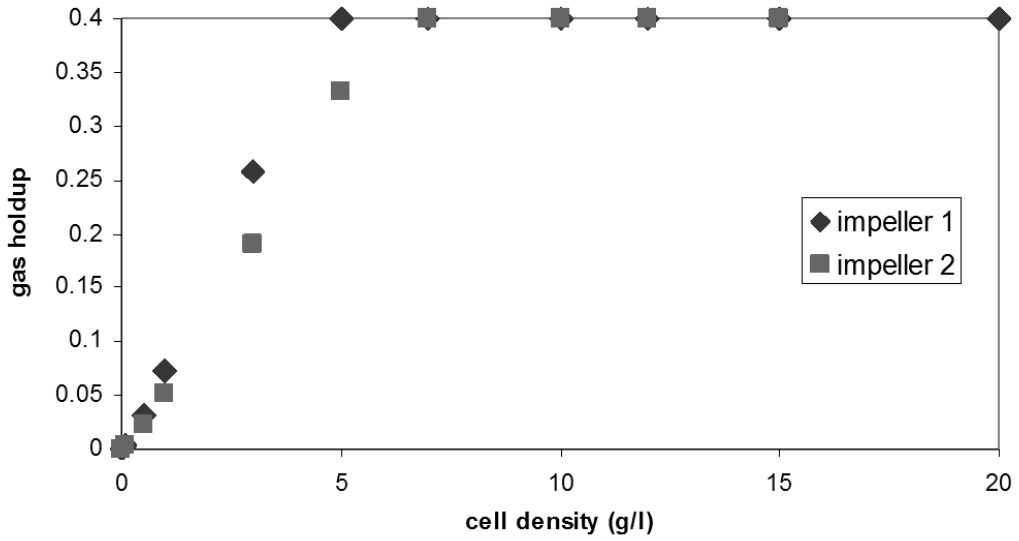

Figure 2.16. Determination of the effect of biomass cell density on gas holdup in the CSTB at cost minimizing culture conditions of aeration and mixing (*S. cerevisiae*, 10 m^3, fresh water medium).

The mixing speed required to meet the oxygen demands of a given amount of biomass, optimized for minimum cost, is shown in Figure 2.17. Increasing mixing is required for increased cell density as expected. Greater mass transfer is required to meet the needs of a denser cell culture. Greater speeds are required for impeller 1 than for impeller 2. This has been observed consistently in Figures 2.7 and 2.10 as well, and would seem to indicate that greater

mixing speeds are necessary to achieve the same mass transfer rates with impeller 1 as with impeller 2.

The optimized operating cost for various steady state cell densities are given in Figure 2.18. Operating cost increases with the amount of biomass being cultured in the CSTB. The difference in cost between the two impeller types becomes apparent at greater cell densities, where the greater mixing speed required when using impeller 1 has an increased impact. Figure 2.19 provides information on the cost minimization as a function of steady state cell density for a 10 m^3 bioreactor. Figure 2.19 highlights the cell density range where the minimum cost per gram of biomass cultured is observed. If only operating cost is considered, this cost increases with biomass density. If the capital and operating cost is considered, then a minimum unit cost occurs near 5 g/l.

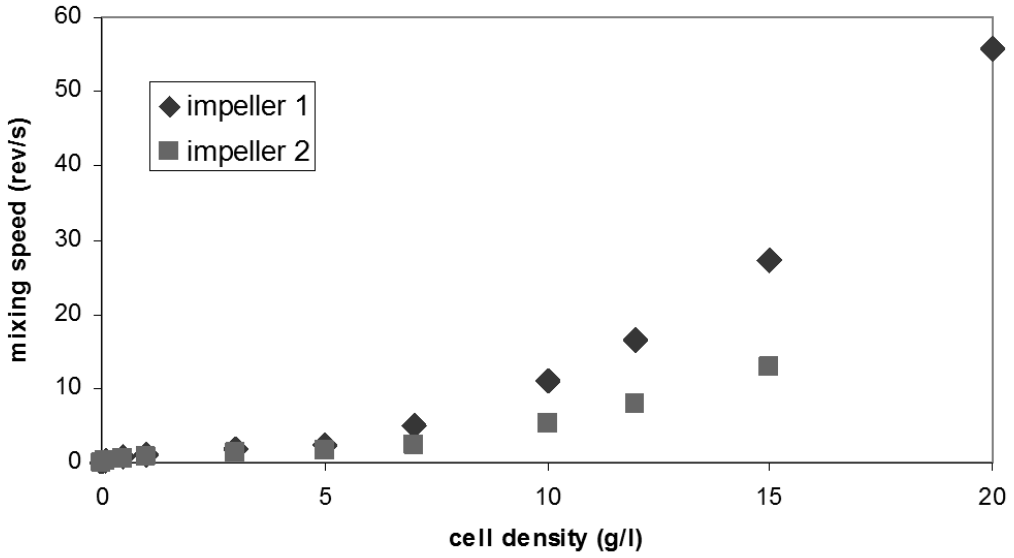

Figure 2.17. Determination of the effect of biomass cell density on mixing in the CSTB at cost minimizing culture conditions (*S. cerevisiae*, 10 m^3, fresh water medium).

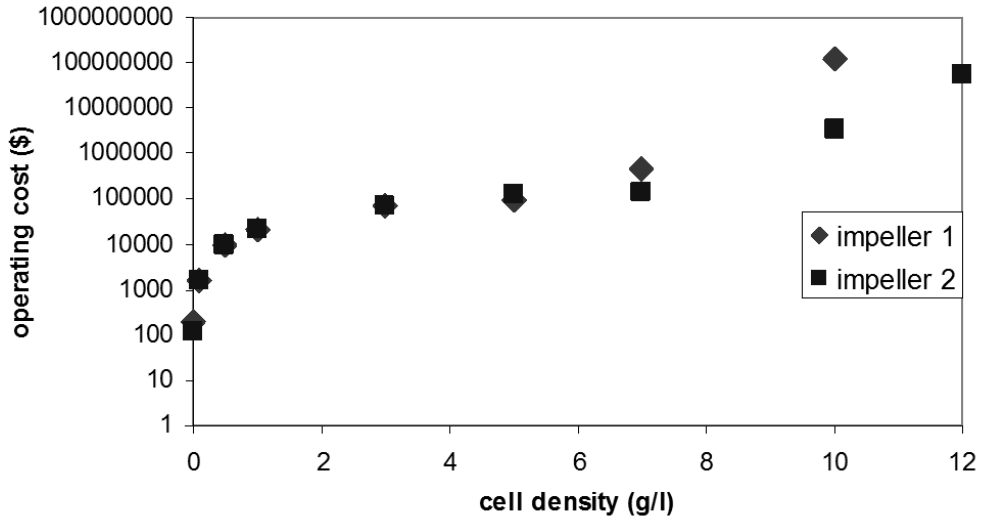

Figure 2.18. Determination of the effect of biomass cell density on minimum operating cost (over 5 years) at cost minimizing culture conditions of aeration and mixing (*S. cerevisiae*, 10 m^3, fresh water medium).

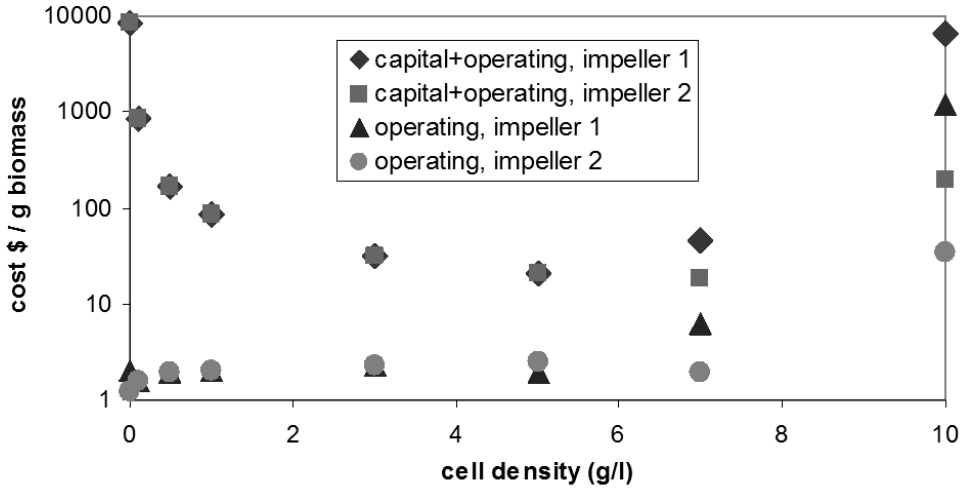

Figure 2.19. Determination of the effect of biomass cell density on minimum production costs at cost minimizing culture conditions of aeration and mixing (*S. cerevisiae*, 10 m^3 reactor volume, fresh water medium).

2.5. Conclusions

A cost minimization strategy and program has been developed for CSTB design. It is suitable for use with a variety of microorganisms and culture mediums. At the cost-minimized optimum conditions, it is possible to evaluate the effect of microbial species, culture medium, and fermentor design aspects on CSTB system characteristics. At minimized cost conditions, a variety of effects were observed.

The species of microbe being cultivated is key to the determination of the design parameters of the optimized system, in particular the oxygen requirements of the cells. This determines the value of k_La and impacts the mixing speed and aeration rate required to supply oxygen to the cells, affecting gas holdup, and the overall operating cost. A comparison of pure water with seawater as culture medium demonstrated that the design strategy is much less sensitive to this parameter than to microbial species, with smaller effect on mixing speed and aeration rate, and therefore cost. Data on the decreasing optimum mixing speed with increasing bioreactor volume, for minimum operating cost, was also obtained. Finally, the effect of increasing steady state biomass density on gas holdup, mixing speed, and cost was determined.

2.6. Nomenclature

C^* adjusted oxygen concentration in liquid phase, mg/l

C_{BMC} compressor cost, bare module, $

C_{BMM} mixer cost, bare module, $

C_{CRIT} critical oxygen concentration for growth, mg/l

C_C total compressor cost, $

C_F total fermentor cost, $

C_M total mixer cost, $

C_{O2IN} oxygen concentration, inlet, mg/l

C_{O2OUT} oxygen concentration, outlet, mg/l

D_I impeller diameter, m

d tank diameter, m

F_{BM} model correction factor

g gravitational constant, m/s^2

H Henry's Law constant

H_{LIQ} liquid height, m

H_{TANK} tank height, m

k_La oxygen mass transfer coefficient, s^{-1}

m_{AIR} mass flow rate, air, kg/s

MW_{AIR} molecular weight, air, g/mol

N mixing speed, rev/s

N_A aeration number

N_{MIN} mixing speed, minimum, rev/s

N_{O2} oxygen demand of cells, mg O_2 / l-h

N_P power number

N_{RE} Reynolds number

N_S oxygen supplied to cells, mg O_2 / l-h

N_{WE} Weber number

n_C number of compressors

n_F number of fermentors

n_M number of mixers

P_{COST} total cost of power, $

P_{EXT} total external power, W

P_G aerated power, W

P_O unaerated power, W

Q aeration rate, m^3/s

Q_{O2} respiratory coefficient, mg O_2 / mg DW-h

S substrate concentration, g/l

S_0 substrate concentration, bioreactor inlet, g/l

S_1 substrate concentration, bioreactor outlet, g/l

t temperature, ^oC

V_L liquid volume, m^3

V_{TANK} tank volume, m^3

V_W working volume, m^3

W_C compressor power, kW

w impeller blade width, m

X biomass input, mg DW / l

Y_{XS} biomass yield factor, mg DW /mg substrate

Greek letters

ε_G gas holdup

γ ratio of specific heats, air relative to water

μ viscosity, N s / m^3

ρ_{AIR} density, kg/m^3

ρ_L density, kg/m^3

σ surface tension, N/m

υ_S superficial gas velocity, m/s

Chapter 3

3. Growth Kinetics of *Chlorella vulgaris* and Its Use as a Cathodic Half Cell

A similar version of this chapter has been published in Bioresource Technology:

Powell, E.E., Mapiour, M.L., Evitts, R.W., and G. A. Hill "Growth kinetics of *Chlorella vulgaris* and its use as a cathodic half cell", Bioresource Technology, **100**, 269-274 (2009).

The topics discussed in this chapter have also been included in an oral paper presented at the following conference:

Powell, E.E., Mapiour, M.L., Evitts, R.W., Hill, G.A. and J. C. Bolster, "Growth Kinetics of a Photosynthetic Microorganism and Its Use in a Fuel Cell", 57th Canadian Society of Chemical Engineering Conference, Edmonton, Alberta
October 30, 2007.

Contribution of Ph.D. Candidate

Experiments were planned and supervised by Erin Powell and performed by summer student Majak Mapiour. Gordon Hill and Richard Evitts provided guidance in planning the experiments. The experimental results were analyzed by Erin Powell. The submitted manuscript was written by Erin Powell, with Gordon Hill and Richard Evitts providing editorial assistance.

Contribution of this Paper to the Overall Study

The primary goal of the Ph.D. research is the cultivation of *C. vulgaris* for the consumption of CO_2. With the literature gap on kinetic growth data for *C. vulgaris*, as discussed in Chapter 1, growth data must be collected as part of this study. This will enable the maximization of yields during cultivation, and therefore the maximization of the CO_2 consumption. The collection of the kinetic growth data is also needed to enable the design of a novel photobioreactor for improved *C. vulgaris* cultivation. Once the growth study was completed, the suitability of a *C. vulgaris* culture to serve as photosynthetic cathodic half cell was evaluated as a novel avenue for production of electricity as a useful by-product during cultivation and CO_2 consumption.

3.1. Abstract

The kinetics of growth of the algal species *Chlorella vulgaris* has been investigated using CO_2 as the growth substrate. The growth rate was found to increase as the dissolved CO_2 increased to 150 mg/L, but fell dramatically at higher concentrations. Increasing the radiant flux also increased growth rate. With a radiant flux of 32.3 mW falling directly on the 500 mL culture media, the growth rate reached up to 3.6 mg of cells/L-h. Both pH variation (5.5 - 7.0) and mass transfer rate of CO_2 (K_La between 6 h^{-1} and 17 h^{-1}) had little effect on growth rate. Growing on glucose, the yeast *Saccharomyces cerevisiae* produced a stable 160 mV potential difference when acting as a microbial fuel cell anode with ferricyanide reduction at the cathode. The algal culture was observed to be a workable electron acceptor in a cathodic half cell. Using an optimum methylene blue mediator concentration, a net potential difference of 70 mV could be achieved between the growing *C. vulgaris* culture acting as a cathode and a 0.02 M potassium ferrocyanide anodic half cell. Surge current and power levels of 1.0 µA/mg of cell dry weight and 2.7 mW/m^2 of cathode surface area were measured between these two half cells.

3.2. Introduction

Alternate technologies to produce energy are of great interest today due to decreasing supplies and increasing costs of petroleum and other sources of energy (Kouroussis and Karimi, 2006). The microbial fuel cell (MFC) is a new technology that generates electrical current from the oxidation – reduction reactions that occur within living microorganisms. So far, all studies have focused on the growth of microorganisms for production of electrons at the anode, primarily by the oxidation of organic compounds and the release of electrons. Studies with pure sugars (Bennetto et al., 1983, 1985; Kim et al., 2000; Park and Zeikus, 2000; Rabaey et al., 2003), alcohols (Kim et al., 2007b), fatty acids (Bond and Lovley, 2003), domestic wastewater (Liu et al., 2004; Kim et al., 2005), food processing wastewater (Oh and Logan, 2005; Min et al., 2005) and marine sediments (Bond et al., 2002) have shown that a single microbial fuel cell can produce voltages up to 800 mV and currents measured in tens of mA. Stacking MFCs can increase both voltage and current.

Figure 3.1a demonstrates the general principles that occur at the anode of a typical MFC. Most microorganisms grow by the uptake of organic chemicals and passing them through a series of metabolic reaction pathways which involve hundreds of oxidation – reduction reactions. Electrons released by these reactions can be captured by mediator chemicals which have the ability to penetrate into the cells in their oxidized state and leave the cells in their reduced state. Once released into the fermentation media, the reduced mediator chemicals spontaneously oxidize to their original state and release electrons at the anode that subsequently enter the electric circuit.

Logan et al. (2006) reviewed some recent advances in microbial fuel cell technology, as well as the limitations. Although many academic studies have focused on the abilities of pure microbial cultures to act as the anode of a MFC, mixed cultures tend to yield higher current densities. MFC designs frequently use graphite or platinum as both the anode and cathode, and include a cation exchange membrane (CEM) or salt bridge to separate the anodic and cathodic half cells. Min et al. (2005a) reported that CEMs had reduced electrical resistance compared to a salt bridge such that the CEMs greatly improved power generation. Resistance depends on the salt bridge construction: its length, diameter and the concentrations of dissolved ionic species. Although several mediator chemicals have been studied to improve the capture and transport of

electrons, recent research has shown that mediator - less anodic cells are feasible, especially when the cells grow as a film coating the anodic electrode. Energy capture efficiencies (power produced relative to the heat of combustion of the food source) of MFCs generally reach up to 50%.

An electrical cell is composed of both an anode and a cathode. Most studies use an electrochemical reduction reaction to act as the cathodic half-cell, such as ferricyanide to ferrocyanide. In this work, using the oxidation of ferrocyanide to ferricyanide at the anode, we show that a photosynthetic culture of *Chlorella vulgaris* can act as a biological electron acceptor at the cathode while simultaneously reducing CO2 to biomass. The overall biochemical reaction that occurs at the cathode is:

$$6\ CO_2 + 12\ H^+ + 12\ e^- \rightarrow\ -C_6H_{12}O_6\text{-(biomass)} + 3\ O_2 \qquad (3.1)$$

Figure 3.1b shows that in this new configuration, electrons are transferred into the media at the cathode and reduce the mediator from its oxidized state to its reduced state. The mediator then penetrates into the cell where it becomes oxidized and releases electrons to the growing cells. The growing cells use these electrons in their metabolic pathways with the net result of converting CO_2 into oxygen and biomass. The oxidized mediator chemicals leave the cells and enter the media where they are once again reduced by the uptake of electrons at the cathode.

The use of a cathodic microbial half cell can transform a MFC into an entirely microbiological system when it is coupled with an anodic microbial half cell. At the same time this device could be used to capture CO_2 gas. In this study, we present the growth behaviour of *C. vulgaris* on CO_2 and also experimental studies designed to demonstrate and optimize the capture of electrons by *C. vulgaris* cultures acting as electron receptors in the cathode half-cell.

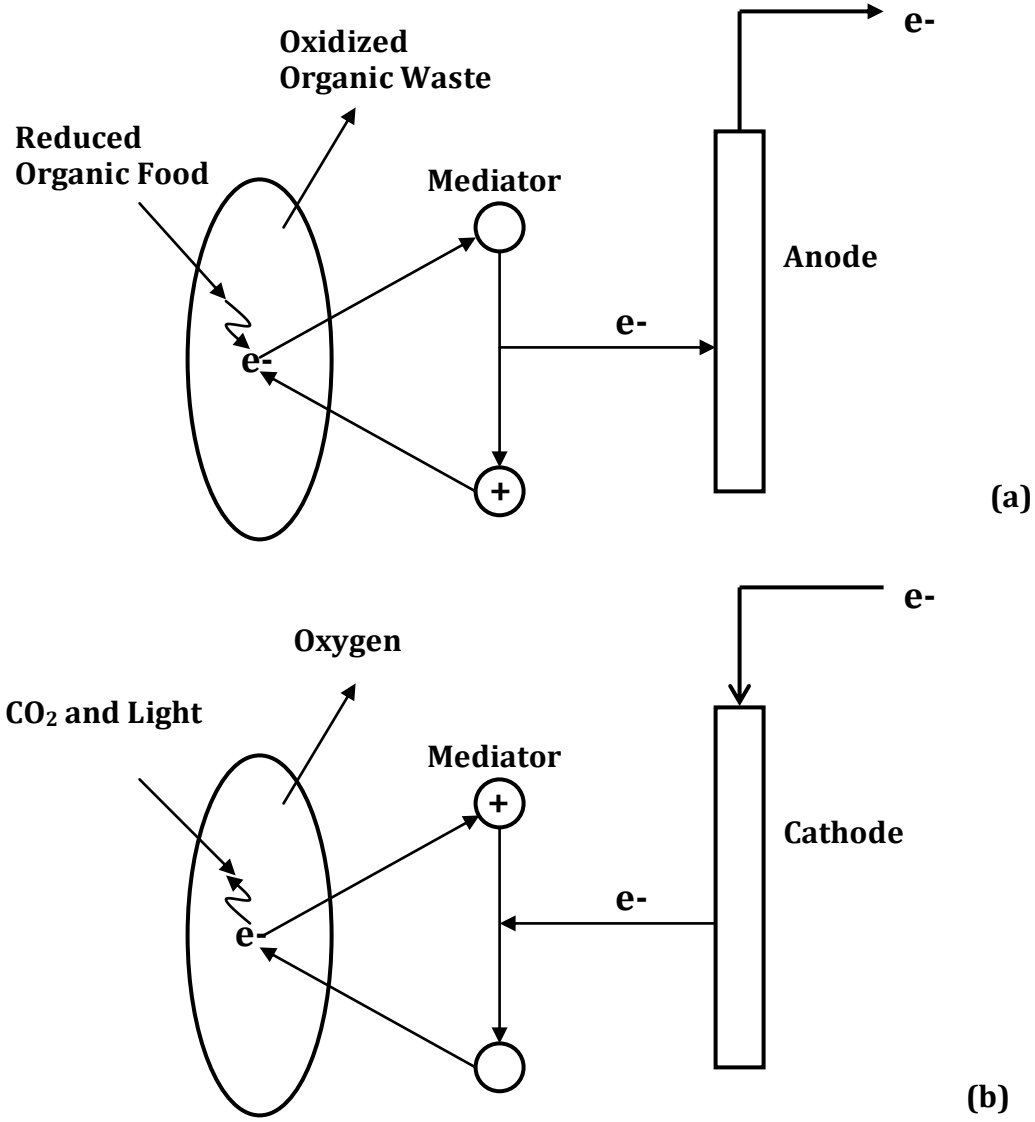

Figure 3.1Schematic of electron flow in a microbial fuel cell: (a) anodic release of electrons by consuming organic compounds, (b) cathodic capture of electrons buy photosynthesis growth on CO_2.

3.3. Methods

C. vulgaris was purchased from Carolina Biological Supply (Burlington, North Carolina, Cataolgue No.15-2075) and grown on a modified Bolds Basic media. The concentrations of nutrients were (mg per litre of reverse osmosis water): 75 KH_2PO_4, 50 K_2HPO_4, 75 NH_4Cl, 25 $MgSO_4.7H_2O$, 12.5 $CaCl_2$, 12.5 NaCl, 60 $NaHCO_3$, 25 EDTA (sodium salt), 2.5 $FeSO_4.7H_2O$, and 0.5 mL of trace mineral solution. The trace mineral solution consisted of (mg per 100 mL of reverse osmosis water): 1250 boric acid, 882 $ZnSO_4$, 70 MoO_3, 50 $Co(NO_3)_2$, 140 $MnCl_2$, 160 $CuSO_4.5H_2O$.

All experiments were conducted at 22.5 ℃. Biomass yield was determined by placing a known amount of liquid nutrient media and CO_2 gas into a sealed glass bulb, which was inoculated through a septum with *C. vulgaris* cells. The initial and final concentrations of both cells and CO_2 were used to determine cell yield. Growth experiments were carried out in 1.0 L Kontes culture vessels that were fitted with baffles and filled with 500 mL of culture solution as shown in Figure 3.2. After the growth media was added to the culture vessel, *C. vulgaris* was inoculated from a fresh shake flask giving an initial cell concentration of approximately 3 mg/L. The culture was exposed to a 40 W fluorescent Sylvania model Gro-lux bulb placed at either 50 cm above or 20 cm to the side of the bioreactor. At this point, air (containing 0.037% by volume CO_2) or CO_2 enriched air (5%, 10% and 20% by volume) was bubbled through two fritted glass bubblers at a total flowrate of 200 mL/min. Samples were then taken from the culture vessel using a hypodermic syringe to measure the increase in cell mass with time.

For MFC studies, 100 mL of the same culture media was used at both the cathode and anode as for the growth studies described above except at the cathode, *C. vulgaris* cells were added to the media to give a starting concentration of 3 mg/L and at the anode 0.02 M potassium ferrocyanide was added to the media. The cathode and anode cells were well stirred, baffled glass beakers that were open to the atmosphere. In the cathode cell, two types of chemicals were tested as mediators carrying electrons from the electrode to the growing cells: methylene blue and thionine blue. In order to reduce electrical resistance, a short, 15 cm, 6 mm ID salt bridge (containing saturated KCl jellified with agar) was used to transport potassium ions to the cathode. The electrodes in both the anode and cathode cells were glassy graphite rods, 5.0 mm in diameter that were immersed 47 mm in the liquid solutions. The cathode was connected to the

anode through a TSI model 1076 volt – ammeter which in turn was connected to a chart recorder to continuously measure voltage and from time to time, current flow through a zero resistance external circuit.

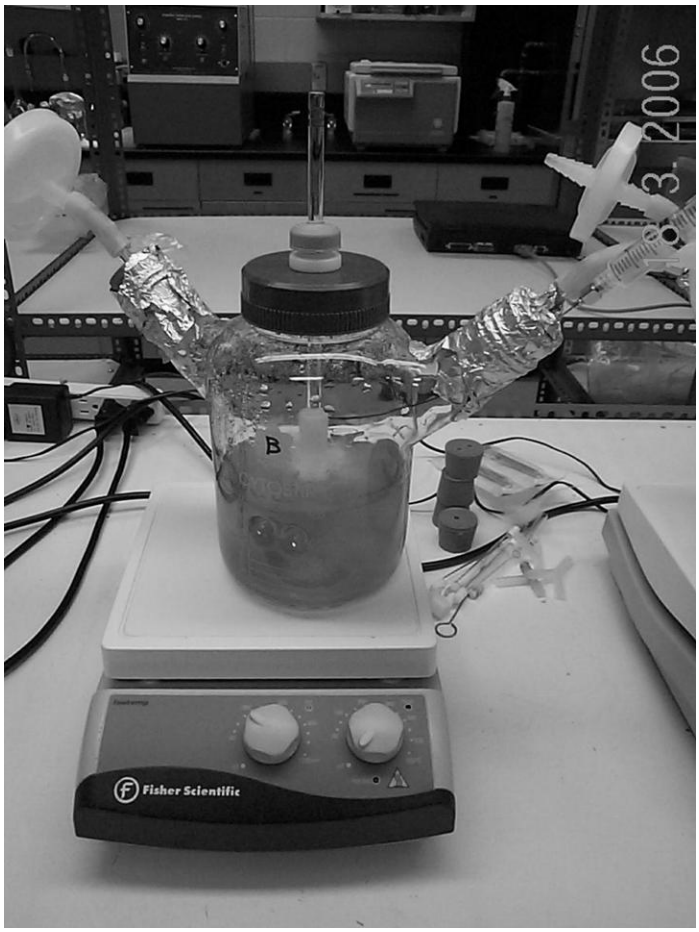

Figure 3.2. *Chlorella vulgaris* culture in the Kontes culture apparatus.

Cell mass was measured by optical density measurements on a Shimadzu model 1240 spectrophotometer at 620 nm. Optical density was converted to dry weight of algae cells using a previously prepared calibration curve. Chlorophyll content within the cells was measured by the standard APHA 10200H method (APHA, 1996) which accounts for chlorophyll degradation products. The pH of culture solutions was measured using an IQ240 pH meter and adjusted several times per day using 0.1 M NaOH or HCl solutions, and maintained within 0.2 pH units of the set point positions. Radiant flux and spectra were measured using an Ocean Optics, model

USB2000 spectrophotometer and an Ocean Optics model P200 fiber optic probe. The spectrophotometer and probe were calibrated to give accurate radiant flux readings using an Ocean Optics model LS1 calibration lamp. CO_2 was measured in the gas phase using a packed column (Carbosieve SII) and a TCD detector on a Hewlett Packard model 5890 gas chromatograph. Initial oven temperature was 100 ℃ which was ramped to 150 ℃ over 8 minutes, inlet temperature was 150 ℃ and the detector temperature was 190 ℃.

Each microbial growth experiment lasted ten days and two operating conditions were repeated in triplicate to determine standard deviations for growth rates. One algae microbial fuel cell condition was performed in duplicate and since glucose concentrations did not affect yeast fuel cell runs, the two yeast runs were combined to demonstrate the reproducibility of transient voltage curves. Standard errors and 95% confidence limits were computed using Excel®. The effects of variables on microbial growth and fuel cell performance were determined using the single factor method (Montgomery, 1991) applied to pH (two values resulting in CO_2 and HCO_3^- forms of dissolved CO_2), radiant flux (low and high), mass transfer (low and high), CO_2 concentration (four values spanning 0.037% to 20% by volume in air) and methylene blue concentrations in media. In all, fourteen algae growth runs and seven microbial fuel cell runs were completed.

3.4. Results and Discussion

3.4.1. Magnitude of Light Radiation

Light radiation from the plant growth, fluorescent bulbs was found to have the irradiance spectra shown in Figure 3.3. The light was initially shone from 50 cm above the reactor which resulted in a total visible radiation level (integration of area under the curve shown in Figure 3.3 times the bioreactor surface area which was 34.3 cm^2) of 6 mW falling on the top glass surface of the bioreactor and into the 500 mL of culture media. The light was also shone from the side of the bioreactor at a distance of 20 cm resulting in 32.3 mW falling on the glass surface (area of 140 cm^2 at the liquid depth) of the *C. vulgaris* cultures.

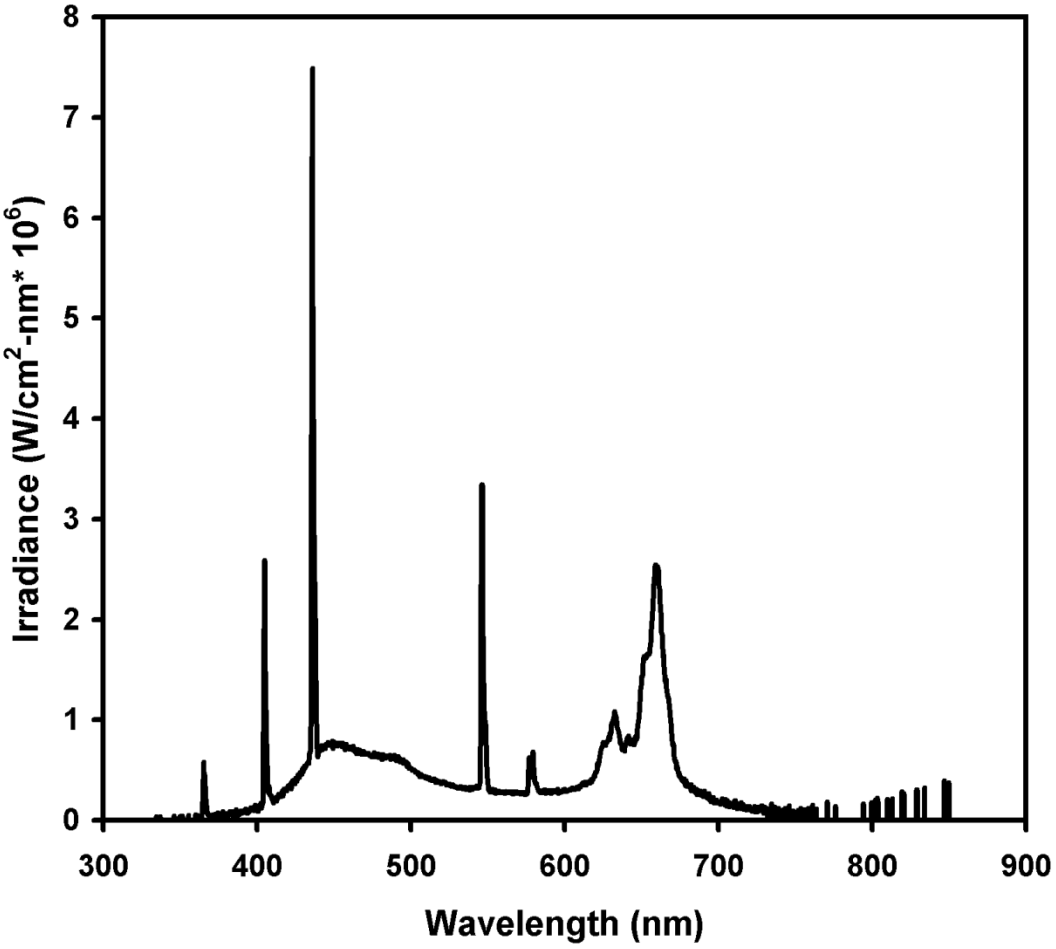

Figure 3.3. Scan of light irradiance from the plant growth fluorescent bulbs.

3.4.2. Magnitude of CO_2 Mass Transfer Rate

Mass transfer from the air into the liquid culture was also varied by performing experiments with air flowing across the top of the fermentation media or alternatively by bubbling into the media directly through two fritted bubblers. The effect this change had on mass transfer rate was determined by measuring the rate of build up of dissolved CO_2 as described earlier (Hill, 2006). It was found that the bubblers improved the rate of transport of CO_2 by a factor of three, with the mass transfer coefficient, K_La, increasing from 6 to 17 h^{-1}.

3.4.3. Yields of Biomass and Chlorophyll

The mean diameter of the *C. vulgaris* cells was found to be 5.7 µm. A photograph of a sample *C. vulgaris* cell taken during a kinetic growth experiment is shown in Figure 3.4. *C. vulgaris* was found to consume CO_2 with a biomass yield coefficient of 0.51 mg biomass/mg CO_2, meaning approximately 2 mg of CO_2 is needed to generate 1 mg of algae biomass. This yield of biomass is in agreement with the value reported by Javanmardian and Palsson (1992). Measurements taken on several samples of actively growing *C. vulgaris* cells demonstrated that the total biomass dry weight consisted of 6% chlorophyll with negligible amounts of chlorophyll degradation products present in the actively growing cells. Myers and Graham (1958) measured up to 5% chlorophyll content in *Chlorella*.

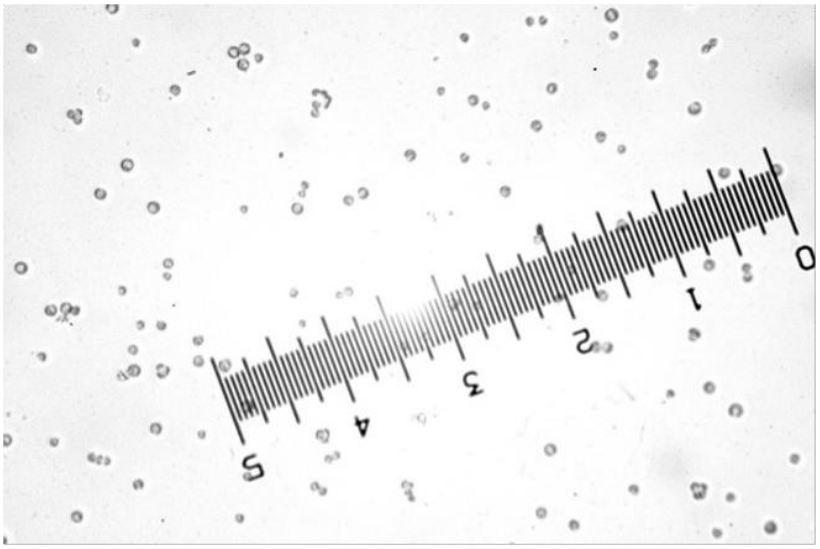

Figure 3.4. *Chlorella vulgaris* cells (small division = 2.6 µm)

3.4.4. Growth Rates of Algae

Rates of growth were determined by measuring the biomass accumulation at various pH values, light intensities, CO_2 concentrations and mass transfer conditions. This linear growth behaviour was observed for every kinetic experiment, with a sample curve being shown in Figure 3.5. Linearity indicates that the algae growth was therefore limited by something other than the cells' abilities to reproduce, which would cause exponential rather than linear increases in biomass concentrations with time. Two important limitations which could cause this linear

growth behaviour are mass transfer of CO_2 from the air bubbles or light penetration into the media.

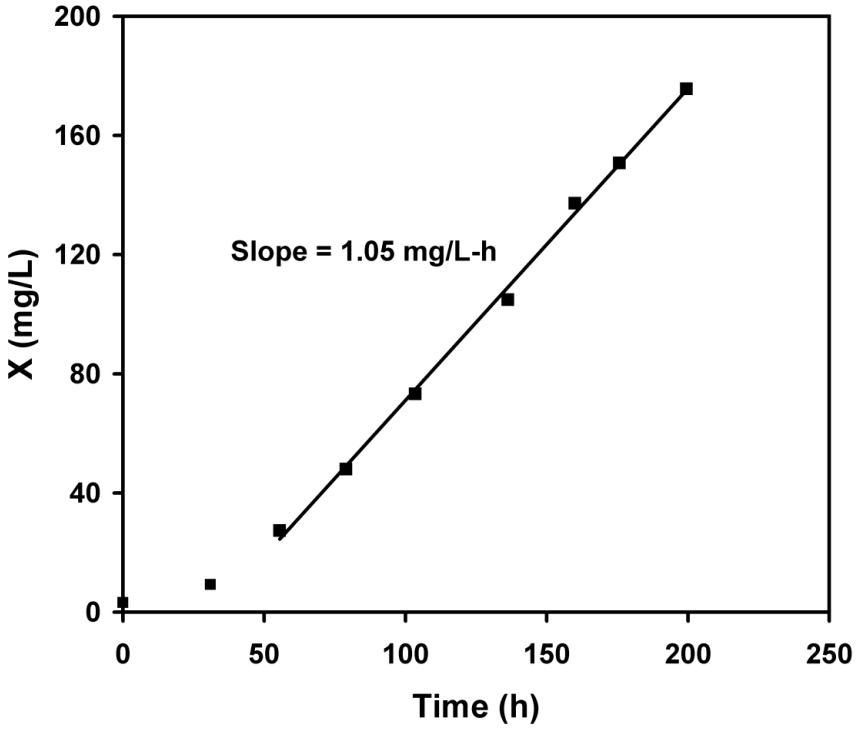

Figure 3.5. Linear biomass increase (pH 5.5, air, radiant flux = 32.3 mW)

The effect of mass transfer rate of CO_2 into the solution (Hill, 2006) was enhanced by using fritted bubblers (K_La = 17 h^{-1}) instead of blowing the air- CO_2 mixtures over the surface of the stirred medium (K_La = 6 h^{-1}). It was found this three-fold increase in mass transfer rate had a negligible effect on the rate of growth of the *C. vulgaris* cells. Measurement of dissolved CO_2 using an ion chromatograph showed no changes in the solution concentration as a function of time using either method of aeration. Therefore, mass transfer of CO_2 from the air was not limiting the ability of *C. vulgaris* cells to grow.

Figure 3.6 demonstrates the effect of three other variables on the kinetics of growth of *C. vulgaris*. Triplicate runs at Condition 1 (both low and high pH) in Figure 3.6 indicated a reproducibility (95% certainty of the slopes) of ± 0.150 mg/L-h, and error bars of this magnitude are shown for all growth rate data points. At pH 5.5 the majority of dissolved CO_2 would be in the form of CO_2 molecules, while at pH 7.0 bicarbonate ions would dominate (Hill, 2006). The rates of growth between the two pH runs at all environmental conditions were consistently within

0.150 mg/L-h of each other and could be greater at either pH. It appears that the aqueous form of the dissolved CO_2 molecules was not a factor limiting *C. vulgaris* growth. Other investigators have shown that certain species of *C. vulgaris* can uptake bicarbonate ions as well as CO_2 molecules (Aizawa and Miyachi, 1986; Moroney and Somanchi, 1999). It can be concluded that pH variations between 5.5 and 7 have no effect on CO_2 assimilation by the *C. vulgaris* species used in this investigation.

The variation of inlet CO_2 concentration had a dramatic effect on the growth rate of the algal cells. Figure 3.6 shows that the growth rate of *C. vulgaris* increased from 1.0 to 3.6 mg/L-h when the CO_2 concentration in the air was increased from 0.037% to 10% by volume at the high radiant flux condition (32.3 mW). Since the mass transfer rate of CO_2 into the media was much faster than the cell growth rate, the increase in CO_2 concentration in the air results in a proportional increase in dissolved CO_2 concentration in the aqueous phase according to Henry's law (Mook and deVries, 2005). . Hill (2006) showed that 10% CO_2 by volume in the gas phase results in a total dissolved CO_2 concentration of 3.5×10^{-3} M (150 mg/L) and is only 1.5×10^{-5} M (0.7 mg/L) under unenriched air (0.037% by volume CO_2). The higher concentration of dissolved CO_2 accounts for the faster growth rate of the *C. vulgaris* cells at high gas phase CO_2 concentrations. However, as the gas phase CO_2 concentration is further increased, the dissolved CO_2 becomes inhibitory. Figure 3.6 demonstrates that at 20% by volume in air (300 mg/L in the aqueous phase) the *C. vulgaris* growth rate dropped over an order of magnitude, from 3.5 to 0.25 mg/L-h. High levels of CO_2 are known to inhibit several metabolic reactions associated with the Krebs cycle. Ammann and Lynch (1967) found that air enriched at the 3% level with CO_2 inhibited the growth of some *Chlorella* species, but Hirata et al. (1999) found *Chlorella* species that were able to tolerate 40% CO_2 by volume in air.

Radiant flux had an important but interacting affect with CO_2 concentration on cell growth. At low dissolved CO_2 concentrations (0.7 mg/L in the media), increasing radiant flux from 6.0 to 32.3 mW resulted in the growth rate of the cells increasing by a factor of 2.5, from 0.4 to 1.0 mg/L-h. Increasing the radiant flux by the same amount but at 150 mg/L of CO_2 in the media, resulted in the growth rate increasing from 0.4 to 3.6 mg/L-h, almost a full order of magnitude. Thus to reach the optimum growth rate of *C. vulgaris* cells, it is important to increase both light radiation and dissolved CO_2 concentration simultaneously. Since radiant flux is clearly a limiting factor for growth rate, it is this factor which limits the growth rate to be

linear with time. Morita et al. (2000) also observed that the availability of light limited photosynthetic productivity in their photobioreactor. Burger et al. (1988) reported that microalgae grown under CO_2 enriched air (> 5% by volume) required different quantum light supplies compared to unenriched air, suggesting there is an interacting effect between CO_2 concentration and light requirements.

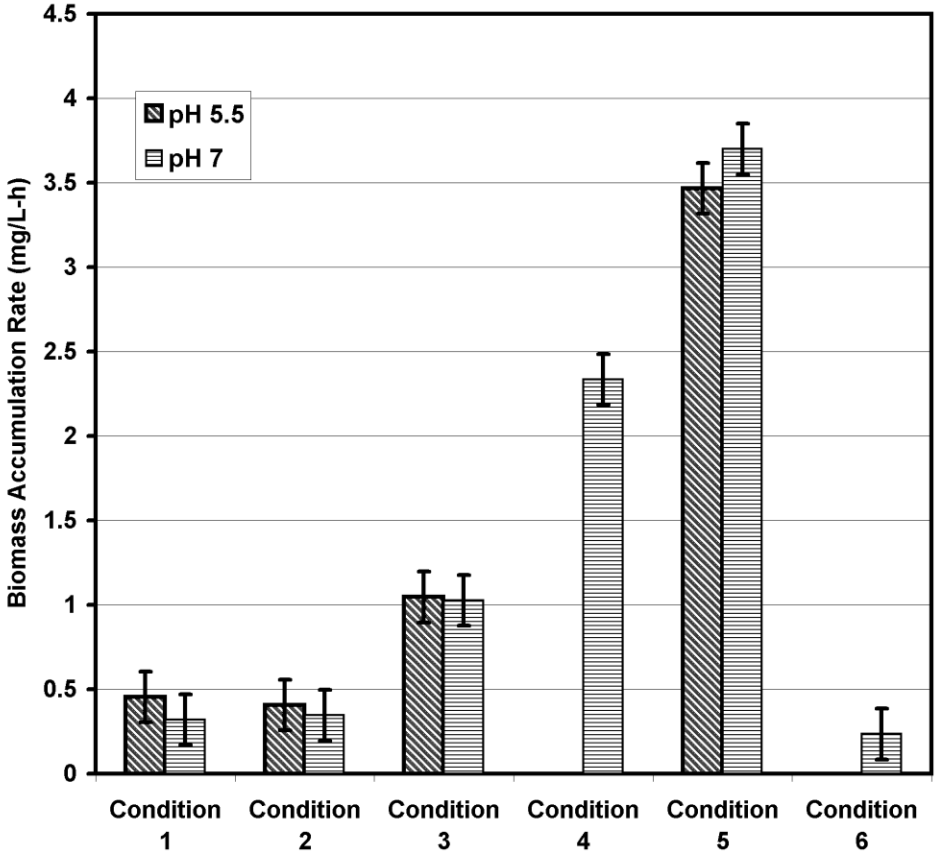

Figure 3.6. Effects of environmental parameters on growth rates of *C. vulgaris*. Conditions: 1: 0.037% CO_2 in Air, Light = 6.0 mW; 2: 10% CO_2 in Air, Light = 6.0 mW; 3: 0.037% CO_2 in Air, Light = 32.3 mW; 4: 5.0% CO_2 in Air, Light = 32.3 mW; 5: 10% CO_2 in Air, Light = 32.3 mW; 6: 20% CO_2 in Air, Light = 32.3 mW.

3.4.5. Microbial Fuel Cell Measurements

Two initial runs were performed using a yeast culture (*S. cerevisiae*, species NRRL Y-132, growing on glucose with nutrients described by Hill and Robinson, 1990) as a conventional MFC anode to generate electrons, and using methylene blue at 1900 mg/L as the mediator. In

this yeast study, a 0.02 M potassium ferricyanide solution was used in the cathodic half-cell with the cathodic reaction being the reduction of ferricyanide to ferrocyanide. Figure 3.7 shows the potential difference as a function of time following inoculation of the two cultures. For the first 20 h the cells are in their stationary phase, no active growth was observed and a 160 mV potential was maintained between the cathode and anode due to the different chemical solutions in each half cell. However, once growth commenced, the voltage difference quickly increased over a time frame of about 20 h, reaching a maximum potential difference of 340 mV in each case. This difference was maintained for 80 h at which point the experiments were stopped. The cells had reached their resting phases but were still able to maintain a high potential difference between the two half cells. It is interesting to note that the potential difference was independent of the initial glucose concentration and the final cell concentration (yield factor was 0.10 in both cases). The curve in Figure 3.7 represents an empirical sigmoid function. Sigmoidal growth behaviour of cells is a common observation. The voltage data from the two batch curves follow this sigmoidal behaviour with an average scatter of only ± 4.2% and maximum scatter of ± 15% for both yeast runs. A surge current of 230 µA was achieved for the 20 g/L glucose run (1.2 µA/mg of cells) when the cathode and anode were shorted, producing a

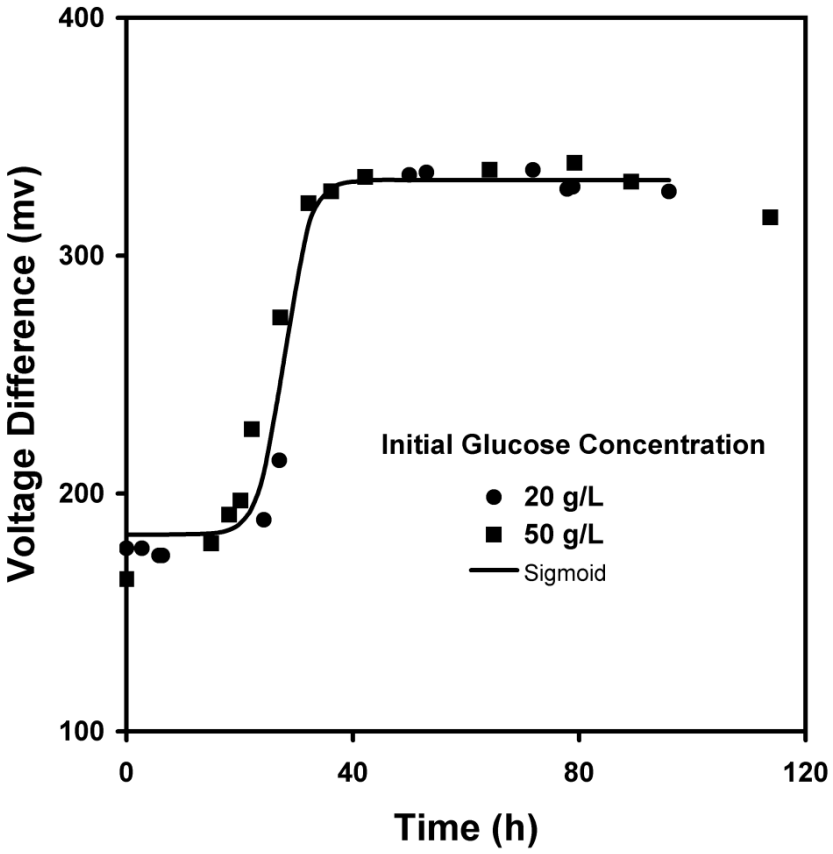

Figure 3.7. Voltage history during anaerobic growth of *Saccharomyces cerevisiae* cells on two concentrations of glucose and acting as a MFC anode (curve represents empirical sigmoid function).

maximum power level of 41 µW. Early work by Bennetto et al. (1983) demonstrated similar voltages for yeast growing anaerobically on glucose along with sustainable current generations of up to 120 µA.

Using the same culture media as for the kinetic studies, four runs were performed to measure the performance of a photosynthetic culture of *C. vulgaris* to act as an electron receptor at the cathode of a MFC using different mediator (methylene blue) concentrations. The results are plotted in Figure 3.8 where time zero represents the point of inoculation. At 10 and 50 mg/L of methylene blue (MB), the cells grew and the potential difference between the *C. vulgaris* culture and the 0.02 M ferricyanide solution increased from an initial value of 0 mV to an ultimate value of 70 mV over a period of 100 h. This time period was five times slower than for the yeast culture due to the much slower growth rate of *C. vulgaris*. The reproducibility of the algae cultures was determined by performing two runs at 50 mg/L methylene blue concentrations. The same form of Sigmoidal empirical curve as was used for yeast cell transient voltage was fit to the algae data. In this case, more scatter was observed with an average scatter of ± 11% between the data and curve and a maximum deviation of ± 25%. Cell counts were made during the 50 mg/L run, and it was observed that the cell number increased from 2.5×10^6 to 9.4×10^6 cells/mL over a period of 130 hours. This represents a doubling time in cell mass of 68 hours. During the kinetic runs, at low light and low CO_2 conditions (air at 0.037% CO_2), the doubling time was 30 hours during the initial phase of the *C. vulgaris* cultures (time less than 50 hours in Figure 3.5). It is likely that the low quantities of light radiation able to penetrate into the 50 mg/L solution of MB limited the ability of *C. vulgaris* to grow. When the MB concentration was further increased to 100 mg/L, Figure 3.8 shows that the potential difference between the cathode and anode actually dropped from 0 to -40 mV and then slowly increased to -20 mV after 150 h of operation. The cell count had increased more slowly than for the 50 mg/L run, from the inoculation level of 2.5×10^6 to 7.6×10^6 cells/ml over 150 h of operation, likely due to the lower amount of light that could penetrate through the more concentrated MB solution. At 800 mg/L MB, a steady drop in potential difference between the two electrodes occurred, reaching -100 mV in 125 h of operation, and it was observed under the microscope that cell count were continuously declining due to cell death. At this concentration, less than 1% of the 420 nm light could penetrate 1 cm into the culture solution. It appears that cell death may release metabolites into the media that causes the solution chemistry in the cathode to change significantly causing

the initial potential difference between the cathode and anode to drop. During the 50 mg/L MB run, a surge current of 28.4 µA was measured when the cell count was 9.4×10^6 cells/mL. This represents a power of 2.0 µW, or based on the cathode surface area, about 2.7 mW/m^2, similar to the value of 2.0 mW/m^2 measured by Min et al. (2005) for an anodic half-cell system also using a salt bridge. Using the average cell diameter of 5.7 µm and moisture content of 60%, an electron uptake of approximately 1.0 µA/mg dry weight of cells was achieved, similar to the electron generation rate of the yeast cultures. But to produce *C. vulgaris* biomass at the growth rate of this run, a net electron uptake rate of 19 µA/mg dry weight of cells would be required, indicating that only about 5% of the electron uptake rate came from the action of the MFC while the rest was due to photosynthesis.

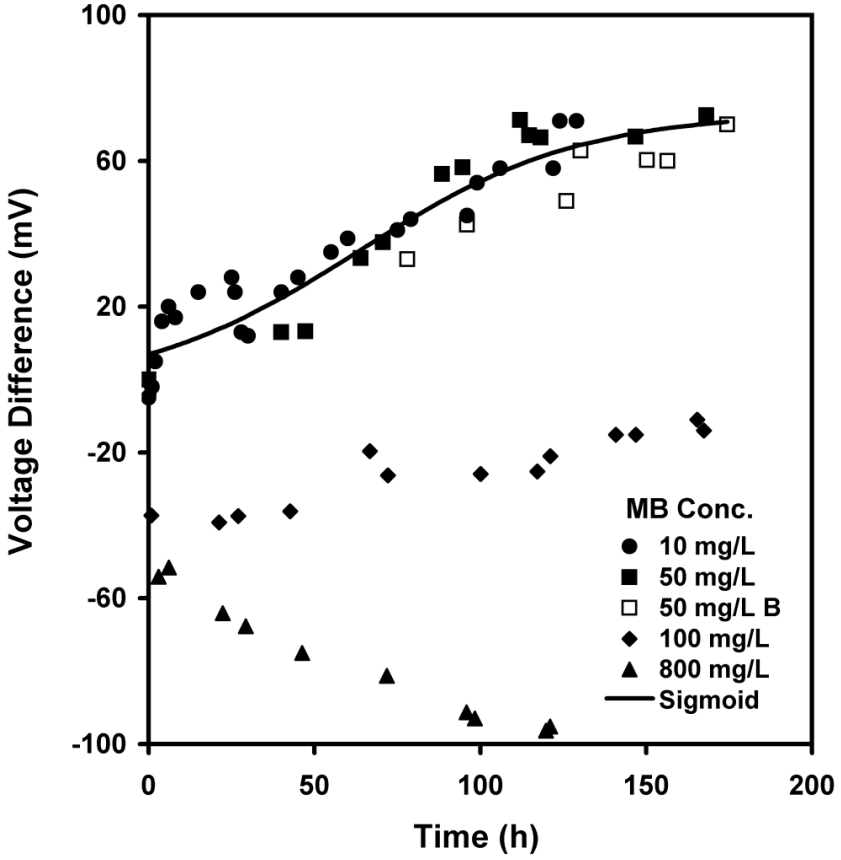

Figure 3.8. Effect of methylene blue concentrations on voltage histories for *Chlorella vulgaris* cells growing on CO_2 in air at high radiant flux and acting as a MFC cathode (curve represents empirical sigmoid function).

Although several anodic MFCs report much higher power levels, this is due primarily to the very high and artificial cell concentration used in those studies (pastes of microbial cells were

immersed in buffer solutions). In our work, a natural culture was used with much lower cell concentrations resulting in much lower current flows. A superior bioreactor design could significantly increase the current measurements either by generating higher *C. vulgaris* cell densities or by use of greater electrode areas.

Finally, a second mediator was tested to see if an improvement in voltage or current could be achieved. But the mixture of 200 mg/L of thionine blue along with 2.0 g/L of $FeSO_4$ (to keep the thionine blue in an oxidized state in the cathode solution) proved to be toxic. After 70 hours of operation, *C. vulgaris* cell count had declined and no change in potential between the anode and cathode was observed. Further studies at other concentrations or using other mediators are planned to help increase the potential difference and current flow when using *C. vulgaris* as the electron acceptor in the cathode chamber of a MFC.

3.5. Conclusions

A novel application of a photosynthetic culture of *C. vulgaris* cells has been shown to act as a suitable cathode chamber in a microbial fuel cell and to simultaneously remove CO_2 from the atmosphere. In addition, *C. vulgaris* growth has been optimized by increasing radiant flux to 32.3 mW falling on the surface of a bioreactor containing 500 mL of culture solution, and by enriching the concentration of CO_2 in the feed air to 10% by volume. Maximum cell growth rates of 3.6 mg/L-h were achieved at these conditions. The photosynthetic growth of *C. vulgaris* on CO_2 produced an ultimate potential difference of 70 mV (using a potassium ferricyanide solution as the oxidant) and current levels of 1.0 µA/mg cell dry weight were achieved, which corresponded to a power density of 2.7 mW/m^2 of electrode surface. This research suggests that a complete microbial fuel cell could be constructed with both the anode and cathode relying on the growth of microorganisms. Under proper operating conditions, electron flow could be sustained to continuously generate a potential voltage and current as an alternate form of energy generation technology.

Chapter 4

4. Microbial Fuel Cell with a Photosynthetic Microalgae Cathodic Half Cell Coupled to a Yeast Anodic Half Cell

A similar version of this chapter has been accepted for publication in the journal Energy Sources, Part A: Utilization, Recovery, and Environmental Effects. This version is considerably longer and includes more experimental details and results:

Powell, E.E., Bolster, J.C., Hill, G.A. and R.W. Evitts "Microbial Fuel Cell with a Photosynthetic Microalgae Cathodic Half Cell Coupled to a Yeast Anodic Half Cell", Energy Sources Part A: Recovery, Utilization, and Environmental Effects, Accepted June 2009.

The topics covered in this chapter have also been included in one short paper:

Powell, E.E., Bolster, J.C., Hill, G.A. and R.W. Evitts "Complete Microbiological Fuel Cell: A Photosynthetic Cathode Coupled to a Fermentative Anode", Proceedings of the Clean Technology 2008 Conference, Boston, MA, USA, June 1-4, 2008.

The work discussed in this chapter was also included in paper presentations at the following conferences:

Powell, E.E., Bolster, J.C., Hill, G.A. and R.W. Evitts "Complete Microbiological Fuel Cell: A Photosynthetic Cathode Coupled to a Fermentative Anode", Clean Technology 2008 Conference, Boston, MA, USA, June 1-4, 2008.

Powell, E.E., Bolster, J.C., Hill, G.A. and R.W. Evitts, "Coupled Microbiological Fuel Cell: A Photosynthetic Cathode Coupled to a Fermentative Anode", AIChE Annual Meeting, Philadelphia, PA, USA, November 16-19, 2008.

Contribution of Ph.D. Candidate

Experiments were planned and supervised by Erin Powell, and performed by summer student John Bolster. Gordon Hill and Richard Evitts provided guidance in planning the experiments. The experimental results were analyzed by Erin Powell. The submitted manuscript was written by Erin Powell, with Gordon Hill and Richard Evitts providing editorial assistance.

Contribution of this paper to overall study

Chapter 3 demonstrated the potential for *Chlorella vulgaris* to act as the biological acceptor in the cathodic half cell of a microbial fuel cell (MFC). A secondary goal of the Ph.D. research is to produce by- products with the microalgae cultivation, in addition to the CO_2 consumption. This phase of the research demonstrates that this novel photosynthetic cathodic half cell can be coupled to a microbial anodic half cell, creating a completely microbiological fuel cell. This makes electricity generation a possible by-product of *C. vulgaris* cultivation for CO_2 consumption. In this case a typical yeast anodic half cell was employed in the experimental study, thus resulting in the possibility of integrating this type of coupled fuel cell into new or existing bioethanol plants.

Additional Details Included in this Chapter

Several Figures were eliminated from the final accepted draft of this manuscript due to the length constraints of the journal Energy Sources. These are Figures 4.1, 4.4, and 4.6, and they have been reintegrated into this chapter. The discussion of the colour change phenomenon (Section 4.4.6) observed during the experimental testing that is included in this chapter was also not part of the final accepted version of the manuscript.

4.1. Abstract

A recently developed photosynthetic cathode has been coupled to a fermentative anode to produce a complete microbial fuel cell. The photosynthetic organism *Chlorella vulgaris* was employed as the electron acceptor in the cathodic half cell with the yeast strain *Saccharomyces cerevisiae* serving as the electron donor in the anodic half cell. Loading effects and the effect of changing culture conditions on fuel cell operation is reported. For instance, an increase in output was achieved with the addition of supplemental glucose to the anodic half cell and the enriching of the feed air bubbled into the cathode half cell with 10% CO_2.

4.2. Introduction

The increasing demand for energy combined with decreasing supplies has led to great interest in alternate energy production technologies (Kouroussis and Karimi, 2006) like the microbial fuel cell (MFC). The MFC generates electrical current from the oxidation – reduction reactions that occur within living microorganisms (Chae et al., 2008). A wide range of fuel cell designs and microbial species have been studied with power densities ranging from 10^{-1} to 10^{3} mW/m^2 of electrode surface area (Rabaey and Verstraete, 2005; Kim et al., 2007a). Existing studies have focused primarily on microbial growth for production of electrons at the anode, principally by the oxidation of organic compounds, and employing a variety of designs, microorganisms, and substrates (Rabaey et al., 2003; Liu et al., 2004; Oh and Logan, 2005). The current output pattern of the MFC changes dramatically when microbial culture conditions are altered, indicating that MFC performance can be manipulated in this manner (Choi et al., 2004).

Figure 4.1 (a) demonstrates the same general processes that occur at the anode of all typical MFCs. The oxidation – reduction reactions inside the cell release electrons. Mediator chemicals can scavenge these electrons by penetrating into the microbial cell in their oxidized state, bonding with the electrons, and exiting in their reduced state. Once released into the fermentation media, the mediator spontaneously oxidizes and releases the electrons at the anode, where they enter the electric circuit. To complete the electrical cell, most microbial fuel cell

studies use an electrochemical reduction reaction in the cathodic half cell, such as ferricyanide to ferrocyanide. Microorganisms have been employed in the cathodic half cell of MFCs to regenerate ions for the electrochemical reaction (He and Angenent, 2006; Prasad et al., 2006), and more recently, have also been employed in MFCs as the electron acceptor in bacterial biocathodes (Rhoads et al., 2005; He and Angenent, 2006; Clauwaert et al., 2007; Jia et al., 2008; Rabaey et al., 2008; Virdis et al., 2008). Powell et al. (2009b) have shown that a photosynthetic microbial culture can act as a biological electron acceptor at the cathode. Figure 4.1 (b) shows that in this configuration, electrons are transferred into the media at the cathode surface and reduce the mediator from its oxidized state. The mediator then penetrates into the cell where it becomes oxidized and releases electrons to the growing cells. The cells use these electrons in their metabolic pathways with the net result of converting CO_2 into oxygen and biomass according to the following equation:

$$6CO_2 + 12H^+ + 12e^- \xrightarrow{light} C_6H_{12}O_6 - (biomass) + 3O_2. \quad (4.1)$$

CO_2 is the only carbon source for growth and the cathode remains at the same oxidation potential (electrically neutral) and there is no H_2 buildup over time.

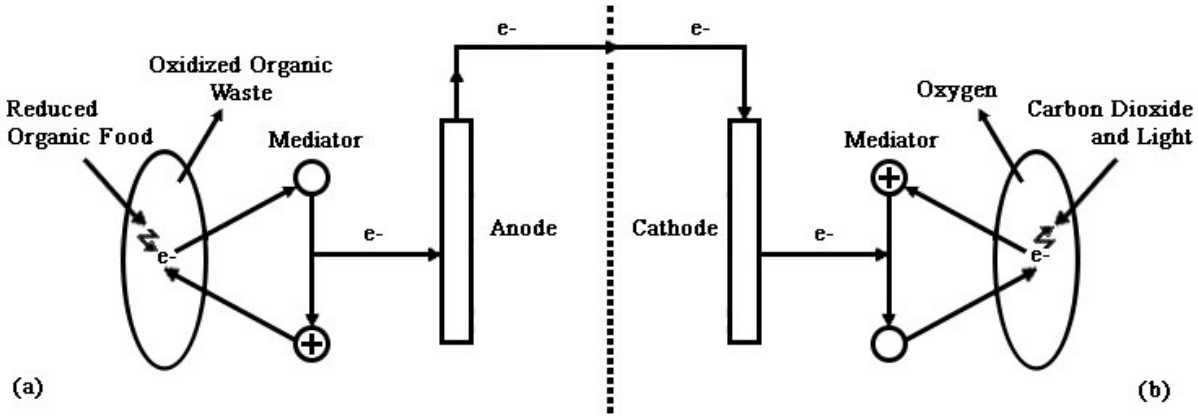

Figure 4.1. Schematic of electron flow in the completely biological microbial fuel cell: (a) anodic release of electrons by consuming organic compounds, (b) cathodic capture of electrons by photosynthetic growth on CO_2.

Operational data for the coupled microbial fuel cell system is presented in this investigation. Sugars are necessary to activate the anode culture while exposure of the cathode culture to light is also a requirement. Since CO_2 generated at the anode can be used as the carbon

source in the photosynthetic cathode, no external carbon source is required to activate the cathode culture.

4.3. Materials and Methods

Chlorella vulgaris was purchased from Carolina Biological Supply (Burlington, North Carolina, Catalogue No. 15-2075) and grown on a modified Bolds Basic media as in Powell et al. (2009b) maintained at pH 6.8. The only carbon source in the cathode half cell during operation is CO_2. The *Saccharomyces cerevisiae* strain NRRL Y132 was purchased from the U.S. Department of Agriculture, and grown using media formulated earlier (Hill and Robinson, 1990) and adjusted to pH 4.0. The yeast culture received no carbon food source (glucose) other than the 20.0 g/L in the initial growth media until otherwise stated in the supplemental glucose feeding study discussed in the results.

The experimental MFC setup (Figure 4.2) consisted of two modified 2 L Kontes culture vessels, one to house the yeast and the anode, and the other for the algae and the cathode. The two vessels were joined by a glass bridge with a NAFION 112 membrane separating the half cells and allowing proton exchange. Beveled glass flanges containing o-ring gaskets were securely clamped to ensure a leak-free system around the membrane. The complete apparatus was placed on two VWR Dyla-Dual stir plates and mixed at 150 rpm. Each vessel was filled with 2 L of its respective media. 200 mg/L of methylene blue (MB) and 93 mg/L 2-hydroxy-p-naphthoquinone (HNQ) were added to the anode and cathode sides, respectively, to act as chemical mediators. Glassy carbon graphite electrodes, with 6.35×10^{-3} m diameter and 8.02×10^{-2} m submerged length, were used as the electrodes in both half cells, and were connected via a Fluke 189 True RMS Multimeter to enable voltage readings. A GE 26 W helical fluorescent bulb was set at 5cm (at the nearest point, Powell et al., 2009b) from the cathode half cell on a timed 16 hour per day light cycle to enable photosynthesis. Airflow of 2.92×10^{-6} m^3/s was blown across the top of both cultures in the coupled fuel cell, providing oxygen to the yeast for cell propagation and synthesis of compounds to maintain cell membrane integrity (Gibson et al., 2007; O'Connor-Cox and Ingledew, 1990) and oxygen and CO_2 to the algae. Experiments were conducted at room temperature, 22.5 ^oC.

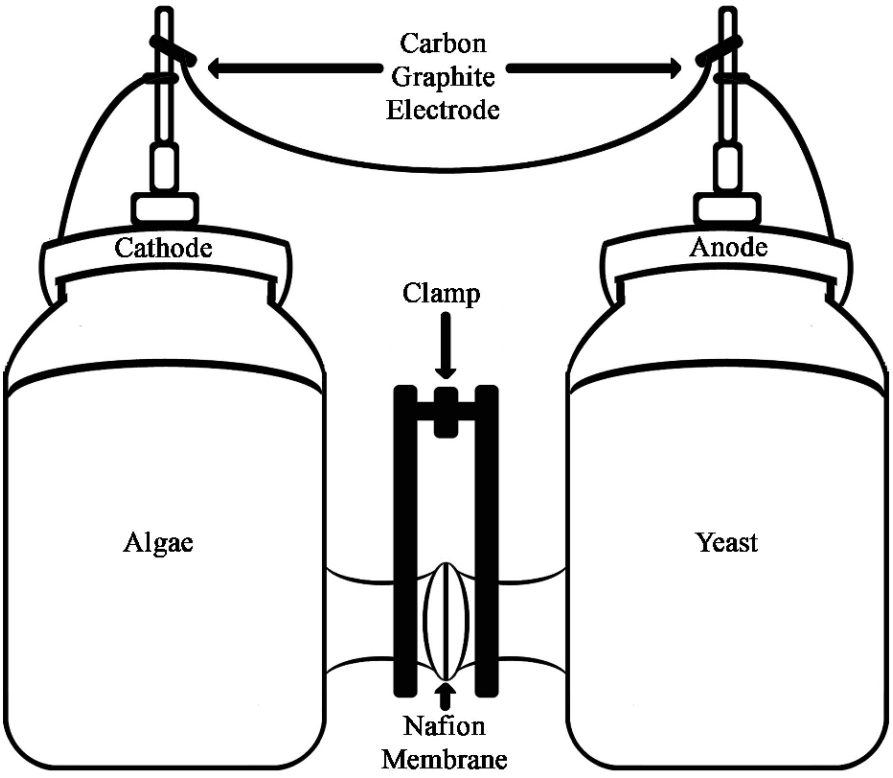

Figure 4.2. Schematic of coupled MFC experimental apparatus.

Fuel cell operation began with 5 mL inoculation of the respective microbial cultures into the media at each half cell. Voltage readings were taken using electronic data logging by the Fluke Multimeter, stored, and analyzed by the computer using FlukeView Forms software. Daily pH monitoring was performed using an IQ240 pH meter. Biomass cell densities were determined daily by microscopic cell counts counted over a specific volume, with samples taken in triplicate, and then averaged. Cell counts were converted to dry weights using average cell diameters determined previously for *C. vulgaris* (Powell et al., 2009b) and published for *S. cerevisiae* (Bailey and Ollis, 1986), and representative microbial cell densities (Bailey and Ollis, 1986) for both species. Half cell voltages of the system were obtained using a Saturated Calomel Electrode placed in close proximity to the anodic graphite electrode and a potential was measured across the electrodes. Resistances were applied to the system by an OHMITE Ohm-Ranger resistance box, connected via electric wires to each electrode. Ethanol concentrations in the anodic half cell were determined by gas chromatography according to Hill and Robinson (1990).

Error bars on voltage, power, and cell concentrations are presented on all figures since multiple measurements were taken (between three and fifty) and averaged into a single data point. All are presented at a 95% confidence level. A duplicate run was performed of a loading experiment at 5000 Ω (see Figure 4.3) as a measure of the reproducibility of the results. A maximum reproducibility error of ± 6.4 % was observed between the two runs.

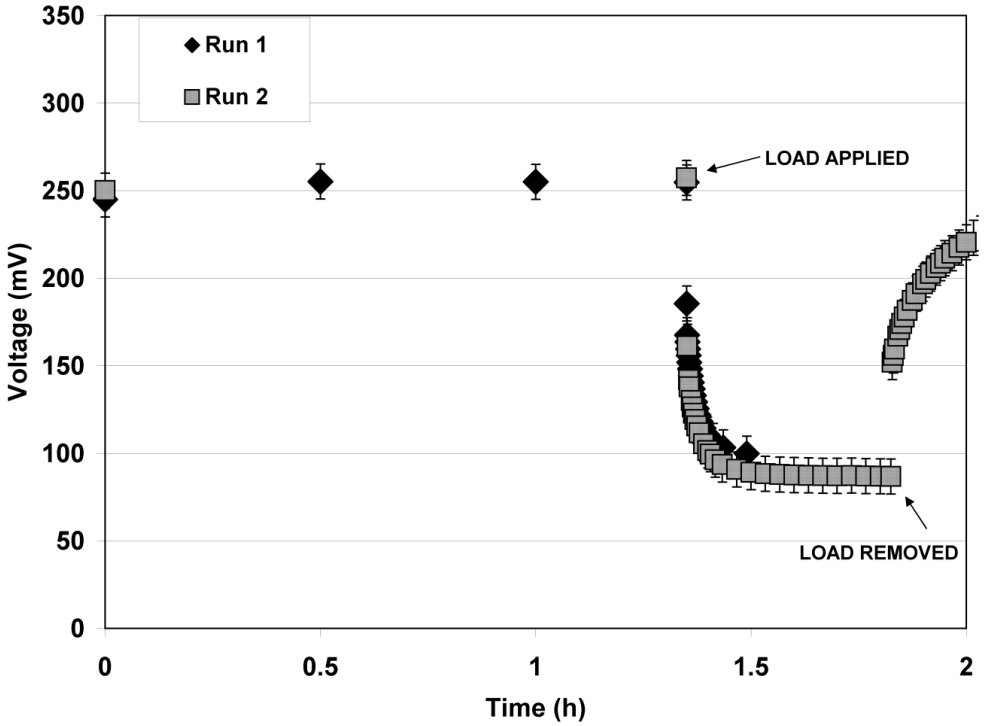

Figure 4.3. Duplicate runs of loading experiment at 5000 Ω (anode = glucose 20g/L initial, cathode = CO_2 atmospheric (0.037%)). Load was applied at 1.35 h and released at 1.82 h.

4.4. Results and Discussion

4.4.1. Mediator Selection

The use of a variety of mediator chemicals has been reported (Park and Zeikus, 2000; Rhoads et al., 2005) to improve the capture and transport of electrons. Before evaluating the coupled MFC, the operation of the photosynthetic cathodic half cell was tested with an alternative chemical mediator. In earlier work (Powell et al., 2009b), MB was found to be a suitable chemical mediator for algae growth. Experiments using the *C. vulgaris* cathodic half

cell coupled to an electrochemical oxidation reaction at the anode, as with previous work (Powell et al., 2009b), were performed using HNQ at various concentrations as an alternative to MB. HNQ has been used with several bacterial microorganisms (He and Angenent, 2006; Rhoads et al., 2005) and by Bennetto et al. (1984) with *C. vulgaris*. The optimal concentration of HNQ in the cathode medium was determined to be 93 mg/L. The earlier transient voltage values (Powell et al., 2009b) generated during batch growth using an optimum 50 mg/L MB are compared to experimental values obtained in this work using 93 mg/L of HNQ (Figure 4.4). Using HNQ enhanced the *C. vulgaris* growth rate by a factor of 1.7 resulting in an algae culture that is denser by a factor of 1.5, and a higher voltage of 100 mV, compared to only 72 mV with the use of MB. This was likely due to HNQ allowing greater light penetration into the medium, and promoting faster photosynthetic growth. HNQ was therefore used as the chemical mediator on the cathode side of the coupled MFC for all subsequent experiments.

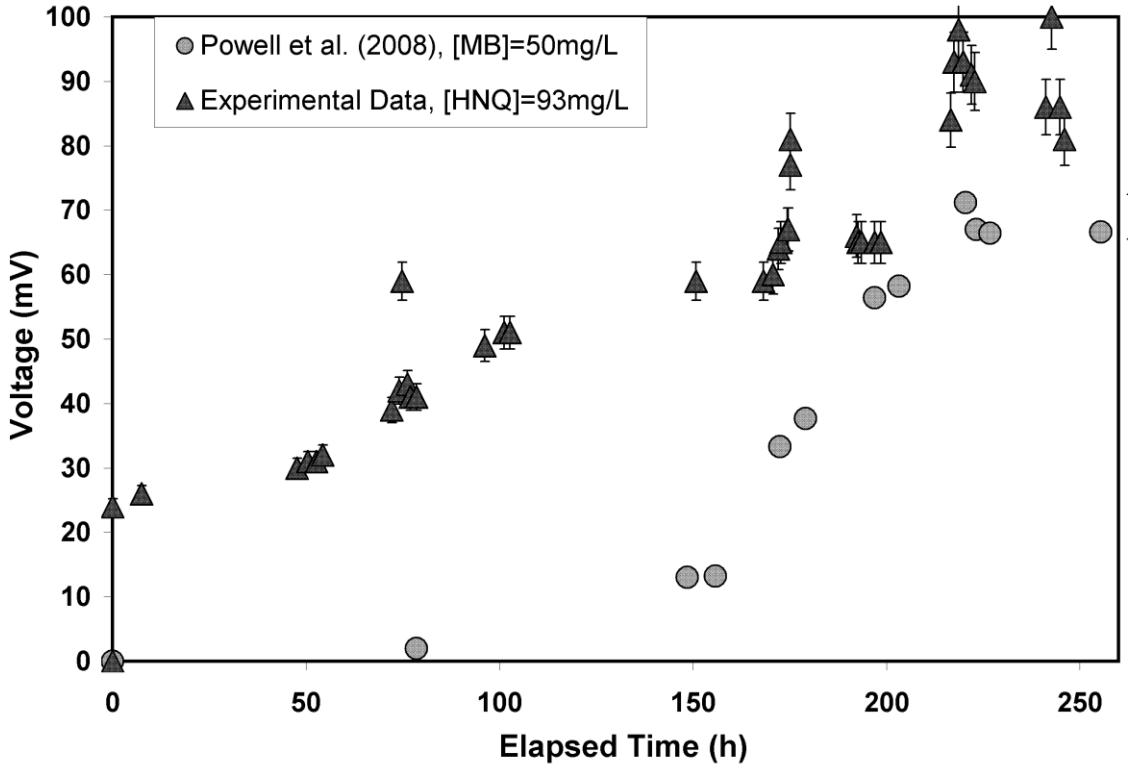

Figure 4.4. Transient open circuit voltage during growth of *C. vulgaris* in a cathodic half cell (anode = ferricyanide oxidation reaction, cathode = CO_2 atmospheric (0.037%)). (MB = methylene blue as mediator, HNQ = 2-hydroxy-p-naphthoquinone as mediator).

4.4.2. Coupled Fuel Cell: Loading Effects and Production of Biomass

Before experiments were performed using cell cultures, a blank run was completed using only the fuel cell apparatus and chemical mediators to ensure that it was not simply the difference in chemical environments that created the current flow and observed voltage. After a very brief sudden spike in voltage immediately after connecting the two half cells, the voltage dropped quickly in the first 30 minutes and then remained negative at -5 mV over a further 24 hours. At this point, culture experiments were begun.

Loading effects on the coupled MFC system were analyzed systematically by placing various resistances in the closed circuit and measuring the voltage as shown in Figure 4.5. Each load was placed in the circuit for a duration of 30 min, and the average recovery time was 22.8 ± 2.1 min. Current is directly related to voltage by Ohm's Law for a given load placed in the circuit, as long as the electrode is not polarized. The known resistances and measured voltages were used to determine the power (per electrode surface area) generated by the fuel cell, shown in Figure 4.5, and presented again versus voltage and current in Figure 4.6. A maximum power

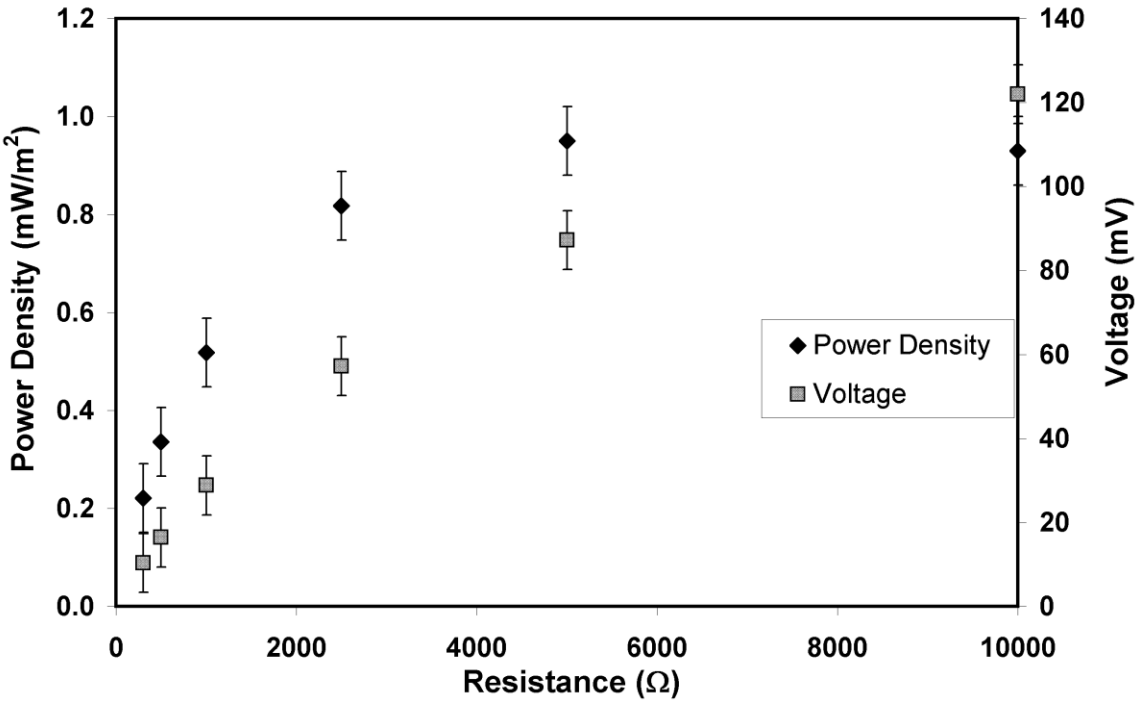

Figure 4.5. Voltage and power output as a function of applied load for the coupled MFC (anode = glucose 20g/L initial, cathode = CO_2 atmospheric (0.037%)).

of 0.95 mW/m^2 of electrode surface area was observed at an applied load of 5000 Ω when a voltage of 90 mV was measured. The power density remains almost unchanged with larger loads. The peak power density of 0.95 mW/m^2 observed in this study was lower than many reported values (Liu and Logan, 2004; Min et al., 2005a; Min et al., 2005b) for purely anodic MFCs, although these vary greatly with design. For coupled MFCs with biocathodes, Jia et al. (2008) reported a power output comparable to that observed in this study. Current flows reached up to 35 µA (Figure 4.6), or on a cell basis, 5.8 x 10^{-2} µA/mg algae and 5.8 x 10^{-3} µA/mg yeast.

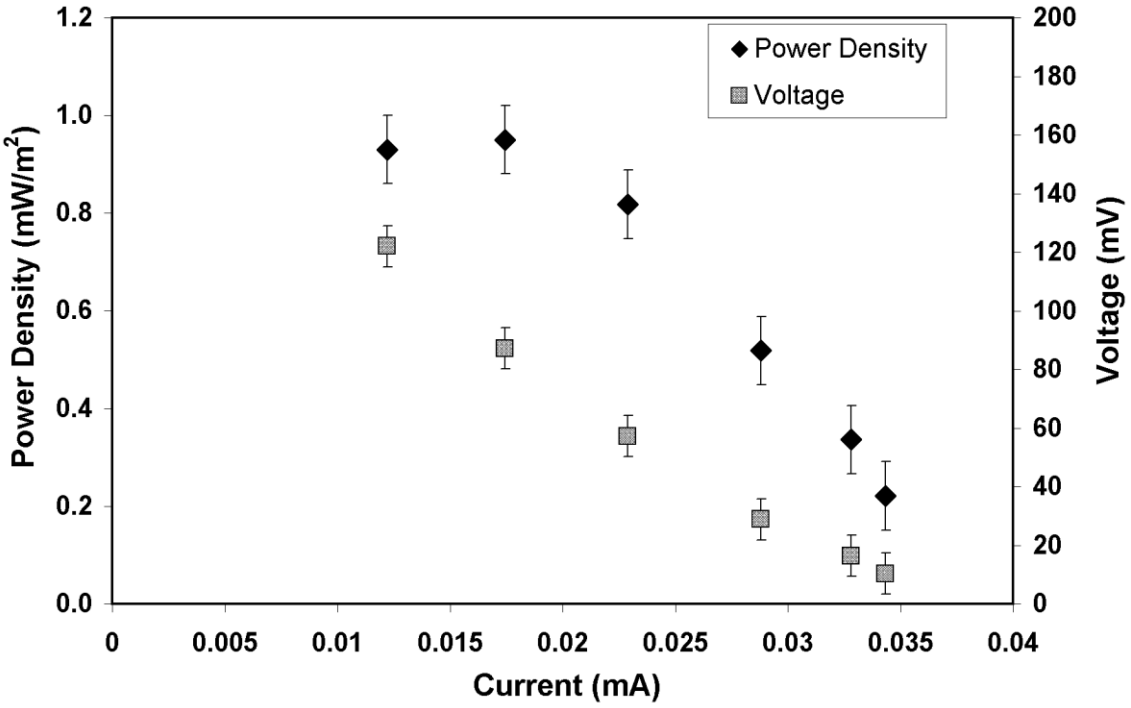

Figure 4.6. Power and voltage as a function of total current for the coupled MFC (anode = glucose 20g/L initial, cathode = CO_2 atmospheric (0.037%)).

Since the coupled system is entirely biological, it produces biomass at both electrodes. Consistent average cell densities were observed during the fuel cell measurements described above. *C. vulgaris* reached an average level of 300 mg/L, while *S. cerevisiae* was measured to be 3025 mg/L. A slower *C. vulgaris* growth rate relative to yeast is likely the cause of the lower algae biomass density, and may be contributing to the reduced voltages and currents observed, in particular when compared to the much faster electrochemical reduction reactions generally used instead at the cathode in MFCs. The lower power densities observed with smaller loads can also

be attributed to the slower growth rate of *C. vulgaris* relative to that of *S. cerevisiae*.

4.4.3. Coupled Fuel Cell: Supplemental Addition of Glucose

The addition of supplemental glucose to the coupled MFC was subsequently studied as it is the growth substrate of the yeast cells. After the initial concentration of 20 g/L of glucose was added to the medium of the anode half cell, and after an initial period where the biological system adjusted to the presence of the sugar, an increase in voltage with time was observed, as shown in Figure 4.7.

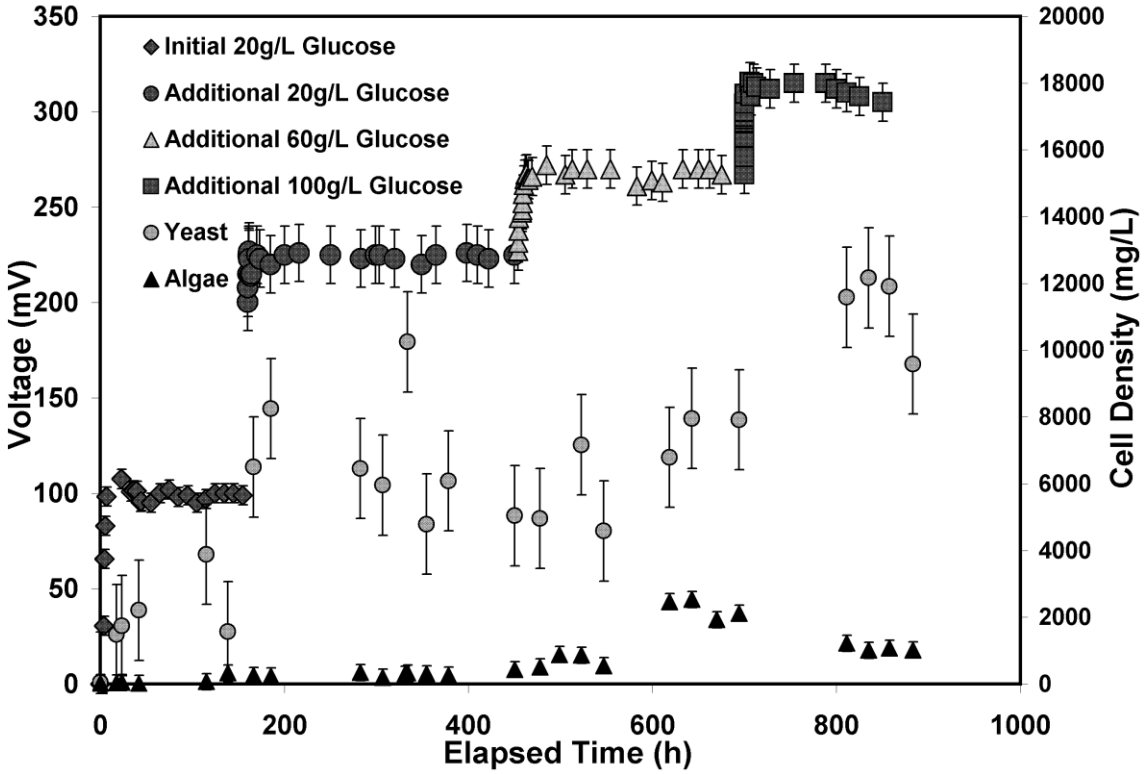

Figure 4.7. Effect of supplemental glucose addition on open circuit voltage and cell densities for the coupled MFC (cathode = CO_2 atmospheric (0.037%)).

Further glucose additions were made up to a total of 200 g/L (20, 60, and 100 g/L). Figure 4.7 shows the transient open circuit voltages for each addition. A closed circuit voltage was also measured under a 5000 Ω load at the 20 g/L and 60 g/L glucose additions, which caused the potential to drop to 100 mV in both cases (data not shown). A peak, maximum

voltage was observed to be 315 mV at the highest glucose concentration. The transient cell densities for both yeast and algae over the course of the glucose study are also shown in Figure 4.7. The maximum cell densities attained were 2500 mg/L algae and 12500 mg/L yeast.

The circuit was closed for a 24 h period until the voltage dropped to zero and the fuel cell was completely drained. When the circuit was subsequently opened, the potential difference between the two cells remained at zero volts. Glucose at 20 g/L was then added to the anode half cell and the voltage returned to the previous level of 100 mV. This confirms that yeast growth is the driving force for the coupled photosynthetic MFC and sugar addition serves as a way to renew a drained MFC.

The results of the supplemental glucose study can be explained by the fact that the potential to release electrons is proportional to yeast cell concentration, and as cells grow exponentially, the voltage increases exponentially. Eventually however, this exponential growth due to excess food ends, and the cells move into a stationary phase and the open circuit voltage then remains constant. An examination of the change in cell densities in the two half cells with each step-wise glucose addition, relative to the increase in open circuit voltage in Figure 4.7, shows a direct link between yeast cell growth and voltage, with subsequent peaks in cell density after supplemental substrate is added at 170 h and after 700 h. All glucose is metabolized by the yeast during batch reactions with a yield of 0.099 g cells/g glucose as reported earlier (Hill and Robinson, 1990). The algae growth in the cathodic half cell also increased with addition of substrate to the anode, although gradually and with minimal sudden changes. *C. vulgaris* growth is enhance because the increased yeast growth at the anode results in increased electrons reaching the cathode. These electrons are then available to be used in increased photosynthetic biomass production by the algae cells. Open circuit voltages observed in this study, up to 315 mV, approach those reported for yeast and bacteria based anodic MFCs (Bennetto et al., 1983; Chiao et al., 2003; Rabaey and Verstraete, 2005), and are comparable to coupled MFCs with bacterial biocathodes (Clauwaert et al., 2007; Virdis et al., 2008).

4.4.4. Coupled Fuel Cell: Ethanol Production

The yeast on the anode side of the MFC produces ethanol, another fuel source. The ethanol present in the yeast medium was measured during the addition of glucose at various

points during the growth/decay cycle. After an additional 60 g/L glucose was added (100 g/L total glucose), the ethanol produced was measured at 31 g/L, or 100%, of the maximum theoretical ethanol yield eight hours after addition, and decreased to 87% of the theoretical yield 24 h later. After adding a further 100 g/L of glucose (200 g/L total glucose), the percentage of the theoretical ethanol produced was only 58%. The reduction in ethanol yield may have been caused by the ability of the cells to metabolize ethanol as a carbon source after being starved before the addition of further glucose. A reduction in ethanol production by yeast may also be observed due to the operation of the coupled MFC, as when electrons are transferred to the anode they are not available for the reduction of pyruvate to ethanol (Slaughter, 2003).

4.4.5. Coupled Fuel Cell: Effect of Carbon Dioxide Addition

In order to test the effect of algae substrate enrichment, a 10% CO_2 enriched stream was bubbled into the cathode. This corresponds to the optimum CO_2 concentration observed earlier for maximum *C. vulgaris* growth (Powell et al., 2009b). The voltage was first measured when only air was bubbled into the cathodic half cell, instead of blown over the top, and then again when air was bubbled in with 10% CO_2 added. The results, where the unenriched run refers to bubbling air into the cathodic half cell and the enriched run refers to 10% CO_2 being added to the bubbled air, are shown in Figure 4.8, along with the increase in algae cell density in the cathodic half cell. The maximum cell density was 780 mg/L of *C. vulgaris*.

It is evident that bubbling unenriched feed air into the cathodic half cell produced a greater open circuit voltage, 173 mV, than when the air was blown over the top of the media, which produced an open circuit voltage of only 100 mV, as is seen in Figure 4.7. Open circuit voltages of up to 260 mV were recorded when the *C. vulgaris* cells were supplied with 10% CO_2, which is 1.5 times larger than the case where unenriched air was bubbled through the medium.

The improved open circuit voltage observed with the use of the bubbler is due to improved mass transfer of CO_2 into the media. The subsequent addition of CO_2 leads to enhanced *C. vulgaris* growth, as confirmed by Powell et al. (2009b), which appears to be directly related to increased voltage. This is supported by the corresponding increase in *C. vulgaris* cell density in the cathodic half cell as CO_2 is added. Biomass in a growing state produces higher voltage than resting cells. This is observed with the addition of substrate, either glucose or CO_2,

by examining the shape of the cell density curves relative to the transient voltages in Figures 4.7 and 4.8. The ability of the cathode side of this MFC to consume CO_2 provides for the possibility of additional environmental benefits. The photosynthetic algae on the cathode side of the MFC will also be able to consume the CO_2 produced by the yeast on the anode side, making this a CO_2 neutral technology.

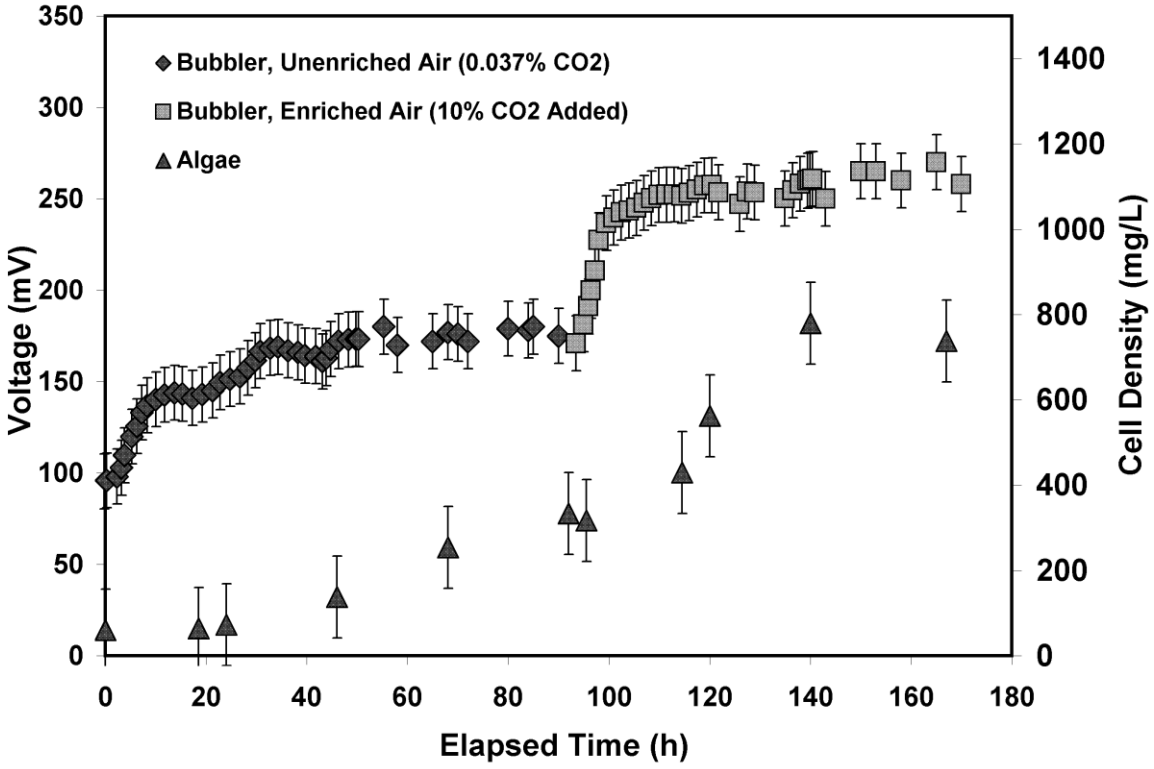

Figure 4.8. Effect of bubbler implementation and CO_2 addition on the open circuit voltage and algae cell density in the coupled MFC (anode = glucose 20g/L initial).

During the CO_2 enrichment study, the voltage of each half cell was determined separately with reference to a Saturated Calomel Electrode (SCE). The anode and cathode half cell voltages were found to be -203 mV_{SCE} and 62 mV_{SCE}, respectively, corresponding to a cell potential of 265 mV. The steady state open circuit potential measured immediately after these measurements was found to be 270 mV. The small discrepancy between these potential differences was within the uncertainty of the reference electrode.

4.4.6. Coupled Fuel Cell: Colour Change Phenomenon

An interesting phenomenon was noted on the anode (yeast) side of the MFC. A colour change was observed during different stages of operation. As the yeast were actively growing and generating electricity, the dark navy blue colour of the MB changed to an off-white colour. When the cells stopped growing and the voltage stopped increasing, the colour changed back to blue. As the steady state voltage was reached for each of the runs and the cells entered a resting stage, the solution remained a light blue. If the voltage dropped off completely, or as the yeast began to die off entirely within the fuel cell, the colour returned to the original dark navy blue colour. MB, as the chemical mediator in the anodic half cell, acts as a visible indicator of the health of the yeast in the medium. This corresponds to the findings of Painting and Kirsop (1989) who found that viable yeast cells decolourize methylene blue due to enzyme activity by oxidation-reduction, whereas dead cells do not. The dye absorbed by the cell membranes of the healthy growing yeast is re-released back into solution as the membranes deteriorate and the cells begin to die. This interaction between the yeast microbes and the MB mediator on the anode side can serve as a useful tool for the MFC operator in judging the state of the yeast cells.

4.5. Conclusions

The chemical mediator 2-hydroxy-p-naphthoquinone, was demonstrated to be superior to methylene blue for use in a cathodic fuel cell with *C. vulgaris*, likely due to greater light penetration into the medium,

The peak power density of 0.95 mW/m^2 observed in this study demonstrates the feasibility of a coupled MFC, which includes a photosynthetic microalgae cathodic half cell. MFCs vary greatly with design, however, for coupled MFCs with biocathodes, comparable power outputs have been reported. The peak open circuit voltage of 315 mV observed in this study approaches those reported in the literature for yeast and bacteria based anodic MFCs and is comparable to coupled MFCs with bacterial biocathodes.

Significantly more yeast cells are produced in the anode half cell than in the algae culture. The slower *C. vulgaris* growth rate relative to yeast is likely limiting this MFC design, in particular when compared to the fast electrochemical reduction reactions generally used at the

cathode in typical MFC designs exhibiting greater power outputs.

Microbial biomass, commercially valuable products, and ethanol can be harvested from the coupled photosynthetic MFC as presented in this study. Therefore, in addition to electricity generation, the coupled MFC remains a source of additional valuable byproducts.

By operating continuous flow bioreactors, it could be possible to have the fuel cell continuously producing biomass by filtering biomass as it exits the bioreactor, while simultaneously generating electricity. This may also allow the fuel cell to produce higher voltages by keeping the biomass in a continuously growing state, which produces significantly higher voltage than resting cells.

The addition of supplemental glucose to the MFC significantly improved the electrical output of the system and sugar addition serves as a way to renew a drained MFC. An examination of the change in cell densities in the two half cells with each step-wise glucose addition, relative to the increase in open circuit voltage, showed the direct link between yeast cell growth and cell output.

The algae growth in the cathodic half cell also increased with addition of substrate to the anode, although very slowly. The increased yeast growth results in increased electrons reaching the cathode which are used in increased photosynthetic biomass production by the algae cells.

The improved open circuit voltage observed with the use of the bubbler is due to improved mass transfer of carbon dioxide into the media for use by the algae. The subsequent addition of CO_2 leads to enhanced *C. vulgaris* growth and fuel cell output.

The ability of the cathode side of this photosynthetic MFC to consume CO_2 provides for the possibility of additional environmental benefits, in addition to producing power. Carbon dioxide is the primary greenhouse gas, and with 740 megatonnes being emitted into the atmosphere annually (Environment Canada, 2006), it is a major environmental concern. Excess atmospheric greenhouse gases are thought be the cause of climate change. The complete MFC could be used as a bioremediation technology, by converting carbon dioxide to oxygen as part of its operation. The photosynthetic algae on the cathode side of the MFC will also be able to consume the CO_2 produced by the yeast on the anode side, making this a unique carbon dioxide neutral "green" technology.

Chapter 5

5. Modeling *Chlorella vulgaris* Growth in an External Loop Airlift Photobioreactor: Light Distribution and Carbon Dioxide Consumption

The manuscript provided in this chapter is very similar to the one submitted to the Canadian Journal of Chemical Engineering. The version provided has been expanded to discuss other growth equations and solution methods that were considered which differ from the one presented in the submitted manuscript.

Powell, E.E., Hill, G.A., and D. Sasi, "Modeling *Chlorella vulgaris* Growth in an External Loop Airlift Photobioreactor: Light Distribution and Carbon Dioxide Consumption", *Can. J Chem Eng.*,**2009**, Submitted for Review.

Contribution of Ph.D. Candidate

The model presented in this chapter was developed by Erin Powell, with supervisory guidance by Gordon Hill. The experimental data used in the development of the model (and for validation purposes) was collected by M.Sc. student Divya Sasi with the help of summer student Andrea Vigueras. This experimental work was planned and supervised by Erin Powell and Gordon Hill. The novel external loop airlift photobioreactor used in the fed-batch experiments was designed by Erin Powell under the guidance of Gordon Hill.

Contribution of this paper to overall study

With the primary goal of the Ph.D. work being *C. vulgaris* cultivation for CO_2 consumption and the production of valuable products, bioreactor design is important. A simple well-mixed stirred tank design was employed during the growth kinetic experiments discussed in Chapter 3. Although the maximum yields and growth rates obtained are significant compared to those reported in the literature for *C. vulgaris* (Powell et al., 2009b), a novel photobioreactor suitable for larger scale cultivation was desired. This led to the design of an external loop airlift photobioreactor, which will be discussed in the next section prior to presentation of the manuscript.

The experimental testing of this novel bioreactor was carried out by a M.Sc. student (Divya Sasi) and so will not be presented here directly. However, the experimental data are used to develop and validate a model for growth of *C. vulgaris* in this novel photobioreactor. The growth of this microalgae species depends on both light and CO_2 concentration, as has been observed from the growth kinetics (Chapter 3), in the literature (Morita et al., 2000; Burger et al., 1988), and in the experimental testing of the ELAPB (Sasi et al., 2009). The growth of each cell is also affected by its position within the bioreactor and so individual cell growth varies with position and time (Parson, 2007). The fluid dynamics of the bioreactor affect the cell's position and so must be included in the model. All of these factors are considered in the growth model discussed in this chapter.

The value of a growth model cannot be understated. Not only can modeling provide a method for demonstrating the relationship between growth parameters and the manner in which they affect the system, but it can also highlight areas where design improvements can be made to both the existing reactor and during any possible future scale-up. As the ultimate goal of this Ph.D. project is obtaining a viable *C. vulgaris* system for industrial scale-up, modeling information will be useful. It takes a very significant time period to obtain experimental data for even one trial at a single set of light, aeration rate, and CO_2 conditions. A representative model of the growth within the ELAPB can predict how the ELAPB should perform under conditions that could not be examined experimentally due to time constraints, providing an easier method to search for the optimum growth conditions.

Relevant Material Not in the Manuscript

Design of the Novel External Loop Airlift Photobioreactor (ELAPB)

A schematic of the design of the ELAPB employed in the present project is shown in Figure 5.1. This is a small experimental laboratory scale reactor with a 50.8 mm (inner) diameter riser, and 38.1 mm (inner) diameter downcomer, both made of clear acrylic. Both are 1.0 m in height. Gas enters at the bottom of the riser and is dispersed by a circular sparger with 12 orifices. The downcomer contains a ball valve to control fluid flow. Instead of a tube connecting the riser and the downcomer and leaving the top of the riser open, the ELAPB uses a tray separator similar to that of Siegel and Merchuk (1988) to separate out the gas phase before the fluid enters the downcomer. This design decision was made to avoid the problems with gas build-up that can occur at the entrance to the top connecting tube between the riser and downcomer that is a frequent problem in other ELAB designs (Chisti, 1989).

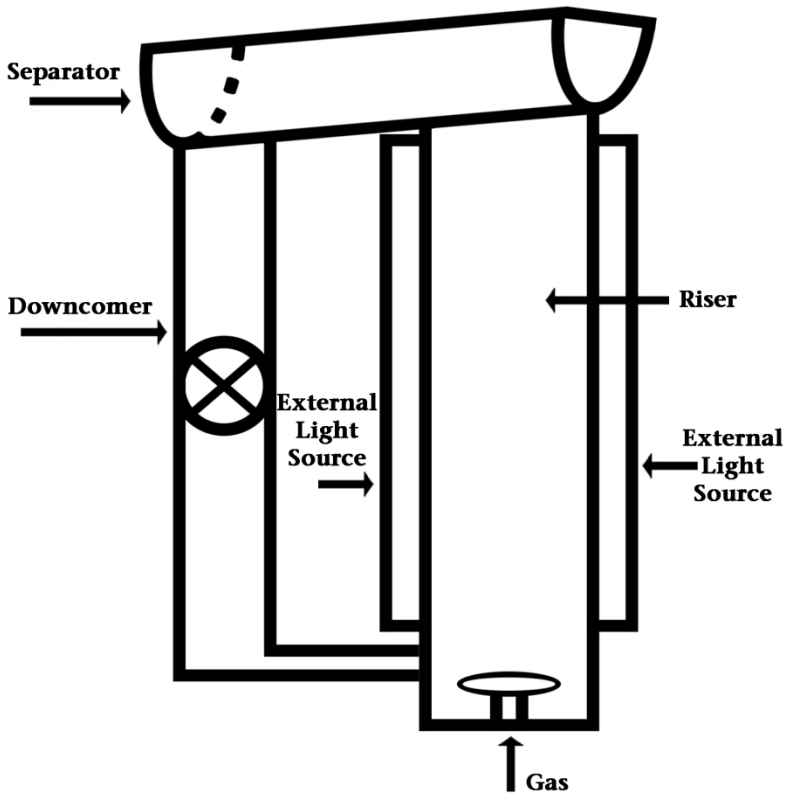

Figure 5.1. Schematic of External Loop Airlift Photobioreactor.

The decision to use an external loop airlift bioreactor was made because the airlift reactor provides a well-mixed environment for photosynthetic microorganisms whose growth is inhibited by shading which is caused by blocking and clumping together of cells. By using the airlift design, constant motion keeps the cells well-mixed thereby reducing adhesion to

the column walls and to each other. This is the most common problem encountered in photobioreactor design for the culture of photosynthetic microorganisms (Richmond, 2005). Wu and Merchuk (2004) observed measurable shear stress on the algae cells with an airlift photobioreactor only under very high gas velocity. Even under that condition, however, the effect on the kinetics of algal growth were negligible for this type of bioreactor design.

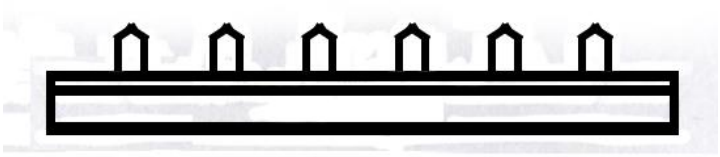

Figure 5.2 Schematic of LED Strip. Each strip is 1.0 m in length and has 60 bulbs.

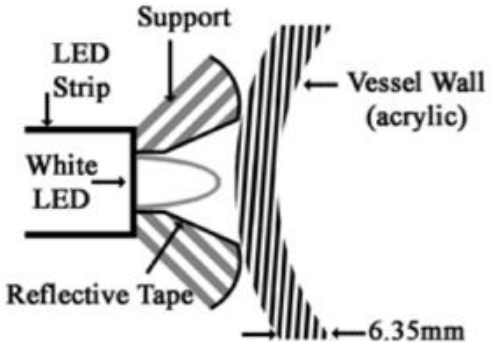

Figure 5.3 Schematic of the Orientation of the LED Bulbs to the Riser Vessel Wall.

External lighting is provided along the entire length of the riser, but the downcomer is kept dark to allow a "rest" period for the algae cells. It has been shown that under high photon flux density, the introduction of a light/dark cycle enhances growth (Wu and Merchuk, 2002; Morita et al., 2000) even for very short light and dark cycles (Lee and Pirt, 1981). This may provide a resting stage for cells, and allow algae to utilize very high photon flux density without entering permanent photoinhibition (Merchuk et al., 1998). The 'light sufficient' riser has a volume that is double that of the 'dark' downcomer to mimic the ratio of daylight hours to nighttime hours in the natural diurnal cycle.

The LED lighting that is being employed for the *C. vulgaris* cultivation consists of a series of white LEDs (as shown in Figure 5.2) in flexible thin PCB strips encapsulated in weather resistant plastic (purchased from ledworldlighting.com, part no. R30-50CM-12V-30-W). Wang et al. (2007) and Michel and Eisentraeger (2004) studied the use of white LEDs for the

cultivation of green andblue-green freshwater microalgae. It was found that LEDs provided an effective and economical light source for microalgae cultivation.These lights have a life of more than 30,000 hours and a low voltage requirement. Each LED strip is 1.0 m in length, is 5 mm wide, and 15 mm thick including the LED bulb.One strip consists of 60 LED lights. These have been arranged in sixteen 1.0 m pieces lengthwise using equidistant spacing around the outside of the ELAPB riser. All of the lights can be lit together at once, or in any combination of the 1.0 m strips surrounding the riser.

Figure 5.4 Completed ELAPB

In order to keep each LED facing directly perpendicular to the vessel wall, a detachable Styrofoam support has been built with equidistant slots for each 1.0 m lighting strip to secure them in place as shown in Figure 5.3. The inside of each slot is lined with reflective tape in order to minimize the loss of light that is not directed towards the riser vessel. The completed ELAPB is shown in Figure 5.4.

Experimental Testing of the Novel ELAPB

A series of fed-batch experiments to test the operation of the ELAPB, and to study the growth of *C. vulgaris*, were performed by Divya Sasi, a M.Sc. student, under the direct supervision of Erin Powell and Gordon Hill. The microalgae growth over time was studied under a range of light and CO_2 conditions. Sasi's experimental data is used for the development and validation of the growth model discussed in this chapter. The novel ELAPB is shown in

Figure 5.5 operating with the LEDs lighting the riser section and the downcomer section darkened. The complete experimental data is presented in Appendix A.1.1.

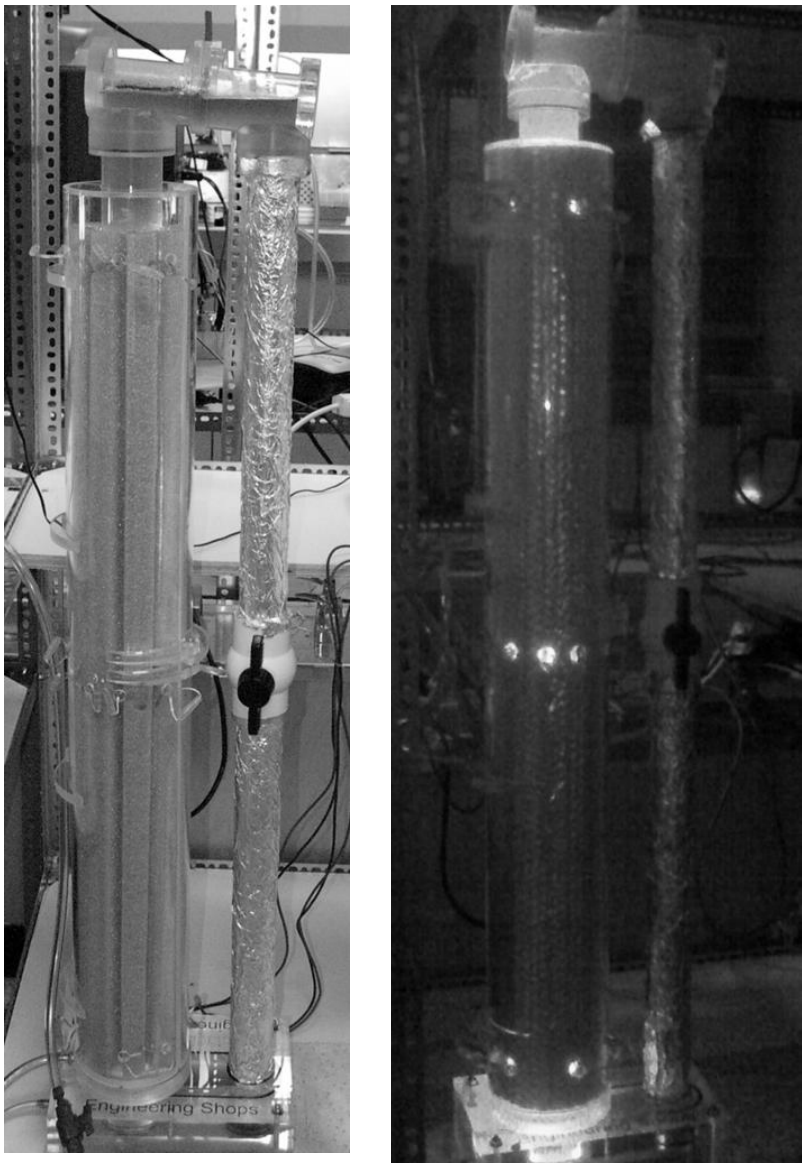

Figure 5.5 Novel ELAPB in Operation

5.1. Abstract

A model was developed to describe the growth of *Chlorella vulgaris* in an external loop airlift photobioreactor. The model includes growth behaviour, light effects, and fluid dynamics for the novel external loop airlift design. The growth behaviour was modeled on experimental work and is dependent on both radiant flux and CO_2 concentration. The model predicts biomass accumulation, light penetration, and transient CO_2concentrations, and compares predictions to experimental data for radiant fluxes of 0.075 – 1.15 W/m^2 and 0 – 20% CO_2 enrichment of feed air, with an average error of 10%. The effect of radiant flux and CO_2 concentration is presented with discussion of radial and vertical profiles along the column. For a fed-batch culture at a biomass density of 170 mg/L, the penetration of the radiant flux was found to decrease by 50% within the first 1 cm, and 75% at 2 cm. Theoretical optimum growth conditions are determined to be 0.30 W/m^2 and a 6% CO_2 enrichment of the inlet feed air. A CO_2 consumption profile is also presented.

5.2. Introduction

Microalgae species are cultivated commercially for their value as biomass or to produce valuable by-products during growth (Pulz and Gross, 2004). Several species have been investigated as a renewable source of fuel owing to the high hydrocarbon content that can be used for biodiesel production (Richmond, 2004). Microalgae have been investigated for their value in CO_2 sequestration as a photosynthetic microorganism that requires significantly less terrestrial surface area for cultivation that traditional crops (Laws, 1991; Chisti, 2007). *Chlorella vulgaris* is a freshwater unicellular microalgae species with a high growth rate relative to other microalgae species (Patino et al., 2007; Ogbonna et al., 1997) and ease of cultivation (Andersen, 2005). Its growth kinetics have been studied in previous work (Powell et al., 2009b), including the CO_2 yield.

Light is the energy source that microalgae use for photosynthetic growth. The growth of *C. vulgaris* is normally light limited, as was observed in previous kinetic growth studies (Powell et al., 2009b) and has been demonstrated by others in the literature (Richmond 2004; Yun and

Park, 2003). It is therefore important to determine the light radiation distribution inside any algae culture vessel. Within a fully lit photobioreactor there can be both regions of high photon flux density and dark regions in which the net biomass production is negative. One way of preventing such negative growth is to increase the volumetric surface area (reduce the depth of the culture) (Wu and Merchuk, 2002), a frequently costly option, or to alter the bioreactor design to reduce shading in the light region. The airlift bioreactor is one design that reduces shading.

The liquid phase in airlift bioreactors is mixed by the rising bubbles of gas dispersed by a sparger located at the bottom of the column. The sparged gas passing through the liquid allows for mass transfer between the liquid and gaseous phases. For instance, these gas bubbles can provide CO_2 to the cells in photosynthetic cultivations. This section is called the riser. The downcomer is a distinct region, both geometrically and hydrodynamically, as it contains minimal gas bubbles. The different gas holdups in the two zones result in two different bulk densities that induce liquid circulation in the bioreactor. The external loop airlift bioreactor is an airlift loop bioreactor in which the two separate columns are normally connected by horizontal tubes near the top and bottom. This external loop allows for liquid circulation between the riser and the downcomer, which provides sufficient mixing for the slow process of microbial cultivation. The enhanced mixing in loop airlift columns forms a homogenous environment for uniform microbial growth (Nikakhtari and Hill, 2005a). The well-mixed environment also reduces shading which in turn would reduce the growth rate achieved by photosynthetic microorganisms. By using the airlift design, the continuous flow through the reactor and mixing effects help prevent algal adhesion (thus reducing the blocking of light) that can inhibit growth in poorly stirred or stagnant tank reactors.

An assessment of local light energy is a prerequisite for modeling and analyzing the light energy transfer in a culture vessel. Either incident light intensity or irradiating surface area per unit culture volume has been widely used as an indication of light transfer efficiency (Ogawa et al., 1971; Prokop and Erickson, 1995; Qi and Rorrer, 1995) in photobioreactors. To model "thin" bioreactors, such as column bioreactors, a simple mean value is frequently taken for the light intensity in many models (Frohlich et al., 1983; Molina Grima et al., 1996), this value being calculated according to the geometry of the reactor. These values are only valid at low cell concentrations and a narrow light path (Suh and Lee, 2003), and give no information on local light distribution inside the culture. Therefore, mathematical models have been developed to

obtain the light distribution profile and average light intensity (Cornet et al., 1992a; Lee et al, 1987; Molina Grima et al., 1997; Rabe and Benoit, 1962). Since the average light intensity can be identical for completely different conditions (Suh and Lee, 2003), the light distribution profile is required to describe the irradiance conditions more precisely.

The present models for light distribution in photobioreactors neglect light attenuation, refraction, and losses due to the vessel wall material (Evers, 1991; Wu and Merchuk, 2004; Cornet et al., 1992a). Reflection inside the vessel is neglected, light is treated monodirectional, and once it enters the vessel it is considered to either be absorbed by the culture or dissipated as heat. It is generally considered sufficient to simply state that the vessel material is considered to be transparent. If the slurry of culture medium and living cells is assumed to be absorbing, scattering, nonemitting, and nonfluorescing, and it is assumed that the scattering and absorption are proportional to the biomass concentration (Cornet et al., 1992a), light radiation diminishes rapidly with depth of penetration (through medium and cell culture).The Beer-Lambert law has typically been used to express the exponential attenuation of the radiant energy flux which results from absorption by the culture (Wu and Merchuk, 2004; Evers 1991; Ten Hoopen et al., 1989; Fredrickson et al., 1961). This model is used extensively in photometry and is based on two assumptions: (1) the light field remains parallel throughout the vessel and (2) the scattering by the solid particles (cells) can be neglected. Attenuation by the actual growth medium is generally neglected, and only attenuation by the biomass in the culture is taken into account. The Lambert-Beer law for light attenuation by biomass is (Parson, 2007):

$$I(r,X) = I_o \exp(-rK_a X) \tag{5.1}$$

where I_o is light intensity at the surface (W/m^2), r is the length of the light path (m), X is the biomass density, (g/L), and K_a is the absorption coefficient (m^2/g). The absorption coefficient, sometimes called the extinction coefficient, must be determined experimentally and is particular to a microalgae species (Yun and Park, 2003). Yun and Park (2001) obtained a value of 435.3 m^2/kg for K_a of *C. vulgaris* suspensions under full spectrum visible light. The Beer-Lambert equation is a simplified description of illuminance attenuation in a bioreactor. A stricter analysis would take into account the geometry of the system and light scattering.

Other published models have accounted for the scattering effect on light within a photobioreactor. Cornet et al. (1992a) proposed a model for light attenuation that may be more appropriate for high biomass concentrations (greater than 1 g/L) that considers scattering and

absorption phenomena separately. It is an adapted version of Schuster's (1905) hypothesis which assumes: (1) the light field remains isotropic throughout the whole culture and (2) light absorption and scattering are independently accounted for by two coefficients, E_a and E_s, respectively. The scattered intensity is assumed to be emitted by the suspended particles in the main direction of the radiation, either positively or negatively. The adapted Schuster and Beer-Lambert models give very different results for dense microbial cultures, indicating the importance of the scattering effect of dense cultures (Cornet et al, 1992a). It should be noted that this model is also monodimensional. Also, for cultures with low biomass densities, or for cultures that have minimal scattering properties, this model and the Beer-Lambert provide the same results.

Light distribution in the bioreactor also depends on the shape of the vessel. Evers (1991) described the modeling of a cylindrical vessel, evenly illuminated from all sides. According to Evers (1991), in a cylindrical reactor, the light intensity at a given point in the vessel can be determined as a function of path length, angle, and light attenuation. Wu and Merchuk (2002) have demonstrated however that the improved accuracy of including the effect of reactor geometry (such as with Evers (1991)) in their own model was not significant, but did greatly increase the complexity of the calculations relative to using the more simple Beer-Lambert Law of light attenuation.

The Beer-Lambert Law of light attenuation has been applied to airlift loop bioreactors with both light and dark zones. For an externally lit internal loop airlift photobioreactor, Wu and Merchuk (2004) based their determination of photon flux density (PFD) in each region of the photobioreactor on the Beer-Lambert law. For the light-sufficient downcomer, the radial mixing is negligible, apparently due to non-developed laminar flow (Wu and Merchuk, 2003). An algal cell that enters this region at a certain radial position will experience a PFD based on the Beer-Lambert law for light attenuation during the entirety of its residence time in the downcomer. It is noted that Wu and Merchuk (2004) neglected the scattering effect of the culture by using the Beer-Lambert law for light attenuation, yet obtained satisfactory agreement with experimental results. This simplification also allowed for combining of algal kinetics and fluid dynamics with light distribution while keeping the solution of the equations in the model manageable.

The specific growth rate of microorganisms has been shown to be affected by the substrate concentration. This relationship can be expressed by the unstructured Monod model of

saturation kinetics. The Monod equation (Shuler and Kargi, 2002) is:

$$\mu = \frac{\mu_m S}{K_s + S} \tag{5.2}$$

where μ is the specific growth rate (h^{-1}), μ_m is the maximum specific growth rate (h^{-1}), S is the rate-limiting substrate concentration (g/L), and K_S is the saturation constant (S at $\mu = \mu_m/2$). According to the Monod equation, increasing the substrate concentration does not affect the specific growth rate when $S >> K_S$. Data obtained by Brune and Novak (1981) from carbon limited batch and chemostat cultures suggest that the specific growth rate of a variety of algae species including *C. vulgaris* are still best represented by the Monod model. However, it has been observed that in most cases, the specific growth rate actually starts to decrease when the substrate concentration increases beyond a certain value. In the case of photosynthetic microorganisms, this phenomenon is termed photoinhibition for light as the substrate. In the case of *C. vulgaris* however, both light and CO_2 are growth substrates, where CO_2may also become inhibitory. The Haldane equation (Aiba, 1982) improves on the Monod model by including the inhibitory effect of excessive light or carbon dioxide:

$$\mu = \frac{\mu_m S}{K_S + S + \frac{S^2}{K_I}} \tag{5.3}$$

where the inhibition constant K_I has been included, and when the substrate S becomes the radiant flux I, then K_I is in fact the photoinhibition constant. If S is CO_2 concentration in the media, then K_I serves as the CO_2 inhibition concentration. This case of CO_2 inhibition was found to describe the actual microalgae production curve far better than the Monod equation by Rehak et al. (2008). Published modeling work on the growth of photosynthetic organisms approach light and CO_2 separately or simply treat one or the other in their model as the only limiting substrate. The other, rather than being considered as the second substrate, is considered to be "in excess, or, as necessary for growth", and only the remaining substrate is modeled (Wu and Merchuk, 2004; Evers, 1991).

There is an indication that the substrate kinetics of the Monod model are considered too simplistic an approach for representing light limitation. The most commonly used models to calculate the growth of a microalgae culture are the P-I models (Camacho Rubio et al. 2002; Molina Grima et al., 1994; Cornet et al., 1992b;Frohlich et al., 1983) which relate productivity P,

or biomass growth rate, to light intensity I. These models differ in the parameters and empirical constants that are included in each model. A mean value is generally taken for light intensity. Similar empirical correlations have been developed for the relationship between growth and CO_2 concentration (Kurano and Miyachi, 2005).

More complicated mechanistic models incorporating reactor geometry or light distribution have also been developed. Cornet et al. (1992a; 1992b) used the Monod model to describe the mean growth rate, but divided the microalgae biomass into several compartments for the purposes of modeling. The goal was to link the biomass growth of cyanobacteria under light limitation to mineral limitations as they affect the different cellular constituents, including those which directly affect photosynthesis such as chlorophyll. Molina Grima et al. (1999) developed their own version of the biomass specific growth rate equation employing multiple empirical coefficients that account not only for photoinhibition, but also for the dependence of specific growth rate on the average irradiance, varying with the incident irradiance level. Lee and Pirt (1981) presented a model that accounts for specific growth rate in both light-sufficient and dark zones in a bioreactor. It also included an endogenous metabolism maintenance term, which differs in light and in darkness.

Wu and Merchuk (2004) simulated microalgae growth in an externally illuminated internal loop airlift photobioreactor that includes kinetic parameters for a system with light/dark cycles. This model constitutes an integration of the kinetics of photosynthesis and photoinhibition with the fluid dynamics of a reactor column, including the effects of shear stress on the kinetics of growth. The maintenance term is modified to take into account the effects of liquid flow in the bioreactor on growth rate. Since light availability varies from point to point in the reaction vessel, the model takes into account the movement of the cells from one region of the bioreactor to another. It also makes possible the prediction of the collapse of cultures under conditions of light deficiency or light excess and the influence of mixing on these critical parameters. This is a dynamic model based on the concept of the photosynthetic factory of the light-trapping system (Eilers and Peeters, 1988) and the three possible states (resting, activated, and inhibited) that may occur upon stimulation by a photon of light. It is however limited to cultures that exhibit the true characteristics of photoinhibition and requires a large amount of experimental data for solution due to the large number of empirical constants. While this model has been used in other work (Vunjak-Novakovic et al., 2005) with good result and should be

applicable to any photosynthetic microbial growth, its application has been found (Wu and Merchuk, 2004) to be best suited to those cultures and experiments where photoinhibition is observed.

Very little literature exists on the quantification of CO_2 mass transfer coefficients in algal cultivation systems, which is dependent on the photobioreactor system being used. Published work frequently assumes that the mass transfer of CO_2 is similar to that of oxygen, and therefore uses the well-known mass transfer rate of oxygen and the diffusion coefficient correction factor (Hill, 2006). Direct study of the rate of carbon dioxide transfer from air bubbles into the aqueous phase has recently been reported by Hill (2006). Hill has developed an empirical equation for predicting the volumetric mass transfer coefficient K_La for CO_2 as a function of temperature, gas flow rate, and mixing speed in a well-mixed, baffled reactor. However, it was clear that the mass transfer rate of CO_2 is indeed also closely modeled by applying a diffusion correction factor to oxygen.

In addition to the previous study on *C. vulgaris* growth kinetics and CO_2 consumption, it was desirous to improve upon the growth rate results observed in a stirred tank bioreactor, although literature indicates that the biomass growth rate obtained by Powell et al. (2009b) is significant relevant to that published in the literature. Therefore, a novel external loop airlift photobioreactor (ELAPB) was designed for *C. vulgaris* cultivation. A growth model based on experimental data obtained using the ELAPB is valuable however in further examining the effects of experimental conditions on growth rate, which are prohibitively time consuming in the laboratory. The model development is presented in detail, and the resulting theoretical data compared to experimental data obtained using the ELAPB. An examination of the effect of light intensity and CO_2 concentration is performed, including any interaction between the two, with determination of the predicted optimum growth rate conditions.

5.3. Experimental

5.3.1. Microbial Species, Media, and Growth Conditions

Chlorella vulgaris was purchased from Carolina Biological Supply (Burlington, North Carolina, Catalogue No. 15-2075) and grown on a modified Bolds Basic media as described in

Powell et al. (2009b) and maintained at pH 6.8. Cultivations were performed at 22.5 ^{o}C. The only carbon source provided during operation is CO_2.

5.3.2. External Loop Airlift Photobioreactor Design

The photobioreactor is an airlift design with an external loop as shown in Figure 5.6. It has a total volume of 4 L with a 50.8 mm diameter riser, and 38.1 mm diameter downcomer (resulting in half the riser volume), made entirely of clear acrylic. The riser is externally lit along its full length with a series of miniature light-emitting diodes. Both columns are 1 m in height. Gas enters at the bottom of the riser and is dispersed by a circular sparger with 12 orifices. The downcomer contains a ball valve to control fluid flow. The riser and downcomer are connected by a tray separator to release undissolved gas from the top of the riser before the fluid enters the downcomer.

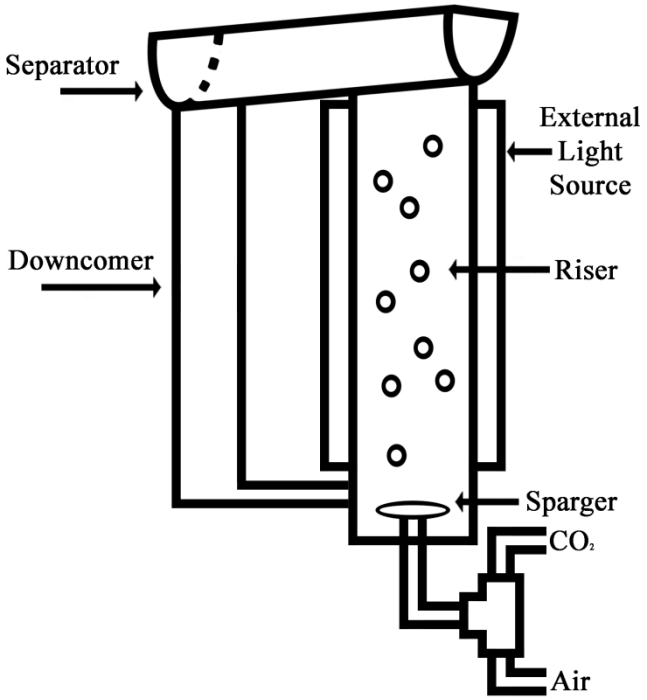

Figure 5.6. Schematic of External Loop Airlift Photobioreactor.

5.3.2.1. Fed-Batch Experiments

The experimental data used in the development of the model was obtained by Sasi et al. (2009). It was collected using the novel ELAPB described in Section 5.3.2 for radiant fluxes ranging from 0.075 W/m^2 – 1.15 W/m^2 and CO_2 inlet air concentrations ranging from 0.038 % (atmospheric) - 15 %. All runs were performed in fed-batch mode, with time periods up to 14 days. These runs are considered fed-batch because CO_2 is continually being supplied, at a total gas flow rate of 3.33 x 10^{-6} m^3/s.

5.4. Model Development

5.4.1. Hydrodynamic considerations

The ELAPB is modeled by treating the riser and downcomer as two distinct regions. This is similar to the work of Wu and Merchuk (2004), who modeled a different design (internal loop airlift bioreactor) in a similar manner. The flow in the riser is also assumed to exhibit a plug flow regime, an assumption supported in the literature for airlift bioreactors (Zhang et al., 2006; Wu and Merchuk, 2004). With plug flow there is no mixing in the axial direction and no variation in axial velocity over the cross section and the cells flow along the tube or column uniformly with the medium, which initially contains all the substrates and factors required for growth. Plug flow is so termed because the contents move along the tube together as an approximation of a plug (Bakker et al., 1997). When fluid moves through a large pipe or channel with a sufficiently large Reynolds number (typically > 2100 in a pipe), it approximates plug flow (Bailey and Ollis, 1986). The assumption of plug flow in the riser is supported by the estimation of the Reynolds number using the liquid velocity. The liquid circulation velocity, V_{LIQ}, was measured experimentally as given in Table 5.1. This was used with the measured gas holdup, θ, to calculate the liquid velocity, U_{LIQ}, in the riser:

$$U_{LIQ} = \frac{V_{LIQ}}{1-\theta} \tag{5.4}$$

Using the density, ρ, and the viscosity μ, for a medium assumed to be primarily water at room temperature and pressure, and the diameter of the riser, D_R, the Reynolds number, Re, was determined by solving (Perry and Green, 1997):

$$\mathrm{Re} = \frac{\rho U_{LR} D_R}{\mu} \tag{5.5}$$

Since the Reynold's number is 6023, indicating a turbulent well-mixed state, plug flow is a reasonable assumption. The same fluid regime is assumed to be present in the downcomer. In the case of the separator, the residence time is very short and the cells can be considered to be undergoing turbulent mixing as they move quickly from the riser to the downcomer during the release of any undissolved gas.

The superficial gas velocity in the riser, U_{GAS}, is calculated from the gas flow rate, AF, and the riser cross-sectional area, A_{Riser},:

$$U_{GAS} = \frac{AF}{A_{Riser}} \tag{5.6}$$

The sparger region and the bottom connecting tube are assumed to be part of the downcomer for modeling purposes. The inclusion of the bottom connector is considered reasonable as it is a short, narrow pipe with negligible gas holdup, and can be considered to have minimal impact on the overall cell growth. This is similar to the assumptions of Wu and Merchuk (2004). In the case of the separator, since for this ELAPB design it can be considered dark (as is the downcomer), with a comparatively short residence time relative to both the riser and the downcomer, it is also included with the downcomer in order to simplify the calculations. The major impact of the separator on the model is on the boundary conditions. Although it will be included in the downcomer's total volume and column height; at the location of the separator where venting of undissolved gas occurs, the downcomer gas phase is released (with the total gaseous CO_2 concentration assumed to now be zero entering the downcomer) and the distribution of the cells within the bioreactor will be randomized due to mixing. Under low gas flow rates, there is gas only in the riser, and the gas holdup in the downcomer can be neglected. Therefore the concentration, y, of CO_2 in the gas phase in the downcomer is zero at all locations and times steps since no gas exists in the downcomer. Randomization of the radial location of the biomass will occur again as the cells re-enter the bottom of the riser for the next cycle. At the base of the riser the gas phase is again infused with the CO_2 enriched feed air. The initial and boundary conditions are summarized in Section 5.4.7.

The cells enter both the riser and downcomer in a random arrangement after the turbulent mixing of either the separator or passage through the bottom connector and past the sparger. At the bottom of the sparger, the influx of inlet gas will increase the gas phase CO_2 again for the next cycle. The cells then assume the plug flow regime as discussed above, remaining each within their own "plug" section throughout their passage through the riser and the downcomer. Therefore, the position of each cell remains at a constant location relative to the wall during a single cycle through either the riser or the downcomer, but changes (randomly) each time the top of the riser or bottom of the downcomer is reached.

Several hydrodynamic parameters were measured experimentally (Sasi et al., 2009), or calculated for the ELAPB during operation. These are summarized in Table 5.1.

Table 5.1 Hydrodynamic Parameters of ELAPB

Parameter	**Value**
Total Bioreactor Loop Length	3.058 m
Average Circulation Velocity	0.12 m/s
Total Circulation Time	26.5 s
Average Gas Holdup (Riser)	0.0045
Liquid Velocity in Riser	0.121 m/s
Superficial Gas Velocity in Riser	1.645×10^{-3} m/s

5.4.2. Light Attenuation

The riser is externally lit, with the total light reaching the cells decreasing both with distance from the riser wall and increasing biomass density. The external lighting is assumed to be distributed homogenously around the riser, and in the case of a cylindrical riser such as an airlift photobioreactor, homogeneous lighting from all sides is a reasonable assumption (Evers, 1991).

The separator and downcomer are both considered to be completely dark, with any ambient exposure to light being neglected. This is considered to be valid given that the downcomer is covered, as is the riser outside the lighting system, and residence time in the separator is very short. The radiant flux at all points in the downcomer is assumed to be zero.

Evers (1991) described the modeling of a cylindrical vessel, evenly illuminated from all sides. Evers (1991) concluded that the cylinder length did not influence the modeling of overall biomass change rate in the vessel if the top and bottom effects were neglected. This is not the case here due to the differing conditions in the riser and downcomer. The direction of the light was also not considered by Evers (1991), due to the assumption of uniform lighting from all sides.

The assumption of uniform lighting is adopted here but any light source is considered mono-directional and to be attenuated according to the Beers-Lambert Law. Light from an external source must pass through the vessel wall and a slurry of culture medium and other living cells (Miyake et al., 1999) to reach an individual algae cell. The light reaching the growing *C.*

vulgaris cells at any point in the ELAPB was determined using the Beers-Lambert Law. This equation determines the light reaching the cells from the distance it must travel and the biomass density attenuation as presented below:

$$I\left(r, X_{(r)}\right) = I_o \exp\left(-rK_a X_{(r)}\right) \tag{5.7}$$

where I_o is light intensity at the inside wall surface (W/m^2), r is the length of the light path from the outer wall to reach that radial position (m), $X_{(r)}$ is the biomass density at that radial position, (g/L), and K_a is the absorption coefficient (m^2/g). This equation applies only to the externally lit riser, where I_o is known and is measured experimentally for each trial. For the separator and downcomer I_o is zero. Since the light reaching the cells (and resulting biomass growth) must be solved over the entire radius of the riser from the wall to the centre, the volume of the riser is divided into equally-spaced radial sections at a distance $rad_{(r)}$ from the riser wall. In each of these radial sections, the average radius is used to determine the average light intensity in that section. The volumetric ratio of each segment (relative to the total), $Rratio_{(r)}$, is also determined for this radial section, with the largest $vol_{(r)}$ being adjacent to the outside wall. This is used to determine the volumetric ratio of the total cells exposed to this level of radiant flux, where Δr is the radial step size, Δz is the vertical step size, H is the column height, and n is the number of the radial location with zero being at the riser wall.

$$rad_{(n)} = \Delta r * (n - 0.5) \quad \text{for } 1 < n < 20,\ 0 < r < R, \text{ all z,} \tag{5.8}$$

$$vol_{(n)} = \pi \Delta z * \left(\left(R_{Riser} - (n-1) * \Delta r\right)^2 - \left(\left(R_{Riser} - n * \Delta r\right)^2\right)\right)$$

$$\text{for } 1 < n < 20,\ 0 < r < R, \text{ all z,} \tag{5.9}$$

$$Ratio_{(n)} = \frac{vol_{(n)}}{A_{Riser} H} \quad \text{for } 1 < n < 20,\ 0 < r < R, \text{ all z,} \tag{5.10}$$

5.4.3. Specific Growth

The growth equation for *C. vulgaris* for both substrates, radiant flux and CO_2, was determined from experimental kinetic growth data collected from fed-batch experiments using the novel ELAPB (Sasi et al., 2009). The radiant flux was measured just inside the riser wall for each experiment and therefore this value is treated as the light source, or maximum flux, I_o, for any given run. The substrate term, S, in any biomass growth equations refers to the CO_2in the

liquid phase, but it is the concentration in the gas phase that is predetermined. The concentration of CO_2 at the gas-liquid interface at any location in the bioreactor can be determined from the concentration in the gas, y (g/L), from Henry's law (Perry and Green, 1997):

$$pCO_2 = \frac{C_g}{100} \tag{5.11}$$

$$y = 1.185 pCO_2 \tag{5.12}$$

$$S^* = \frac{y}{H_e} \tag{5.13}$$

where C_g = % CO_2 in the gas phase, g/L, S* = CO_2 concentration at the gas-liquid interface, g/L, and H_e = Henry's Law constant, g/L/g/L. The value of H_e was determined to be 0.682 g/L/g/L from Hill (2006).

The best fit equation for the specific growth rate was found to be one employing a series of empirical constants with an error of 0.83% (95% confidence level). An equation using a "double" Haldane format was also fit to the data, although the error between this model and the data is higher at 1.8% ± 0.75% (95% confidence level). The effect of light is presented in a Haldane kinetic relationship, as although no inhibiting level was reached in this experimental data, photoinhibition is a well-known phenomenon. In the case of the CO_2 liquid phase concentration, a Haldane inhibition constant was included because at high concentrations growth inhibition was observed in multiple experiments (Sasi et al., 2009). The constants presented in the equation are best-fit constants. The error inherent in using the "double" Haldane form equation is not significantly higher than any empirical equations that were available, and the recognizable form is considered beneficial to work with. The effect of the two substrates was combined as shown below:

$$\mu_L = 0.113 \left(\frac{I}{0.03 + I + \frac{I^2}{1.5}} \right) \left(\frac{S}{0.005 + S + \frac{S^2}{0.1}} \right) \tag{5.14}$$

In the case of growth under dark conditions (in the separator and downcomer) the value of the illumination is zero, but the growth rate is not zero as the dark reactions continue (Wu and Merchuk, 2002). The change in the growth rate when the light is zero can be accounted for by using a second equation for growth in the dark. In the dark downcomer, the radiant flux-dependant portion of the growth equation becomes equal to zero, giving an unreasonable value

for the specific growth rate also equal to zero. The use of a constant dark phase growth rate was used in order to fit the growth data to the model throughout the ELAPB. The best-fit equation for the dark zone of the bioreactor is:

$$\mu_D = 1.00x10^{-4} \tag{5.15}$$

This is similar to accounting for a change in the growth maintenance between the light and dark phases, as has been done in other work (Lee and Pirt, 1981). The low aqueous solubility of CO_2 (Hill, 2006)) results in a growth rate that is approximately constant regardless of the CO_2 concentration in the dark downcomer. The two growth equations (5.14) and (5.15) have been adopted as the growth equations for the primary model used in this work.

An attempt was made to fit a second Haldane style equation that would not produce a zero growth rate in the downcomer (when I = 0), making it applicable to all regions of the ELAPB. This equation form was chosen simply in order to include both the radiant flux and CO_2 concentration. In this case, the effect of radiant flux was considered to be exponential so that the growth rate would become unity and not zero in the downcomer. Exponential-form Haldane- and Monod-type equations have been reported earlier (Molina Grima et al., 1999). The error for this growth equation was higher however at 3.3% (95% confidence level) and required the use of a maintenance coefficient that differed for the light and dark regions of the ELAPB.

5.4.4. Fluid dynamics: carbon dioxide and biomass accumulation

The fluid dynamics of the ELAPB are similar to those reported by Nikakhtari and Hill (2006), with three equations to describe the steady state change in biomass, substrate, and in CO_2 (in both the gas and liquid phases) over the vertical height of an external loop airlift bioreactor riser column. The equations of Nikakhtari and Hill (2006) are:

$$D\frac{d^2S}{dz^2} - U_{LR}\frac{dS}{dz} + K_L a(S^* - S) - \frac{\mu X_T}{Y_{XS}} = 0 \tag{5.16}$$

$$D\frac{d^2X}{dz^2} - U_{LR}\frac{dX}{dz} + \mu X_T = 0 \tag{5.17}$$

$$-U_{GR}\frac{dy}{dz} - K_{La}\frac{1-\theta_{GR}}{\theta_{GR}}(S^* - S) = 0 \tag{5.18}$$

where D is dispersion coefficient (m^2/s), S is the liquid phase CO_2 concentration (g/L), z is the vertical position (m), k_{La} is the mass transfer coefficient (s^{-1}), S* is the CO_2 concentration at the

interface (g/L), μ is the growth rate (s^{-1}), X_T is the total biomass concentration (g/L), Y_{xs} is the yield (mg/mg), U_{LR} is the liquid velocity in the riser (m/s), X is the biomass concentration (g/L), U_{GR} is the gas flow rate in the riser (m/s), y is the CO_2 concentration in the gas phase (g/L), θ_{GR} is the gas holdup. These equations are for a steady state situation, whereas the concentrations of biomass and substrate change with time in the ELAPB. This can be accounted for by including a time differential in each equation, giving three first order partial differential equations. The second order differential terms in equations (5.16) and (5.17) refer to axial diffusion. However in this model, the flow regime in both the riser and the downcomer is considered to be plug flow; therefore the dispersion term can be neglected. When changes with time are considered and dispersion is neglected:

$$-U_{LR}\frac{dS}{dz}+K_L a(S^*-S)-\frac{\mu X_T}{Y_{XS}}=\frac{dS}{dt} \tag{5.19}$$

$$-U_{LR}\frac{dX}{dz}+\mu X_T=\frac{dX}{dt} \tag{5.20}$$

$$-U_{GR}\frac{dy}{dz}-K_{La}\frac{1-\theta_{GR}}{\theta_{GR}}(S^*-S)=\frac{dy}{dt} \tag{5.21}$$

A further simplification of the above equations was also considered. Although there are multiple mass transfer considerations, the low aqueous solubility of CO_2 (Hill, 2006) does make the mass transfer from the gas to the liquid phase a slow process. The photosynthetic growth of microalgae is significantly slower however, and it is assumed that since the transfer rate of CO_2 from the gas phase to the liquid phase is much faster than the rate at which the cells can uptake the dissolved CO_2, that phase transfer from gas to liquid can be considered instantaneous from a relativistic standpoint. The boundary layer around each cell can also be assumed to be minimal due to the continuous flow around the microalgae particles, and so can be neglected. Therefore, it may be possible to include only the convective mass transfer in the above differential equations. All other CO_2 mass transfer considerations would be neglected.

The assumption that the growth rate, and corresponding uptake of CO_2 from the liquid, is significantly slower than the mass transfer from gas to the liquid phase greatly simplifies the calculations. If the cell density is sufficiently low, and the continuous supply of gas is sufficiently high, then the amount of CO_2 consumed by the cells will not be significant enough to change to the CO_2 concentration. This allows for the assumption that both the gas and liquid phases remain saturated with CO_2 and at equilibrium at all times throughout the cultivation. If

this can be considered to be a valid assumption then the gas phase concentration, y, and the liquid phase concentration, S, can be assumed to remain constant at the initial equilibrium values for all time periods in the riser. In the downcomer, the gas phase CO_2 concentration is zero as any undissolved gas is released and the gas holdup is assumed to become negligible. The phase concentrations are therefore constant in the riser. These are determined by the CO_2 concentration in the inlet feed air.

In order to confirm whether the rate of mass transfer of CO_2 from the gas to the liquid phase was significantly greater than the rate of uptake by the cells, a comparison of these rates was calculated. The rate of mass transfer of CO_2 was estimated from the following:

$$\frac{dS}{dt} \approx k_{La}\left(S^* - S\right) \tag{5.22}$$

Therefore, using a conservative k_{La} of 1.0 h^{-1}, for a 10% CO_2 inlet concentration (y = 0.1185 g/L, S*=0.1466 g/L), the value of dS/dt is 147 mg/L-h if the liquid phase S is at atmospheric concentration, and 73.3 mg/L-h if it is assumed to be at a higher 50% of the interface S*.

The rate of CO_2 uptake by the cells was estimated from the maximum growth rate observed in the fed-batch experiments and the Monod-form equation for CO_2 and the CO_2 yield:

$$\frac{dCO_2}{dt} \approx \mu_{\max} \frac{X_{\max}}{Y_{X/S}} \tag{5.23}$$

Therefore, using the maximum growth rate and biomass concentration observed by Sasi et al. (2009) of 0.04 h^{-1}, a maximum cell concentration of 200 mg/L and the yield of 0.5 mg DW/ mg CO_2 measured in Chapter 3, the value of dCO_2/dt is 16 mg/L-h. As the rate of phase mass transfer is of an order of magnitude greater than the rate of uptake by the cells, the assumption of CO_2 saturation and constant gas and liquid concentrations is considered valid.

The assumption of negligible CO_2 mass transfer would greatly simplify the solution, however it was found that the numerical solution was still very sensitive to step size. In order to achieve solution stability, an extremely small step size in the time dimension was required which resulted in large simulation times (measured in hours) using the MATLAB® software. Therefore, the model including transient CO_2 concentrations in both the riser and downcomer (Equations (5.19), (5.20), and (5.21)) was employed instead for reasons of both improved accuracy and practicality.

5.4.5. Constants Used in Calculations and Solution of Model

Several constants obtained from the literature, in addition the measured parameters (Table 5.1), are required for the solution of these equations. These are summarized in Table 5.2.

Table 5.2. Constants Required for Model Solution.

Constant, (symbol)	**Value, (units)**	**Source**
Biomass Extinction Coefficient, K_a	0.4353, (m^2/g)	Yun and Park (2003)
CO_2 mass transfer coefficient, k_{La}	1.0 h^{-1}	Ritchie (1995)
Density of CO_2, ρ_{CO2}	1.98 g/L	Perry and Green (1997)
Density of air, ρ_{air}	1.185 g/L (25 ^oC, 1atm)	Perry and Green (1997)
Molar mass of CO_2, m_{CO2}	43.99 g/mol	
Henry's constant, H_e	0.682 g/L / g/L	Hill (2006)
Average Density of Culture Fluid (water assumed), ρ	998 g/L	Perry and Green (1997)
Average Viscosity of Culture Fluid (water assumed), μ	0.890 cP	Perry and Green (1997)

5.4.6. Assumptions

The assumptions made in the development of this model and its solution are summarized below:

- There is gas only in the riser and the gas holdup in the downcomer can be neglected.
- The flow regime in both the riser and downcomer is that of plug flow.
- The separator and bottom connector are part of the downcomer.
- The biomass is perfectly and randomly mixed in the both the separator and the bottom connector during each cycle.
- Dispersion in the riser and downcomer is negligible.

- The riser is uniformly lit.
- The radiant light in the riser is mono-directional, non-scattering, and non-absorbing.
- The downcomer is completely dark.
- The only CO_2 mass transfer resistance considered is that between the gas-liquid interface and the liquid phase. The effect of the rate of CO_2 uptake by the growing cells is considered separately.

5.4.7. Solution Method

The three differential equations (5.19), (5.20), and (5.21) and two conservation equations (5.7), (5.13), and the best fit Haldane –form growth equations (5.14) and (5.15), were solved simultaneously with time, vertical column position, and radial position (within the riser only). These are summarized:

$$I\left(r, X_{(r)}\right) = I_o \exp\left(-rK_a X_{(r)}\right) \tag{5.7}$$

$$S^* = \frac{y}{H_e} \tag{5.13}$$

$$\mu_L = 0.113\left(\frac{I}{0.03 + I + \frac{I^2}{1.5}}\right)\left(\frac{S}{0.005 + S + \frac{S^2}{0.1}}\right) \quad \text{for the riser} \tag{5.14}$$

$$\mu_D = 1.00x10^{-4} \quad \text{for the downcomer} \tag{5.15}$$

$$-U_{LR}\frac{dS}{dz} + K_L a\left(S^* - S\right) - \frac{\mu X_T}{Y_{XS}} = \frac{dS}{dt} \tag{5.19}$$

$$-U_{LR}\frac{dX}{dz} + \mu X_T = \frac{dX}{dt} \tag{5.20}$$

$$-U_{GR}\frac{dy}{dz} - K_{La}\frac{1-\theta_{GR}}{\theta_{GR}}\left(S^* - S\right) = \frac{dy}{dt} \tag{5.21}$$

All three differential equations were solved explicitly using forward differencing. The step sizes chosen for each variable, in order to achieve solution stability, are given in Table 5.3. This

numerical problem is a stiff problem, requiring a very small time step initially (over the course of the first complete circulation loop).

Table 5.3. Numerical solution step sizes.

Variable, (units)	**Step size**
Time, t, (s)	0.001 if $0 \geq t \geq 30s$ 0.1 if $30s > t$
Vertical Location, z, (m)	0.05 (20 steps in 1m column)
Radial Location, r, (m)	0.0254 (10 steps in riser radius and volume)

The riser and downcomer are treated as separate regions with different initial and boundary conditions. In order to maintain the separation of the riser and downcomer in the solution, they were treated as two sequential columns in a single loop. The initial conditions for each region differ as do the boundary conditions. In order to ensure that the solution mimics the flow of the cultivation from one region to another, the boundary conditions also at the start of one region also reflect the conditions at the end of the previous region for each cycle. The initial and boundary conditions are summarized below.

The initial conditions (t = 0) for the solution of the equations are:

For the riser:

$X_{t=0} = X_0$ for all z, for all r, (5.24)

$S_{t=0} = S_0$ for all z, for all r, (5.25)

where S_o is assumed to be in equilibrium with atmospheric air y_o.

$y_{t=0} = y_0$ for z > 0, for all r, (5.26)

$y_{t=0} = y_{z=0}$ for z = 0, for all r, (5.27)

where y_o is assumed to be the CO_2 concentration in atmospheric air (0.038%),

and $y_{z=0}$ is the CO_2 concentration in the enriched inlet air at the bottom of the riser.

In the downcomer:

$X_{t=0} = X_0$ for all z, for all r, (5.28)

$S_{t=0} = S_0$ for all z, for all r, (5.29)

where S_o is assumed to be in equilibrium with atmospheric air y_o.

$y_{t=0} = y_0$ for all z, for all r, (5.30)

where y_o is assumed to be the CO_2 concentration in atmospheric air (0.038%),

The boundary conditions are summarized as:

In the riser:

$y = y_{z=0}$ for z = 0, for all r, (5.31)

and $y_{z=0}$ is the CO_2 concentration in the enriched inlet air at the bottom of the riser.

For t > 0:

$S_{Riser} = S_{Downcomer}$ for z = 0, for all r, (5.32)

$X_{Riser} = X_{Downcomer}$ for z = 0, for all r, (5.33)

$I_R = I_o$ for z = 0,for r = R. (5.34)

In the downcomer:

$y = y_{z=0}$ for z = 0, (5.35)

$I_R = 0$ for all z, (5.36)

and for t > 0:

$S_{Downcomer} = S_{Riser}$

$X_{Downcomer} = X_{Riser}$ for z = 0, (5.37)

for z = 0. (5.38)

The growth model was solved using MATLAB (The MathWorks Inc., Natick, MA, USA) (see Appendix A.2.2 for full source code). The main program variables include the radiant flux inside the bioreactor wall (I_0) in W/m^2, total cultivation time (t_{final}) in s, the CO_2 concentration in the feed air ($y_{z=0}$) in g/L, the biomass inoculation concentration (X_0) in mg/L, and the numerical step sizes in the time (Δt), vertical space (Δz), and radial (Δr) dimensions.

5.5. Modeled Growth: Results and Discussion

The complete model incorporates the biomass growth equation, accounts for each cell's light exposure history (based on fluid flow and radial position), and links it mathematically with the fluid dynamics of the bioreactor. The growth in the ELAPB as predicted by the model is discussed below.

5.5.1. Comparison to Experimental Data

The output of the model was compared to the data of Sasi et al. (2009) for multiple combinations of growth conditions. The data of Sasi et al. (2009) is presented in Figure 5.7 with the results of the model output for multiple growth conditions of radiant flux and % CO_2 enrichment of inlet air. An average agreement of 21.3 mg/L (95% confidence level) was observed between the model and the data. With final biomass concentrations ranging from 170 mg/L to 300 mg/L, this represents an error of 7 – 13 %. The increase in error in comparison to that measured with just the best fit specific growth rate equation is due to the increased complexity of the full model. Equations for growth rate, light attenuation, hydrodyanmics and mass transfer have all been combined using both measured and published values for the requisite constants. There is also a degree of error in any experimental data during the cultivation of living cells, such as that which is used for comparison and validation.

From previous experimental work on the growth kinetics of *C. vulgaris* (Powell el al., 2009b), it was observed that the radiant flux and the CO_2 concentration have an interacting effect on biomass growth. Examination of the experimental data used in the development of this model indicates the same relationship (Sasi et al., 2009). The relationship between light and CO2 concentration, and their effect on the *C. vulgaris* cultivation is complex as the two factors interact to affect overall photosynthesis and biomass production. The model simulates this interacting effect and therefore effectively predicts growth behaviour in the ELAPB. This allows for the determination of the predicted optimum growth conditions without the need for time-consuming experimentation.

5.5.2. Examination of Effect of Cultivation Conditions

While an increase in either radiant flux or CO_2 concentration usually results in an increase in biomass growth, that increase is not significant unless both substrates are increased together. It was also observed that CO_2 becomes inhibitory at high concentrations. It is known that light also becomes inhibitory once photoinhibition is reached, and although this point was not blatantly attained during the ELAPB experiments used in this study, there are indications that a plateau was approached at certain radiant fluxes (Sasi et al., 2009).

The effect of both radiant light flux and CO_2 concentration in the inlet air were examined to further explore their affect on *C. vulgaris* growth, and therefore CO_2 sequestration. A three-dimensional graph of the specific growth rate, as predicted by the growth portion of the model is presented in Figure 5.8. The most significant peak growth rate is observed at a radiant flux between 0.30 – 0.45 W/m^2 when the CO_2 concentration corresponds to a value between 5% and 10% in the inlet air. This allows the theoretical optimum to be determined so that *C. vulgaris* growth and subsequent CO_2 consumption can be optimized without the time-consuming trial and error of the laboratory as a starting point. According to the model, the optimum growth conditions in order to maximize the biomass accumulation are a radiant flux of 0.30 W/m^2 at a 5.8 % inlet CO_2 concentration.

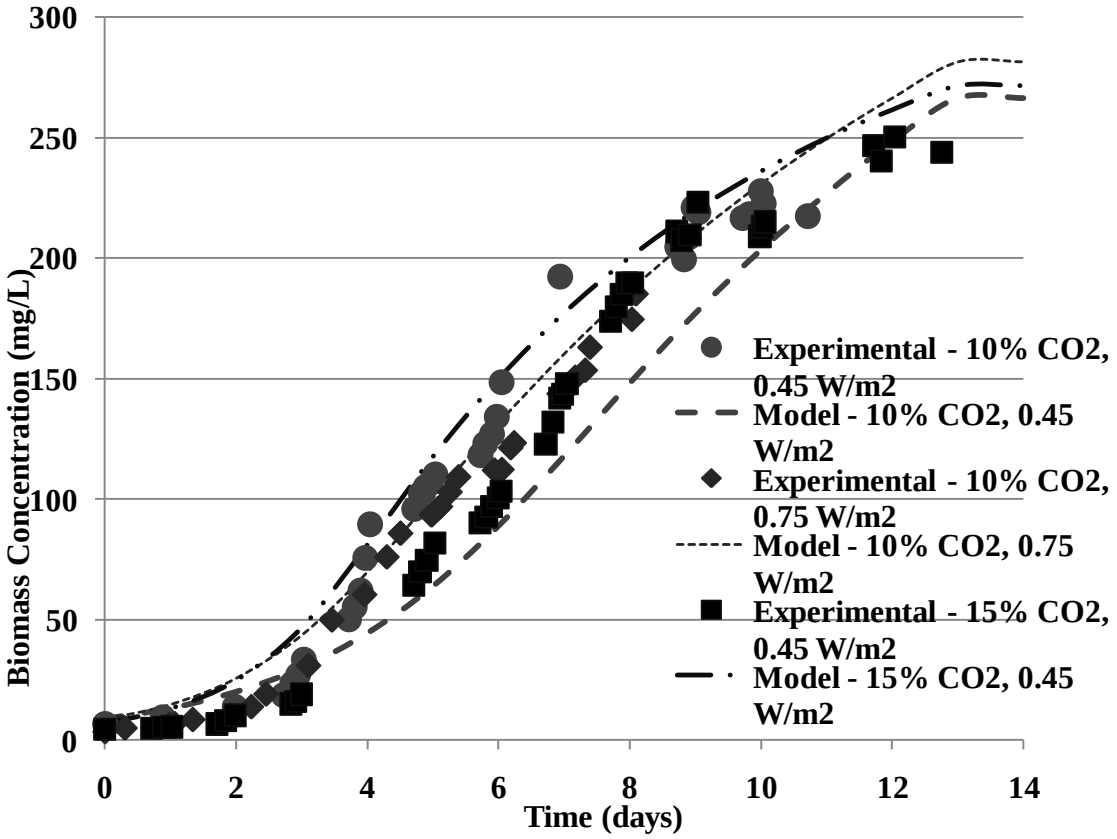

Figure 5.7 Comparison of experimental (Sasi et al., (2009)) and modeled data for the *C. vulgaris* cultivation in the ELAPB.

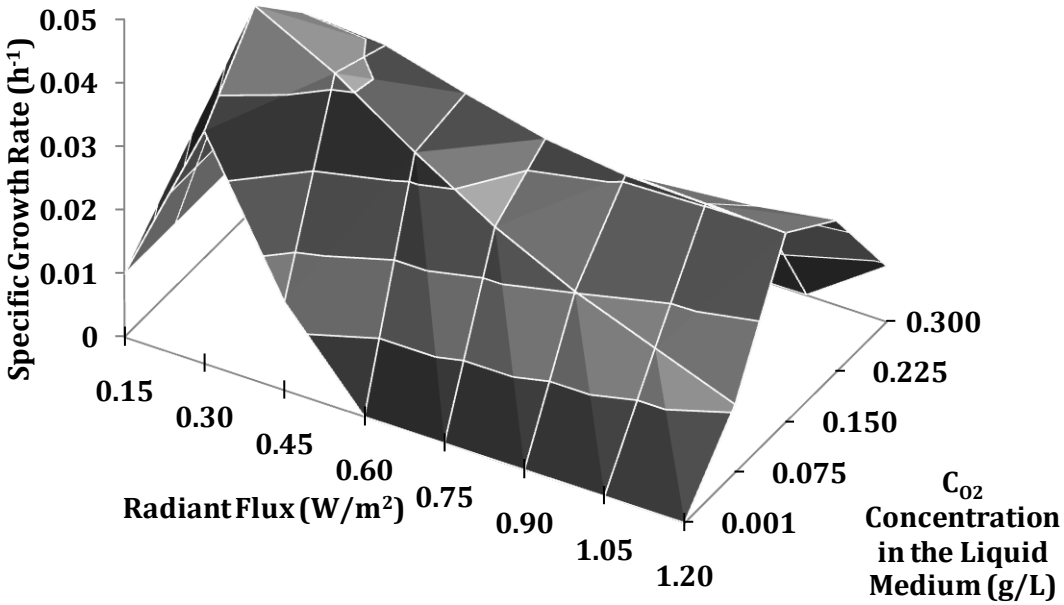

Figure 5.8. Effect of radiant flux and concentration of CO_2 in liquid medium on biomass specific growth rate.

5.5.3. CO_2 consumption and Model Validation

With the ultimate application of the microalgae cultivation in the ELAPB being CO_2 consumption, the cumulative CO_2 consumption was determined for one of the cultivation trials with a high growth rate for which experimental data was available. The CO_2 consumption was determined from the increase in the biomass accumulation rate over the course of the cultivation, with each increase requiring CO_2, and this CO_2 consumption rate was then compared to the rate of CO_2injection into the riser. The resulting values of cumulative CO_2 consumption are given in Figure 5.9 over an 8 day period for growth at 0.45 W/m^2 and 5 % CO_2. An experimental trial performed at those same cultivation conditions, yet not used in the model development, is presented as validation of the results. As expected, the % CO_2 consumed increases with time as more biomass is produced. This is due to the use of CO_2 in photosynthesis for biomass production. However, as the cultivation progress, although the total % CO_2 consumed increases,

the rate at which the total increases is reduced. Interestingly, this is caused by the higher concentration of biomass in the ELAPB near the end of the experiment, where a greater concentration of cells results in less light penetration into the cell culture and a lower growth rate inside the cell culture. A lower growth rate means a smaller rate of biomass increase, and hence a smaller rate of CO_2 consumption rate by the algae.

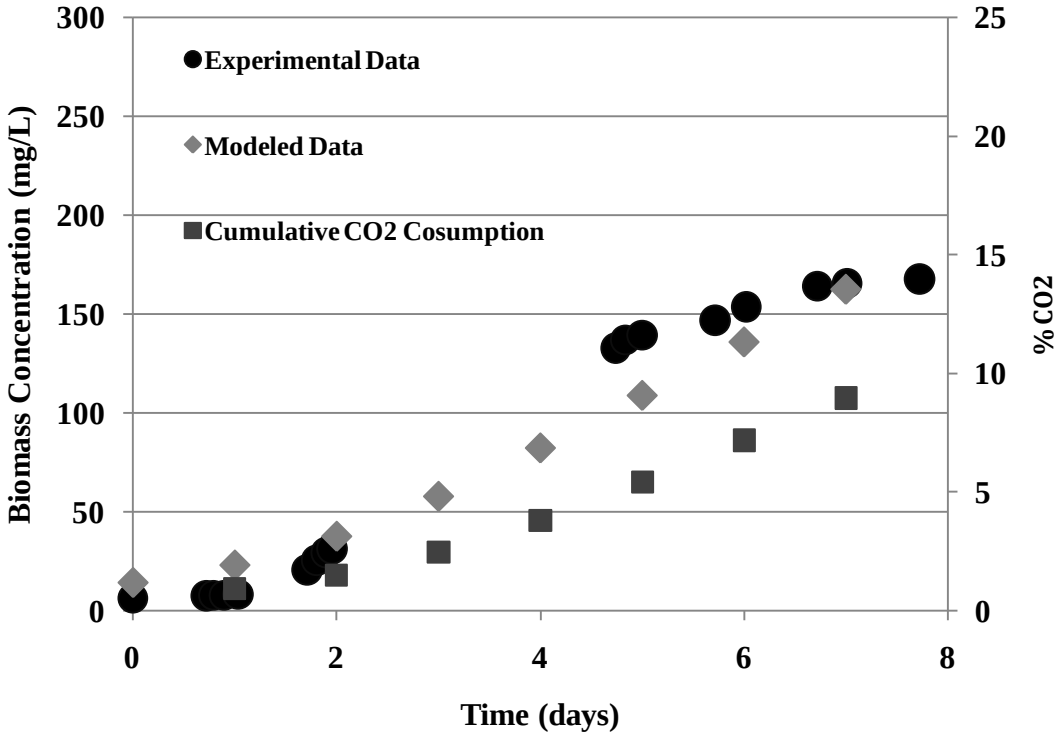

Figure 5.9. Cumulative CO_2 consumption with *C. vulgaris* growth. (0.45 W/m2 radiant flux, 5% CO_2 enrichment).

5.5.4. Radial Light Penetration and Biomass Profile

The radial light and biomass profile for a cultivation trial is presented in Figure 5.10. The simulation is for 0.45 W/m^2 of radiant flux and 10% CO_2 enrichment of the feed air. Once the simulation is underway (t .> 0), the shape of the two profiles becomes evident as seen in the Figure. The biomass in each radial section of the riser decreases with distance from the wall, due to both the decreased volume of the radial section and the decreased growth occurring due to shading and distance from the light source. The radiant flux is also directly proportional to the

distance from the riser wall, as well as to the biomass concentration in that radial section. This results in the complex relationship between radial distance and biomass as shown in Equation (5.1). For the fed-batch culture shown in Figure 5.10, with a biomass density of 170 mg/L, the penetration of the radiant flux was found to decrease by 50% within the first 1 cm distance from the riser wall, and 75% at 2 cm.

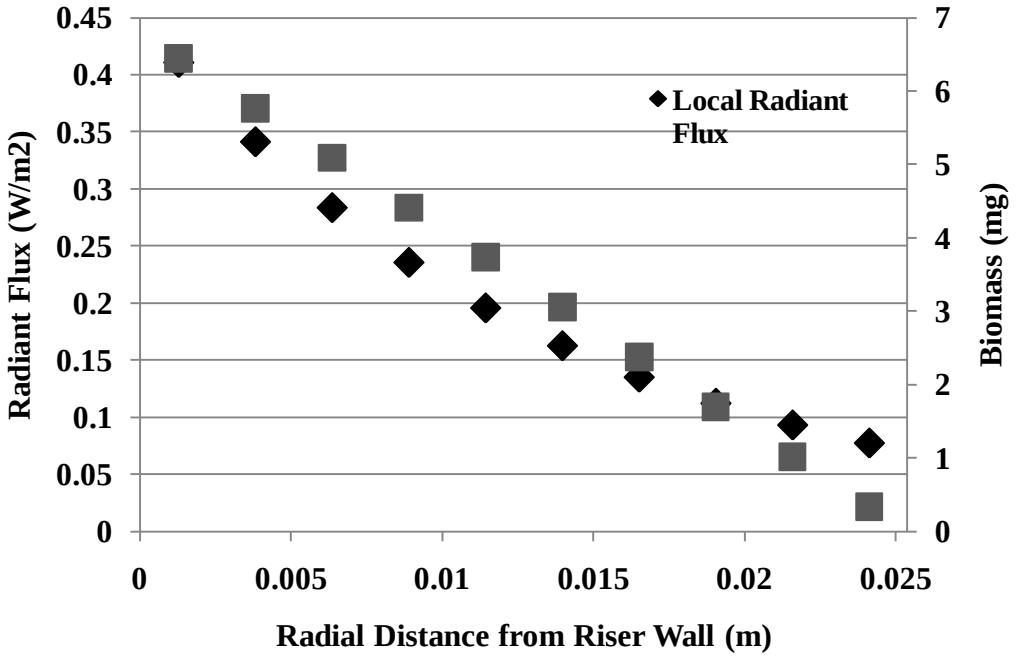

Figure 5.10. Radial profile of radiant flux and biomass in a small vertical section of the ELAPB riser on day 14 of cultivation.

5.5.5. CO_2 Concentration Profile along Column

The CO_2 concentration profile along the length of both the riser and downcomer columns was generated for one set of cultivation conditions. Figure 5.11 shows the change in CO_2 concentration in the gas phase, at the interface, and in the liquid media for one loop through the riser and downcomer. This simulation was performed at 0.45 W/m2 and 5% CO2 enrichment of the feed air. The profile is presented at the start of the cultivation. As expected, the gas phase CO_2 concentration decreases as it travels up the riser due to mass transfer from the gas to the liquid phase (after an initial increase at the sparger gas inlet). The assumption of perfect gas venting results in the zero of gas phase CO2 in the downcomer. The liquid phase

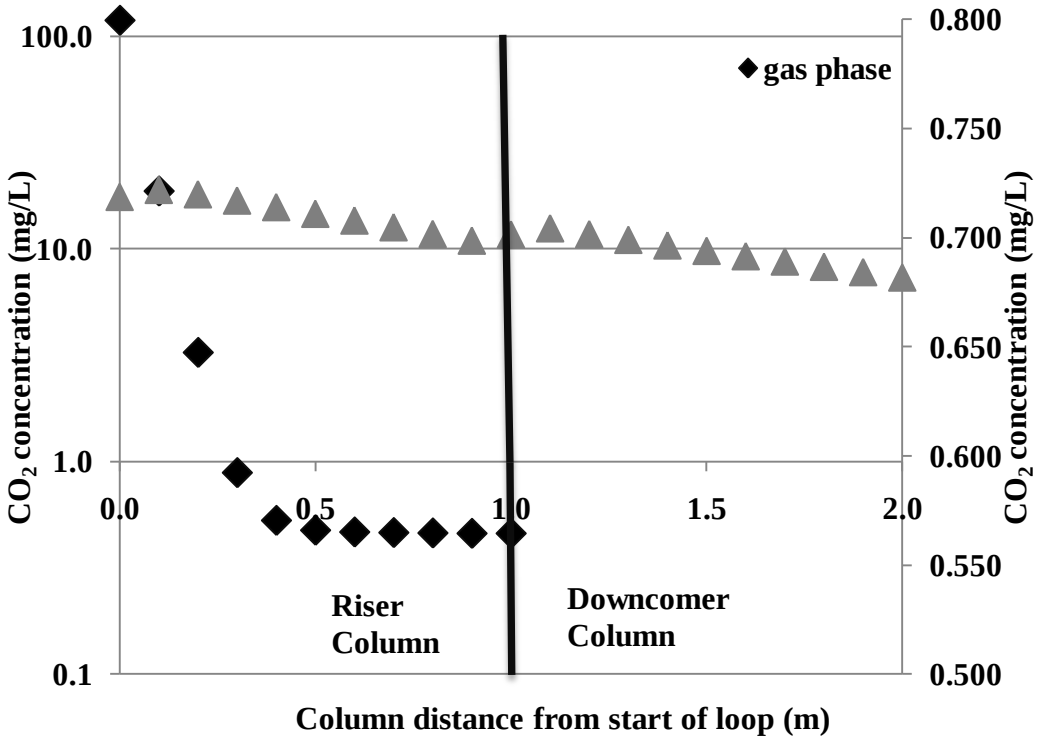

Figure 5.11 CO_2 concentration profile along the length of the column. 0 < Riser < 1 m, 1 m < Downcomer < 2 m. (0.45 W/m2, 5 % CO2 enrichment, 1 minute after cultivation start)

CO_2 concentration also decreases, although this value remains nearly constant. Although the liquid phase receives CO_2 from the gas phase continuously, that CO_2 is also continuously consumed by the growing *C. vulgaris* cells. Therefore, the decrease in the liquid phase concentration is small over the course of the column. An initial increase is also observed at the start of each new loop due to the influx of gaseous CO_2 into the bottom of the riser, which then impacts on the liquid phase. There is therefore a cumulative increase in the gas and liquid phase CO_2 concentrations with each loop through the reactor until saturation is reached.

5.6. Conclusions

A model incorporating the growth behaviour of *C. vulgaris*, the characteristics of light penetration, and the fluid dynamics of a novel external loop airlift photobioreactor (ELAPB) was developed. The simulated growth describes not only the biomass accumulation, but also the radial and vertical profiles of biomass and growth rate, radiant flux, and CO_2 concentrations in

the gas and liquid media phases. This model was found to be in agreement within 10% of experimental data collected during fed-batch cultivation in the ELAPB. The model was also used to predict optimum light and CO_2 concentration to be 0.30 W/m^2 and 5.8 % enrichment of the inlet feed air for *C. vulgaris* cultivation without time-consuming experimental trials.

5.7. Nomenclature

A_{Riser} cross sectional area of riser, m^2

AF gas flow rate, m^3/s

C_g CO_2 in inlet gas, %

D_R diameter of riser, m

H height of ELAPB column, m

H_e Henry's Law constant, g/L/g/L

I local radiant flux, W/m^2

I_o radiant flux at riserwall, W/m^2

K_a absorption coefficient, m^2/g

K_{SI} radiant flux saturation constant, W/m^2

K_{SS} CO_2saturation constant, g/L

K_{II} radiant fluxinhibition constant, W^2/m^4

K_{IS} CO_2inhibition constant, g^2/L^2

k_{La} mass transfer coefficient, h^{-1}

M_e maintenance coefficient, h^{-1}

pCO_2 partial pressure of CO_2 in inlet gas, atm

R radius of the riser, m

Ratio volumetric ratio of radial section to total riser volume, m^3/m^3

Re Reynolds's number, dimensionless

r length of light path, m

rad radial location within the riser, m

S liquid phase CO_2 concentration, g/L

S^* interface CO_2 concentration, g/L

S_o initialliquid phase CO_2 concentration, g/L

T time, s

U_{LIQ} liquid velocity in the riser, m/s

U_{GAS} superficial gas velocity in the riser, m/s

V_{LIQ} liquid circulation velocity, m^3/s

vol volume of radial section, m^3

X biomass density, g/L

X_o initial biomass density, g/L

X_T total biomass density, g/L

Y_{XS} yield coefficient, mg /mg

Y gas phase CO_2 concentration, g/L

y_o initial gas phase CO_2 concentration, g/L

z spatial column location, m

Greek letters

D dispersion coefficient, m^2/s

μ specific growth rate , h^{-1}

μ_m maximum specific growth rate , h^{-1}

μ_D dark zone specific growth rate , h^{-1}

μ_L light zone specific growth rate , h^{-1}

μ_F fluid viscosity,cP

ρ_F fluid density, kg/m^3

θ_G gas holdup, dimensionless

Chapter 6

6. Economic Assessment of an Integrated Bioethanol-Biodiesel-Microbial Fuel Cell Facility

A similar version to this chapter has been accepted and is presently in press in the journal Chemical Engineering Research and Design:

Powell, E.E., and G.A. Hill, "Economic Assessment of an Integrated Bioethanol-Biodiesel-Microbial Fuel Cell Facility Utilizing Yeast and Photosynthetic Algae", *ChERD,* **2009**, In Press.

The topics covered in this chapter have also been included in a short paper and presentation:

Powell, E.E., Hill, G.A., Evitts, R.W. and J.C. Bolster, "Novel Photosynthetic Cathode Coupled To A Fermentative Anode Used In A Bioethanol-Biodiesel Processing Facility", Conference Proceedings of the ECI Bioenergy II:Fuels and Chemicals from Renewable Resources, Rio de Janeiro, Brazil, March 8-13, 2009.

The material discussed in this chapter was also included in a paper presentation at the following conference:

Powell, E.E., Hill, G.A., Evitts, R.W., Sasi, D., Bolster, J.C., and M.L. Mapiour,"Integrated Biofuel Facility: Carbon Dioxide Consumption & Power Generation", IEA Bioenergy Conference, Vancouver, B.C., Canada, August 23-26, 2009.

Contribution of Ph.D. Candidate

The economic assessment was based on calculations and a design developed by Erin Powell, with guidance provided by Gordon Hill. Experimental data from previous work already presentedin previous chapters (Chapters 3, 4, and 5) was used as a basis for some of these calculations. The manuscript was written by Erin Powell, with editorial advice being provided by Gordon Hill.

Contribution of this paper to the overall study

The primary objective of this research is CO_2 consumption using microalgae cultivation, with concurrent by-product production. The growth kinetics and CO_2 consumption of *C. vulgaris* have been studied and discussed in Chapter 3, enabling the design of the novel ELAPB in which *C. vulgaris* growth is modeled in Chapter 5. However, the ultimate goal of any engineering research project is to determine what practical use it might have, particularly on an industrial scale. With the determination that a *C. vulgaris* culture can act as the cathode electron acceptor in a photosynthetic MFC in Chapter 3, and operate coupled to a yeast culture anode in Chapter 4, the opportunity for large-scale integration in a bioethanol plant presents itself. This chapter presents an analysis to demonstrate the economic feasibility of integrating thistechnology into an existing industrial, batch bioethanol facility.

Additional Information Not in the Manuscript

The manuscript presented in this chapter describes a design method (and analysis of the economic feasibility) forthe integration of a *C. vulgaris* cultivation into a large scale bioethanol plant. This is one industrial possibility suggested by the research results for coupled MFCs using yeast cultures at the anode described in Chapter 4. There are a variety of other industries where the *C. vulgaris* cultvation for CO_2 consumption could be integrated on its own just for environmental benefit. Harvest of the microalgae biomass and its byproducts would offset the cost of integration and operation, in addition to the government Carbon Credit program (Haugen-

Kozyra, 2007). In addition to the value of governmental Carbon Credits, part of the harvested biomass could be used for biodiesel production and the remaining biomass sold as an animal feed supplement.The study discussed in this chapter also describes the case where the photobioreactor design has been adapted for use with sunlight. This is achievable as there exist both outdoor photobioreactor cultivation facilities (Grima et al., 1999; Lee and Low, 1992) and indoor facilities using sunlight transmission systems such as lenses and optical fibres (Ogbanna and Tanaka, 2000).

One such use that may be ideal for wide-scale industrial implementation of the ELAPB and microalgae culture is the bioremediation of CO_2 from flue and flaring gases. Flue and flaring gases typically contains between 5-15% CO_2 as exhaust from power plants (Kingsley, 2009; Li et al., 2008; Doucha et al., 2005). Kinetic growth data collected as part of this work (Chapter 3) and using the novel ELAPB (Chapter 5), indicates that *C. vulgaris* grows well at an inlet gas concentration of 10% CO_2. The integration cost could be offset in many of the same ways as those described in Chapters 6 and 7. A complete economic feasibility study would need to be performed to determine if integration on a large scale for a facility of this specific type is practical at this time. Feng (2008), Doucha et al. (2005), and Maeda et al. (1995) have already performed promising preliminary experimental work on using flue gas from coal-fired power plants for CO_2 fixation by microalgae. The work of Doucha et al. (2005) reported that for flue gas containing 6-8% CO_2, 10-50% mitigation should be achievable using *Chlorella* species.

The first practical consideration would be the need for cooling before sending the exhaust gas to the photobioreactor as flue gas temperatures are greater than 200 ^{O}C, while the maximum temperature that *C. vulgaris* can tolerate is 36 ^{O}C, but depends to some extenton the pH (Zargar and Ghosh, 2007, Mayo, 1997). Investigation ofthe toxic effects of some components of the flue gas would also need to be investigated, although in general, microalgae such as *C. vulgaris* are able to grow under many stressful nutrient conditions. Possible algae toxicity might result from the components of the flue gas, such as toxic particulates, alkanes, carbon monoxide, nitrogen oxides and sulfur oxides,.Li et al. (2008), Doucha et al. (2005), and Maeda et al. (1995) reported that *Chlorella* species did not exhibit significant inhibition due to exposure to compounds such as nitrogen oxides and sulfur oxides in flue gas. Many of these compounds are presently scrubbed from plant exhaust using existing processes (Doucha et al.,

2005), but toxins such as mercury may still be present and either inhibit algae growth or depress any microalgae biomass market value.

6.1. Abstract

A strategy for the integration of a novel CO_2 photosynthetic culture and power generation system into a commercial bioethanol plant is presented. Photosynthetic microalgae column photobioreactors, acting as cathodic half cells, are coupled with existing yeast fermentors at a bioethanol plant, acting as anodic half cells, to create coupled microbial fuel cells. The microalgae photobioreactors also sequester CO_2 emitted by the yeast fermentors. Incorporating microbial fuel cells into an existing bioethanol plant generates some of the power used in bioethanol production and the microalgae species *Chlorella vulgaris* contains oil, which acts as a byproduct for the production of biodiesel.

The goal of the study is to determine the required design specifications of novel, airlift photobioreactor cathodes to make the integrated system economically feasible at an existing bioethanol plant. Data from previous experimental studies was used to develop the optimum integration strategy. The reported parameters include photobioreactor size, number of integrated microbial fuel cells, fuel cell outputs, oil (for biodiesel) production rate, and CO_2 consumption rate.

6.2. Introduction

The increasing demand for energy combined with decreasing supplies of fossil fuels has led to great interest in alternate energy production technologies (Kouroussis and Karimi, 2006). The ongoing use of petroleum-based fossil fuels is now also widely considered to be unsustainable due to both diminishing supplies and the contribution of these fuels to the accumulation of carbon dioxide in the environment (Chisti, 2007). The microbial fuel cell (MFC) is a new power generation technology, which uses the electrons released in the oxidation-reduction reactions of microbial metabolism to generate electricity. Studies employing a wide

variety of designs, microorganisms, and substrates, have been performed using microbial anodic half cells (Kim et al., 2007a; Oh and Logan, 2005; Rabaey et al, 2003) coupled to electrochemical half cells, and more recently microbial bacterial cathodes have also been developed (Clauwaert et al., 2007; He and Angenent, 2006). A novel photosynthetic microbial cathodic half cell (Powell et al, 2009b), employing the microalgae species *Chlorella vulgaris* as the direct electron acceptor was developed earlier by us. Recent work (Powell et al., 2009a) coupled this photosynthetic half cell to a fermentative yeast anode, creating a complete, coupled MFC. Present experimental work is focusing on improving *C. vulgaris* biomass production using a novel external loop airlift photobioreactor (PBR) (Sasi et al., 2009).

This novel loop external airlift PBR is being equipped to operate as the cathodic half cell in an improved coupled MFC. This novel photosynthetic MFC design can then be integrated into an existing bioethanol plant to create coupled MFCs with the existing industrial yeast fermentors acting as anodic half cells. This integrated system will generate power for use in the existing bioethanol plant, and through photosynthesis by the microalgae growth in the cathodic PBR half cell, will consume CO_2 emitted from the production of bioethanol at the existing facility. The large scale of the yeast fermentors in the existing bioethanol plant, and the significantly greater growth rate of yeast relative to algae (Powell et al., 2009a), necessitates the use of multiple smaller PBRs columns operating in parallel around each fermentor.

The production of microalgae during operation also provides the opportunity for the production of another energy byproduct. Renewable transport fuels are becoming increasingly important as environmentally friendly and sustainable energy sources. Biodiesel derived oil crops are a potentially renewable and "carbon neutral" alternative to fossil fuels. Of the many oil-producing sources, microalgae are considered (Christi, 2007) to be the only source of renewable biodiesel capable of meeting global demand for transport fuels. Microalgae use light to produce oil by photosynthesis, but more efficiently and at higher productivities than agricultural plants. Among microalgae species, oil contents can reach up to 80 % (d.w.), and levels of 20-50% are quite common (Spolaore et al., 2006). The eukaryotic green microalgae species *C. vulgaris*, while containing a more modest 28-32% oil (Christi, 2007), also grows extremely rapidly (Powell et al., 2009b) and is easy to cultivate (Richmond, 2004). The microalgae produced in the PBRs of a bioethanol plant could therefore be sold for the production of biodiesel.

An integrated plant design that incorporates both CO_2 consumption and biofuel production appears to be the best approach to enable industrial application of these new technologies for environmental benefit. The integration of the novel microalgae PBR/MFC cathodic half cell systems into an existing bioethanol plant is made economically feasible by the generation of three new revenue streams: electrical power generation, oil (for biodiesel) production, and the capture of CO_2 from the yeast fermentation stage of the existing bioethanol facility.

6.3. Integrated System Methodology

6.3.1. Bioethanol Production Plant

The bioethanol production facility used as a model for this work is a typical large-scale production facility, assumed to be already in operation in Western Canada. It produces 130 million L of ethanol annually using 28,570 tonnes per year of grain as feed. The portion of the existing facility that needs to be modified for integration with microalgae PBR cathodes to create MFCs is the fermentation stage, where glucose is converted to ethanol by yeast in large stirred tank fermentors. A facility that produces 130 million L has 15 tanks in use at any time, with an additional four filling and four emptying, for a total of 23 tanks. Each fermentor has a working volume of 1.0 million L, with an assumed diameter of 10 m and a height of 15 m, and only the 15 in use can be used as part of a working MFC. Typically, saccharification and fermentation are carried out together (Lin and Tanaka, 2005), with the dextrins produced from grain starch during the liquefaction stage being converted to glucose by amyloglucosidase enzyme and to ethanol and CO_2 by yeast, simultaneously. Excess glucose is assumed to be present during fermentation (with it all being consumed (Hill and Robinson, 1990)), and ethanol production reaches 9.5 wt % alcohol (Lin and Tanaka, 2005). The batch fermentation stage of the process typically requires 48 hours. The number of operating days in a year, t, for both the existing and integrated plants is assumed to be 330, or a 90% operating factor (Ulrich and Vasudevan, 2004).

Each of the existing 23 yeast fermentation tanks, having a volume of 15000 m^3, must be equipped with electrodes to make them usable as the anodes of integrated MFCs. The electrodes

employed in both microbial half cells are carbon graphite mesh rather than the rod electrodes used experimentally in previous work (Powell et al., 2009a; Prasad et al., 2006; Rhoads et al., 2005). This type of electrode is a graphite mesh synonymous to tower column packing that provides a large amount of electrode surface area without impeding microbial growth (Nikakhtari and Hill, 2005a). The graphite wire has a diameter of 4.6×10^{-4} m (Nikakhtari and Hill, 2006) and is packed within the full height of the tank working volume. A porosity of 99% is employed to minimize detrimental impact on microbial growth (Nikakhtari and Hill, 2005d). Electrodes must be placed in all 23 tanks, although only 15 will be in use at any one time.

The electrode capital cost in each fermentor was determined from the $150 purchase cost, P_m, of each 100 m x 5 m, 25 commercial mesh sheet (Anping Web Wire Mesh Company, West Wardsboro, Vermont, USA). The total cost depends on the volume of packing per sheet, and the number of sheets required to fill the vessel volume at 99 % packing porosity, h. The volume of graphite wire is a single mesh sheet, V_m, is:

$$V_m = \left(\left(\frac{\pi}{4}(d_m)^2 l_m\right)\left(\frac{n_m}{0.0254}\right)w_m\right) + \left(\left(\frac{\pi}{4}(d_m)^2 w_m\right)\left(\frac{n_w}{0.0254}\right)l_w\right) \tag{6.1}$$

where l_m is the length of mesh sheet (m), w_m is the width of the mesh sheet (m), d_m is the wire diameter (m), n_m is the strands per inch of mesh ($inch^{-1}$).

The total cost of mesh, C_{PA}, required to fill 1 % of the volume of each existing yeast fermentor is:

$$C_{PA} = \left(\frac{100-\eta}{100}\right)\frac{1000}{V_m}P_m \tag{6.2}$$

Also, a chemical mediator, methylene blue (MB), must be added to the yeast fermentation media to enable in the transfer of electrons between the yeast cells and the electrode. According to previous work (Powell et al, 2009b), the chemical mediator is only required at a low concentration and will not affect the yeast growth kinetics.

6.3.2. Microalgae PBR/Cathode Design

The microalgae PBR is a novel airlift external loop design currently being tested experimentally in our laboratory (Sasi et al., 2009) for both enhanced biomass growth and as a MFC cathodic half cell. Maximum column height is limited to 50 m by the acrylic Plexiglas®

construction material, and riser diameter is constrained to 1 m to ensure light penetration inside the riser to the algae cells. The feed air contains 10% CO_2, determined to be the optimum level for *C. vulgaris* growth (Powell et al., 2009b), and is bubbled directly into the cell culture by sparger. The novel PBR will be operated continuously with nutrient feed flowing in at the bottom of the riser and spent culture being withdrawn after the downcomer. The light source provided to the microalgae cells for photosynthesis in the novel PBR is sunlight. The airlift PBR would include a unique, external lighting system that transmits light from the outdoor source to the outside surface of the PBR.

The electrode employed in the microalgae cathode is identical to that employed in the adapted yeast fermentors discussed in the previous section. The carbon graphite mesh electrode has the same 4.6×10^{-4} m diameter, d_m, and is packed within the full height of the riser tank working volume with a porosity, η, of 99%. A chemical mediator will also be added to the algae culture medium, in this case 2-hydroxy-p-napthoquinone (HNQ) at 93 mg/L, to enable electron movement between the electrode and the microorganisms.

A schematic of a yeast fermentation tank connected to a microalgae PBR, to create a coupled MFC, is shown in Figure 6.1. The CO_2 produced by the yeast fermentation is split and pumped directly into the surrounding PBRs and combined with air to form 10% CO_2 enriched air for photosynthetic microalgae growth. The electrode packing in both vessels is connected through an electric circuit. The fermentor and surrounding PBRs are attached through proton exchange channels containing Nafion proton exchange membranes (PEMs). This is shown schematically in Figure 6.2. There are no significant pH changes observed in the media of the PBRs. The hydrogen ions crossing the PEMs into the PBRs are likely used by the algae in their own metabolism.

6.3.3. Cost of PBR Cathodic Half Cell(s)

The capital cost of installing a single microalgae PBR, C_T, to act as a cathodic half cell for a coupled MFC, and for CO_2 consumption and biodiesel production, includes the cost of the vessel, with lighting system, electrode, and sparger. Each one is operated in continuous mode, with a biomass density of 15 g/L and a constant flow rate, F, of 2.0 m^3/h. The PBR, complete with sunlight lighting system, C_L, was modeled as a shell and tube heat exchanger for cost

purposes. This cost is based on the surface area that must be available for sunlight in order to have adequate light penetration into the algae PBR. Using the data of Ulrich and Vasudevan (2004), an equation was developed for the cost of the lighting transfer system as a function of vessel height, H, and diameter, D. The cost of the Nafion® PEM is included with the microalgae reactor. Membrane replacement cost is included in the maintenance costs discussed in the following section regarding operating costs.

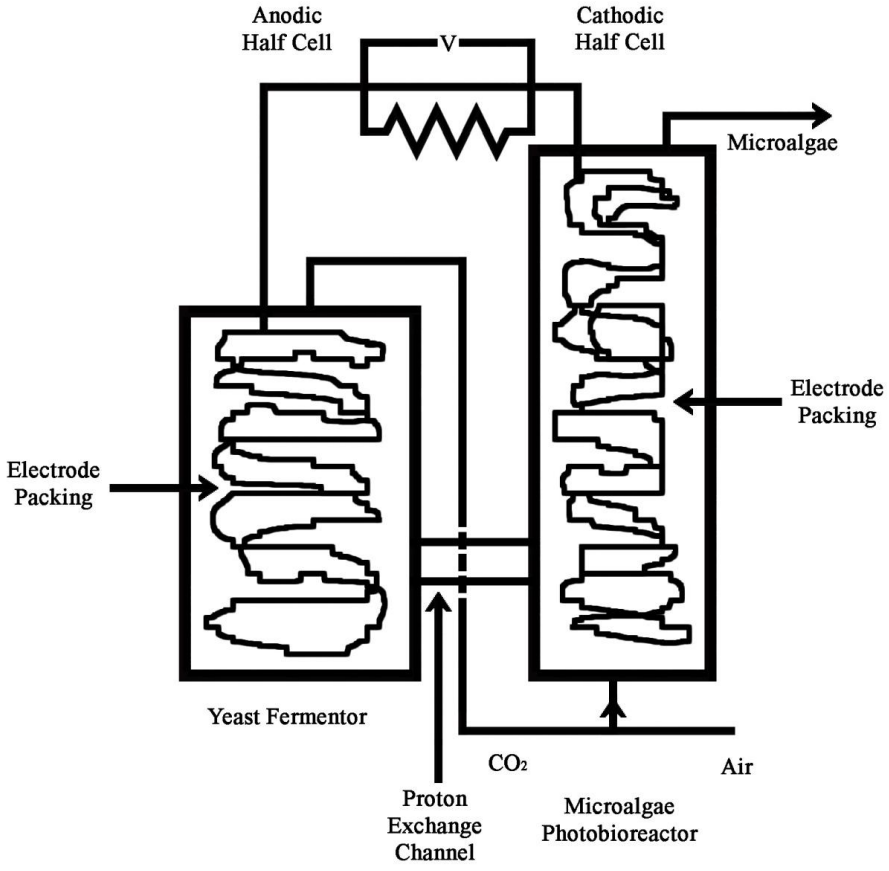

Figure 6.1. Schematic of a coupled MFC, showing a single yeast fermentor and a microalgae PBR.

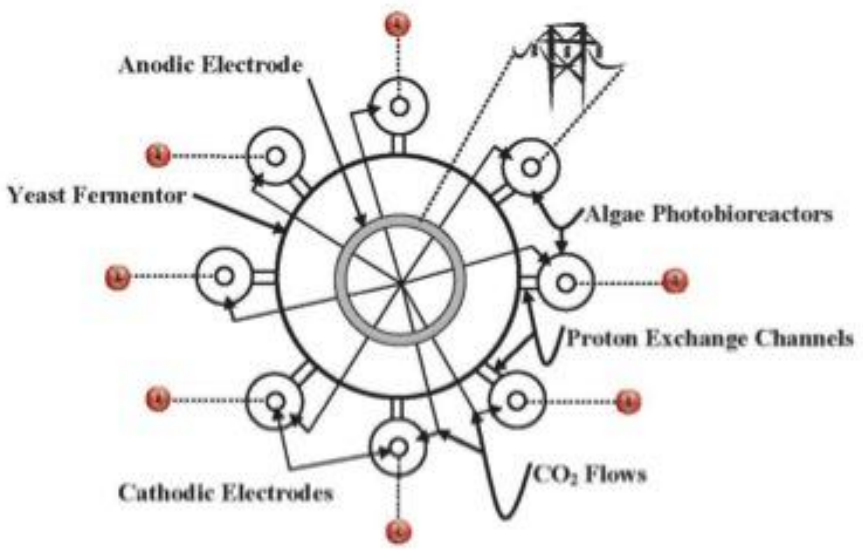

Figure 6.2. Sketch demonstrating the location of photobioreactors around a yeast fermentor.

$$C_L = 25906.82\ln(HD) - 16773.9 \tag{6.3}$$

The cost of the required sparger, C_S, for each airlift vessel was determined to be:

$$C_S = 45332.55D^{1.2047} \tag{6.4}$$

from the work of Ulrich and Vasudevan (2004), where the sparger diameter was related to the PBR vessel diameter, D, by the equation D_s=0.6D to give the above equation. The Chemical Plant Cost Index was 400. The cathode electrode packing, C_{PC}, for a single airlift vessel was determined in a manner similar to Equation (6.2), but for each cathodic PBR:

$$C_{PC} = \left(\frac{100-99}{100}\right)\frac{\pi}{4}D^2 H \frac{1}{V_m}150 \tag{6.5}$$

The capital cost of installing the PBR vessel(s), C_t, into an existing ethanol production plant is therefore the sum all PBR capital costs, multiplied by the number of PBR vessels, N, and the cost of anode packing multiplied by the number of fermentation vessels, $N_{F,}$, (in this case 23):

$$C_t = 3\left(N\left(C_S + C_{PC} + C_L\right) + N_F\left(C_{PA}\right)\right) \tag{6.6}$$

The purchase cost of this equipment must also be increased by a factor of 3 (Ulrich and Vasudevan, 2004), as shown in Equation (6.6) to obtain the installation cost for the required

equipment. With fee and contingency, the capital cost must be increased by a factor of 1.2 (Ulrich and Vasudevan, 2004). This results in a total capital cost of :

$$C_T = 1.2C_t \tag{6.7}$$

The capital cost will be acquired by loans and paid off over the life of the plant. The interest on the loan required to purchase the capital equipment also needs to be repaid. A low interest government loan can be obtained in Canada at 4% for an environmental "green" initiative such as this project to encourage such sustainable technology developments. Therefore, a 4% interest rate, i, is applied to the total capital remaining to be repaid each year and amortized over the 20 year life, Y, of the new integrated portion of the plant:

$$A = C_T \frac{i(1+i)^Y}{(1+i)^Y - 1} \tag{6.8}.$$

This annual payment, A, of both principal and interest, in fact becomes part of the yearly operating costs of the plant.

6.3.4. Operating Costs

The additional operating costs of the integrated system include labour, materials, maintenance, utilities, administration, and marketing for the operation of the installed PBRs. Annual material cost for each PBR consists of *C. vulgaris* inoculant and nutrient media, P_f, ($0.029/L) for continuous operation, 330 days of the year. Annual labour, P_l, cost is one technician for every four PBR vessels, at $60,000/year.

The total material cost, N_{ut}, required annually is the amount required to fill the column with culture medium (nutrients) entirely three times each year, as well as the nutrient media required to operate it continuously during the remainder of the year. The need to refill each column three times each year is due to stoppages required for cleaning, maintenance, or plant shutdowns. This cost includes algae innoculant. The cost of continuously adding nutrient medium to the PBRs at a flow rate F is a function of both the PBR volume, and the total number of PBRs, N, integrated into the existing ethanol plant (during annual plant years t).

$$N_{ut} = 3NP_f\left(\frac{\pi}{4}1000D^2H\right) + NP_f 1000Ft \tag{6.9}$$

The total annual labour cost, L, is the annual labour cost per four vessels, P_L, multiplied by the total number of PBRs integrated into the existing plant.

$$L = N\frac{P_L}{4} \tag{6.10}$$

The annual cost of maintenance, M_t, includes the cost to maintain all new equipment, including replacing Nafion membranes. Maintenance costs are estimated to be 6% of the total capital cost (Ulrich and Vasudevan, 2004). Therefore the annual maintenance cost is given by:

$$M_t = 0.06C_T \tag{6.11}$$

The main utility cost is the power required to operate the pumps and compressors, estimated at 0.5 kW for each PBR column installed, to and from the PBR columns. Utilities, U_p, are estimated at a power cost, P_w, of \$0.12/kW-h as:

$$U_p = 0.5tP_w \tag{6.12}$$

Annual administrative costs, A_m, include all administrative salaries, materials, and benefits to all labourers. Administrative salaries and wages are assumed to be 20% of the plant labour wages, with further administrative operating costs estimated to be 25% of the plant's overall utilities. This is estimated using guidelines in Ulrich and Vasudeven (2004). This is determined from:

$$A_m = 0.2L + 0.25U_p \tag{6.13}$$

Chemical mediators must be purchased for both the cathodic and anodic half cells. The estimated annual cost of mediators, CM, supplied in bulk from the manufacturer is estimated at a price, P_{HNQ}, \$0.337/g, and a price, P_{MB}, \$0.018/g for the HNQ and the MB, respectively. The concentration, $[C_{HNQ}]$, of HNQ in each PBR is 93 mg/L, which must be multiplied by the volume of each PBR, the total number of PBRs, and although the mediator is re-used, a 10% factor for losses throughout the year must be accounted for:

$$CM_{HNQ} = P_{HNQ}\frac{[C_{HNQ}]}{1000}\frac{\pi}{4}D^2HN0.1 \tag{6.14}$$

The concentration, $[C_{MB}]$, of MB in each fermentation tank is 200 mg/L, which again must be multiplied by the volume, V_F, of each tank (1 million L), the total number of tanks in operation at any one time, N_f., The yeast fermentors in the existing plant are operated in batch mode (48 hours typically), therefore when they are emptied and refilled, the chemical mediator must be re-

introduced in to the fermentation tank so it can act as an anodic half cell. The mediator is re-used, but a 10% factor for losses throughout the year included:

$$CM_{MB} = P_{MB}\frac{[C_{MB}]}{1000}V_F N_F 0.1 \tag{6.15}$$

Marketing may be required for the newly integration plant. These costs, M_r, are typically 10% of the operating costs (Ulrich and Vasudevan, 2004). Therefore,

$$M_r = 0.1\left(N_{ut} + L + M_t + U_p + A_m + CM_{HNQ} + CM_{MB}\right) \tag{6.16}$$

The total annual operating cost is:

$$Op = N_{ut} + L + M_t + U_p + A_m + M_r + CM_{HNQ} + CM_{MB} \tag{6.17}.$$

6.3.5. Microalgae Production in PBR Cathode

Past work using a simple well-mixed bioreactor (Powell et al., 2009b), reported a maximum biomass production rate of 4 mg/L-h, similar to maximum rates reported elsewhere in the literature. However, results from present experimental work using the airlift PBR with *C. vulgaris* (Sasi et al., 2009) indicate biomass growth rates approaching an order of magnitude higher than this value. Therefore, given the greater biomass growth rate and the use of the continuous operation mode, a biomass concentration, [a], of 15 g/L is assumed to be constantly maintained in the microalgae PBRs. With a constant flow rate, F, of 2.0 m^3/h, at a dilution of 0.05, the production rate of *C. vulgaris*, $\overset{o}{m}$, in a novel PBR of a given volume is therefore:

$$\overset{o}{m} = [a]F\frac{\pi}{4}D^2H \tag{6.18}$$

The total annual algae biomass production, m, cultivated in one PBR is based on 330 operating days, t, per year (using a 90% operating factor from Ulrich and Vasudevan, (2004)).

$$m = t\overset{o}{m} \tag{6.19}.$$

6.3.6. Carbon Dioxide Consumption

The determination of the CO_2 consumption due to microalgae growth in the integrated PBRs was based on previous experimental work. Powell et al. (2009b) found that *C. vulgaris* produced 0.51 mg biomass / mg CO_2 during growth. A CO_2consumption rate, r, of double this

value, 1.02 mg biomass / mg CO_2, is employed in this study based on present experimental work using the airlift PBR (Sasi et al., 2009). This higher value is due to the use of CO_2 for both growth and maintenance under more stressful conditions. The total annual CO_2 consumed by the microalgae, CO_{2C}, can be determined from this consumption rate and the annual biomass production (Equation 6.19), and the total number of PBR half cells that are integrated into the existing ethanol plant.

$$CO_{2C} = Nr\frac{m}{1x10^6} \tag{6.20}$$

The total CO_2 produced in the 130 million L/yr ethanol facility, CO_{2P}, is 1.114 x 10^8 kg/year. The amount of that CO_2 that is left after uptake, as a percentage b, by *C. vulgaris* growth is

$$b = (CO_{2P} - CO_{2C})100 \tag{6.21}$$

The present value of carbon credits, P_{CO2}, is \$15/tonne CO_2 (Haugen-Kozyra, 2007), which are awarded for every tonne of greenhouse gas that is removed prior to venting to the atmosphere. These make up one of the revenue streams, E, of the integrated plant.

$$E = \frac{P_{CO_2}}{1000}CO_{2C} \tag{6.22}.$$

6.3.7. Biodiesel from *C .vulgaris*

The *C. vulgaris* cells collected continuously from the PBR are assumed to contain 25% oil (Chisti, 2007). As the PBR algae output stream will be sold for biodiesel production, but will require further processing after sale, its market value is assumed to be only 25% of that of crude oil. The crude oil price, P_O, was assumed to be \$80 /barrel (USD), a representative market value from August and September 2008 (Nymex, 2008). The annual biomass production, m, is as described in Equation (6.19), and for a total number N of PBR vessels, the annual oil production, B, is:

$$B = N0.25\frac{m}{1000}0.25\left(\frac{P_O}{158.98}\right) \tag{6.23}$$

An inflation of 10% in the value of biodiesel is assumed each year over the course of the life of the plant. The current biodiesel price, P_{Dy}, is therefore a function of the year from start-up and the inflation rate.

$$P_{Dy} = 80(1 + (0.1y)) \tag{6.24}.$$

6.3.8. Power Output of Integrated MFC

The power generation obtained from the coupled MFCs in the integrated plant is based on previous work using a similar coupled MFC (Powell et al., 2009a). This photosynthetic cathode, when coupled to a fermentative yeast anode, can be expected to produce a current, c, of 1.0 A/kg DW algae cells at a measured potential, v, of 1.0 V. This results in a power output, w, of approximately 1.0 W/mg DW algae cells present in the PBR cathodic half cell. Growth on the algae side the coupled MFC is significantly slower that that on the yeast side (Powell et al., 2009a), and with a much larger capacity fermentation vessel, multiple PBR columns in parallel can be supported by a single yeast fermentor, each one forming a coupled MFC.

The annual power output, P, from all the integrated MFCs in the entire bioethanol plant is therefore based first on the output from a single installed column operating continuously. This column has a constant biomass concentration, [a], in a column of known volume, based on diameter, D, and column height, H, giving the constant power output. Once the total number of PBRs is considered:

$$P = wN[a]1000\frac{\pi}{4}1000D^2H \tag{6.25}$$

Calculating the annual revenue, R, returned from the coupled MFC power regeneration in terms of kW-h over the operating year, t, with an electrical cost, P_W, of \$0.12/kW-h:

$$R = \frac{P}{1000}tP_w \tag{6.26}$$

Actual voltage and power outputs may reach higher levels in a system fully integrated into an industrial bioethanol plant than those studied experimentally (Powell et al., 2009a). The effect of glucose concentration in the anodic half cell of the MFC was studied up to 200 g/L, and yeast biomass concentrations of 12500 mg/L. With the existing industrial yeast fermentors serving as anodic half cells, and with grain feeding at high volumetric loadings, of which 2/3 is starch that is liquefied to glucose, further increases in MFC power output may be observed in practice. Also, when microbial cells are stressed they typically consume more of their food supply to compensate, and in the case of the microalgae, this could mean increased CO_2 consumption, but also perhaps increased use of nutrient feed.

6.3.9. Taxation on Profits

In Western Canada, a very low taxation rate of 2% (Government of Canada, 2007) is applied to energy processes until the capital costs have been repaid. The taxation rate then increases to 21%. Taxes are applied to the net income of a business. This will include the income from the sale of the *C. vulgaris* produced (for oil for biodiesel). The value of the power generated by the coupled MFCs integrated into the existing bioethanol plant is not taxed as it is used internally. The carbon credits obtained for removal of CO_2 from the bioethanol plant emissions are non-taxable benefits. The depreciation of the cost of the capital equipment is calculated by straight line depreciation of 10% per year over 10 years, a standard value according to Canadian Corporate Taxation Law (Government of Canada, 2007). The annual taxes, T, are only calculated for the 20 year life of the plant, over which the capital loan is to be repaid, so the tax rate, x, is limited to 2% for the purposes of this integration study. For operating years, y, one through ten (which include depreciation):

$$T = x\left(B + C_T - C_T(0.1y) - A - Op\right) \tag{6.27}$$

and for operating years eleven through twenty (once the value of the capital equipment has fully depreciated):

$$T = x\left(B - A - Op\right) \tag{6.28}.$$

If the annual tax value in any year is negative, then the taxes paid in that year are zero.

6.3.10. Final PBR/MFC Integration Design

The optimized design parameters for the integrated plant design are the dimensions of the microalgae column PBRs, namely height, H, and diameter, D, giving a specific volume, and the total number of PBRs being installed in the existing ethanol plant creating an equivalent number of coupled MFCs. The optimum design is such that the annual net cost of implementing *C. vulgaris* production into the described existing ethanol plant is zero. The net annual cash flow of the integrated PBR/MFCs operating in the existing plant must be positive. Time zero is the year in which operation of the PBR/MFC system begins. The plant is assumed to be built instantaneously for the purposes of this economic study. Both the bioreactor dimensions and number of total PBRs, N, placed in the plant was determined by maximizing the net present

worth (NPW) of the integrated plant. The pre-existing ethanol production facility was not included in the cash flow, taxation, and cost analyses as it is already in operation and assumed to be operating profitably.

The maximum number of cathodic PBR half cells that can be supported by a single large anodic fermentor half cell, at maximum output, is determined by several factors. There is a maximum amount of current that the number of yeast cells present during fermentation can produce. The sharing of a single yeast fermentation tank by multiple microalgae PBRs to create multiple MFCs is shown schematically in Figure 6.3. Because there are only 15 of the 23 fermentation tanks in operation at any one time, multiple connections exist between the cathodic PBR half cells and the anodic fermentors. Since the yeast growth rate is significantly higher than that of microalgae, and the volume of the yeast fermentors is significantly greater than that of the PBR columns, the yeast fermentors are capable of supporting a significant number of PBR columns operating in parallel.

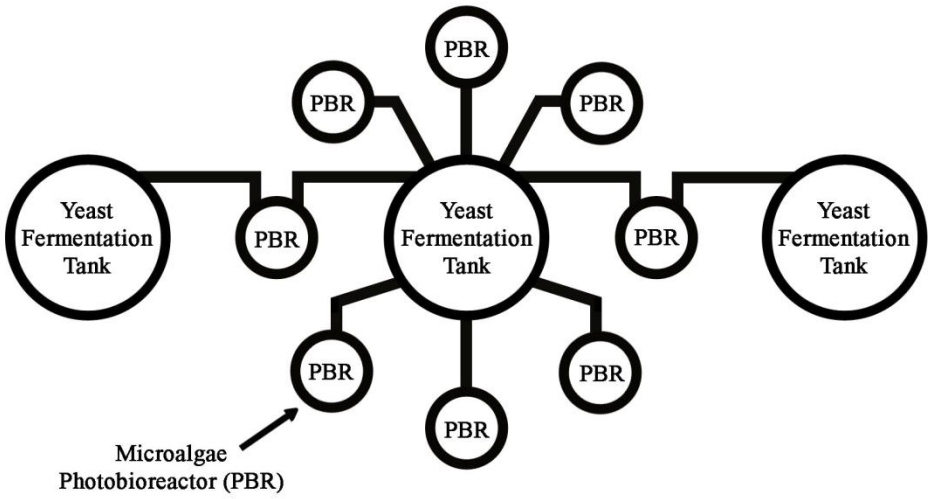

Figure 6.3. Multiple PBRs surrounding a single existing fermentation tank. Electrical connections are required to multiple fermentors.

The yeast inoculation is typically 5% of the ultimate concentration. The yeast concentration reaches 20 g/L over the course of the fermentation stage (Hill and Robinson, 1990). Because the yeast fermentor stage of the bioethanol production in the existing plant has

such a varying concentration, an average value of 10 g/L (10,000 mg/L) is used as the representative yeast concentration in the fermentor for the purposes of this study. The current obtained on a mass basis for yeast fermentation cultures from previous work (Powell et al., 2009a) using batch cultures with 200 g/L glucose is 1 A/ mg cells. Therefore there is a limit to how many microalgae cathodic columns a single fermentative anode would be able to support with sufficient electrons to achieve the desired current and power levels. Given the significantly larger fermentation tank relative to the column PBR volume, the number of PBR columns that can be operating in parallel around a fermentor is far greater than would be practical for this design. The amount of CO_2 available could also become limiting, as it is required for photosynthesis. The maximum number of PBR columns therefore, and the CO_2 requirements of the resulting algae biomass production, cannot exceed the physical space available in the existing bioethanol plant.

The maximum number of PBR columns that can be installed around a single yeast fermentor is determined from the column diameter, the spacing, and the fermentor circumference. The circumference, CR, of the a single fermentor is calculated from the fermentor diameter, D_F. An additional 1 m (0.5 m on each side) is allotted to ensure space is available outside of the fermentor for the PBR columns themselves. The fermentor circumference is:

$$CR = 2\pi\left(\frac{D_F + 1}{2}\right) = \pi(D_F + 1) \tag{6.29}$$

The space for PBR columns around each fermentor is therefore CR, and each fermentor uses its own diameter, D, of space plus another 0.5 m for attached equipment and maintenance access. Therefore the maximum number of columns, n_{max}, which can be attached to a single fermentor, according to the space limitations is:

$$n_{\max} = \frac{CR}{(D + 0.5)} \tag{6.30}$$

The positive cash flow for the integrated section of the plant for each year includes the revenue from the sale of the biomass (with oil) from *C. vulgaris* for biodiesel production, the value of power regeneration from the coupled MFCs, and the carbon credits from bioremediation.

$$CF_{Py} = B + R + E \tag{6.31}$$

The negative cash flow each year includes the yearly loan payment on the capital, taxes, and operating costs.

$$CF_{Ny} = A + T + Op \tag{6.32}$$

The NPWof the integrated section of the plant assumes that the business requires a 10% return from its operation, and is determined from the positive and negative cash flows for each year of operation (over the 20 year plant life) and the required return on investment.

$$NPW = \sum_{y=1}^{20} \frac{\left(CF_p - CF_N\right)_y}{\left(1+0.1\right)^y} \tag{6.33}$$

The optimum dimensions of height, diameter, and resulting volume, of each identical microalgae PBR column, as well as the total number installed, were determined using the Newton-Raphson method. All of the constraints and equations discussed in the previous sections were incorporated in order to maximize the NPW of the plant. The NPW of a particular design provides a measure of the economic feasibility of building the integrated plant according to that design and the desired return on the investment. A positive NPW value indicates that the integrated biofuel facility will be profitable while returning a 10% return on investment.

6.4. Results and Analyses

The optimum design of the cathodic PBRs for integration into the existing ethanol plant is based on the installation of multiple tall, narrow columns around the existing fermentor tanks. Each optimum airlift PBR is 50 m in height, with a 1 m diameter, resulting in a working volume of 39.3 m^3. The results of the optimization of the design of the newly integrated portion of the biofuel facility demonstrate that it is necessary to maximize the PBR column dimensions in order to offset the column installation costs. The column height of 50 m is the maximum considered practical, due to the construction material, and the diameter of 1 m cannot be exceeded if light penetration is to be adequate. Smaller columns cannot be built if an economically viable design is to be achieved. This column design however does result in a positive NPW, with a rate of return of 10%, for any number of installed columns studied. These results indicate that each PBR column essentially "pays for itself" with the multiple revenue streams from its operation,

assuming there at least as many total PBR/MFCs installed in the plant as there are fermentation tanks in operation at any one time.

Since only one column design has been demonstrated to produce sufficient microalgae yields (and therefore revenue in the form of oil (for biodiesel), electricity, and CO_2 consumption) to offset the cost of installation and operation, all calculations of NPW will be performed using this PBR column design. The effect of the total number of PBRs, and hence the total number of coupled MFCs, integrated into the existing bioethanol production facility is shown in Figure 6.4. The dimensions of the microalgae PBR cathodes are the optimum values (D = 1 m and H = 50 m). Figure 6.4 demonstrates the NPW of the newly integrated PBR portion of the facility as well as the annual power generation, % of CO_2 bioremediation from the existing bioethanol plant, and the volume of oil produced for biodiesel production. The number of PBR cathodes per single existing fermentation tank anode, n, is the total number of coupled MFCs, N, divided by 15. The number of installed PBR columns studied varies from one per fermentor (in use) to the maximum number that is theoretically possible in practice.

The total amount of CO_2 (from the existing bioethanol facility) consumed by the *C. vulgaris* growth, the volume of oil (for biodiesel) produced, and the power generated all increase with the number of MFCs integrated into the bioethanol plant. These three revenue streams all provide positive cash flow for the integrated facility to offset costs. As expected, each one increases with the number of coupled MFCs in the biofuel facility, since each represents a PBR column and increased microalgae production. The NPW of the integrated facility design also increases with the number of PBR columns (and coupled MFCs). The NPW continues to increase with the number of coupled MFCs in the biofuel facility, but as seen in Figure 6.4 at CO_2 consumption of 100%, that number cannot increase beyond N = 120 (or 8 per fermentor in use). This is limited by the CO_2 available for photosynthetic growth from the existing bioethanol plant. Also, while the NPW does increase with the number of PBR/MFCs installed, it does not do so linearly. Some of the capital cost of the integrated plant is due to modification of the existing fermentation tanks which is not significantly affected by the number of columns installed. As well, some operating costs do not increase appreciably with the addition of extra columns in parallel at the same fermentor.

The design requires that multiple coupled MFCs be created throughout the existing bioethanol plant, meaning that the PBRs will be connected to each of the 15 operating yeast

fermentors. However, the total number of PBRs must be distributed among the 23 fermentation tanks present in the plant, with permanent connections to multiple fermentors, and switches will open and close the circuits to the 15 fermentors in use at any one time. Therefore, this same number of coupled MFCs will always be in continuous operation, as are the microalgae PBRs, but the electrical connections will be open and closed automatically every 48 hours (batch time period of the yeast fermentation stage) such that only 15 of the 23 fermentors are working as anodic half cells at any one time.

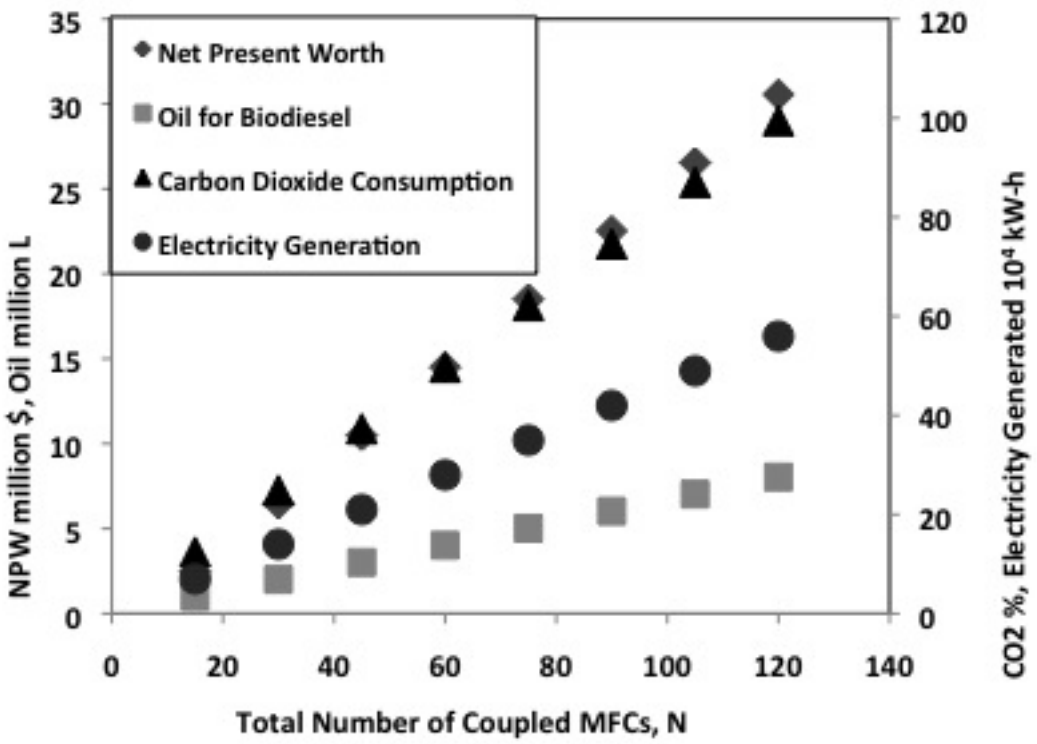

Figure 6.4. Total number of coupled MFCs, N, in integrated Plant. (Dimensions of cathodic PBR are D = 1 m, H = 50 m; number, n, of cathodic PBR half cells per anodic yeast fermentor half cells is N/15).

6.5. Discussion and Conclusions

The results of this economic feasibility study demonstrate that it is possible to integrate photosynthetic microalgae MFCs that capture CO_2, generate electrical power, and yielding oil for

biodiesel, into an existing bioethanol production facility. This is demonstrated by the positive NPW achieved over the 20 year life of the plant, at a 10% rate of return on investment. The new integrated facility would produce not only bioethanol, but would generate, by coupled MFCs, part of the power used in the existing bioethanol production process, produce microalgae and oil in the PBR cathodic half cell for sale for biodiesel production, and have reduced CO_2 emissions from the bioethanol production process. The CO_2 is used during photosynthesis in the PBR cathodic half cells. It should be noted that while a positive NPW is achieved for this integrated biofuel design, it is measured at the minimum rate of return of 10% that is generally considered desirable when evaluating economic viability.

Possible improvements to the existing integrated facility may be made with the use of a microalgae species with a significantly higher oil yield than *C. vulgaris* and further processing of the algae biomass onsite. Unfortunately, not all algal oil sources are suitable for production of biodiesel (Chisti, 2007), since many high oil content algal cells grow very slowly. The oil could also be removed from the algae as part of the integrated plant design, and sold at a higher price, and the remaining biomass sold as an animal feed supplement. Also, the present value at which carbon credits are trading is still considered low at $15/tonne, and is expected to increase significantly in value in the future (Haugen-Kozyra, 2007). In fact, it has been hypothesized that a governmental valuation of carbon credits of $100/tonne (Stern, 2006) would likely be required before CO_2 bioremediation technologies become profitable enough to enjoy widespread implementation.

6.6. Nomenclature

A amortized loan payment, $

[a] biomass concentration, kg DW/m^3

A_m, annual administrative operating cost, $/year

B revenue from sale of oil for biodiesel, $/year

b CO_2 from bioethanol plant remaining after microalgae uptake , %

C_L capital cost of PBR vessel, including lighting apparatus, $

C_{PA} capital cost of anode packing (per vessel), $

C_{PC} capital cost of cathode packing (per vessel), $

C_S capital cost of spargers (per PBR), $

C_T total capital cost, $

C_t overall total capital cost, $

CF_{Ny} negative cash flow in a given year, $/year

CF_{Py} positive cash flow in a given year, $/year

CM_{HNQ} annual chemical mediator cost for HN, $/year

CM_{MB} annual chemical mediator cost for MB, $/year

CO_{2C} total annual CO_2 consumed by *C. vulgaris*, kg/year

CO_{2P} total annual CO_2 produced in bioethanol facility, kg/year

CR fermentor circumference, m

$[C_{HNQ}]$ concentration, HNQ, mg/L

$[C_{MB}]$ concentration, MB, mg/L

D photobioreactor diameter, m

D_F fermentor diameter, m

d_m electrode mesh wire diameter, m

E value of carbon credits for total CO_2 consumed, $/year

F photobioreactor flow rate, m^3/h

H photobioreactor column height, m

i interest rate, fraction

L annual operating cost for labour, $/year

l_m length of electrode wire mesh sheet, m

m total *C. vulgaris* biomass (per PBR), kg

$\overset{o}{m}$ *C. vulgaris* production rate (per PBR), kg/h

Mat annual material operating cost, $/year

M_r annual marketing cost, $/year

M_t annual cost of maintenance, $/year

N total number of coupled MFCs

N_F total number of fermentors in operation at any one time

N_{ut} annual material cost, $/year

n number of PBRs per single fermentation tank

n_m strands per inch of mesh, $inch^{-1}$

n_{max} maximum number of cathodic PBRs per anodic fermentor

η electrode packing porosity, %

NPW net present worth of integrated facility, $

Op total annual operating cost, $/year

P annual total power output from coupled MFCs, W

P_{CO2} value of carbon credits, $/tonne CO_2

P_{DY} future price of biodiesel, $/L

P_f, nutrient media, $/L

P_{HNQ} cost of chemical mediator, HNQ, $/g

P_L annual labour cost per four vessels, $/column

P_m cost of electrode wire mesh, $/sheet

P_{MB} cost of chemical mediator, MB, $/g

P_O current price of biodiesel, $

P_W electrical cost, P_W, $/kW-h

R revenue from annual power output, $/year

r carbon dioxide consumption rate, mg biomass / mg CO_2

SA_E electrode surface area, m^2

T taxation on profits, $/year

t operating hours in the year, h

U_p annual utilities operating cost, $/year

V_F, fermentor volume, L

V_m volume of wire mesh packing sheet, m^3

w power output, W/mg DW algae

w_m width of electrode wire mesh sheet, m

Y total life of integrated plant, years

y present year

x taxation rate, fraction

Chapter 7

7. Economic Assessment of an Integrated Bioethanol-Biodiesel-Microbial Fuel Cell Facility, with Continuous Operation and On-Site Algae Processing

A similar version to this chapter has been accepted for publication in Energy Journal.

Powell, E.E., and G.A. Hill, "Carbon Dioxide Neutral, Integrated, Continuous Biofuel Facility", *Energy Journal*, Accepted September 2009.

A shorter, summarized version of the material discussed in this chapter has already been presented and published in the proceedings of the conference below:

Powell, E.E., and G.A. Hill "Carbon Dioxide Neutral, Integrated Biofuel Facility", Proceedings of 3rd Sustainable Energy and Environmental Protection Conference, Dublin, Ireland, August 12-15, pp 42-46, 15, 2009.

Contribution of Ph.D. Candidate

The economic assessment was based on calculations and a design developed by Erin Powell, with guidance provided by Gordon Hill. Experimental data discussed in previous chapters (Chapters 3, 4, and 5) was used as a basis for the calculations. The manuscript was written by Erin Powell, with editorial advice being provided by Gordon Hill.

Contribution of this paper to overall study

As discussed at the beginning of Chapter 6, the ultimate goal of a research project in engineering work is to determine what practical use it might have industrially. This chapter builds on the economic feasibility study and integration design of Chapter 6, but now examines the design option of extracting the oil for biodiesel from the *C. vulgaris* on-site, and processing the remaining biomass for sale at a full-scale facility. The effect of integrating the microalgae cultivation technology into a bioethanol facility employing continuous biofuel production, rather than a batch system (as evaluated in Chapter 6), is also examined here.

Additional Details not in the Manuscript

The original submitted manuscript presented in this chapter was subject to strict length limitations and was meant to provide a summary of an integration study. Therefore, the discussion of the design scheme and economic study presented only an overview of the design and results of the economic analysis. In order to clarify the analytical process, several equations and further details have been included in the presented version. Due to the brief nature of the requested manuscript however, the optimization of Chapter 6 was not repeated. Instead, the major design characteristics observed to be beneficial to the economics of the process, such as maximizing column height and number, were incorporated directly into the proposed design.

When the manuscript presented in this chapter was submitted, the details of the novel ELAPB design had not yet been released. As a result, discussion of the ELAPB is vague and any calculations based on the photobioreactor are based on the volume of the riser column alone. In regards to photobioreactor volume and algae growth, the riser is the illuminated region where the majority of growth and carbon fixation occurs and so this assumption was considered acceptable for the purposes of this article.

7.1. Abstract

Algae are efficient biocatalysts for both capture and conversion of carbon dioxide in the environment. It is estimated that of the 160 gigatonnes of CO_2 captured each year from the atmosphere, 60% occurs in surface waters to support the growth of diverse microalgae species. In earlier work, we have optimized the ability of *Chlorella vulgaris* to rapidly capture CO_2 from man-made emission sources by varying environmental growth conditions and bioreactor design. In this presentation, we demonstrate that a coupled biodiesel-bioethanol facility, using yeast to produce ethanol and photosynthetic algae to produce biodiesel, can result in an integrated, economical, large-scale process for biofuel production. The algae utilize CO_2 released from the yeast fermentation as their carbon source for growth. Since each bioreactor acts as an electrode for a coupled complete microbial fuel cell system, the integrated cultures produce electricity that is consumed as an energy source within the process. Finally, both the produced yeast and spent algae biomass can be used as added value byproducts in the feed or food industries. Using cost and revenue estimations, an IRR of 10% is calculated using a 5 year project lifespan.

7.2. Introduction

The development of new, environmentally friendly sources of energy is of great interest to humanity given the prospect of both peak oil production and global warming (Nel and Cooper, 2009). In recent work, we have characterized the growth kinetics of *Chlorella vulgaris* and developed a coupled photosynthetic microbial fuel cell (MFC) that generates an electrical current from *Saccharomyces cerevisiae* growth at the anode and *C. vulgaris* growth at the cathode (Powell et al., 2009a, Powell et al., 2009b; Sasi et al., 2009). In this work, a plan to incorporate this dual culture MFC into an existing large scale bioethanol facility is investigated.

A continuous flow, bioethanol fermentation facility is assumed to already be in operation and producing 130 million L/yr of fuel grade ethanol. This is a typical capacity for a bioethanol plant in Canada. The economics (capital cost, operating cost, and profitability) of installing efficient continuous flow column photobioreactors that consume the CO_2 from the bioethanol fermentors and produce electricity, algae biomass, and oil for biodiesel production as

new co-products from the existing bioethanol facility are to be determined. In addition, it is assumed that a cash inflow is generated due to carbon credits received from capture and conversion of CO_2 during microalgae growth. The algae bioreactors are designed similar to a new external loop airlift photobioreactor under development in our laboratories (Sasi et al., 2009). Algae growth kinetics and biomass yield are taken from data being generated in those studies and previous work (Powell et al., 2009b).

7.3. Integrated Facility Design

7.3.1. Nutrient Sources

The algae cultures require mineral supplements, light and enriched CO_2 to support optimum growth (Powell et al., 2009b). The mineral supplements are provided by a continuous fresh feed of medium containing plant growth media (10 kg/m^3 of Plant-Prod® Fertilizer, 30-10-10, Sure-Gro Inc., Brantford, ON). Light is provided free of charge by sunlight. CO_2 is provided free of charge from the gas discharges of the existing *S. cerevisiae* fermentors.

7.3.2. Existing Yeast Fermentors

In order to produce 130 million L/year of fuel grade ethanol, it is assumed that three, continuous flow fermentors are in operation that contain steady state concentrations of yeast and ethanol equal to 20 and 100 kg/m^3 (Hill and Robinson, 1990), respectively. Each fermentor is 10 m in diameter, 15 m high and contains 810 m^3 of fermentation broth. The flow of medium through each fermentor results in the production of 242 m^3/h of beer. Once formed, the beer is sent to downstream processing to produce a pure stream of fuel grade ethanol. The three commercial bioethanol fermentors release 12.6 tonnes/hr of carbon dioxide, which can be diverted for photosynthetic growth in the microalgae columns.

7.3.3. Novel Column Photobioreactors

In order to provide sufficient light penetration into the algae cultures, high density, clear polyethylene columns are used to culture the microalgae, and are equally spaced around each

yeast fermentor as shown in Figure 7.1. Each photobioreactor is 1 m in diameter and 30 m tall, containing 23.5 m^3 of algal broth at a concentration of 15 kgDW/m^3. The cell density was determined from anticipated concentrations for a continuous cultivation with cell recycle (Shuler and Kargi, 2002). High density cell concentrations of microalgae approaching this value have been reported (Ogbanna and Tanaka, 2000). At a dilution rate, D, of 0.05 h^{-1}, the volumetric flow rate, F_P, through each bioreactor is 1.2 m^3/h from the photobioreactor algal broth volume, V_P:

$$F_P = DxV_P \tag{7.1}$$

Any number of photobioreactors could be installed, however the physical dimensions of each yeast fermentor, and those of the surrounding installed column photobioreactors, limit the number of photobioreactors that can be placed around each fermentor. The circumference of a single yeast fermentor is determined from the diameter, but extra space must be allotted for equipment between the fermentor and surrounding photobioreactor. An additional 0.5 m was allotted around the outside of the fermentor in addition to the 10 m diameter, d_F. The circumference was determined to be 34.56 m from:

$$C_F = \pi(d_F + 1) \tag{7.2}$$

Each photobioreactor requires its own width equal to its diameter of 1m, d_P, with an additional 0.5 m on either side for equipment and access. The maximum number of photobioreactors that can therefore surround a single fermentor, N_F, is determined to be 23 from the following:

$$N_F = \frac{C_F}{d_P + 0.5} \tag{7.3}$$

with the total number of photobioreactors, N_T, being given by:

$$N_T = 3N_F \tag{7.4}$$

The column photobioreactors are filled with stainless steel, platinum doped mesh packing that acts as a cathodic surface. The yeast fermentors contain the same packing material as the photobioreactors, but now this material acts as an anodic surface. These two electrodes make up the driving force for current flow, but in order for that to occur, proton exchange channels are located between each photobioreactor and the yeast fermentor. The channels contain Nafion proton exchange membranes (PEMs), which permit only protons to flow between the two cell cultures. CO_2 gas, which exits the top of each yeast fermentor, is split and piped to the bottom of each photobioreactor, where it rises and is consumed by the growing algae cultures. The algae cells are cultured at optimum conditions, which include a light intensity of

0.45 W/m^2 and 10% CO_2 entering in the bottom of the vessel (Sasi et al., 2009). Sufficient algae photobioreactor volume is provided to consume a significant amount of the CO_2 emitted by the fermentors, and significantly reduce the greenhouse gas emissions from the existing bioethanol facility.

7.3.4. Downstream Algae Processing

The liquid effluent of the continuous algae photobioreactors is mixed and sent for further downstream processing to generate both oil (biodiesel) and biomass products. Figure 7.2 demonstrates this downstream processing scheme. First, the dilute algae broth is concentrated by a factor of 13.3 using a spiral wound, membrane filter. This results in a thick broth that is pumped into a continuous flow, hot hexane extraction/settling tank system. The sudden temperature change and violent mixing causes the microalgae cells to release their oils, which are quickly dissolved in the hexane. These oils are then easily separated in a flash tank, and all the hexane is recycled while the oil leaves as the desired co-product. The bottoms of the extractor go to a continuous tunnel dryer where hot, low pressure steam evaporates the remaining water and generates a 10% moisture content, dried algae biomass co-product.

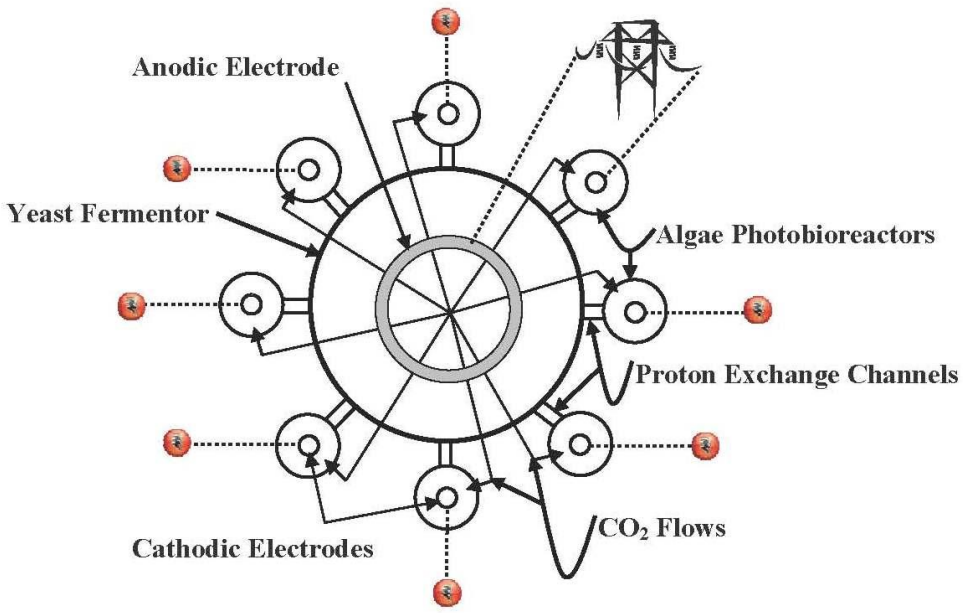

Figure 7.1. Sketch demonstrating the location of photobioreactors around a yeast fermentor.

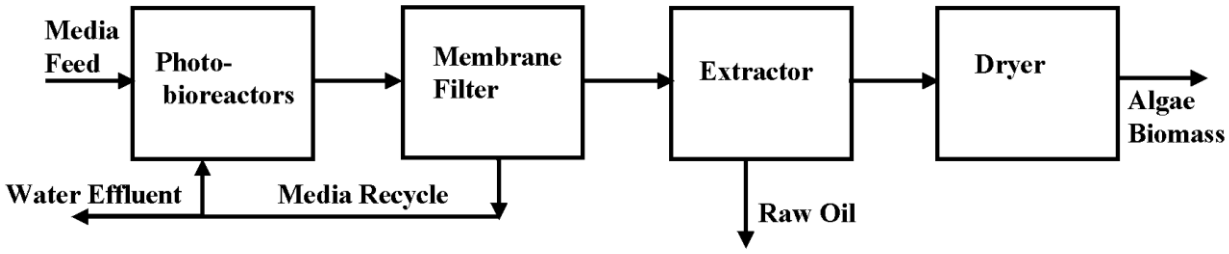

Figure 7.2. Block diagram of algae and oil processing system.

7.3.5. Economic Analysis

The economic analysis evaluates only the newly integrated portion of the biofuel facility, which includes all equipment installation and operation costs related to the column photobioreactors, microalgae downstream processing, and adaptation of the existing yeast fermentors for operation as MFC anodic half cells. The existing bioethanol facility itself was neglected in the economic analysis as being separate from the new installation and already operating profitably.

Installed capital costs of the column photobioreactors were estimated using Ulrich and Vasudevan's costing data (Ulrich and Vasudevan, 2004). This includes the cost of the platinum doped electrodes. Operating expenses included labour, maintenance and power to operate pumps and agitators. Steam usage to flash the hexane and dry the biomass was not included in costs since it was assumed that this was available free of charge from the existing bioethanol plant. Platinum doped electrodes must also be installed in the fermentors in the existing facility.

Revenue was calculated for the extracted oil using the current spot price for crude oil ($52 /bbl) (Nymex, 2008), and the algae biomass was costed as an animal feed supplement ($0.25 /kg). Electricity costs were determined using the same utility value as used for operating expenses ($0.12 /kW-h). The monetary value of carbon credits was calculated using a price of $100 /tonne. This is a high, subsidized value, which is needed in order to curb global warming (Stern, 2006). However, in reality, carbon credits have a present value in Western Canada of only $15/tonne (Haugen-Kozyra, 2007).

7.4. Results and Discussion

7.4.1. Sizing of Equipment

The flow of CO_2 from each yeast fermentor is mixed with air to obtain a carbon dioxide concentration of 10% by volume, and distributed to the column photobioreactors that encircle the fermentor. Two different design scenarios are evaluated. The total volumetric flow rate of algae broth from all integrated photobioreactors is given by:

$$F_{TP} = N_T F_P \tag{7.5}$$

and the total algae production rate is therefore determined from the cell density, X:

$$m = F_{TP} X \tag{7.6}$$

The theoretical CO_2 consumption is determined from the yield, Y_{XS}, and the algae production rate. The algae yield was determined experimentally in previous work (Powell et al., 2009b) to be 0.51 mg biomass / mg CO_2, and recent experiments indicate that when stressed the yield decreases by a factor of 2 (Sasi et al., 2009):

$$\overset{o}{X} = \frac{m}{\left(Y_{X/S} \diagup 2 \right)} \tag{7.7}$$

This value was then compared to the CO_2 production rate and converted to a percentage:

$$P_{CO_2} = \frac{\overset{o}{X}}{\overset{o}{C}} 100 \tag{7.8}$$

In the first design, all equipment was sized in order to capture one third of the CO_2 produced in the bioethanol plant. This requires a total of 36 microalgae photobioreactors to be integrated into the facility, with 12 columns surrounding each yeast fermentor. The total volumetric flow of algal broth through all 36 photobioreactors is 42.3 m^3/h giving a total algae production rate of 636 kgDW/h. This design produces enough algae to sequester 21% of the CO_2 produced by the bioethanol fermentors. The second design scenario examines the maximum number of columns possible surrounding each fermentor, according to the physical dimensions. With 23 columns per fermentor, or 69 in total, to be integrated into the existing bioethanol facility, 40% of the CO_2 produced by the existing yeast fermentations can be consumed. The total volumetric flow of algal broth through all 69 photobioreactors in this scenario is 81.3 m^3/h, giving a total algae production rate of 1219 kgDW/h.

The algae broth flows through 114 m^2 of spiral wound membrane filter cartridges that concentrate the algae to a thick broth containing 200 $kgDW/m^3$ of algae biomass. 90% of the water stream from the membrane is recycled to the photobioreactors such that only 5 m^3/h of fresh nutrient broth needs to be supplied to the photobioreactors.

The concentrated algae broth flows into a 1.0 m^3 hexane extraction tank, which operates at 65 ˚C. This is a two tank system such that while one tank is mixing the second tank is settling. The hexane from the second tank proceeds to a small flash tank where hexane is separated with negligible losses and returned to the extractor after condensing in a heat exchanger. The heat exchanger is also used to heat up the thick algae broth. The bottoms of the settling tank enter a 10 m long, 1 m wide tunnel dryer where supersaturated steam at 150 ˚C dries the algae into a saleable powder containing 10% moisture.

7.4.2. Costing of Equipment

Each column photobioreactor, complete with electrode, had an installed cost of $200K. For 36 and 69 installed columns, the total photobioreactor cost is $7.20 million and $13.8 million, respectively. The spiral wound membrane filter costs $0.10 million. The dual tank extractor complete with flash tank and heat exchange, installed was costed at $0.2 million, while the tunnel dryer was costed at $0.15 million, installed. Other equipment included the electrodes for the bioethanol fermentors and small pumps to move the algae feed, broth and hexane through the system costed at $0.50 million for the first design, and $0.95 million for the second. The total installed equipment cost is therefore estimated at $8.15 million (2009, Cdn dollars) for the design employing 36 columns. Allowing for fee and contingency, the estimated total project capital cost is $9.62 million. For the second design, where the maximum 69 columns are installed, the total installed equipment cost is estimated at $14.9 million (2009, Cdn dollars). Allowing for fee and contingency, the estimated total project capital cost for the second design is $17.9 million.

7.4.3. Operating Costs

Operating expenses are due to labour, nutrient feed, maintenance, administration, marketing, and electricity. Operators are required at 0.27 operators/column at a cost of $60 K/year. Ten new operators are hired at a cost of $600 K/year, and 19 operators at a cost of $1.14 million/yr, for the fewer and greater column design scenarios, respectively. Nutrient costs are low due to the low flowrate of fresh media, estimated at $5 K/year and $9.5 K/year (both fresh water and fertilizer), respectively. 7.9×10^4 kW-h of power, at $0.12/kw-h is needed to pump the fluids and mix the extractors at a cost of $9 K/year when 36 columns are installed, and $ 14.4 K/year when 69 columns are installed. Maintenance (includes replacing the Nafion membranes) is $577 K/year, or $ 1106 K/year for the scenario with the maximum number of columns. This is based on 6% of the total project capital cost. The cost of administration and benefits is determined to be 20% of the labour cost and 60 % of the combined labour and maintenance costs. Marketing is assumed to be 10% of all operating expenses and costs of goods. Administration costs (and benefits) and marketing are estimated to be $830 K/yr and $202 K/year, respectively, for the design employing a total of 36 photobioreactor columns. Administration costs (and benefits) and marketing are estimated to be $1590 K/year and $387 K/year, respectively, for the design employing a total of 69 photobioreactor columns. The total annual operating cost is $1.71 million for the design scenario where 36 photobioreactors are installed, and $3.2 million for the scenario where 69 photobioreactors are installed.

7.4.4. Revenues

CO_2 revenue (in the form of carbon credits), at $100 per tonne of capture, provides the most substantial positive cash flow for the integrated facility. An annual positive cash flow of $2.1 million can be achieved with a total of 36 column photobioreactors installed in the plant. This provides consumption of 21% of the CO_2 produced by the existing yeast fermentors. An annual positive cash flow of $4.0 million can be achieved by installing the maximum number of photobioreactors around each fermentor, consuming 40% of the CO_2 from the bioethanol plant.

Power generated by the novel MFC system is based on both algae cell density (1.0 A/kgDW of algae cells) and high glucose fed yeast fermentors generating an operating potential of 1.0 V (Powell et al., 2009a). This provides 1.0×10^5 kW-h of power or a revenue stream of

$12 K/year, for the lesser column design, and 1.9 x 10^5 kW-h or $23 K/year, for the maximum column design, both at a value of $0.12/kW-h.

For the design scenario in which 36 photobioreactors are installed, the 5000 tonnes DW of algae generated each year is assumed to be 30% oil (Chisti, 2007) giving a production of 1500 tonnes/year (or 11,500 bbl of oil) worth $600 K/year. When the total number of algae columns is increased to the maximum of 69, the 9700 tonnes DW of algae produced each year results in 2900 tonnes/year of oil valued at $1088 K/year. Finally, the dried algae powder (post-oil removal) is considered to be a valuable animal nutrient. It is sold, giving an annual positive cash flow of $875 K/year, and $1690 K/year, for the two designs, respectively.

The total positive annual cash flow to the plant, due to the addition of the microalgae system, is therefore estimated to be $4.72 million when 36 photobioreactor columns are installed, and $8.50 million when 69 columns are installed in the bioethanol facility.

7.4.5. Profitability

The facility modification is assumed to be built instantaneously and is financed 50% by loans (6% APR), 25% by a government "green" grant, and 25% by equity. The plant and loan are written off over 5 years after start up at a tax rate of 21% and using the declining balance depreciation (half in the first year) methodology.

The After Tax Cash Flow (ATCF) must be determined for each year of the five year life of the plant, including year zero when the plant is built. The ATCF is the summation of all net costs and revenues. In year zero, this would include the total investments (capital), with borrowings (loan) and the government green grant serving as positive cash flow. After operation has begun, the cash flow includes all operating costs, revenues, interest on the loan, and depreciation. The ATCF is also determined after taxes are remitted at a rate of 21%, on positive cash flow only, and therefore only in years 1 - 5 (plant operation).

The ATCF over the five year life of the plant is used to determine the Internal Rate of Return (IRR). The rate at which the IRR discounts the ATCF is given by:

$$R_{IRR_y} = \left(\frac{1}{1 + \left(IRR / 100 \right)} \right)^y \qquad \text{for years } 0 - 5 \tag{7.9}$$

The Discounted Cash Flow (DCF) for each year is then determined from the ATCF:

$$DCF_y = ATCF_y \times R_{IRR_y} \qquad \text{for years } 0 - 5 \tag{7.10}$$

The Cumulative Discounted Cash Flow (CDCF) is then determined for each year by adding the DCF for that year to the CDCF from the previous year:

$$CDCF_y = CDCF_{y-1} + DCF_y \tag{7.11}$$

The IRR can then be determined by solving equations (7.9) – (7.11) so that $CDCF_5$ is equal to zero. For the first design scenario, in which 12 microalgae columns surround each fermentor, for a total of 36, an analysis of the cumulative cash flow results in an IRR of 6.05%. The cumulative cash flow profile for this plant is shown in Figure 7.3.

For the second scenario, in which the maximum number of microalgae columns surround each fermentor, for a total of 69, an analysis of the cumulative cash flow results in an IRR of 9.93%. The cash flow profile for this plant design is shown in Figure 7.4. Since the IRR of the integrated microalgae plant increases significantly when the number of columns attached to each fermentor is increased to 23, the profitability was evaluated again, but using the more realistic carbon credit value of \$15/tonne of CO_2. However, even with the increased capacity of this larger design is was not possible to achieve any positive cash flow without the subsidized high revenue value of carbon consumption.

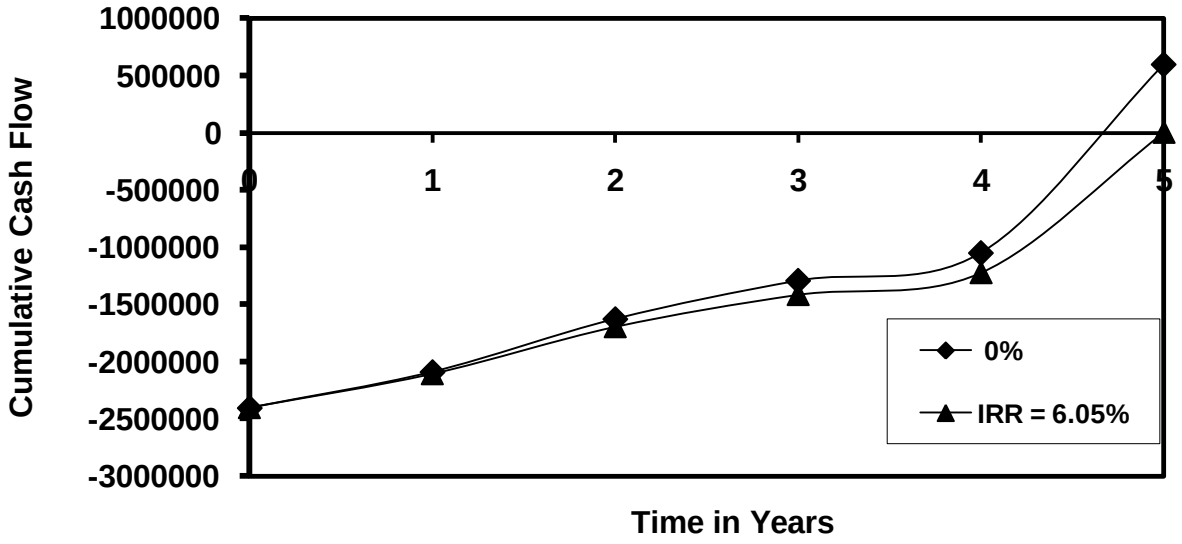

Figure 7.3. Cumulative cash flow of integrated facility with 36 total photobioreactors.

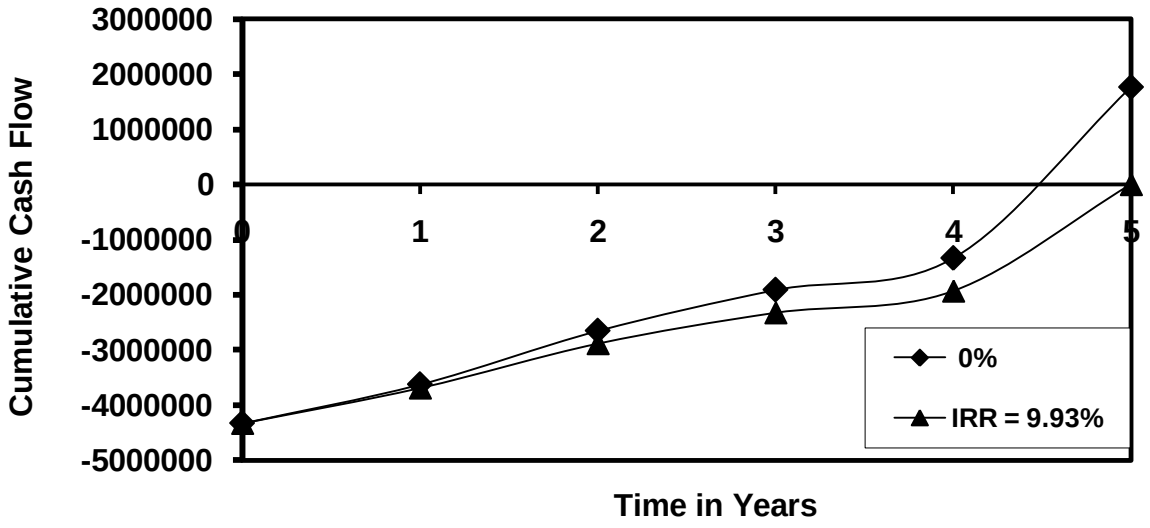

Figure 7.4. Cumulative cash flow of integrated facility with 69 total photobioreactors.

7.5. Conclusions

Algae photobioreactors can be used to capture significant CO_2 released from existing bioethanol plants. It is also possible to process the effluent from the bioreactors to produce oil and dried biomass. However, the economics of this process are only positive if the government provides financial assistance in the form of generous carbon credits ($100 per tonne of CO_2 captured) and a 25% capital equipment grant.

With these investments, the plant is just barely profitable with a low IRR of only 6.05% if only 21% of the released CO_2 is captured. By increasing the number of microalgae columns to the maximum spatially possible, 40% of the CO_2 released can be captured and the IRR increases to 9.93%. Given the greater IRR that can be achieved with the greater number of installed photobioreactor columns, it would appear that the design of this integrated plant is profitable. However, it does not remain so if the profitability is evaluated using a monetary value for carbon credits less than the highly subsidized $100/tonne. At this point in time, therefore, the construction of such a facility is not recommended from an economical standpoint.

7.6. Nomenclature

$ATCF_y$ after tax cash flow, $

C^o CO_2 production rate, kg/h

C_F circumference, fermentor, m

$CDCF_y$ cumulative disounted cash flow, $

D dilution rate, h^{-1}

DCF_y discounted cash flow, $

d_F diameter, fermentor, m

d_P diameter, fermentor, m

F_P volumetric flow rate, photobioreactor, m^3/h

F_{TP} total volumetric flow rate, all photobioreactors, m^3/h

IRR internal rate of return, %

m total algae production rate, kg DW/h

N_F number of photobioreactors per fermentor, dimensionless

N_T total number of photobioreactors, dimensionless

P_{CO2} overall CO2 consumption, %

R_{IRR} IRR discount rate, dimensionless

V_P algal broth volume, photobioreactor, m^3

X algae cell density, kg DW/m^3

X^o CO_2 consumption rate, kg/h

Y_{XS} biomass yield, kg DW/kg CO_2

y year

Chapter 8

8. General Discussion

8.1. Overall Ph.D. Project Discussion

This Ph.D. study involved the engineering of *Chlorella vulgaris* cultivation for CO_2 consumption. This involved many aspects of *C. vulgaris* cultivation including the study of growth kinetics, production of byproducts, scale-up and economic calculations, design of a novel external loop airlift photobioreactor (ELAPB) and the development of a model to describe growth in that cultivation system.

The growth kinetics of *C. vulgaris* were studied in a series of batch experiments using a well-mixed bioreactor. This data was needed in order to operate and design a photobioreactor for CO_2 consumption, and sufficient data was lacking in the literature. *C. vulgaris* growth was optimized by increasing radiant flux to 32.3 mW falling on the surface of a bioreactor containing 500 mL of culture solution, and by enriching the concentration of CO_2 in the feed air to 10% by volume. Maximum cell growth rates of 3.6 mg/L-h were achieved at these conditions. Under the growth conditions determined to be optimum during the kinetic experiments (32.3 mW, 10% CO_2), the yield was found to be 0.51 mg biomass d.w. / mg CO_2. The kinetic growth data for *C. vulgaris* collected was invaluable in the engineering of an improved photobioreactor design for the larger scale cultivation of this microalgae species for CO_2 consumption.

The biomass growth rate did increase with either increasing radiant flux or increasing CO_2 concentration in the feed air, however an interacting affect between the two variables was observed. A significant increase in the biomass accumulation rate was only observed when both variables were increased to their optimum levels. A high CO_2 concentration in the feed air, at which it becomes inhibitory to biomass growth, was observed at 20%. No maximum radiant flux was reached during the batch well-mixed reactor growth experiments. A maximum radiant flux, where photoinhibition occurs, should be observed if the light level is increased sufficiently.

Linear growth curves were observed for all batch kinetic growth experiments in the continuously stirred tank bioreactor. Results indicate that the *C. vulgaris* cells exhibit light limited growth, as expected for a photosynthetic microorganism, rather than being simply limited by their own ability to reproduce. While the light limitation observed in the kinetic growth study is frequently observed for microalgae in the literature, including for *C. vulgaris* specifically, overcoming this growth limitation is desirous in any improved photobioreactor design.

A novel external loop airlift photobioreactor (ELAPB) was designed and constructed using the kinetic growth data collected at the beginning of the Ph.D. project with the goal of improving *C. vulgaris* biomass yields. An airlift design was selected to provide an environment with excellent gas-liquid CO_2 mass transfer and consistent mixing to minimize mutual shading of the cells from the external light source. The light source is a series of white (visible spectrum) LEDs surrounding the entire riser, with the darkened downcomer providing a resting stage for the cells that improves growth rate. Experimental testing of the operation of this novel ELAPB using a fed-batch *C. vulgaris* growth study of light and CO_2 concentration was used to develop a model. The actual data collection was performed by a M.Sc. student under the supervision of the Ph. D. student Erin Powell and therefore the raw data is not directly part of this project. The design of the ELAPB however is part of the Ph.D. project and it is worth noting that in the batch growth experiments performed using the novel ELAPB, the growth curves are less linear than when cultivation was performed in a well-mixed tank bioreactor. The observed growth curves, while not fully exponential as one might expect to see in a bacterial microbe, begin to approach a more exponential growth curve than a completely linear one. The specific growth rate has also been increased fourfold from 0.008 h^{-1} to 0.04 h^{-1}, now reaching more than 1/3 of the typical growth rate of a bacterial species. This indicates that the ELAPB design has significantly improved on the continuously stirred tank bioreactor, and several designs published by others as well.

A model was developed using the ELAPB cultivation data collected by the M.Sc. student. This growth model couples the specific growth characteristics of *C. vulgaris*, light attenuation due to reactor geometry and biomass density, and the fluid dynamics of the ELAPB. The model predicts biomass accumulation, light penetration, and transient CO_2 concentrations, and compares predictions to experimental data collected using the novel ELAPB for radiant fluxes of 0.075 – 1.15 W/m^2 and 0 – 20% CO_2 enrichment of feed air, with an average error of

10%. The effect of radiant flux and CO_2 concentration was examined with radial and vertical profiles along the riser and downcomer columns of the ELAPB. For a fed-batch culture at a biomass density of 170 mg/L, the penetration of the radiant flux was found to decrease by 50% within the first 1 cm, and 75% at 2 cm, with the centre of the riser being located at 2.54 cm from the riser outer wall. Theoretical optimum conditions for maximum biomass growth were determined to be a radiant flux of 0.30 W/m^2 and a 5.8% enrichment of the inlet feed air.

A difference is observed in the predicted results of the model and the initial kinetic growth trials performed in the early stages of the PhD project. The scope of the experimental trials and the number of runs performed was limited, and the data indicated that a CO_2 enrichment of 10% was superior to 5%. Experiments were not performed at enrichments between 5 and 10% in the initial kinetic growth study. The radiant light fluxes employed in the initial kinetic growth study were also significantly different from those studied and modeled in the ELAPB. An interacting effect between radiant flux and CO_2 enrichment has been demonstrated. The CO_2 enrichment level of 10% was employed in all work subsequent to the initial kinetic study, prior to the completion of the modeling work and the ELAPB experimental trials, specifically the MFC and facility integration economic feasibility studies.

Simultaneous to the *C. vulgaris* growth study using continuously stirred tank reactors, a cost minimization strategy and program was developed for CSTB design. This design program determines the aeration rate and mixing speed required to meet the oxygen needs of the cells being cultured, at cost minimizing conditions. The decision to make the major design criteria cost minimization was made in order to create a program with practical application. It is suitable for use with a variety of microorganisms and culture media, and for bioreactor vessels ranging in size from small laboratory to large industrial scale. At the cost-minimized optimum conditions, the CSTB design program was used to evaluate the effect of microbial species, culture medium, and fermentor design aspects on CSTB system characteristics. A variety of effects were observed. The species of microbe being cultivated is key to the determination of the design parameters of the optimized system, in particular the oxygen requirements of the cells. This determines the value of the mass transfer coefficient and impacts the mixing speed and aeration rate required to supply oxygen to the cells, affecting gas holdup, and the overall operating cost. A comparison of pure water with seawater as culture medium demonstrated that the design strategy is much less sensitive to this parameter than to microbial species, with smaller effect on

mixing speed and aeration rate, and therefore cost. Data on the decreasing optimum mixing speed with increasing bioreactor volume, for minimum operating cost, was also obtained. Finally, the effect of increasing steady state biomass density on gas holdup, mixing speed, and cost was determined.

In addition to the major goal of engineering the cultivation of *C. vulgaris* for CO_2 consumption, a secondary goal remained the investigation of by-products to improve the economic feasibility of industrial implementation of large scale *C. vulgaris* cultivation. A novel application of the photosynthetic culture of *C. vulgaris* cells is as the direct electron acceptor in a biocathode in a microbial fuel cell (MFC). When coupled to an electrochemical anodic half cell, the photosynthetic growth of *C. vulgaris* on CO_2 produced an ultimate potential difference of 70 mV (using a potassium ferricyanide solution as the oxidant) and current levels of up to 1.0 μA/mg cell dry weight, which corresponded to a power density of 2.7 mW/m^2 of electrode surface. This research suggested that a coupled MFC could be constructed, with both the anode and cathode relying on the growth of microorganisms. This discovery indicated that the development of an alternate form of energy generation technology was possible that would incorporate *C. vulgaris* cultivation and CO_2 consumption.

The recently developed photosynthetic *C. vulgaris* cathode was coupled to a fermentative anode to produce a completely microbial fuel cell. The yeast strain *Saccharomyces cerevisiae* served as the electron donor in the anodic half cell. Loading effects and the effect of changing culture conditions on fuel cell operation were studied. A maximum power density of 0.95 mW/m^2 was observed at 90 mV and 5000 ohms during the loading study. An increase in this output was achieved with the addition of supplemental glucose to the anodic half cell (increase by a factor of 3 with a 180 g/L glucose addition) and the enriching of the feed air bubbled into the cathode half cell with 10% CO_2 (increase by a factor of 1.7). As these are the growth substrates of the yeast and microalgae, respectively, this is a predictable response. A correlation between cell growth and output was observed. The growth rate and biomass concentration was significantly less in the cathode half cell than in the anode half cell, likely due to the much slower growth rate of microalgae relative to yeast. Improvements to the microalgae cultivation and cathode design are required to balance the energy flow between the two half cells. The fact that lower outputs were obtained with the coupled MFC than with the photosynthetic biocathode alone, or with reported bioanodes alone, can be attributed to the use of

microorganisms on both sides of the fuel cell. When a microbial half cell is coupled to an electrochemical half cell, the coupled reaction is much faster than is the case with two cells entirely dependent on microbial growth. Also, microalgae growth is very slow relative to the yeast and bacteria used in the majority of reported MFCs. Further improvements to the coupled MFC are also possible as the design used in this initial feasibility study was very simple. A distinct benefit of the novel photosynthetic design used in this work however is that the biocathode consumes CO_2, both that generated by the growth at the anode (by the yeast) and additional CO_2 due to its significant photosynthetic consumption. Therefore, this novel photosynthetic MFC, under proper operating conditions, could be sustained to continuously generate a potential voltage and current as an alternate form of energy generation technology. This provides a useful technology to enable economical integration of *C. vulgaris* cultivation into a variety of industrial operations.

An economic feasibility study was performed to demonstrate that it is possible to integrate photosynthetic microalgae ELAPBs into an industrial facility. This integration study operated the microalgae cultivation ELAPBs as biocathodes in coupled MFCs that capture CO_2 from an existing bioethanol plant, generate electrical power, and yield oil for biodiesel. The anodes for the coupled MFCs are the existing yeast batch fermentors, and the CO_2 to be sequestered comes from the existing bioethanol production within the plant. While CO_2 sequestration remains the primary goal of the project, the power generation and oil production aspects provide operational revenue to offset costs. This new integrated facility would produce not only bioethanol, but would generate, by coupled MFCs, part of the power used in the existing bioethanol production process, produce microalgae and oil in the ELAPB cathodic half cell for sale for biodiesel production, and have reduced CO_2 emissions from the bioethanol production process. It should be noted that the ELAPB was assumed to be under continuous operation for this study. This economic feasibility is demonstrated by the positive NPW achieved over the 20 year life of the plant, at a 10% rate of return on investment. The profitability was maximized by installing the tallest columns that were considered practical, and integrating the maximum number possible according to space and CO_2 constraints. It should be noted that while a positive NPW is achieved for this integrated biofuel design, it is measured at the minimum rate of return that is generally considered desirable when evaluating economic viability.

Possible improvements to the existing integrated facility may be made with the use of a microalgae species with a significantly higher oil yield than *C. vulgaris* and further processing of the algae biomass onsite. The oil could also be removed from the algae as part of the integrated plant design, and sold at a higher price, and the remaining biomass sold as an animal feed supplement. Also, the present value at which carbon credits are trading is still considered low at $15/tonne, and is expected to increase significantly in value in the future, which would increase the economic value of plant integration.

A second economic feasibility study was performed on the integration of the *C. vulgaris* ELAPB cultivations into an industrial facility. In this case, the facility was once again a bioethanol plant, but both the ELAPB and the bioethanol fermentors are being operated continuously. The concept of harvesting the biomass and removing the oil for biodiesel on-site, and then selling the remaining dried biomass as an animal feel supplement was included in this second study. The economics of this process are only positive however if the government provides financial assistance in the form of generous carbon credits ($100 per tonne of CO_2 captured) and a 25% capital equipment grant. With these investments, and by increasing the number of microalgae columns to the maximum spatially possible (23), the IRR is 9.93%. Given the IRR that can be achieved with the greater number of installed photobioreactor columns, it would appear that the design of this integrated plant is profitable. However, it does not remain so if the profitability is evaluated using a monetary value for carbon credits less than the highly subsidized $100/tonne which is a speculative value that may not be implemented for years, if ever. At this point in time therefore, the construction of such a facility is not recommended from an economical standpoint.

8.2. Achievement of Research Objectives

All the research objectives listed in Chapter 1 (Section 1.7) have been achieved over the course of the Ph.D. project. These are listed from i to iv as in Section 1.7 to indicate which objective has been attained. The thesis chapters in which the thesis objectives are achieved are included in brackets after each numbered listing for reference.

i. The necessary study of the growth kinetics of *C. vulgaris* was initially performed using a well-mixed bioreactor, in order to aid in the cultivation of this microalgae species for CO_2 consumption. The biomass yield of CO_2 was also determined. (Chapters 3, and 5)

ii. In order to assist in the determination of the optimum design of such a continuously stirred tank bioreactor, an optimization scheme was designed which determines the best design and operating conditions for the bioreactor(s) for microbial growth. (Chapter 2)

iii. As part of the ongoing search for ways to make microalgae cultivation and CO_2 bioremediation economically feasible with valuable cultivation byproducts, an examination of using the *C. vulgaris* culture as a novel photosynthetic biocathode in a microbial fuel cell was performed and determined to be feasible. It was further shown that this microalgae biocathode could be coupled to a fermentative anode to form a completely microbiological fuel cell. The economics of using the coupled microbial fuel to integrate the *C. vulgaris* bioreactor industrially for CO_2 bioremediation was studied. The economics of selling the microalgae for oil for biodiesel, harvesting that oil on-site, and selling the remaining biomass as animal feed were all examined. (Chapters 3, 4, 6, and 7)

iv. With the growth kinetic study completed using a stirred tank bioreactor, an improved novel external loop airlift photobioreactor was designed and built. This novel bioreactor has both light and dark zones for improved growth and the mixing of the airlift design increases light penetration to each cell by reducing shading and cell adhesion without excessive shear. (Chapter 5)

v. The novel airlift photobioreactor was tested experimentally by a M.Sc. student under the supervision of Erin Powell. Several growth experiments were performed which have been incorporated into a model that includes light and CO_2 effects, reactor cell position, and fluid dynamics. (Chapter 5)

vi. The economic feasibility of integrating the novel external loop airlift photobioreactor into an industrial bioethanol plant was analyzed. This was performed for two cases: batch and continuous bioethanol plant operations. The microbial fuel cell with *C. vulgaris* biocathode concept was used to facilitate integration. Also, both off-site and on-site microalgae oil extraction (for biodiesel) was examined. (Chapters 6 and7)

Chapter 9

9. Conclusions and Recommendations

9.1. Project Conclusions

To optimize carbon dioxide consumption and byproduct formation in a large, continuous stirred tank bioreactor, it is important to consider the installation and operating economics of such a vessel. A cost minimization strategy and software program was developed for continuously stirred tank bioreactor (CSTB) design that optimizes aeration rate and mixing speed to meet the oxygen needs of the cells under cultivation. It is suitable for use with a variety of microorganisms, culture mediums, and bioreactor vessel sizes. This design program can also be used to evaluate the effect of microbial species, culture medium, and fermentor design aspects on CSTB system characteristics in order to design a superior CSTB cultivation operation.

Chlorella vulgaris batch growth in a continuously stirred tank bioreactor has been optimized by increasing radiant flux to 32.3 mW and by enriching the concentration of CO_2 in the feed air to 10% (by volume). Maximum cell growth rates of 3.6 mg/L-h were achieved at these conditions. Although the biomass growth rate increased with both increasing light and increasing CO_2 concentration in the feed air, an interacting effect between the two variables was observed. A maximum CO_2 concentration in the feed air at which it becomes inhibitory to biomass growth was observed at 20%. No inhibitory radiant flux was reached during the batch well-mixed reactor growth experiments. Linear growth curves were observed for all batch kinetic growth experiments in the continuously stirred tank bioreactor. Results indicate that the *C. vulgaris* cells exhibit light limited growth, rather than being simply limited by their own ability to reproduce.

The *C. vulgaris* cells used in the experimental aspects of the Ph.D. project were found to have an average diameter of 5.7 mm. Under the growth conditions determined to be optimum

during the initial kinetic experiments (32.3 mW, 10% CO2), the yield was found to be 0.51 mg biomass d.w. / mg CO_2.

C. vulgaris cells have been shown to act as a suitable cathode chamber in a microbial fuel cell (MFC). This serves as a novel MFC biocathode, being the first reported photosynthetic implementation of this technology. When coupled to an electrochemical anode of potassium ferricyanide solution, a maximum potential difference of 70 mV and current levels of 1.0 µA/mg cell dry weight were achieved, which corresponded to a power density of 2.7 mW/m^2 of electrode surface area.

The novel developed photosynthetic *C. vulgaris* cathode was coupled to a fermentative *Saccharomyces cerevisiae* anode to produce a MFC based only on the activity of microorganisms. A potential difference was measured across the coupled MFC, demonstrating that this is a feasible technology. A study of the loading effects measured a maximum power density of 0.95 mW/m^2 was observed at 90 mV and 5000 Ω. A lower power density was observed when the photosynthetic cell was coupled to a microbial half cell due to the much slower reactions occurring relative to that of the electrochemical oxidation reaction used in the previous experiment. The effect of changing culture conditions on fuel cell operation determined that an increase in output is achieved with the addition of growth substrates to the half cells. This includes addition of supplemental glucose to the anode half cell, and the enriching of the feed air bubbled into the cathode half cell with 10% CO_2.

A novel external loop airlift photobioreactor (ELAPB) was designed and constructed using the kinetic growth data collected at the beginning of the Ph.D. project. This novel design resulted in significantly increased biomass growth rates relative to growth in a continuous flow, CSTB (0.04 h^{-1} vs 0.01 h^{-1}). Experimental data generated from this novel ELAPB using fed-batch *C. vulgaris* cultures, varying radiant flux and CO_2 concentration, were used to develop a growth model incorporating the specific growth characteristics of *C. vulgaris*, light attenuation, and the fluid dynamics of the ELAPB. This model was found to be in agreement within 10% of experimental data collected during fed-batch cultivation in the ELAPB collected by D. Sasi (Sasi et al. (2009).

The model developed to describe the growth of *C. vulgaris* in the ELAPB is therefore useful in examining the theoretical interaction of the growth parameters. This provides valuable information for the cultivation of *C. vulgaris* without time consuming laboratory

experimentation, indications as to what type of improvements can be made to the ELAPB itself, and the prediction of the optimum growth conditions. The predicted optimum growth conditions are a radiant flux of 0.30 W/m^2 and 5.8% CO_2 enrichment of the inlet feed air.

The optimum CO_2 enrichment level predicted by the model differs from that determined in the initial kinetic growth study performed using well-mixed batch reactors. This is a result of the predicted value of 5.8% falling between two experimental trial points from this initial study, and the study being performed at significantly different radiant flux levels than the ELAPB work. As the MFC and economic feasibility studies were performed prior to the completion of the modeling, the optimum CO_2 enrichment concentration of 10% was assumed.

The growth model incorporating light and fluid dynamics was used to generate the radial and vertical profiles along the ELAPB column of biomass and growth rate, radiant flux, and CO_2 concentrations in the gas and liquid media phases. This provides valuable information on the interaction of growth conditions and bioreactor design with biomass growth.

An economic feasibility study demonstrated that it is possible to integrate photosynthetic microalgae ELAPBs that capture CO_2 into an existing bioethanol production facility. However, these microalgae cultivation ELAPBs, operating continuously, must serve as biocathodes coupled to the existing yeast batch fermentors as anodes in MFCs in order generate electrical power, as well microalgae biomass (containing oil for biodiesel) in order to generate sufficient revenue to offset costs. This is demonstrated by the positive NPW achieved over the 20 year life of the plant, at a 10% rate of return on investment.

When both the microalgae and yeast are produced in continuous mode, and the biomass is harvested and treated on-site the results of the economic differ significantly. It was thought that the oil extraction and drying of the remaining biomass for animal feed on-site at the integrated plant would increase revenue but this design is less profitable. With the maximum number of ELAPB cathodes spatially possible, the IRR increases to 9.93% but this is only if the government provides financial assistance in the form of generous carbon credits ($100 per tonne of CO_2 captured) and a 25% capital equipment grant. At this point in time, therefore, the construction of such a facility is not recommended from an economical standpoint.

9.2. Project Recommendations

Important kinetic growth data, which was key to optimizing the *C. vulgaris* cultivation and the design of the novel ELAPB was collected as part of the initial phase of the project. Further data was collected during the experimental testing of the novel ELAPB. As always, the time available limits the number of experimental trials that can be performed. Additional kinetic data could be collected focusing on those points of interest (areas of maximum growth) from the previous work. The theoretical optimum growth conditions in the ELAPB as predicted by the growth model should also be examined experimentally.

The CSTB design optimization program provides a valuable resource for design of a suitable CSTB for microbial growth while minimizing cost. This program could be expanded further to encompass more design options and to take into account more design parameters. For example, more than two impeller design options could be included, and a choice of more than four microbial species (without requiring additional user input).

All *C. vulgaris* growth experiments using the novel ELAPB were performed in fed-batch mode. Consequently, the resulting model is for fed-batch growth in the bioreactor. Further experimentation using a fed-batch (with a source other than CO_2) mode, continuous mode of operation, or cell-recycle, would provide more growth data for use in implementation for large-scale integration and for expansion of the growth model presented in the Ph.D. thesis.

Further growth experiments should be performed using *C. vulgaris* regarding its relationship to radiant flux until observable photoinhibition is reached. A plateau in the growth rate was observed with higher radiant flux, but not a decrease in growth. The reality of photoinhibition was assumed in the developed growth equation. Trials at growth inhibiting levels would provide valuable kinetic data, which could be incorporated into the specific growth model to provide more accurate results.

With the information obtained from the modeling performed at the end of the Ph.D. work, further studies can be performed on the novel ELAPB, the coupled MFC, and the integrated facility concept.

The cells in the ELAPB should be measured for shear stress effects. The airlift bioreactor is known to have a low shear stress relative to other designs, and microalgae cells are not particularly sensitive to the shear stress relative to other microorganisms, therefore it was

neglected in the modeling work carried out in this study. However, shear stress can sometimes have a small to moderate effect at high airflow rates and this should be investigated.

The change in viscosity with increasing cell density within the ELAPB was neglected in the development of the model. The viscosity only becomes a significant factor at very high cell concentrations, and while it should not be significant in this work, it could become so if further experiments are performed under conditions designed to obtain high density cell concentrations. It may therefore require measurement and study.

The novel external loop airlift photobioreactor has not been tested for its operation as a biocathode. Previous experimental work included in the Ph.D. work employed a stirred tank bioreactor design to test the concept. Performance of the *C. vulgaris* culture as an electron acceptor in an ELAPB microbial fuel cell biocathode should be comparable, but should be tested with the new bioreactor design.

Many of the modifications to the novel ELAPB as well as the biorefinery installation plan included in the integrated biorefinery design schemes were based on theoretical analysis. A more accurate evaluation of the economical feasibility could be made if the design modifications and scale-up were tested experimentally. These could include scale-up for industrial use, modification for use with sunlight, and testing of the bioelectrodes on a large scale.

The experiments with the *C. vulgaris* biocathode, both alone and as part of a coupled microbial fuel cell employed simple carbon graphite rods as electrodes. As discussed in Chapters 6 and 7 as part of a plan for industrial integration, a wire mesh electrode design would be more suitable for use in the riser of the novel ELAPB. It would also be more practical for use in large industrial tanks if integration in a bioethanol facility is the ultimate goal. The operation and output of the photosynthetic microalgae biocathode and coupled MFC using these new electrodes, as well as other electrode materials, should be measured experimentally.

Toxic impairment of the growth of the microalgae cultivation was observed at high concentrations of the chemical mediators needed for the biocathode of a MFC. Two different chemical mediators were evaluated during the photosynthetic biocathode work, but the choice was made based on which compound allowed for superior cell growth rates and electron flow at low concentration. This distinction was likely due to the differences in the ability of light to penetrate the two mediator chemicals that were evaluated. No actual toxicity measurements were performed (such as MicroTox) either for the chemical mediators or on possible resulting

by-products. This would be important if industrial integration of the microalgae cultivation for CO_2 consumption is to be implemented.

Economic feasibility studies were performed on the integration of the *C. vulgaris* ELAPB cultivation and CO_2 consumption into existing bioethanol facilities. Further economic studies should be performed on other industrial applications of the technology. One possible application is bioremediation of flue gas from coal-fired power plants, an ideal source of CO_2 with an average concentration of 10-13%. *C vulgaris* was shown to grow well under such conditions. Such a study would need to consider the toxic effects of the many chemicals (such as nitrogen oxides) in industrial flue gas.

Although microalgae by-products were discussed as part of the Ph.D. work, none were measured specifically. Valuable by-products such as oil for biodiesel, biochemicals for medicinal purposes, and nutritional and animal food supplements should be quantified and the impact of culture conditions on their production studied.

Improvements can be made to the design of the coupled MFC. The design used in the feasibility study was a simple electrode connection of two growing cultures, however several MFC design advances that improve performance have been reported in the literature. The development of a superior coupled MFC design that provides greater electrical output during *C. vulgaris* cultivation for CO_2 consumption would result in a new technology with improved practical application. The possibility of operating several fuel cells in series to improve voltage output could also be explored.

Chapter 10

10. References

Acien Fernandez, F. G., F. Garcia Camacho, J. A. Sanchez Perez, J. M. Fernandez Sevilla and E. Molina Grima, "A Model for Light Distribution and Average Solar Irradiance Inside Outdoor Tubular Photobioreactors for the Microalgal Mass Culture," Biotechnol. Bioeng. **55**, 701-714 (1997).

Aiba, S., "Growth kinetics of photosynthetic microorganisms," Adv. Biochem. Eng. **23**, 85-156 (1982).

Aizawa, K. and S. Miyachi, "Carbonic anyhydrase and CO_2 concentrating mechanisms in microalgae and cyanobacteria," FEMS Microbiol. Rev. **39**, 215-233 (1986).

Altman, P.L. and D.S. Dittmer, "Biology data book", Federation of American Societies for Experimental Biology, Bethesda, MD (1972).

Amann, J.-M., M. Kanniche, and C. Bouallou, "Natural Gas combined cycle power plant modified into an O2/CO2 cycle for CO2 capture," Energy Conservation and Management 50, 510-521, (2009).

Ammann, E. C. B. and V. H. Lynch, "Gas exchange of algae. III. Relation between the concentration of carbon dioxide in the nutrient medium and the oxygen production of *Chlorella pyrenoidissa*," Appl. Microbiol. **15**, 487-495 (1967).

Andersen, R. A., "Algal Culturing Techniques," Elsevier Academic Press, San Diego, CA (2005), pp. 189-203.

APHA (American Public Health Association), "Standard Methods for the Examination of Water and Wastewater," 20th ed., Washington, D.C. (1996).

Babcock, R. W., J. Malda and J. C. Radway, "Hydrodynamics and mass transfer in a tubular airlift photobioreactor," J. Appl. Phycol. **14**, 169-184 (2002).

Bailey, J. E. and D. F. Ollis, "Biochemical Engineering Fundamentals," 7th ed., McGraw-Hill, Toronto, ON (1986), pp. 101-104, 382-391, 394-404, 535-543, 551-552, 595-598, 609-610, 641, 772, 926.

Bakker, W. A. M., P. E. M. Overdevest, H. H. Beeftink, J. Tramper and C. D. de Gooijer, "Serial air-lift bioreactors for the approximation of aerated plug flow," Trends Biotechnol. **15**, 264-269 (1997).

Baquerisse, D., S. Nouals, A. Isambert, P. Ferreira dos Santos and G. Durand, "Modelling of continuous pilot photobioreactor for microalgae production," J. Biotechnol. **70**, 335-342 (1999).

Bennetto, H.P., J.L. Stirling, K. Tanaka and C.A. Vega, "Anodic reactions in microbial fuel cells," Biotechnol. Bioeng. **25**, 559-568 (1983).

Bennetto, H.P., Tanaka, K., and K. Matsuda. "Biofuel cells containing algae", in "Charge and Field Effects in Biosystems", Allen, M.J. and P.N.R. Usherwood, Eds., Abacus Press, Tunbreidge Wells, pp. 515-522 (1984).

Bennetto, H.P., G.M. Delaney, J.R. Mason, S.D. Roller, J.L. Stirling and C.F. Thurston, "The sucrose fuel cell: efficient biomass conversion using a microbial catalyst," Biotechnol. Let. **7**, 699-705 (1985).

Bond, D.R., D.E. Holmes, L.M. Tender and D.R. Lovley, "Electrode-reducing microorganisms that harvest energy from marine sediments," Science **295**, 483-485 (2002).

Bond, D.R. and D.R. Lovley, "Electricity production by Geobacter sulfurreduccens attached to electrodes," Appl. Environ. Microbiol. **69**, 1548-1555 (2003).

Borowitzka, M. A., "Commercial production of microalgae: ponds, tanks, tubes and femerenters," J. Biotechol, 70, 313-321 (1999).

Brune, D. E. and J. T. Novak, "The Use of Carbonate Equilibrium Chemistry in Quantifying Algal Carbon Uptake Kinetics," European J. Appl. Microbiol. Biotechnol. **13**, 71-76 (1981).

Burger, J., S. Miyachi, P. Galland, and H. Senger, "Quantum requirements on photosynthetic oxygen evolution and 77K fluorescence emission spectra in unicellular green algae grown under low and high CO_2 conditions," Botanica Acta. **101**, 229-232 (1988).

Camacho-Rubio, F. and M. E. Martinez-Sancho, "Development of a model for the effect of the intensity of light on on the growth of *Chlorella pyrenoidosa*," Int. Chem. Eng. **25**, 289-294 (1985).

Camacho-Rubio, F., A. Padial-Vico and M. E. Martinez-Sancho, "The effect of the mean intensity of light on the cultivation of *Chlorella pyrenoidosa*," Int. Chem. Eng. **25**, 283-288 (1985).

Camacho Rubio, F., F. G. Acien Fernandez, J. A. Sanchez Perez, F. Garcia Camacho and E. Molina Grima, "Prediction of Dissolved Oxygen and Carbon Dioxide Concentration Profiles in Tubular Photobioreactors for Microalgal Culture," Biotechnol. Bioeng. **62**, 71-86 (1999).

Camacho Rubio, F., Garcia Camacho, F., Fernendez Sevilla, J.M., Chisti, Y. and E. Molina Grima, "A Mechanistic Model of Photosynhtesis in Micorlagae," Biotechnol. Bioeng. **81**, 461-473 (2003).

Carvalho, A. P., and F. X. Malcata, "Transfer of Carbon Dioxide within cultures of Microalgae: Plain bubbling versus hollow fiber modules," Biotech. Prog. 17, 265-272, (2000).

Chae, K. J., M. Choi, F. F. Ajayi, W. Park, I. S. Chang and I. S. Kim, "Mass Transport through a Proton Exchange Membrane (Nafion) in Microbial Fuel Cells," Energ. Fuel. **22**, 169-176 (2008).

Cheremisinoff, N. P., "Fixed Flow Hydrodynamics," Gulf Publishing Co., Houston, TX (1996), pp. 499-519.

Chiao M., K. Lam and L. Lin, "Micromachined Microbial Fuel Cells," IEEE **3**, 383-386 (2003).

Chisti, M. Y., "Airlift Bioreactors," Elsevier Applied Science, New York, NY (1989), pp. 8, 40-41, 87-100, 203-229.

Chisti, Y., "Biodiesel from microalgae," Biotechnol Advances, **25**, 294-306 (2007).

Choi Y., E. Jung, H. Park, S.R. Paik, S. Jung and S. Kim, "Construction of Microbial Fuel Cells Using Thermophilic Microorganisms, *Bacillus licheniformis* and *Bacillus thermoglucosidasius*," *Bull. Korean Chem. Soc.* **25**, 813-818 (2004).

Clauwaert, P., K. Rabaey, P. Aelterman, L. De Scamphelaire, T.H. Pham and P. Boeckx, "Corporate Taxation Info-Guide," Government of Canada, Ottowa, ON, Canada (2007).

Cornet, J. F., C. G. Dussap and G. Dubertret, "A Structured Model for Simulation of Cultures of the Cyanobacterium *Spirulina platensis* in Photobioreactors: I. Coupling Between Light Transfer and Growth Kinetics," Biotechnol. Bioeng. **40**, 817-825 (1992a).

Cornet, J. F., C. G. Dussap, P. Cluzel and G. Dubertret, "A Structured Model for Simulation of Cultures of the Cyanobacterium *Spirulina platensis* in Photobioreactors: II. Identification

of Kinetic Parameters under Light and Mineral Limitations," Biotechnol. Bioeng. **40**, 826-834 (1992b).

DePinto, J.V., J.F. Atkinson, J. Song, C. Cheng, T. Slawecki and P.W. Rodgers, "Development and application of a coupled GIS-modeling system for watershed analysis", Proceedings of Watersheds '96 , June 8–12, Baltimore, MD, 896–899 (1996).

Doucha, J., S. Frantisek, and K. Livansky, "Utilization of flue gas for cultivation of microalgae (*Chlorella* sp.) in an outdoor open thin-layer photobioreactor," Journal of Applied Phycology, **17**, 403-412, (2005).

Droop, M. R., "Heterotrophy of carbon," in "Algal Physiology and Biochemistry," W. Stewart, Ed., University of California Press, Berkeley, CA, (1974), pp. 530.

Eilers, P. H. C. and J.C.H. Peeters, "A model for the relationship between light intensity and the rate of photosynthesis in phytoplankton," Ecolog. Model, vol. 42, 199-215, (1988).

Eliezier, E.D., "Power Absorption by New and Hybrid Mixing Systems under Gassed and Ungassed Conditions", in "Ho, C.S. and J.Y. Oldshue, "Biotechnology Processes: Scale-up and Mixing", American Institute of Chemical Engineers, New York, NY (1987).

Ellison, W., "Simultaneous scrubbing of the full array of flue gas acid gases,", Proceedings of the EPA-DOE-EPRI-A and WMA Power Plant Air Pollutant Control Mega Symposium 2006, **3**, 1236-1251, (2006).

Endo, H. and M. Shirota, "Studies on heterotrophic growth of *Chlorella* in a mass culture," in "Fermentation and Technology Today, Proceedings of the Fourth International Fermentation Symposium," Terui, Ed., Kyoto, Japan, March 19-25, 1972, pp. 533.

Environment Canada, "Canada's National Environmental Indicator Series 2003: Climate Change", Government of Canada, Ottawa, ON, Canada (2003).

Environment Canada, “Canada’s 2006 Greenhouse Gas Inventory”, Government of Canada, Ottawa, ON, Canada (2006).

Environment Canada, “From Impacts to Adaptation: Canada in a Changing Climate 2007”, Natural Resources Canada, Ottawa, ON, Canada (2007).

Environment Canada, “Canada’s Greenhouse Gas Emissions 2007”, Government of Canada, Ottawa, ON, Canada (2008).

Etheridge, D.M., Steele, L.P., Langenfelds, R.L. and R.J. Francey. “Historical Co2 record derived from a spline fit (20 year cutoff) of the Law Dome DE08 and DE08-2 ice cores”, Division of Atmospheric Research, Aspendale, Victoria, Austrialia (1998).

Evers, E. G., “A Model for Light-Limited Continuous Cultures: Growth, Shading, and Maintenance,” Biotechnol. Bioeng. **38**, 254-259 (1991).

Feng, M., “Microalgae cultivation in bioreactors for CO2 mitigation from power plant flue gas and fuel production by supercritical CO2 extraction,” Proceedings of the AIChE 2008 Spring Annual Meeting, (2008).

Fleck-Schneider, P., F. Lehr and C. Posten, “Modelling of growth and product formation of *Porphyridium purpureum*,” J. Biotechnol. **132**, 134-141 (2007).

Fredrickson, A. G., A. H. Brown, R. L. Miller and H. M. Tsuchiya, “Optimum conditions for photosynthesis in optically dense cultures of algae,” ARS J. **31**, 1429-1435 (1961).

Frohlich, B. T., I. A. Webster, M. M. Ataai and M. L. Shuler, “Photobioreactors: Models for Interaction of Light Intensity, Reactor Design, and Algal Physiology,” Biotechnol. Bioeng. Symp. **13**, 331-350 (1983).

Galaction, A.-I., D. Cascaval, C. Oniscu and M. Turnea, "Prediction of oxygen mass transfer coefficients in stirred tank bioreactors for bacteria, yeasts and fungus broths", Biochem. Eng. J. **20**, 85-94 (2004).

Garcia-Malea, M. C., C. Brindley, E. Del Rio, F. G. Acien, J. M. Fernandez and E. Molina, "Modelling of growth and accumulation of carotenoids in *Haematococcus pluvialis* as a function of irradiance and nutrients supply," Biochem. Eng. J. **26**, 107-114 (2005).

Gibson, B.R., S.J. Lawrence, J.P.R. Leclaire, C.D. Powell and K.A. Smart, "Yeast responses to stresses associated with industrial brewery handling," FEMS Microbiol. Rev. **31**, 535-569 (2007).

Gordon, J. M. and J. E. W. Polle, "Ultrahigh bioproductivity from algae," Appl. Microbiol. Biotechnol. **76**, 969-975 (2007).

Grima E.,M., F.G.A. Fernendez, F.G. Camacho, and Y. Chisti, "Photobioreactors: light regime, mass transfer, and scale-up," Journal of Biotechnology, 70, 231-247, (1999).

Hanagata, N., T. Takeuchi, Y. Fukuju, D. J. Barnes and I. Karube, "Tolerance of microalgae to high CO_2 and high temperature," Phytochemistry. **31**, 3345-3348 (1992).

Hassan, I.T.M. and C.W. Robinson, "Stirred-Tank Mechanical Power Requirement and Gas Holdup in Aerated Aqueous Phases," AIChE J. **23**, 48-56 (1977).

Haugen-Kozyra, K., "Carbon Credit Markets in Alberta, Canada and North America – Where are we at?" Climate Change Central, Government of Alberta, Edmonton, AB, Canada, (2007).

He, Z., and L.T. Angenent, "Application of bacterial biocathodes in microbial fuel cells," Electroanalysis **18**, 2009-2015 (2006).

Herzog, H., D. G0lomb, and S. Zemba, "Feasibility, modeling and economics of sequestering power plant CO2 emissions in the deep ocean,", Environmental Progress, **10**, 64-74, (1991).

Hill, G.A. and C.W. Robinson, "Minimum tank volumes for CFST bioreactors in series," Can. J. Chem. Eng. **67**, 818-824 (1989).

Hill, G.A. and C.W. Robinson, "A modified Ghose model for batch cultures of *Saccharomyces cerevisiae* at high ethanol concentrations," Chem. Eng. J. **44**, B69-B80 (1990).

Hill, G. A., "Measurement of Overall Volumetric Mass Transfer Coefficients for Carbon Dioxide in Well-Mixed Reactor Using a pH Probe," Ind. Eng. Chem. Res. **45**, 5796-5800 (2006).

Hirata, S., M. Hayashitani, M. Taya and S. Tone, "Carbon dioxide fixation in batch cultures of *Chlorella* sp. using a photobioreactor with a sunlight collection device," J. Ferment. Bioeng. **81**, 470-472 (1999).

Ho, C.S., M.J. Stalker and R.F. Baddour, "The Oxygen Transfer Coefficient in Aerated Stirred Reactors and Its Correlation with Oxygen Diffusion Coefficients", in "Biotechnology Processes: Scale-up and Mixing," C.S. Ho and J.Y. Oldshue, Eds., American Institute of Chemical Engineers, New York, NY (1987).

Huisman, J., "Population Dynamics of Light-Limited Phytoplankton: Microcosm Experiments," Ecology. **80**, 202-210 (1999).

Iehana, M., "Kinetic analysis of the growth of Chlorella vulgaris," Biotechnol. Bioeng. **36**, 198-206 (1990).

Javanmardian, M. and B.O. Palsson. "Continuous photoautotrophic cultures of eukaryotic alga *Chlorella vulgaris* can exhibit stable oscillatory dynamics", Biotechnol. Bioeng. **39**, 487-497 (1992).

Jia Y.-H., H.-T. Tran, D.-H. Kim, S.-H. Oh, D.-H. Park, R.-H. Zhang and D.-H. Ahn, "Simultaneous organics removal and bio-electrochemical denitrification in microbial fuel cells," Bioprocess. Biosyst. Eng. **31**, 315-321 (2008).

Kim, N., Y. Choi, S. Jung and S. Kim, "Development of microbial fuel cells using *Proteus vulgaris*," Bull. Korean Chem. Soc. **21**, 44-48 (2000).

Kim, J.R., M. Booki and B.E. Logan, "Evaluation of procedures to acclimate a microbial fuel cell for electricity production," Appl. Microbiol. Biotechnol. **68**, 23-30 (2005).

Kim, H., I.S. Chang and G.M. Gadd, "Challenges in microbial fuel cell development and operation," Appl Microbial Biotechnol **79**, 485-494 (2007a).

Kim, J.R., S.H. Jung, J.M. Regan and B.E. Logan, "Electricity generation and microbial community analysis of alcohol powered microbial fuel cells," Bioresource Technol. **98**, 2568-2577 (2007b).

Kingsley, F., "Simplified results from flue-gas analysis," The Engineering Record, **60**, 220-221 (2009).

Krichnavaruk, S., W. Loataweesup, S. Powtongsook and P. Pavasant, "Optimal growth conditions and the cultivation of *Chaetoceros calcitrans* in airlift photobioreactor," Chem. Eng. J. **105**, 91-98 (2005).

Kouroussis, D. and S. Karimi, "Alternative fuels in transportation," Bull. Sci. Technol. Soc. **26**, 346-355 (2006).

Kurano, N. and S. Miyachi, "Selection of microalgal growth model for describing specific growth rate-light response using extended information criterion," J. Biotechnol. Bioeng.. **100**, 403-408 (2005).

Laws, E. A., "Photosynthetic efficiency optimization studies with the macroalga *Gracilaria tikvihae*: implications for CO2 emission control from power plants," Bioresource Technology, **37,** 25-33, (1991).

Lee, Y.-K. and S. J. Pirt, "Energetics of Photosynthetic Algal Growth: Influence of Intermittent Illumination in Short (40 s) Cycles," J. Gen. Microbiol. **124**, 43-52 (1981).

Lee Y.-K. and C.-S. Low, "Productivity of Outdoor Algal Cultures in Enclosed Tubular Photobioreactor," Biotechnology and Bioengineering, 40, 1119-1122, (1992).

Lee, H. Y., L. E. Erickson and S. S. Yang, "Kinetics and bioenergetics of light limited photoautotrophic growth of *Spirulina platensis*," Biotechnol. Bioeng. **29**, 832-843 (1987).

Lee, C.-G. and B. O. Palsson, "Photoacclimation of Chlorella vulgaris to Red Light from Light-Emitting Diodes Leads to Autospore Release Following Each Cellular Division," Biotechnol. Prog. **12**, 249-256 (1996).

Li, J., N. S. Xu and W. W. Su, "Online estimation of stirred-tank microalgal photobioreactor cultures based on dissolved oxygen measurement," Biochem. Eng. J. **14**, 51-65 (2003).

Li Y., M. Horsman, N. Wu, C.Q. Lan and N. Dubois-Calero, "Biofuels from Microalgae" AIChE (2008).

Lin, Y. and S. Tanaka, "Ethanol fermentation from biomass resources: current state and prospects," Appl Microbiol Biotechnol **69**, 627 –642 (2005).

Liu, H. and B.E. Logan, "Electricity generation using an air-cathode single chamber microbial fuel cell in the presence and absence of a proton exchange," Environ. Sci. Technol. **38**, 4040-4046 (2004).

Liu, H., R. Ramnarayanan and B.E. Logan, "Production of electricity during wastewater treatment using a single chamber microbial fuel cell," Environ. Sci. Technol. **28**, 2281-2285 (2004).

Logan, B.E., B. Hamelers, R. Rozendal, U. Schroder, J. Keller, S. Freguia, P. Aelterman, W. Verstraete and K. Rabaey, "Microbial fuel cells: methodology and technology," Environ. Sci. Technol. **40**, 5181-5192 (2006).

Maeda, K., M. Owada, N. Kimura, K. Omata and I. Karube, "CO_2 fixation from the flue gas on coal-fired thermal power plant by microalgae," Energy Conservation and Management, **36**, 717-720, (1995).

Malcata, F.X., "A heuristic approach for the economic optimization of a series of CSTR's performing Michaelis-Menten reactions," Biotechnol. Bioeng. **33**, 251-255 (1989).

Mantzouridou, F., T. Roukas and P. Kotzekidou, "Effect of the aeration rate and agitation speed on b-carotene production and morphology of Blakeslea trispora in a stirred tank reactor: mathematical modeling," Biochem. Eng. J, **10**, 123-135 (2002).

Matthijs, H. C. P., H. Balke, U. M. Van Hes, B. M. A. Kroon, L. R. Mur and R. A. Binot, "Application of Light- Emitting Diodes in Bioreactors: Flashing Light Effects and Energy Economy in Algal Culture (*Chlorella pyrenoidosa*)," Biotechol. Bioeng. **50**, 98-107 (1996).

Mayo, A. W., "Effects of temperature and pH on the kinetic growth of unialga *Chlorella vulgaris* cultures containing bacteria," Water Environment Research, **69**, 64-72, (1997).

Meng, A. X., G.A. Hill, A.K. Dalai, "Hydrodynamic characteristics in an external loop airlift bioreactor containing a spinning sparger and a packed bed," Ind. Eng. Chem, Res. 41, 2124-2128 (2002).

Merchuk, J. C., M. Ronen, S. Giris and S. Arad (Malis), "Light/Dark Cycles in the Growth of the Red Microalga *Porphyridiun* Sp.," Biotechnol. Bioeng. **59,** 705-713 (1998).

Michel, K. and A. Eisentraeger, "Light-Emitting Diodes for the Illumination of Algae in Ecotoxicity Testing," Environ. Toxicol. **19**, 609-613 (2004).

Min B., S. Cheng and B.E. Logan, "Electricity generation using membrane and salt bridge microbial fuel cells," Wat. Res. **39**, 1675-1686 (2005a).

Min B., J.R. Kim, S.E. Oh, J.M. Regan and B.E. Logan, "Electricity generation from swine wastewater using microbial fuel cells" Wat. Res. **39**, 4961-4968 (2005b).

Miyake, J., M. Miyake and Y. Asada, "Biotechnological hydrogen production: research for efficient light energy conversion," J. Biotechnol. **70**, 89-101 (1999).

Molina Grima, E., F. Garcia Camacho, J. A. Sanchez Perez, J. M. Fernandez Sevilla, F. G. Acien Fernandez and A. Contreras Gomez, "Mathematical model of microalgal growth in light-limited chemostat culture," J. Chem. Technol. Biotechnol. **61**, 167-173 (1994).

Molina Grima, E., J. M. Fernandez Sevilla, J. A. Sanchez Perez and F. Garcia Camacho, "A study on simultaneous photolamination and photoinhibition in dense microalgal cultures taking into account incident and averaged irradiances," J. Biotech. **45**, 59-69 (1996).

Molina Grima, E., F. Garcia Camacho, J. A. Sanchez Perez, F. G. Acien Fernandez and J. M. Fernandez Sevilla, "Evaluation of photosynthetic efficiency in microalgal cultures using averaged irradiance," Enzyme Microb. Technol. **21**, 375-381 (1997).

Molina Grima, E., F. G. Acien Fernandez, F. Garcia Camacho and Y. Chisti, "Photobioreactors: light regime, mass transfer, and scaleup," J. Biotechnol. **70**, 231-247 (1999).

Montgomery, D.C., "Design and Analysis of Experiments", John Wiley and Sons, Toronto, Canada (1991).

Mook, W.G. and J.J. deVries, "Environmental isotopes in the hydrological cycle: Principles and applications", IAEA Publication, Vienna, Austria (2005).

Morita, M., Y. Watanabe and H. Saiki, "Investigation of photobioreactor design for enhancing the photosynthetic productivity of microalgae," Biotechnol. Bioeng. **69**, 693-698 (2000).

Moroney, J. V. and A. Somanchi, "How Do Algae Concentrate CO_2 to Increase the Efficiency of Photosynthetic Carbon Fixation?," Plant Physiol. **119**, 9-16 (1999).

Myers, J. and J.R. Graham, "On the mass culture of algae. II. Yield as a function of cell concentration under continuous sunlight irradiance", Plant Physiol. **34**, 345-352 (1958).

Nel, W. P., and C. J. Cooper, "Implications of fossil fuel constraints on economic growth and global warming," Energy Policy, **37**, 166-180 (2009).

Nikakhtari, H. and G. A. Hill, "Enhanced Oxygen Mass Transfer in an External Loop Airlift Bioreactor Using a Packed Bed," Ind. Eng. Chem. Res. **44**, 1067-1072 (2005a).

Nikakhtari, H. and G. A. Hill, "Hydrodynamic and oxygen mass transfer in an external loop airlift bioreactor with a packed bed," Biochem. Eng. J. **27**, 138-145 (2005b).

Nikakhtari, H. and G. A. Hill, "Modelling Oxygen Transfer and Aerobic Growth in Shake Flasks and Well-Mixed Bioreactors," Can. J. Chem. Eng. **83**, 493-499 (2005c).

Nikakhtari, H. and G. A. Hill, "Volatile Organic Chemical Mass Transfer in an External Loop Airlift Bioreactor with a Packed Bed," Ind. Eng. Chem. Res. **44**, 9299-9306 (2005d).

Nikakhtari, H. and G. A. Hill, "Continuous Bioremediation of Phenol Polluted Air in an External Loop Airlift Bioreactor with a Packed Bed," J. Chem. Technol. Biotechnol. **81**, 1029-1038 (2006).

Nymex, New York Mercantile Exchange, (2008) http://www.nymex.com/index.aspx.

O'Connor-Cox, E.S.C. and W.M. Ingledew, "Effect of the timing of oxygenation on very high gravity brewing fermentations," J. Am. Soc. Brew. Chem. **48**, 26-32 (1990).

Ogawa, T., H. Kozawa and G. Terui, "Studies on the growth of *Spirulina platensis* (II) growth kinetics of an autotrophic culture," J. Ferment. Technol. **50**, 143-149 (1971).

Ogbonna, J. C., H. Yada, H. Masui and H. Tanaka. "A novel internally illuminated stirred tank photobioreactor for large-scale cultivation of photosynthetic cells," J. Ferment. Bioeng. **82**, 61-67 (1996).

Ogbonna, J. C., H. Masui and H. Tanaka, "Sequential heterotrophic/autotrophic cultivation – An efficient method of producing *Chlorella* biomass for health food and animal feed," J. Appl. Phycol. **9**, 359-366 (1997).

Ogbonna, J. C. and H. Tanaka, "Light requirement and photosynthetic cell cultivation – Development of processes for efficient light utilization in photobioreactors," J. Appl. Phycol. **12**, 207-218 (2000).

Oh, S.E. and B.E. Logan, "Hydrogen and electricity production from food processing wastewater using fermentation and microbial fuel cell technologies," Wat. Res. **39**, 4673-4682 (2005).

Oldshue, J. Y., "Fluid Mixing Technology," McGraw-Hill Publications Co., New York, NY (1983), pp. 1-23, 493-503.

Otsuki, T., "A study for the biological CO_2 fixation and utilization system," Sci.Total Environ. **277**, 21-25 (2001).

Painting, K. and B. Kirsop, "A quick method for estimating the percentage of viable cells in a yeast population, using methylene blue staining," National Collection of Yeast Cultures, AFRC Institute of Food Research, (1989).

Park, D.H. and J.G. Zeikus, "Electricity generation in microbial fuel cells using neutral red as an electonophore," Appl. Environ. Microbiol. **66**, 1292-1297 (2000).

Parson, W. W., "Modern Optical Spectroscopy," Springer-Verlag Heidelberg, New York, NY (2007), pp. 1-23, 73-100.

Patino, R., M. Janssen and U. von Stockar, "A Study of the Growth for the Microalga Chlorella vulgaris by Photo-Bio-Calorimetry and Other On-line and Off-line Techniques," Biotechnol. Bioeng. **96**, 757-767 (2007).

Perry, R.H. and D.W. Green, "Perry's Chemical Engineers' Handbook", 7th ed, Toronto, On (1997).

Physical Science Study Committee, "Physics," The Copp Clark Publishing Co., Ltd., Toronto, ON (1960), pp. 179-300.

Pirt, S. J., Y. K. Lee, A. Richmond and M. Watts Pirt, "The photosynthetic efficiency of *Chlorella* biomass growth with reference to solar energy utilization," J. Chem. Tech. Biotechnol. **30**, 25-34 (1980).

Popovic, M. K. and C. W. Robinson, "Mass Transfer Studies of External-Loop Airlifts and a Bubble Column," AIChE J. **35**, 393-405 (1989).

Powell, E.E., J.C. Bolster, G.A. Hill and R.W. Evitts, "Complete Microbiological Fuel Cell: A Photosynthetic Cathode Coupled to a Fermentative Anode," Energy Sources Part A, In Press (2009a).

Powell, E.E., Mapiour, M.L., Evitts, R.W., and G. A. Hill "Growth kinetics of *Chlorella vulgaris* and its use as a cathodic half cell", Bioresource Technology, **100**, 269-274 (2009b).

Powell, E.E., Hill, G.A., and D. Sasi, "Modeling *Chlorella vulgaris* Growth in an External Loop Airlift Photobioreactor: Light Distribution and Carbon Dioxide Consumption", *Can. J Chem Eng.*, Submitted for Review (2009).

Powell, E.E., and G.A. Hill, "Economic Assessment of an Integrated Bioethanol-Biodiesel-Microbial Fuel Cell Facility Utilizing Yeast and Photosynthetic Algae", *ChERD,* In Press (2009).

Prasad, D., T.K. Sivaram, S. Berchmans and V. Yegnaraman, "Microbial fuel cell constructed with a micro-organism isolated from sugar industry effluent," J Power Sources, **160**, 991-996 (2006).

Prokop, A. and L. E. Erickson, "Photobioreactors," in "Bioreactor system design," J. A. Asenjo and J. C. Merchuk, Eds., Marcel Dekker, New York, NY (1995), pp. 441-477.

Pulz, O. and W. Gross, "Valuable products from biotechnology of microalgae," Appl. Microbiol. Biotechnol. **65**, 635-648 (2004).

Qi, H. and G. L. Rorrer, "Potolithotrophic cultivation of *Laminaria sacharina* gametophyte cells in a stirred-tank bioreactor," Biotechnol. Bioeng. **45**, 251-260 (1995).

Rabaey, K. and W. Verstraete, "Microbial fuel cells: novel biotechnology for energy generation," Trends Biotechnol. **23**, 291-298 (2005).

Rabaey K., G. Lissens, S.D. Siciliano and W. Verstraete, "A microbial fuel cell capable of converting glucose to electricity at high rate and efficiency," Biotechnol. Lett. **25**, 1531-1535 (2003).

Rabaey K., S.T. Read, P. Clauwaert, S. Freguia, P.L. Bond, L.L. Blackall and J. Keller, "Cathodic oxygen reduction catalyzed by bacteria in microbial fuel cells," ISME Journal **2**, 519-527 (2008).

Rabe, A. E. and R. J. Beniot, "Mean light intensity – a useful concept in correlating growth rates of dense cultures of microalgae," Biotechnol. Bioeng. **4**, 377-390 (1962).

Ratledge, C. and B. Kristiansen, "Basic Biotechnology," 3rd ed., Cambridge University Press, Cambridge, (2006).

Rehak, B., S. Celikovsky and S. Papacek, "Model for Photosynthesis and Photoinhibition: Parameter Identification Based on the Harmonic Irradiation O_2 Response Measurement," Special Issue on Systems Biology, 101-108 (2008).

Rhoads, A., H. Beyenal and Z. Lewandowski, "Microbial Fuel Cell using Anaerobic Respiration as an Anodic Reaction and Biomineralized Manganese as a Cathodic Reagent," Environ. Sci. Technol. **39**, 4666-4671 (2005).

Richmond, A., Ed., "Handbook of Microalgal Culture: Biotechnology and Applied Phycology," Blackwell Science Ltd., Ames, IA (2004), pp. 3-39, 255-263.

Ritchie, B. J., "Biodegradation of Phenol from Contaminated Air by *Pseudomonas putida* in an External Loop Airlift Bioreactor," M.Sc. Thesis, University of Saskatchewan, Saskatoon, SK (1994).

Ritchie, B. J. and G. A. Hill, "Biodegradation of Phenol-Polluted Air using an External Loop Airlift Bioreactor," J. Chem. Tech. Biotechnol. **62**, 339-344 (1995).

Sansawa, H. and H. Endo, "Production of Intracellular Phytochemicals in *Chlorella* under Heterotrophic Conditions," J Biosci Bioeng **98**, 437-444 (2004).

Sasi, D., E. Powell and G. Hill, "Effect of light intensity on growth of *C. vulgaris* in a novel photobioreactor," in "Proceedings of the 8th World Congress for Chemical Engineering," Montreal, Canada, August (2009).

Schell, D. J., J. Farmer, J. Hamalton, B. Lyons, J. D. McMillan, J. C. Saez and A. Tholudur, "Influence of Operating Conditions and Vessel Size on Oxygen Transfer During Cellulase Production," Appl. Biochem. Biotechnol. **91**, 627-642 (2001).

Schuster, A., "Radiation through a foggy atmosphere," Astrophys. J. **21**, 1-22 (1905).

Shackelford, J. F. and W. Alexander, "The CRC Materials Science and Engineering Handbook," CRC Press, Boca Raton, FL (2001).

Shafeen, A., E. Croiset, P. L. Douglas and I. Chatzis, "CO_2 sequestration in Ontario, Canada. Part I: storage evaluation of potential reservoirs" Energy Conversion and Management, **45**, 2645-2659 (2004).

Shuler, M. L. and F. Kargi, "Bioprocess Engineering: Basic Concepts," 2nd ed., Prentice Hall, Upper Saddle River, NJ (2002), pp. 155-199, 207-216, 245-275, 413.

Siegel, M. and J.C. Merchuk, "Mass Trasnfer in a Rectangular Air-Lift Reactor: Effects of Geometry and Gas Recirculaation", Biotechnol. Bioeng. **32**, 1128-1137 (1988).

Slaughter, J.C., "The biochemistry and physiology of yeast grwoth," in "*Brewing Microbiology*," 3rd ed., F.G. Priest and I. Campbell, Eds., Kluwer Academic Press, New York, NY (2003), pp. 19-66.

Sorensen, B., "Hydrogen and Fuel Cells: Emerging technologies and applications," Elsevier Academic Press, Burlington, MA (2005), pp.58-59.

Spolaore, P., C. Joannis-Cassan, E. Duran and A. Isambert, "Commercial applications of microalgae," J Biosci Bioeng **101**, 87-96 (2006).

Stanier, R. Y., M. Doudoroff and E. A. Adelberg, "The microbial world," 3rd ed., Prentice Hall, Englewood Cliffs, NJ (1970), pp. 99-108, 179, 218-221, 298-321.

Stern, N., "The Stern review report on the economics of climate change," Cambridge University Press, Cambridge, UK (2006).

Stryer, L., "Biochemistry," 3rd ed., W.H. Freeman & Company, New York, NY (1988), pp. 603-689.

Suh, I. S. and S. B. Lee, "A Light Distribution Model for an Internally Radiating Potobioreactor," Biotechnol. Bioeng. **82**, 180-189 (2003).

Suh, I. and S. Lee, "Cultivation of cyanobacterium in an internally radiating air lift photobioreactor," Journal of Applied Phycology, 13, 381-388, (2001).

Ten Hoopen, H. G. J., J. A. Roels, J. M. Van Gemert, P. J. Nobel and A. Fuchs, "An unstructured model of algal growth in continuous cultures," in "Advances in biotechnology. International Fermentation Symposium," Pergamon, Elmsford, NY (1989), pp. 315-321.

Ulrich, G.D. and Vasudevan, P.T., "Chemical engineering: Process Design and Economics A practical Guide," Process Publishing, Durham, New Hampshire, USA (2004), pp. 383, 386-389, 410.

Van't Riet, K., "Review of Measuring Methods and Results in Nonviscous Gas-Liquid Mass Transfer in Stirred Vessels," Ind. Eng. Chem. Proc. D. D., **18**, 357-364 (1979).

Virdis, B., K. Rabaey, Z. Yuan and J. Keller, "Microbial fuel cells for simultaneous carbon and nitrogen removal," Wat. Res. **42**, 3013-3024 (2008).

Voloshin, Y., A. Lawal and N. Panikov, "Continuous Plug-Flow Bioreactor: Experimental Testing With *Pesudomonas putida* Culture Growth on Benzoate," Biotechnol. Bioeng. **91**, 254-259 (2005).

Vunjak-Novakovic, G., Y. Kim, X. Wu, I. Berzin and J. C. Mercuk, "Air-Lift Bioreactors for Algal Growth on Flue Gas: Mathematical Modeling and Pilot-Plant Studies," Ind. Eng. Chem. Res. **44**, 6154-6163 (2005).

Wang, C.-Y., C.-C. Fu and Y.-C. Liu, "Effects of using light-emitting diodes on the cultivation of *Spirulina platensis*," Biochem. Eng. J. **37**, 21-25 (2007).

Warren, R. K., G. A. Hill and D. G. MacDonald, "Continuous Cell Recycle Fermentation to Produce Ethanol," Trans. I. Chem E. **72**, 149-157 (1994).

White, C. M., B. Strazisar, E. Granite, J. S. Hoffman, and H. W. Pennline, "Separation and capture of CO2 from large stationary sources and sequestration in geological formations – Coalbeds and deep saline aquifers," Journal of the Air and Waste Management Association, **53**, 645-715, (2003).

Winkler, M. A., "Critical Reports on Applied Chemistry Volume 29: Chemical Engineering Problems in Biotechnology," Society of Chemical Industry, Elsevier Applied Science, New York, NY (1990), pp. 228-229, 264.

Wu, X. and J. C. Merchuk, "Simulation of Algae Growth in a Bench-Scale Bubble Column Reactor," Biotechnol. Bioeng. **80**, 156-168 (2002).

Wu, X. and J. C. Merchuk, "Measurement of fluid flow in the downcomer of an internal loop airlift reactor using an optical trajectory tracking system," Chem. Eng. Sci. **58**, 1599-1614 (2003).

Wu, X. and J. C. Merchuk, "Simulation of algae growth in a bench scale internal loop airlift reactor," Chem. Eng. Sci. **59**, 2899-2912 (2004).

Yoon, D., H. Lee and Y. Park, "Effect of process variables in oxidation of paraffin wax in a stirred tank reactor," J. Ind. Eng. Chem., **13**, 194-198 (2002).

Yun, Y.-S. and J. M. Park, "Attenuation of monochromatic and polychromatic lights in *Chlorella vulgaris* suspensions," Appl. Microbial. Biotechnol. **55**, 765-770 (2001).

Yun, Y.-S. and J. M. Park, "Kinetic Modeling of the Light-Dependent Photosynthetic Activity of Green Microalga *Chlorella vulgaris*," Biotechnol. Bioeng. **83**, 303-311 (2003).

Zargar, S., and T. K. Ghosh, "Thermal and Biocidal (Chlorine) Effects on Select Freshwater Plankton," Archives of Environmental Contamination and Toxicology, **53**, 191-197, (2007).

Zhang, T, B. Zhao, and J. Wang, "Mathematical models for macro-scale mass transfer in airlift loop reactors," Chem. Eng. J. 119, 19-26, (2006).

Zheng, X., Y. Diao, W. Feng, C. Chen, X. Xu and H. Boshu, "Recovery of carbon dioxide by ammonia scrubbing in power plants," Energy and the Environment – Proceedings of the International Conference on Engery and the Environment, **2**, 1244-1247, (2003).

Appendix A - Data Used in Model Development (Chapter 5) - Collected by D. Sasi

A.1. Summary of Fed-Batch ELAPB Experimental Growth Data

Table A.1.1 Specific Growth Rate with Light and CO_2 Concentration

No. of LED Light Strips	Illuminance (mW)	Radiant Flux (W/m^2)	CO_2 Added to Feed Air (%)	Specific Growth rate (h^{-1})
6	162	0.45	0	0.014
6	162	0.45	5	0.041
6	162	0.45	5	0.043
6	162	0.45	10	0.037
8	216	0.60	10	0.037
10	269	0.75	10	0.034
10	269	0.75	10	0.029
16	431	1.15	10	0.030
6	162	0.45	15	0.013
10	269	0.75	15	0.015

A.2. Detailed Fed-Batch ELAPB Experimental Growth Data

Table A.2.1 Biomass Accumulation with Time: 0.45 W/m^2 (6 LED strips) and 0% CO_2 Added

Time (h)	Biomass Concentration (mg DW/L)
0.00	6.95
5.8	7.70
25.5	9.47
34.5	12.5
46.3	13.5
49.0	15.0
54.3	17.3
70.5	20.1
73.5	24.6
74.5	27.4
76.5	29.9
167	32.9
171	33.9

Table A.2.2 Biomass Accumulation with Time: 0.45 W/m^2 (6 LED strips) and 5% CO_2 Added

Time (h)	Biomass Concentration (mg DW/L)
0.00	7.96
20.5	8.46
30.3	12.2
44.3	15.3
48.5	19.3
52.7	25.1
73.7	63.9
78.2	77.5
94.1	90.9
116	108
123	115
148	176
177	191
235	219
241	219
259	221

Table A.2.3 Biomass Accumulation with Time: 0.75 W/m^2 (10 LED strips) and 10% CO_2 Added

Time (h)	Biomass Concentration (mg DW/L)
0.00	10.2
72.0	18.8
96.0	29.1
144	118
168	130
192	127
216	122

Table A.2.4 Biomass Accumulation with Time: 0.45 W/m^2 (6 LED strips) and 10% CO_2 Added

Time (h)	Biomass Concentration (mg DW/L)
0.00	6.70
21.0	9.47
47.5	13.8
65.3	18.5
68.5	23.6
70.5	27.1
72.8	33.2
89.3	50.1
91.3	55.3
93.5	61.9
95.3	75.8
97.0	89.6
113	95.9
116	102
117	105
119	107
121	110
137	118
139	123
141	127
143	134
145	149
167	192
210	204
212	199
214	209
216	221
217	219
233	217
236	218
240	228
241	223
257	218

Table A.2.5 Biomass Accumulation with Time: 0.60 W/m^2 (8 LED strips) and 10% CO_2 Added

Time (h)	Biomass Concentration (mg DW/L)
0.0	3.42
5.0	3.92
12.7	6.20
19.0	7.96
22.8	9.73
24.8	11.24
29.8	16.3
33.3	20.1
36.9	22.6
40.1	25.6
46.5	30.1
50.6	29.9
52.9	33.4
54.0	35.9
54.8	37.2
55.4	38.4
60.6	48.8
71.5	52.0
80.7	79.0
102	112
118	149
143	174
156	178

Table A.2.6 Biomass Accumulation with Time: 0.75 W/m^2 (10 LED strips) and 10% CO_2 Added

Time (h)	Biomass Concentration (mg DW/L)
0.0	3.42
7.25	4.93
23.6	6.44
25.5	6.70
32.1	8.46
45.8	10.2
53.5	13.8
58.9	19.1
74.4	30.9
83.0	49.8
94.9	60.4
103	76.0
108	85.8
119	93.4
120	94.2
121	95.9
122	96.9
126	102
129	109
142	112
145	112
148	121
149	123
166	143
168	145
170	148
172	150
175	153
177	163
192	174
194	185

Table A.2.7 Biomass Accumulation with Time: 1.15 W/m^2 (16 LED strips) and 10% CO_2 Added

Time (h)	Biomass Concentration (mg DW/L)
0.00	4.68
7.00	4.94
7.75	7.71
16.0	9.98
27.7	32.2
29.7	35.7
31.7	40.7
33.7	45.7
34.7	49.6
35.2	50.8
51.2	69.7
53.2	73.8
55.2	81.0
57.2	90.1
59.2	98.4
75.2	130
77.7	147
79.5	162
81.9	176
83.2	179
99.2	196
101	197
102	202
105	213
107	219
123	210
126	210

Table A.2.8 Biomass Accumulation with Time: 0.45 W/m^2 (6 LED strips) and 15% CO_2 Added

Time (h)	Biomass Concentration (mg DW/L)
0.00	4.43
17.0	4.93
21.5	5.19
24.5	5.44
41.0	6.70
44.3	7.96
47.8	10.2
67.9	15.0
69.8	16.0
72.0	19.0
113.	64.1
115	69.7
117	74.5
120	81.8
137	90.1
139	92.4
141	96.9
143	100
145	103
161	123
164	132
166	142
167	144
169	148
185	174
187	180
189	185
191	190
193	190
209	211
211	207
213	210
217	223
239	209
240	213
241	215
281	247
284	240
289	250
306	244

Table A.2.9 Biomass Accumulation with Time: 0.75 W/m^2 (10 LED strips) and 15% CO_2 Added

Time (h)	Biomass Concentration (mg DW/L)
0.00	4.68
7.00	5.19
23.0	5.69
28.3	6.95
30.8	7.46
48.8	11.5
52.3	13.2
53.8	14.0
71.5	23.8
76.2	33.9
80.8	48.3
119	105
121	109
123	115
125	116
126	117
143	146
145	165
148	173
151	184
167	211
170	218
172	227
175	230
190	242
193	252
195	255

Appendix B - Computer Programs Created in Support of This Study

B.1. Excel Design Output for CSTB Optimization – Chapter 2

Fermentor Design

INPUT DATA

Input the Fermentor Working Volume (m^3)	**10**
Number of Tanks in Parallel Required	**1**
Working Volume per Tank (m^3)	**10**
Input Impeller Style (1 only)	**1**
Input Mixing Speed (rev/s)	**5.050**
Input Aeration Rate (m^3/s)	**0.023**
Input Temp (^oC)	**25**
Input Steady State X (mgDW/L)	**7000**
Maximum X (mgDW/L)	**50000**
Ccrit (mg/l)	**1**
Input Respiratory Coefficient (mgO2/mgDW-h)	**0.36**
turbine impeller type	**1**

note: multiple fermentors are of equal size and all values except step 9 are for one of those identical fermentors operated in parallel

Does this design meet the cell oxygen requirements? YES

STEP 1: Tank Design	
Total working volume required (m^3), V	**10**
Number of tanks in parallel required	**1**
Liquid volume per tank (m^3), Vw	**10**
Tank diameter (m), T	**2.34**
Height of liquid in tank (m), Hliq	**2.34**
Height of tank (m), Htank	**3.50**
Volume of individual tank(s) (m^3), Vtank	**15**
STEP 2: Impeller Characteristics	
Impeller Style	**1**
Impeller Diameter (m), DI	**0.93**
STEP 3: Specify Stirring Rate	
Stirring Rate (rev/s), N	**5.050**
STEP 10: Unaerated Power	
Reynold's number, NRe	**4304505**
Turbine power number, Np	**5**
Unaerated power (W), Po	**447288**
STEP 4: Specify Aeration Rate	
Aeration rate (m^3/s), Q	**0.023**
Superficial air velocity (m/s), vs	**0.005467**

Step 11: Compressor Power	
Air mass flow rate (kg/s), m_{AIR}	**0.029**
Compressor power (kW), ($\dot{W}_{ELEC}$)	**6.31**
Step 5: Power for Aerated Fermentor	
Aeration number, NA	**0.005689**
Weber number, New	**312374**
Gas Hold-up, ϵG	**0.400000**
Aerated power (W), PG	**179863**
Step 12: Size and Cost of Compressor(s) and Mixer(s)	
Number of compressors per fermentor, Nc	**1**
Base compressor cost ($), Cp,c	**34431**
Carbon steel compressor cost ($), $C_{BM,C}$	**86078**
Number of mixers per fermentor, Nm	**1**
Base mixer cost ($), Cp,m	**160884**
Stainless steel mixer ($), $C_{BM,M}$	**402210**
Step 13: Total External Power	
Total external power (W), P ext	**186170**
Step 6: Oxygen Mass Transfer Coefficient	**0**
oxygen mass transfer coefficient (s^{-1}), kLa	**0.096787**
Step 14: Oxygen Concentration Exiting Fermentor	
Oxygen demand of cells (mg O2 / L h), NO2	**2520**
Concentration of oxygen exiting fermentor (mg/L), C*air	**267**
Step 15: Adjusted Oxygen Exit Concentration	
Adjusted Oxygen Exit Concentration (mg/L), C*	**8.23**
Step 20: Compare Oxygen Supply to Demand	
Oxygen demand of cells (mg O2 / L h), NO2	**2520**
Oxygen supplied (mg O2 / L h), Ns	**2520**
Comparison of NO2 to Ns (NO2 - Ns)	**0**
Step 8: Change Stirring Speed and/or Aeration Rate?	
Does this design meet the cell oxygen requirements?	**YES**
If NO, increase stirring speed and/or aeration rate in input box.	
Continue to change one or both values until red box reads YES.	
Step 9: Economy	
Operating period (days)	**1000**

Fermentor(s) cost ($), Cf	**307845**
Compressor(s) cost ($), Cc	**430391**
Mixer(s) cost ($), Cm	**2011051**
Cost of power ($), Pcost	**446808**
Operating Cost (Utilities) ($)	**446808**
Operating Cost (Utilities) (millions of $)	**0.447**
Total Cost (Capital and Operating) ($)	**3196095**
Total Cost (Capital and Operating) (millions of $)	**3.196095**

B.2. MATLAB Source Code for ELAPB Modeling – Chapter 5

ELAPBmodel.m

```
clear
clc
format long

s = 20;          %Number of spacial steps vertically along the ELAPB columns.

% Define riser dependent variables and initialize to zero. Each has a matrix of size 's' vertical
steps and 10 radial steps.
Sriserk = zeros(s,10);  %Liquid phase CO2 concentration in the riser, g/L, previous time step.
Sriserk1 = zeros(s,10);          %Liquid phase CO2 concentration in the riser, g/L, present time
step.
Xriserk = zeros(s,10);           %Biomass in the riser, mg, previous time step.
Xriserk1 = zeros(s,10);          %Biomass in the riser, mg, present time step.
yriserk = zeros(s,10);  % Gas phase CO2 concentration in the riser, g/L, previous time step.
yriserk1 = zeros(s,10);          % Gas phase CO2 concentration in the riser, g/L, present time step.
radriserk = zeros(s,10);         %Radial location in riser, m, previous time step.
radriserk1= zeros(s,10);         % Radial location in riser, m, present time step.
Sstarriserk = zeros(s,10);       %Interface CO2 concentration in the riser, g/L, previous time step.
Sstarriserk1 = zeros(s,10);      %Interface CO2 concentration in the riser, g/L, present time step.
Iriserk = zeros(s,10);           %Local radiant flux in riser, W/m2, previous time step.
Iriserk1 = zeros(s,10);          %Local radiant flux in riser, W/m2, present time step.
uriserk = zeros(s,10);  %Specific growth rate in riser, s-1, previous time step.
uriserk1 = zeros(s,10);          %Specific growth rate in riser, s-1, present time step.
volriserk = zeros(s,10);         %Volume of radial section of riser, m3, previous time step.
volriserk1 = zeros(s,10);        %Volume of radial section of riser, m3, present time step.
Rratiok = zeros(s,10); %Volumetric ratio of radial section to total in riser, previous time step.
Rratiok1 = zeros(s,10);          %Volumetric ratio of radial section to total in riser, previous time
step.
Xsum1k = zeros(s,10);            %Total biomass in riser, mg, previous time step.
Xsum1k1 = zeros(s,10);           % Total biomass in riser, mg, present time step.

% Define downcomer dependent variables and initialize to zero. Each has a matrix of size 's'
vertical steps and a single radial step (no radial variation assumed).
Sdownk = zeros(s,1);  %Liquid phase CO2 concentration in the downcomer, g/L, previous time
step.
Sdownk1 = zeros(s,1);            %Liquid phase CO2 concentration in the downcomer, g/L, present
time step.
Xdownk = zeros(s,1); %Biomass in the downcomer, mg, previous time step.
Xdownk1 = zeros(s,1);            %Biomass in the downcomer, mg, present time step.
```

ydownk = zeros(s,1); % Gas phase CO_2 concentration in the downcomer, g/L, previous time step.
ydownk1 = zeros(s,1); % Gas phase CO_2 concentration in the downcomer, g/L, present time step.
Sstardownk = zeros(s,1); %Interface CO_2 concentration in the downcomer, g/L, previous time step.
Sstardownk1 = zeros(s,1); %Interface CO_2 concentration in the downcomer, g/L, present time step.
Idownk = zeros(s,1); %Local radiant flux in downcomer, W/m^2, previous time step.
Idownk1 = zeros(s,1); %Local radiant flux in downcomer, W/m^2, present time step.
udownk = zeros(s,1); %Specific growth rate in downcomer, s^{-1}, previous time step.
udownk1 = zeros(s,1); %Specific growth rate in downcomer, s^{-1}, present time step.
Xsum2k = zeros(s,1); %Total biomass in downcomer, mg, previous time step.
Xsum2k1 = zeros(s,1); %Total biomass in downcomer, mg, present time step.

% Define auxiliary variables.
NI = 6.; %Number of lights illuminated on ELAPB.
W = NI/37.1118793; %Light intensity inside reactor (at wall), W.
Driser = 0.0508; %Diameter of riser, m.
Rriser = Driser/2.; %Radius of riser, m.
z = 1.; %Height of column m.
Ariser = (PI)*(Rriser^2); %Cross-sectional area of riser, m^2.
Vriser = Ariser*z; %Volume of riser, m^3.
Ddown = 0.0381; %Diameter of downcomer, m.
Rdown = Ddown/2.; %Radius of downcomer, m.
Adown = (PI)*(Rdown^2); %Cross-sectional area of downcomer, m^2.
Vdown = Adown*z; %Volume of downcomer, m^3.
PI = 3.14159; %Numerical value of $\prod$.
Io = W/(2*PI*Rriser*z); %Light intensity inside reactor (at wall), W/m^2.
CO = 10.; %Percentage of CO_2 in ELAPB feed air, %.
yo = (CO*1.185)/100.; %Initial CO_2 concentration in gas phase, g/L.
t = 0.; % Initial value of time, s.
dt = 0.001; % Step change in time, s.
tend = 14*24*3600; % Time to simulation end, s. This is 14 days.
dz = z/s; % Spatial step change vertically along column, m.
dr = Rriser/10.; %Step change in radial position, m, riser only.
Xo = 5.; %Initial biomass concentration at inoculation, mg/L.
AF = 200.; % Airflow rate of gas, mL/min)
AV =(AF/60.)/(1000000.); % Airflow rate of gas, m^3/s.
Ka = 435.3/1000.; %Extinction coefficient of C. vulgaris, m^2/g.
k_{La} = 1./3600.; %Mass transfer coefficient, s^{-1}.
H = 0.682; %Henry's Law coefficient, g/L/g/L.
So = 0.00038/H; %Initial liquid phase CO_2 concentration, g/L , assumed atmospheric.
Sstaro = (CO/100.)/H; %Initial gas-liquid interface CO_2 concentration, g/L.
ghold = 0.0045; %Gas holdup in riser.

```
Bheight = 0.1;                  %Height of bottom connector, m.
Ungas = 1.142;                  %Ungassed height of column, m.
Rheight = 1.0;                  %Column height (of riser), m.
Sheight = Ungas*(1+ghold)- Rheight -Bheight;        %Separator height, m.
EDheight = Bheight + Sheight + z;           %Total height included with downcomer, m.
CircLiq = 0.12;                 %Average liquid circulation velocity, m/s.
tCirc = 26.5;                   %Average circulation time, s.
ULiq = CircLiq/(1-ghold);     %Liquid velocity in riser, m/s.
UGas = AV/Ariser;               %Gas velocity in riser, m/s.
Yxs = 0.51;                     %Yield coefficient (mg biomass / mg CO2).
VELAPB = 4./1000.;                  % Total ELAPB volume, m3.
umax = 0.113;
KSI = 0.03;
KII = 1.5;
KSS = 0.005;
KIS = 0.1;
Me = 0.15315:
udown = 0.0001;
uo = (1./3600.)*(umax*(Io/(Io+KSI+((Io^2)/KII)))*(So/(So+KSS+((So^2)/KIS)))); %Specific
growth equation, for growth in the riser.
Xvolk = Xo;                     %Overall biomass concentration in ELAPB, mg/L.
Xallk = Xo*(VELAPB*1000.);          %Total biomass in ELAPB, mg.
Xtotalk = Xo*(VELAPB*1000.)/(2*s);          %Total biomass in ELAPB, mg, per spatial step.
Xtotalk1 = 0.;
Xtotalk2 = 0.;

% Create a matrix to hold the approximate times at results are printed.
tprint =  0 : 3600 : tend;          %Print every hour of data.
iprint = 1;

fid = fopen('6light10carbon5EqFMSd.txt','wt');          %Create a file for the results.
fprintf(fid,'% 12.8e\r',NI);
fprintf(fid,'% 12.8e\r',CO);

%Set initial values at t=0 time step.
radriserk(:,:)= 0.;
volriserk(:,:) = 0.;
Rratiok(:,:) = 0.;
Sriserk(:,:)= So;
Xriserk(:,:) = 0.;

   for n = 1:10             %Initialize for all ten radial "step" locations.
         radriserk(:,n) = dr*(n-0.5);
         volriserk(:,n) = PI*dz*((Rriser-(n-1)*dr)^2-((Rriser-n*dr)^2));
         Rratiok(:,n) = volriserk(:,n)/(Vriser*(dz/z));
          radriserk1(:,n) = dr*(n-0.5);
```

```
        volriserk1(:,n) = PI*dz*((Rriser-(n-1)*dr)^2-((Rriser-n*dr)^2));
        Rratiok1(:,n) = volriserk1(:,n)/(Vriser*(dz/z));
         Xriserk(:,n) = Xtotalk*Rratiok(1,n); %Partition Xo over all radial divisions.
        Xsum1k(s,n) = (Xo*(VELAPB*1000)/(2*s))*Rratiok(1,n);
         Xsum2k(s,1) = Xo*(VELAPB*1000)/(2*s);

   end

yriserk(:,:) =(0.038*1.185)/100;        %Initial gas phase CO2 concentration in ELAPB is
assumed to be atmospheric.
yriserk(1,:) = yo;        %Initial gas phase CO2 concentration at the riser inlet is assumed to be at
                          yo.
Sstarriserk(:,:) = Sstaro;
Iriserk(:,:) = Io;
uriserk(:,:) = uo;
Sdownk(:,:)= So;
Xdownk(:,:) = Xo*(VELAPB*1000.)/(2*s);
ydownk(:,:) = 0.;
Sstardownk(:,:) = 0.;
Idownk(:,:) = 0.;
udownk(:,:) = 0.;
Stransfer = So;
Xtransfer = Xo*(VELAPB*1000.)/(2*s);
ytransfer = yo; %Boundary condition.
Sstartransfer = Sstaro;
Itransfer = Io;
utransfer = uo;

%Print the initial conditions in the riser and downcomer.
fprintf(fid,'% 12.8f\t',t);
fprintf(fid,'% 12.8e\t',uriserk(1,1));
fprintf(fid,'% 12.8e\t',Xriserk(1,1));
fprintf(fid,'% 12.8e\t',Sriserk(1,1));
fprintf(fid,'% 12.8e\t',yriserk(1,1));
fprintf(fid,'% 12.8e\t',Xtotalk);
fprintf(fid,'% 12.8e\t',Sstarriserk(1,1));
fprintf(fid,'% 12.8e\t',Sdownk(1,1));
fprintf(fid,'% 12.8e\t',Xdownk(1,1));
fprintf(fid,'% 12.8e\t',ydownk(1,1));
fprintf(fid,'% 12.8e\t',Sstardownk(1,1));
fprintf(fid,'% 12.8e\t',udownk(1,1));
fprintf(fid,'% 12.8e\t',Xallk);
fprintf(fid,'% 12.8e\r',Xvolk);

% Create the loop to step through time.  Use a variable time for first circulation loop due to
problem stiffness.
```

```
while (t<tend)

  if (t < 30)
        dt = 0.001;

  else
        dt = 0.1;

  end

  if (t>0)

        % Step through riser and downcomer, explicitly solving for k+1 timestep

%For the Riser.
         %Ensure output of downcomer is used as input to riser.
         Stransfer = Sdownk(s,1);       % Liquid phase CO2 entering riser from downcomer, mg.
        Xtransfer = Xsum2k(s,1);       % Biomass entering riser from downcomer, mg.
        ytransfer = yo;           %Boundary condition: CO2 concentration in feed air.
         Sstartransfer = Sstardownk(s,1);
        Itransfer = Io;             %Boundary condition: radiant flux at riser wall is known.
         utransfer = udownk(s,1);
         z = 1.;           %Riser column  height.
         dz = z/s;

  end

   for i = 1      %At riser bottom (step 1), boundary conditions exist which affect the
                  calculations.

       for j = 1:10
         z = 1.0;
         Sriserk1(i,j) = Sriserk(i,j) + dt*(-(ULiq/dz)*(Sriserk(i,j)-Stransfer)+kLa*(Sstarriserk(i,j)-
                  Sriserk(i,j))-(uriserk(i,j)*Xtotalk*Rratiok(i,j)/Yxs));
         Xriserk1(i,j) = Xriserk(i,j) + dt*(-(ULiq/dz)*(Xriserk(i,j)-
                  Xtransfer*Rratiok(i,j))+(uriserk(i,j)*Xtotalk*Rratiok(i,j)));
         yriserk1(i,j) = yo;       %Boundary condition at bottom of riser.
         Sstarriserk1(i,j) = yriserk(i,j)/H;
         Iriserk1(i,j) = Io*exp(-radriserk(i,j)*Ka*Xriserk(i,j));
         uriserk1(i,j) =
                  (1./3600.)*(umax*(Iriserk(i,j)/(Iriserk(i,j)+KSI+((Iriserk(i,j)^2)/KII)))*(Sriserk(i,j
                  )/(Sriserk(i,j)+KSS+((Sriserk(i,j)^2)/KIS))));

       end

   end
```

```
  for i = 2:s

     for j = 1:10
        z = 1.0;
      Sriserk1(i,j) = Sriserk(i,j) + dt*(-(ULiq/dz)*(Sriserk(i,j)-Sriserk(i-
                1,j))+kLa*(Sstarriserk(i,j)-Sriserk(i,j))-(uriserk(i,j)*Xtotalk*Rratiok(i,j)/Yxs));
      Xriserk1(i,j) = Xriserk(i,j) + dt*(-(ULiq/dz)*(Xriserk(i,j)-Xriserk(i-
                1,j))+(uriserk(i,j)*Xtotalk*Rratiok(i,j)));
      yriserk1(i,j) = yriserk(i,j) + dt*(-(UGas/dz)*(yriserk(i,j)-yriserk(i-1,j))-(kLa*((1-
                ghold)/ghold)*(Sstarriserk(i,j)-Sriserk(i,j))));
        Sstarriserk1(i,j) = yriserk(i,j)/H;
        Iriserk1(i,j) = Io*exp(-radriserk(i,j)*Ka*Xriserk(i,j));
       uriserk1(i,j) =
                (1./3600.)*(umax*(Iriserk(i,j)/(Iriserk(i,j)+KSI+((Iriserk(i,j)^2)/KII)))*(Sriserk(i,j
                )/(Sriserk(i,j)+KSS+((Sriserk(i,j)^2)/KIS))));

     end

  end

 for m = 1:10
        Xsum1k1(s,m) = Xriserk1(s,m
        Xtotalk1 = Xtotalk+(Xsum1k1(s,m)-Xsum1k(s,m));
        Xallk = (2*s)*Xtotalk1;
        Xvolk = (2*s)*Xtotalk1/(VELAPB*1000);

  end

% For the Downcomer.
        %Ensure output of riser is used as input to downcomer.
Stransfer = Sriserk1(s,10);
counter = 0;
Xtransfer = 0.;

     for p = 1:10  %Biomass entering downcomer, mg.  This is summed from all radial "steps".
        counter = Xtransfer;
        Xtransfer = counter+Xsum1k1(s,p);

     end

  ytransfer = 0;          %Boundary condition: assume negligible gas holdup.
  Sstartransfer = Sstarriserk1(s,10);
  Itransfer = 0;
  utransfer = uriserk1(s,10);
  z = EDheight;          %Downcomer height with separator and bottom tube.
```

```
j = 1;
for i =1        %At downcomer bottom (step 1), boundary conditions exist which affect the
                calculations.
   z = EDheight;
   dz = z/s;
  Sdownk1(i,j) = Sdownk(i,j) + dt*(-(ULiq/dz)*(Sdownk(i,j)-
       Stransfer)+kLa*(Sstardownk(i,j)-Sdownk(i,j))-(udownk(i,j)*Xtotalk/Yxs));
  Xdownk1(i,j) = Xdownk(i,j)+ dt*(-(ULiq/dz)*(Xdownk(i,j)-
       Xtransfer)+(udownk(i,j)*Xtotalk));
   ydownk1(i,j) = ydownk(i,j) + 0.;          %Assume negligible gas holdup.
   Sstardownk1(i,j) = ydownk(i,j)/H;
   Idownk1(i,j) = 0.;                  % Downcomer is "dark".
  udownk1(i,j) = 0.0001;

end

for i = 2:s
   z = EDheight;
   dz = z/s;
   Sdownk1(i,j) = Sdownk(i,j) + dt*(-(ULiq/dz)*(Sdownk(i,j)-Sdownk(i-
       1,j))+kLa*(Sstardownk(i,j)-Sdownk(i,j))-(udownk(i,j)*Xtotalk/Yxs));
  Xdownk1(i,j) = Xdownk(i,j)+ dt*(-(ULiq/dz)*(Xdownk(i,j)-Xdownk(i-
       1,j))+(udownk(i,j)*Xtotalk));
   ydownk1(i,j) = ydownk(i,j) + 0.;          %Assume negligible gas holdup.
   Sstardownk1(i,j) = ydownk(i,j)/H;
   Idownk1(i,j) = 0.;                  % Downcomer is "dark".
   udownk1(i,j) = 0.0001;

end

for m = 1
   Xsum2k1(s,m) = Xdownk1(s,m);
  Xtotalk2 = Xtotalk1+(Xsum2k1(s,m)-Xsum2k(s,m));
   Xallk = (2*s)*Xtotalk2;
   Xvolk = (2*s)*Xtotalk2/(VELAPB*1000);

end

% Update current time step values to previous time step values.

Sriserk = Sriserk1;
Xriserk = Xriserk1;
yriserk = yriserk1;
Sstarriserk = Sstarriserk1;
```

```
Iriserk = Iriserk1;
uriserk = uriserk1;
radriserk = radriserk1;
volriserk = volriserk1;
Rratiok = Rratiok1;
Xsum1k = Xsum1k1;
Sdownk = Sdownk1;
Xdownk = Xdownk1;
ydownk = ydownk1;
Sstardownk = Sstardownk1;
Idownk = Idownk1;
udownk = udownk1;
Xsum2k = Xsum2k1;
Xtotalk =Xtotalk2;

%Print results.

if (t > tprint(iprint))
        iprint = iprint + 1;

        % Output results.
      fprintf(fid,'% 12.8f\t',t);
      fprintf(fid,'% 12.8e\t',uriserk(s,1));
      fprintf(fid,'% 12.8e\t',Xriserk(s,1));
      fprintf(fid,'% 12.8e\t',Sriserk(s,1));
      fprintf(fid,'% 12.8e\t',yriserk(s,1));
      fprintf(fid,'% 12.8e\t',Xtotalk);
      fprintf(fid,'% 12.8e\t',Sstarriserk(s,1));
      fprintf(fid,'% 12.8e\t',Sdownk(s,1));
      fprintf(fid,'% 12.8e\t',Xdownk(s,1));
      fprintf(fid,'% 12.8e\t',ydownk(s,1));
      fprintf(fid,'% 12.8e\t',Sstardownk(s,1));
      fprintf(fid,'% 12.8e\t',udownk(s,1));
      fprintf(fid,'% 12.8e\t',Xallk);
      fprintf(fid,'% 12.8e\r',Xvolk);

        end

        t = t + dt;             % Increment time to ensure simulation ends.

end

fclose(fid)
```